THE MOLECULAR BEAM MASER EMPLOYING QUASI-OPTICAL RESONATORS: OSCILLATION BEHAVIOUR AND SPECTROSCOPIC APPLICATIONS

by

GHASSAN YASSIN

M.Sc.

A thesis submitted to the University of Keele

for the Degree of Doctor of Philosophy

Department of Physics
University of Keele
Staffordshire

November 1981

The following has been redacted from this digital copy of the original thesis at the request of the awarding university:

"Publications from the present works", Pages 160-176

PAGE NUMBERING AS ORIGINAL

TO MY FATHER SHARIF

CONTENTS

ACKNOWLEDGEMENTS

The Author would like to thank

Dr. D.C. Laine for his enthusiastic guidance and unfailing help throughout this work.

Professor W. Fuller for the provision of experimental facilities.

Dr. A.M. Al-Jumaily for his technical help and many useful discussion.

Dr. D.E. Dugdale for many helpful discussions.

Mr. M.G. Davies of the Electronics Workshop for his continuous assistance.

Mr. H. Wardell and the staff of the University Workshop for preparing the vacuum chamber and machining the cavity mirrors for the roof-top experiment.

Mr. G. Duddley and the technical staff of the Physics Department - Mr. G. Marsh and Mr. E.J.T. Greasley - for their continued assistance throughout the experimental work.

Mr. F. Rowerth and Mr. C.B. Harrison for their invaluable assistance.

Mr. M. Wallace for preparing the drawings in this thesis.

Mr. S. Cartledge for his technical assistance.

Mr. M. Daniels for preparation of the photographs reproduced in this thesis.

His Wife Frida for typing this thesis and for her continuous assistance over three years.

The University of Birzeit for provision of the study leave.

The British Council for personal finance.

Jim Gillespie for his help in correcting the English.

ABSTRACT

The spectroscopic and oscillation properties of the molecular beam maser, employing quasi-optical resonators are investigated. A new type of cavity, the roof-top resonator, is introduced for molecular beam work. The theoretical discussion reveals that it exhibits low diffraction losses at microwave frequencies. Its successful operation in conjunction with a single beam ammonia maser shows that the cavity is ideal for molecular beam spectroscopy in the cm-mm-wave spectral region.

Although the oscillation behaviour of the ammonia maser operated with disc resonators has been throughly investigated, very little has hitherto been known about the mode polarization properties of these resonators, especially at microwave frequencies. The employment of a new method of detection in the present work, facilitated the observation of the vectorial aspect of the maser oscillation. Such observations have led to the successful interpretation of unusual phenomena in the maser oscillation characteristics, for example, the drop in the amplitude of oscillation at high levels of excitation and the jumps in the frequency of oscillation while tuning the cavity through the molecular resonance. Investigation of the maser oscillation polarization also revealed some new effects directly linked to those previously observed in He-Ne lasers. These included oscillation polarization bistability and rotation of the plane of polarization in a weak axial magnetic field. These effects strongly influence the maser frequency stability and thus its applications as a frequency standard.

Finally, the isotropic properties of the disc resonator were exploited to enhance spectrometer sensitivity. This was done by the use of Faraday rotation as a basis for a new type of molecular beam maser spectrometer. An alternative method, employed detection of weak spectral lines via the low-noise elliptically polarized maser oscillation.

CHAPTER 1

THE MASER

1.1 INTRODUCTION

The principle of stimulated emission, which is employed by all quantum mechanical amplifiers, was first introduced by Einstein (1917) in his theory about interaction between electromagnetic waves and quantum-mechanical systems.

Let E_a and E_b be a pair of energy levels of a molecular ensemble separated by a frequency $\nu_o = (E_b - E_a)/h$ where h is Planck's constant (Fig. 1.1). According to Einstein's theory the probability of inducing transitions from the upper to the lower energy states ($b \rightarrow a$) by an external signal whose frequency $\nu \approx \nu_o$ is proportional to N_b and the transition probability, $a \rightarrow b$, is proportional to N_a where N_a and N_b are respectively the molecular densities of the levels E_a and E_b. At thermal equilibrium, the population distribution is given by the Boltzman law

$$N_b/N_a = \exp(-h\nu/kT) \qquad 1.1$$

Therefore electromagnetic radiation of frequency $\nu \approx \nu_o$ passing through such an ensemble will suffer attenuation. Although this principle was widely employed in bulk gas absorption spectroscopy for many years, the idea of obtaining stimulated emission by inverting the population of the energy levels (making $N_b > N_a$) was first put into practice in 1954 by Gordon, Zeiger and Townes. The first MASER which is an acronym for "Microwave amplification by stimulated emission of radiation" was then successfully operated.

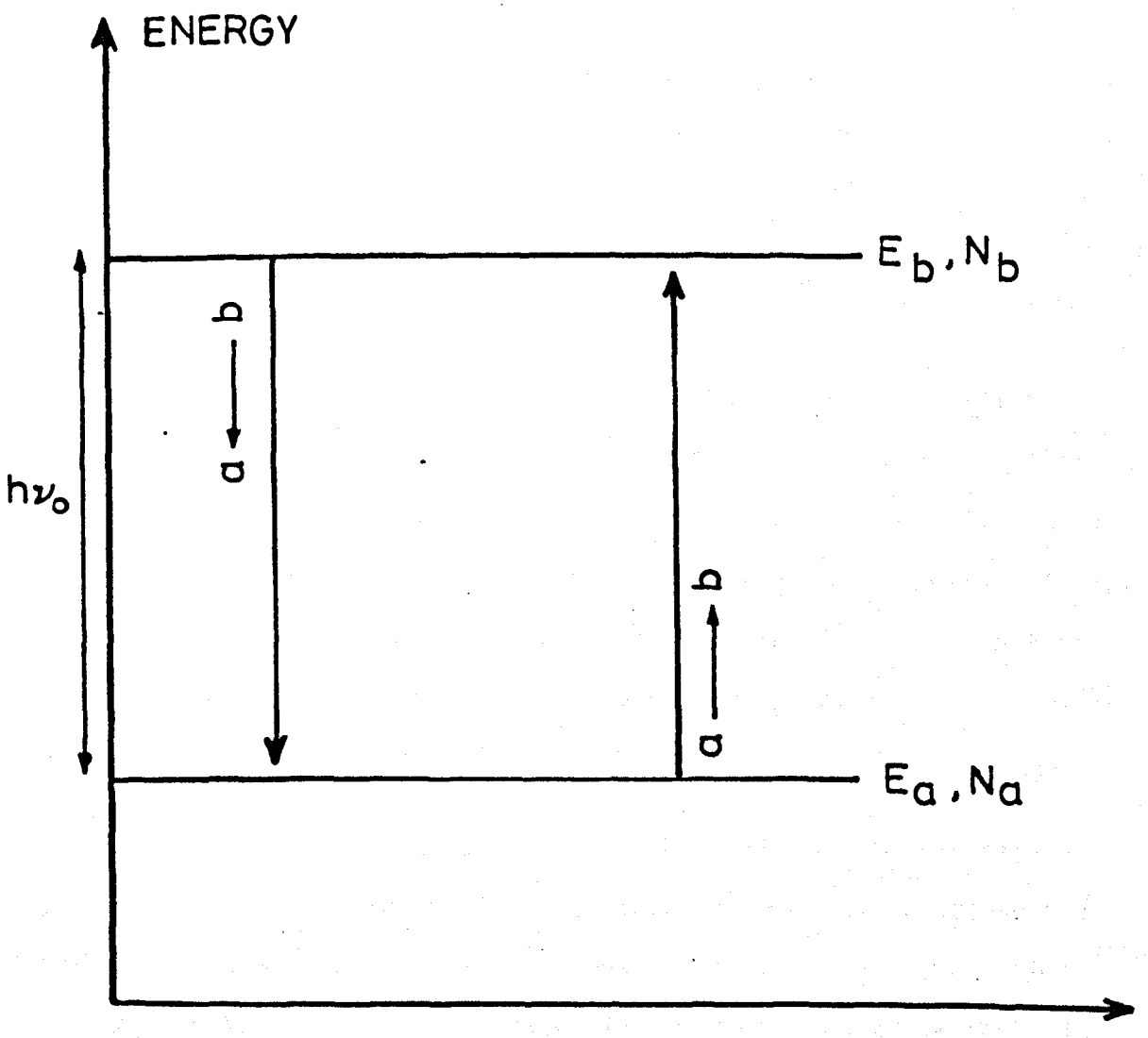

FIG. 1·1 EMISSION AND ABSORPTION BETWEEN A PAIR OF QUANTUM STATES.

The molecular beam maser has three main components: Gas source, state selector and resonator. The gas source is required to produce an intense and a highly collimated molecular beam. This is now achieved by using a single hole nozzle source of small diameter ($\sim$ 0.1mm), where advantage is taken of the dynamic cooling effect which enhances the population of the low-lying rotational states.

Population inversion for an electric dipole transition is obtained by electrostatic spatial separation of molecules in different energy states. Molecules at the low energy level E_a are deflected and pumped away and molecules at the higher energy E_b are focused into the resonator. This is done by letting the molecular beam pass through a device called a "state selector" or sometimes is refered to as "state separator".

The choice of a particular type of state selector depends, among other factors, on the type of resonator where interaction between the focused upper energy level molecules and the stimulating input signal is maintained. A schematic diagram of the maser is shown in Fig. 1.2.

1.2 STATE SEPARATION OF MOLECULES

The principle of state selection of molecules is based on the well known Stark effect in gases where molecules which possess a large electric dipole moment can be readily deflected by the use of a non-uniform external electric field with a gradient perpendicular to the molecular beam axis. Usually, the Stark field is treated as a small perturbation on the zero field Hamiltonian. The perturbed energies are then expressed as a power series in a non-dimensional quantity, smaller than unity, and proportional to the Stark interaction term. However,

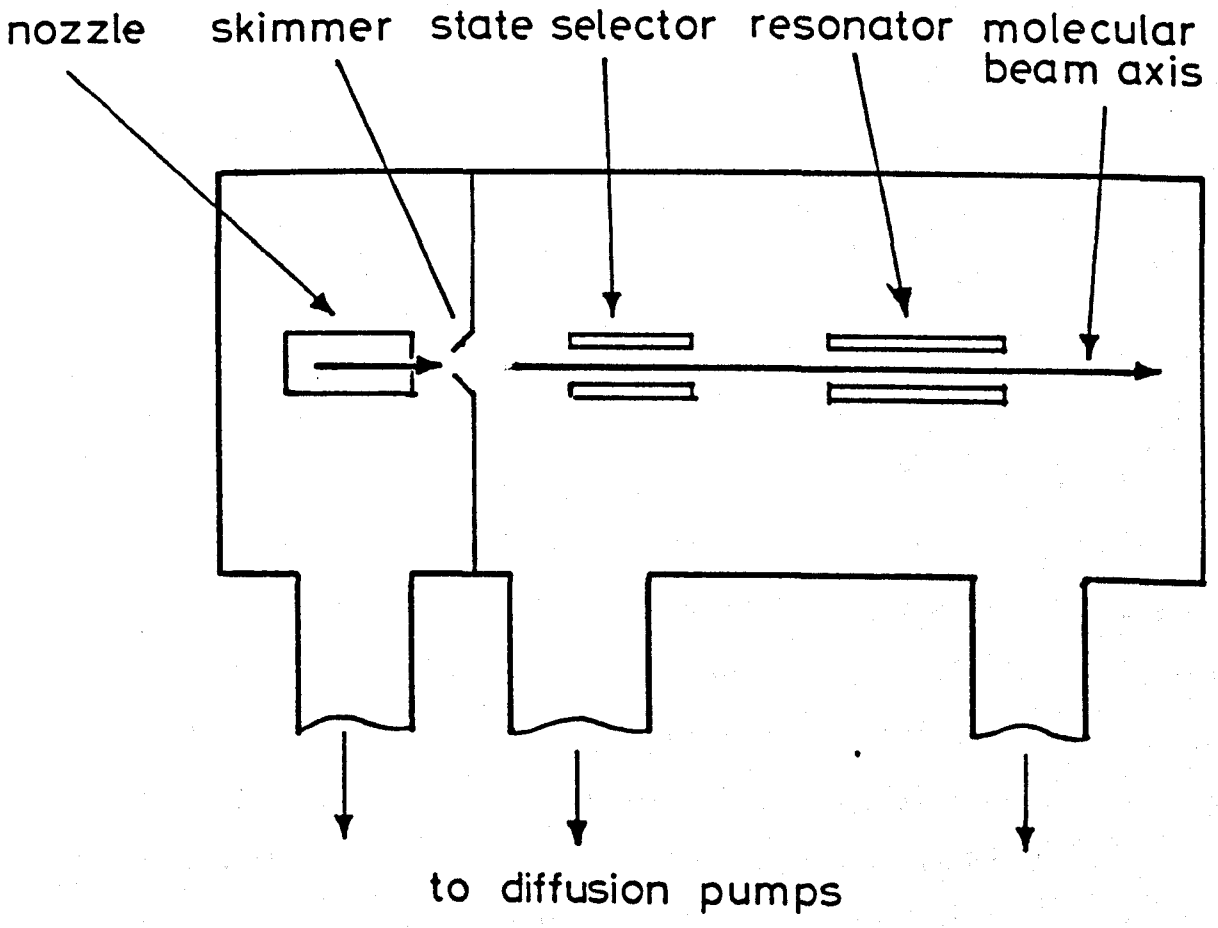

FIG. 1·2 TYPICAL TWO-CHAMBER MOLECULAR BEAM MASER.

if the frequency separation of the pair of energy levels in question is much smaller than with any other level, the perturbed Hamiltonian can be easily diagnolized and the problem is reduced to the solution of a quadratic secular equation. The perturbed energies can then be written as (Schiff, 1968)

$$E_{\pm} = \frac{E_b + E_a}{2} \pm \left[\left(\frac{h\nu_o}{2} \right)^2 + \mathcal{E}^2 \left| \langle \psi_+ | \mu | \psi_- \rangle \right|^2 \right]^{\frac{1}{2}} \qquad 1.2$$

where ψ_+ and ψ_- are the wave-functions corresponding to the energies E_b and E_a respectively, $\mathcal{E}$ is the magnitude of the external electric field and μ is the dipole moment tensor. For the NH_3 molecule the transition $J \rightarrow J + 1$, $J = 1,2,3$; where J is the total angular momentum excluding the nuclear spin, lies in the infra-red region while the inversion transition $J,K \rightarrow J,K$ is in the microwave range. Therefore Eqn. 1.2 is valid for the Stark effect with the inversion spectrum of ammonia which is employed in the present study. Ignoring the hyperfine structure, the perturbed energy levels are thus given by

$$E_{\pm} = E_o \pm \left[\left(\frac{h\nu_o}{2} \right)^2 + \left(\frac{\mu \mathcal{E} K M_J}{J(J+1)} \right)^2 \right]^{\frac{1}{2}}$$

where ν_o is now the inversion frequency, $E_o = (E_b + E_a)/2$; M_J is the projection of the rotational angular momentum along the external field and μ is the permanent dipole moment. If the Stark field provided by the state separator is non-uniform along the z-direction as shown in Fig. 1.3 then molecules travelling along the x-direction will experience the force component

$$F_{z\pm} = -\frac{\partial E_{\pm}}{\partial z} = \mp \frac{E_s \mathcal{E} \partial \mathcal{E}/\partial z}{\left[(h\nu_o/2)^2 + E_s^2 \right]^{\frac{1}{2}}} \qquad 1.3$$

where

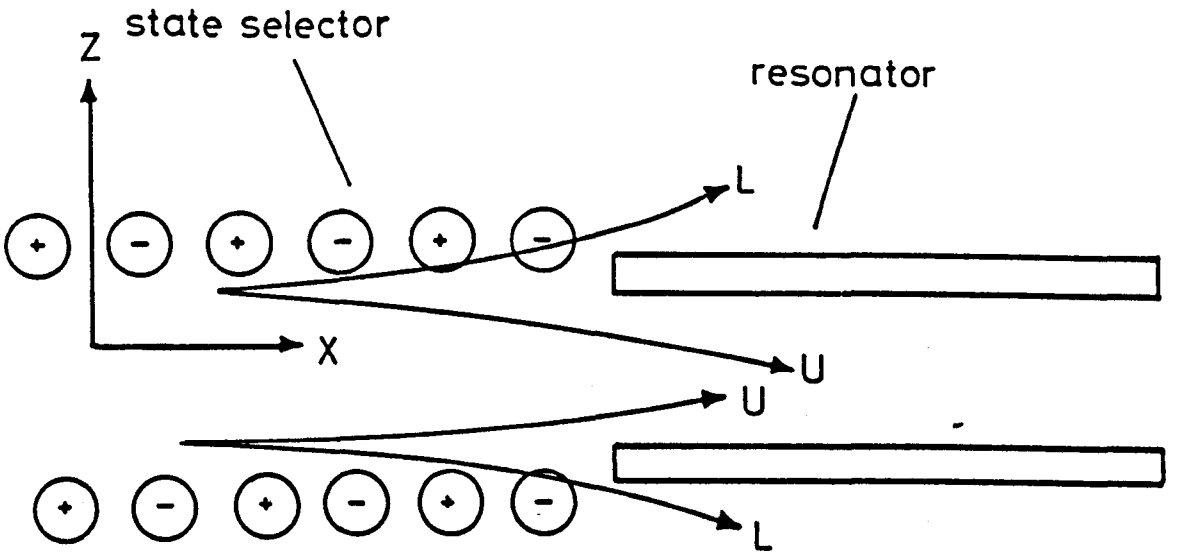

L : MOLECULES AT THE HIGHER INVERSION LEVEL
U : MOLECULES AT THE UPPER INVERSION LEVEL

FIG. 1·3 STATE SELECTION AND FOCUSING OF MOLECULES INTO THE RESONATOR.

$$E_s = \frac{\mu K M_J}{J(J+1)}$$

Molecules at the higher energy levels are then attracted towards the state selector axis and if their velocity is not large they are focused into the resonator. Molecules at the lower inversion level are deflected towards the state selector electrodes and removed by the diffusion pumps.

From Eqn. 1.3 it can easily be seen that for small Stark fields ($E_s \ll h\nu$) the focusing force is proportional to M_J^2. Therefore, in practice only molecules with a dipole moment orientated along the beam axis are sorted. This creates an emissive anisotropy whose high gain oblique axis lies along the beam axis. For higher state selection voltages (and thus Stark fields) the anisotropy is somehow weakened as the focusing force becomes proportional to M_J.

1.3 THE AMMONIA ROTATIONAL SPECTRA

1.3.1 The Rotational Inversion

The Hamiltonian representing the rotation of a symmetric-top molecule can be written as (Gordy and Cook, 1970)

$$H_r = \frac{P^2}{2I_b} + \tfrac{1}{2}\left[1/I_z - 1/I_b\right] P_z^2 \qquad 1.4$$

where $\underline{P}$ is the angular momentum of the molecule with respect to its centre of mass and P_z its projection along the axis of symmetry. I_z is the molecule moment of inertia along the axis of symmetry and I_b is the moment of inertia along an axis perpendicular to Z and passes through the centre of mass. The eigenstates of H_r can be found by expressing the operators P^2 and P_z in the laboratory reference frame coordinates. It turns out that these operators are diagonalized by a set of wave-

functions characterized by the two integers J, K where K is the projection of $\underline{J}$ along the molecule's axis of symmetry. Let these wave-functions be written as "ket" vectors $\langle J,K|$. It is easy to show that

$$\langle JK|P^2|JK\rangle = \hbar^2 J(J+1) \qquad 1.5(a)$$

$$\langle JK|P_z|JK\rangle = \hbar K \qquad 1.5(b)$$

where $\hbar = h/2\pi$. The rotation energies can then be found by direct substitution in Eqn. 1.4 yielding

$$E_{JK} = \langle JK|H_r|JK\rangle = hBJ(J+1) - h(A-B)K^2$$

where for ammonia A = 189GHz and B = 298GHz and with the selection rules $\Delta J = 0, \pm 1$; $\Delta K = 0, \pm 1$. Therefore the frequency of the transition $J \longrightarrow J+1$ is $\upsilon_{JK} = 2B(J+1)$ which lies in the submillimeter wavelength range.

Like other symmetric-top molecules of the type XY_3, ammonia has a fine structure caused by the inversion splitting of the rotational levels. This originates from the fact that the X atom moves through the Y_3 plane to achieve identical but inverted pyramidal configuration. The potential energy of the NH_3 molecule as a function of the nitrogen atom's distance from the H_3 plane is shown in Fig. 1.4 where the wave-functions ψ_+ and ψ_- correspond to the upper and lower inversion states respectively. If the height of the potential barrier between the two equilibrium positions of the nitrogen atom was infinite the molecule would only execute vibrations in the potential valley on either side of the potential barrier and the eigenstates $\psi_\pm$ would be degenerate. However, although the inversion barrier is higher than the lowest vibration state v = 0 it is quantum mechanically possible for the nitrogen atom to achieve inversion through "tunnelling" giving rise to

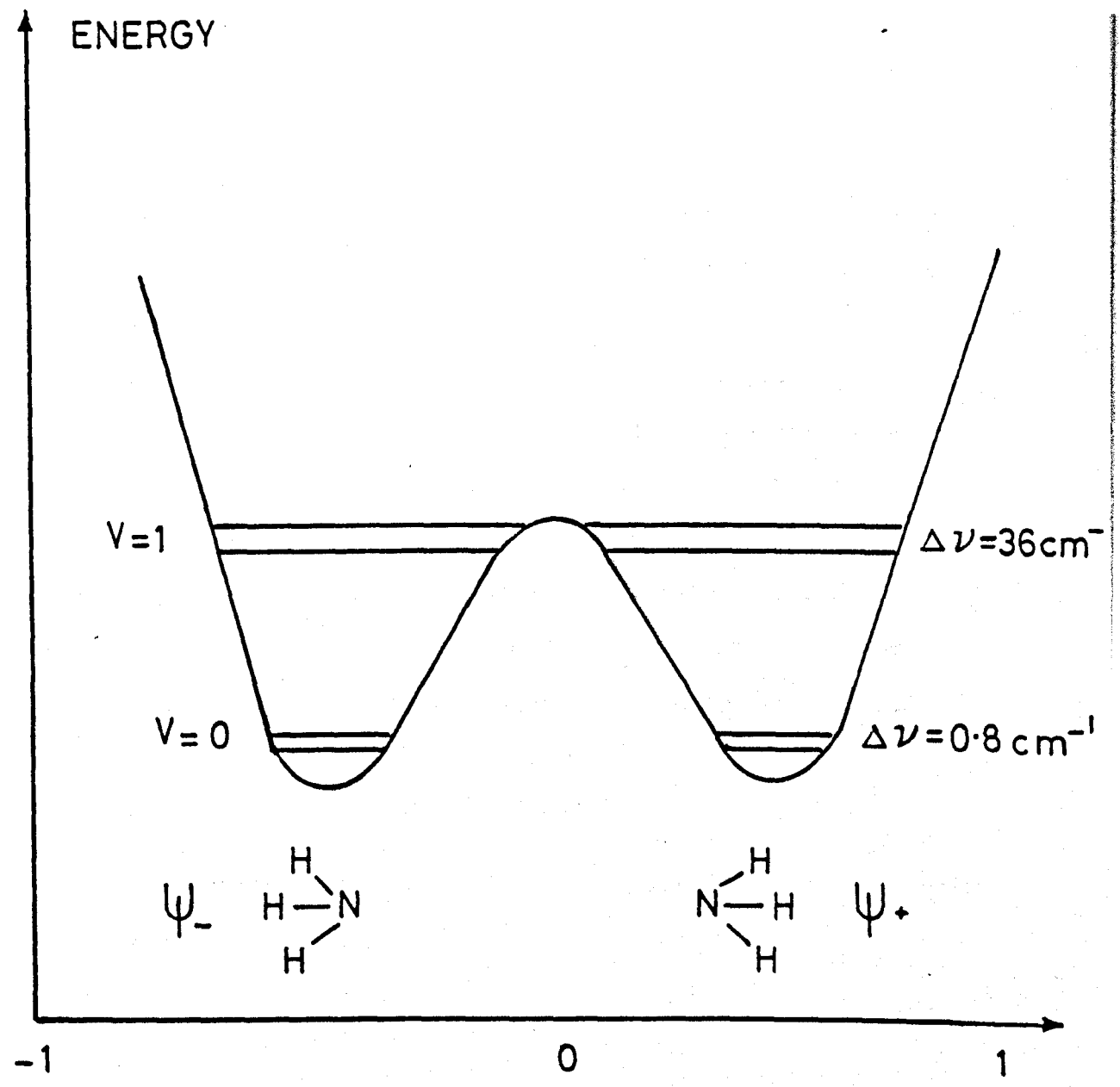

FIG. 1·4 POTENTIAL ENERGY OF THE NH_3 INVERSION

the strong inversion lines at ~ 24GHz.

Expressions for the dependence of the inversion frequencies on the rotational quantum number are given by Oraevskii (1964) and Schnabel et al. (1965). The spectral lines of ammonia in this region are relatively intense owing to the large dipole moment of the molecule ($\mu = 1.47 \times 10^{-8}$CGS.). It was also shown that the transition matrix element is maximized when J = K since the latter is proportional to K and that the intensity of the lines having lower values of J,K increases with low temperature while lines having higher values of J,K would decrease. A plot of the relative amplitude of the absorption spectrum for the first few inversion lines of ammonia is shown is Fig. 1.5.

1.3.2 The Hyperfine Structure of Ammonia.

The interaction Hamiltonian of the hyperfine structure of ammonia can be written as

$$H = H_q + H_{nj} + H_{hj} + H_{nh} + H_h \qquad 1.6$$

where

H_q: The nitrogen quadrupole interaction.

H_{nj}: The magnetic interaction of the nitrogen spin with the molecular rotation.

H_{hj}: The magnetic interaction of the resultant hydrogens spin with the molecular rotation.

H_{nh}: The hydrogen-nitrogen spin-spin interaction.

H_h: The hydrogen-hydrogen spin-spin interaction.

The splitting of the inversion energy levels due to the hyperfine interaction can be explained by the way the angular momentum of the different interactions couple with each other. The coupling

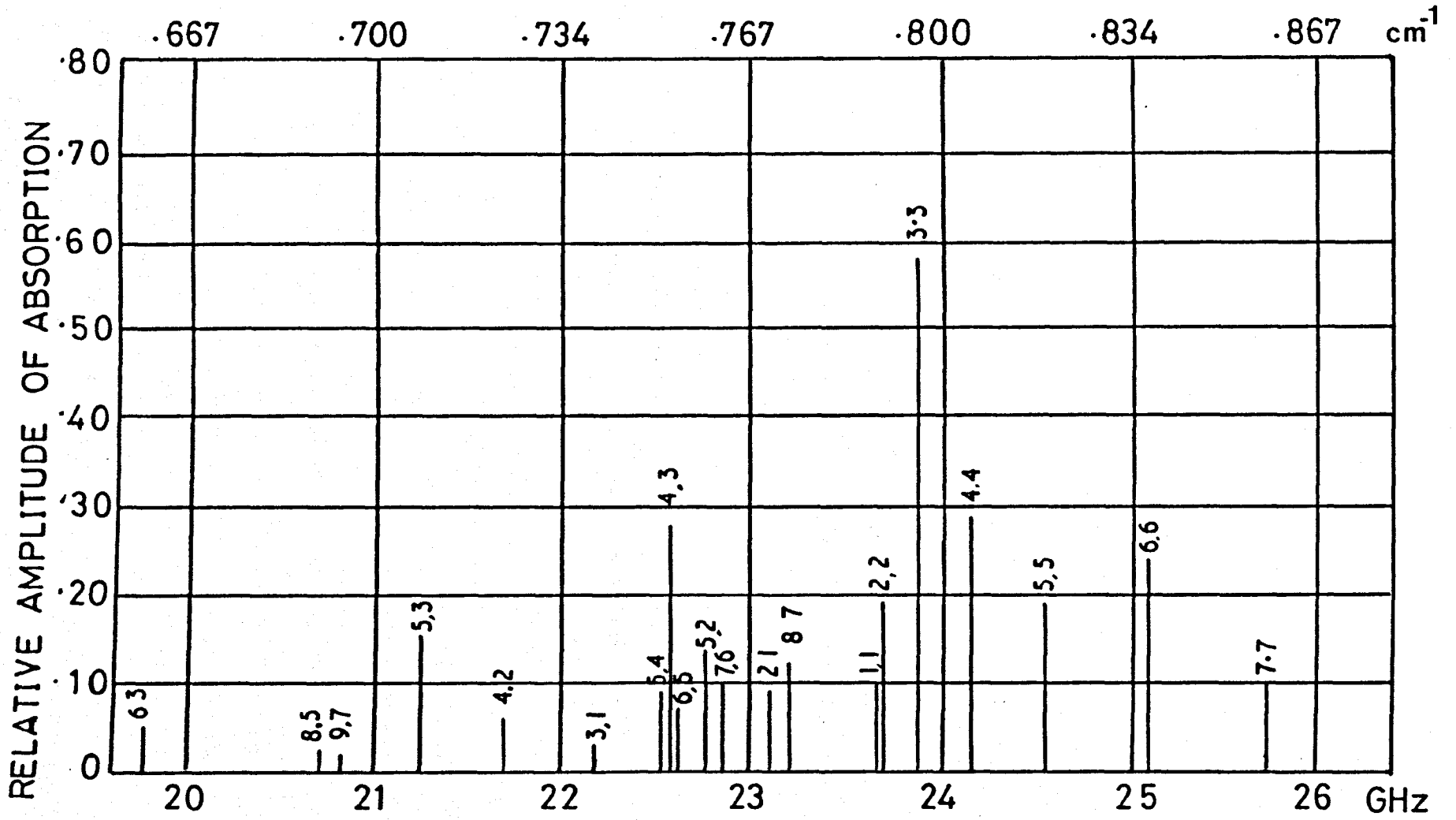

FIG. 1·5 AMMONIA INVERSION SPECTRUM. TEMPERATURE 195 K, PRESSURE 5×10^{-2} MM H_g (AFTER GOOD, 1946)

scheme in the molecular frame suggested by Van Vleck (1953) is as follows: Since the quadrupole interaction energy of the nitrogen nucleus is much stronger than the magnetic interaction energy of the hydrogen atoms, the nitrogen spin I_N is first coupled to J to produce the good quantum number F_1 defined as

$$\underline{F}_1 = \underline{J} + \underline{I}_N$$

For the inversion lines J = K = 1,2,3 of ammonia $I_N = 1$ and thus each inversion level is split into $2I_N + 1 = 3$ sublevels, (F_1 = 3,2,1 for J = 2 and F_1 = 4,3,2 for J = 3).

The protons spins are first added vectorially together in the molecular frame (Fig. 1.6) to give a resultant $\underline{I}_H = \underline{I}_1 + \underline{I}_2 + \underline{I}_3$, which in turn is coupled to F_1 to give the total angular momentum F given by

$$\underline{F} = \underline{F}_1 + \underline{I}_H$$

where $I_H = \frac{1}{2}$ for J = K = 1,2 and 3/2 for J = K = 3. Therefore in the case of the inversion line J = K = 2, each quadrupole state splits into two levels corresponding to the different F-numbers. A schematic diagram of the hyperfine levels of the inversion line J = K = 2 is shown in Fig. 1.7.

The eigenstates of the Hamiltonian given by Eqn. 1.6 were calculated by Gordon (1955) based on the theoretical analysis and the experimental study of Gunther-Mhor et al. (1954A; 1954B). The calculations were carried out by the conventional method using Condon and Shortley (1951) matrix elements. However, the resulting expressions for the transition frequencies and their intensity were very lengthy and the actual computation of their values was extremely inconvenient. The 3n-j (n = 1,2,3,...) method developed by Edmonds (1960) on the

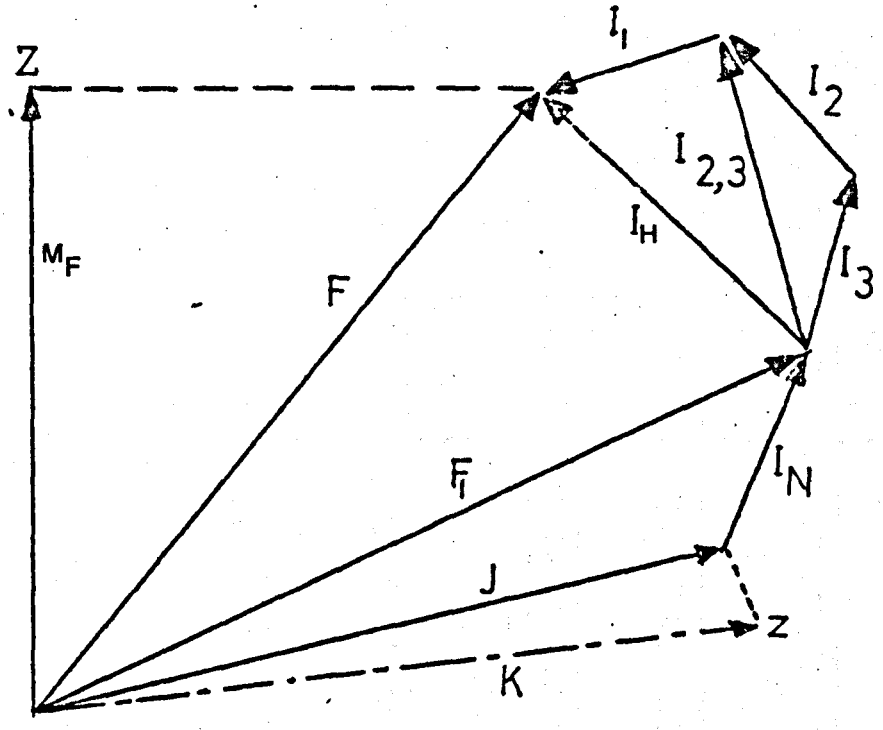

FIG. 1.6 VAN VLECK MOLECULAR COUPLING SCHEME FOR NH_3 REFERED TO THE LABORATORY Z-AXIS.

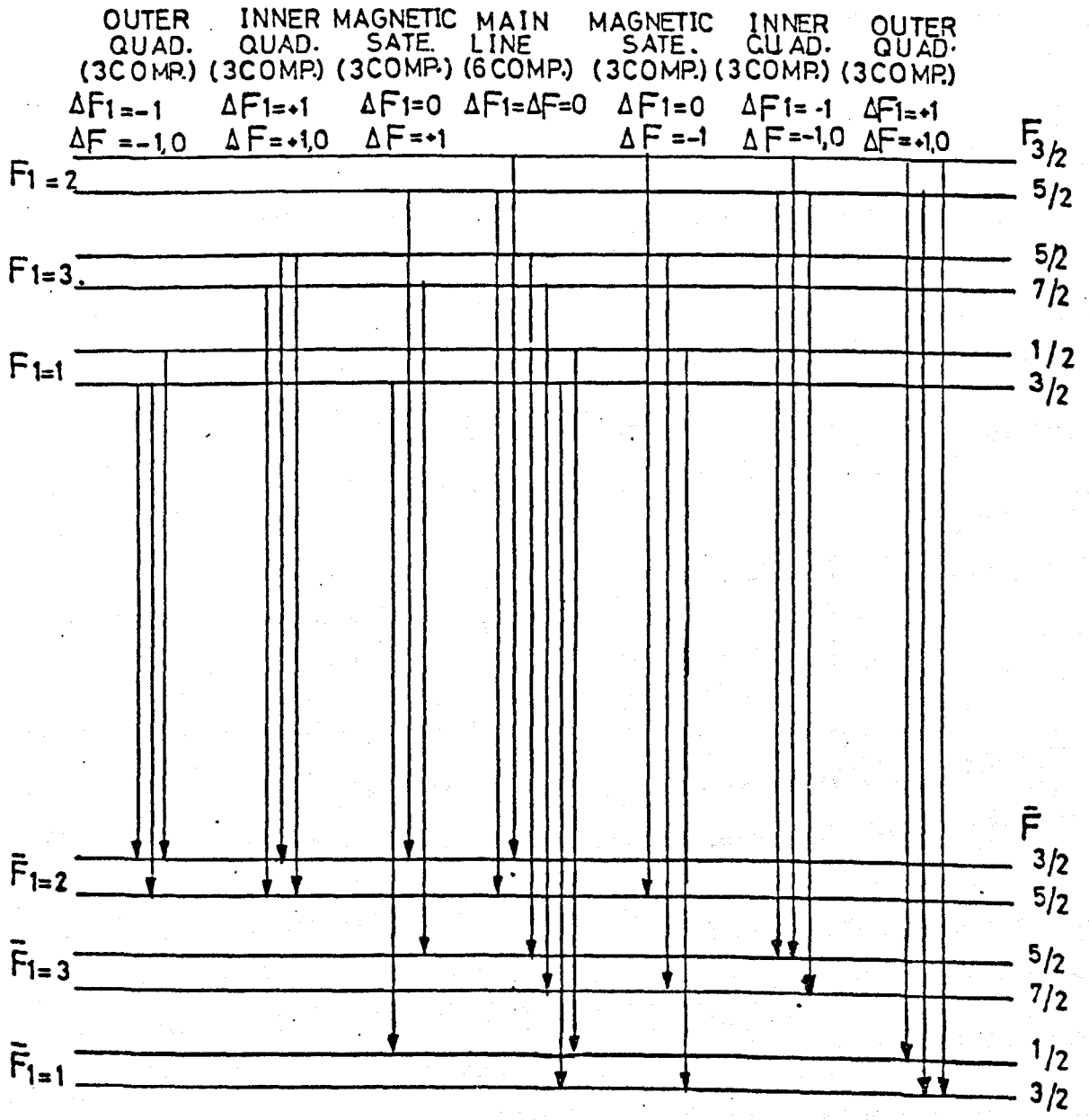

Fig.1.7. Schematic diagram of energy levels for J=K=2 inversion line of ammonia molecule.

other hand helps to simplify the mathematical formulation a great deal. This approach which is suitable for numerical computation in particular was employed by Kukolich (1967) to measure the inversion hyperfine structure of ammonia. The method becomes even more appropriate when the Stark splitting of the hyperfine sub-levels is considered.

Let the method be illustrated for the inversion lines $J = K = 2,3$ of ammonia. If the energy is written in the form

$$W_{JKF_1F} = \sum_{n=1}^{5} W_n$$

where W_n correspond to the n'th term in Eqn. 1.6. Following Kukolich's calculation, the quadrupole energy term is given by

$$W_1 = (-1)^{l_1} (15/8)^{\frac{1}{2}} C_Q (2J+1) \begin{pmatrix} J & 2 & J \\ -K & 0 & K \end{pmatrix} \begin{Bmatrix} F_1 & 1 & J \\ 2 & J & 1 \end{Bmatrix}$$

where $l_1 = J + 1 + F_1$ and the last two products are the Wigner 3-j and 6-j symbols respectively (Edmonds, 1960). In the above expression the value $I_N = 1$ was substituted. The quadrupole coupling coefficient is given by

$$C_Q = 4089 \left\{ 1 + 7.7 \times 10^{-5} [\, J(J+1) + K^2 \,] \right\} \pm 1.5\text{KHz}$$

and tables for the calculations of Wigner symbols can be found in Edmonds.

The nitrogen spin coupling term with $\underline{J}$ is given by Kukolich as

$$W_2 = (-1)^{l_1} \; C_{nj} \left[6J(J+1)\,(2J+1) \right]^{\frac{1}{2}} \begin{Bmatrix} F_1 & 1 & J \\ 1 & J & 1 \end{Bmatrix}$$

where $C_{nj} = 6.7409\text{KHz}$ for $J = K = 2$ and 6.7326KHz for $J = K = 3$.

The hydrogen's interaction term with the molecular rotation can be written in the form

$$W_3 = (-1)^{l_2} C'_{hj} \left[J(J+1)\,(2J+1) \right]^{\frac{1}{2}} (2F_1+1) \times$$

$$\times \begin{Bmatrix} J & F_1 & 1 \\ F_1 & J & 1 \end{Bmatrix} \begin{Bmatrix} F & I_H & F_1 \\ 1 & F_1 & I_H \end{Bmatrix}$$

The strength of the interaction is represented by the coupling constant

$$C'_{hj} = C_{hj} \left[I_H(I_H+1)\,(2I_H+1) \right]^{\frac{1}{2}}$$

where $C_{hj} = -18.6181$KHz for $J = K = 2$ and -18.6976KHz for $J = K = 3$, and $l_2 = 2 + J + I_H + F + 2F_1$.

It can be shown that the Hamiltonian representing the hydrogen-nitrogen spin-spin interaction for $K \neq 1$ is given by (Gordon, 1955; Kuckolich, 1967)

$$H_{hn} = \sqrt{6}\, D_1 T(1, I_H)$$

where D_1 is the interaction coupling constant and T is a second-rank tensor. The interaction energy is then given by

$$W_4 = (-1)^{l_3} C_{hn}(2J+1)\,(2F_1+1)$$

$$\begin{pmatrix} J & 2 & J \\ -K & 0 & K \end{pmatrix} \begin{Bmatrix} I_H & F_1 & F \\ F_1 & I_H & 1 \end{Bmatrix} \begin{Bmatrix} F_1 & F_1 & 1 \\ 1 & 1 & 1 \\ J & J & 2 \end{Bmatrix}$$

where the last product is the 9j-symbol, $l_3 = F + I_H + F_1 + 1$ and

$$C_{hn} = -\sqrt{30}\, D'_1$$

where

$$D_1' = D_1 I_H (I_H + 1)(2I_H + 1)$$

and $D_1 = 2.3854$KHz for $J = K = 2$ and 2.4881KHz for $J = K = 3$.

Finally the mutual interaction energy of the hydrogens spins is written as

$$W_5 = (-1)^{l_4} C_h (2J + 1)(2F_1 + 1) \times \begin{pmatrix} J & 2 & J \\ -K & 0 & K \end{pmatrix} \begin{Bmatrix} F_1 & J & 1 \\ J & F_1 & 2 \end{Bmatrix} \begin{Bmatrix} I_H & F_1 & F \\ F_1 & I_H & 2 \end{Bmatrix}$$

where $l_4 = J + 1 + 2F_1 + F + 3I_H$ and

$$C_h = -\frac{1}{4} D_3 \left[(2I_H - 1)(I_H)(I_H + 1)(2I_H + 1)(2I_H + 3)\right]^{\frac{1}{2}}$$

and $D_3 = 27.1734$KHz.

The theoretical expression for the transition's intensity was calculated by Thaddeus et al. (1964) and can be written in Edmonds formalism as

$$I = (2F_1' + 1)(2F_1 + 1)(2F' + 1)(2F + 1) \times \left[\begin{Bmatrix} J & F_1' & 1 \\ F_1 & J & 1 \end{Bmatrix} \begin{Bmatrix} F_1' & F' & I_H \\ F & F_1 & 1 \end{Bmatrix} \right]^2$$

for the transition $(F_1' \; F') \longrightarrow (F_1 \; F)$. In Fig. 1.8 the calculated relative intensities and frequencies for the quadrupole satellites of the inversion line $J = K = 2$ are shown. The intensity was in fact averaged on the low and the high frequency sides since the intensity of the latter is stronger due to the adiabatic focusing effects. The relative intensity of the high frequency side satellite components are

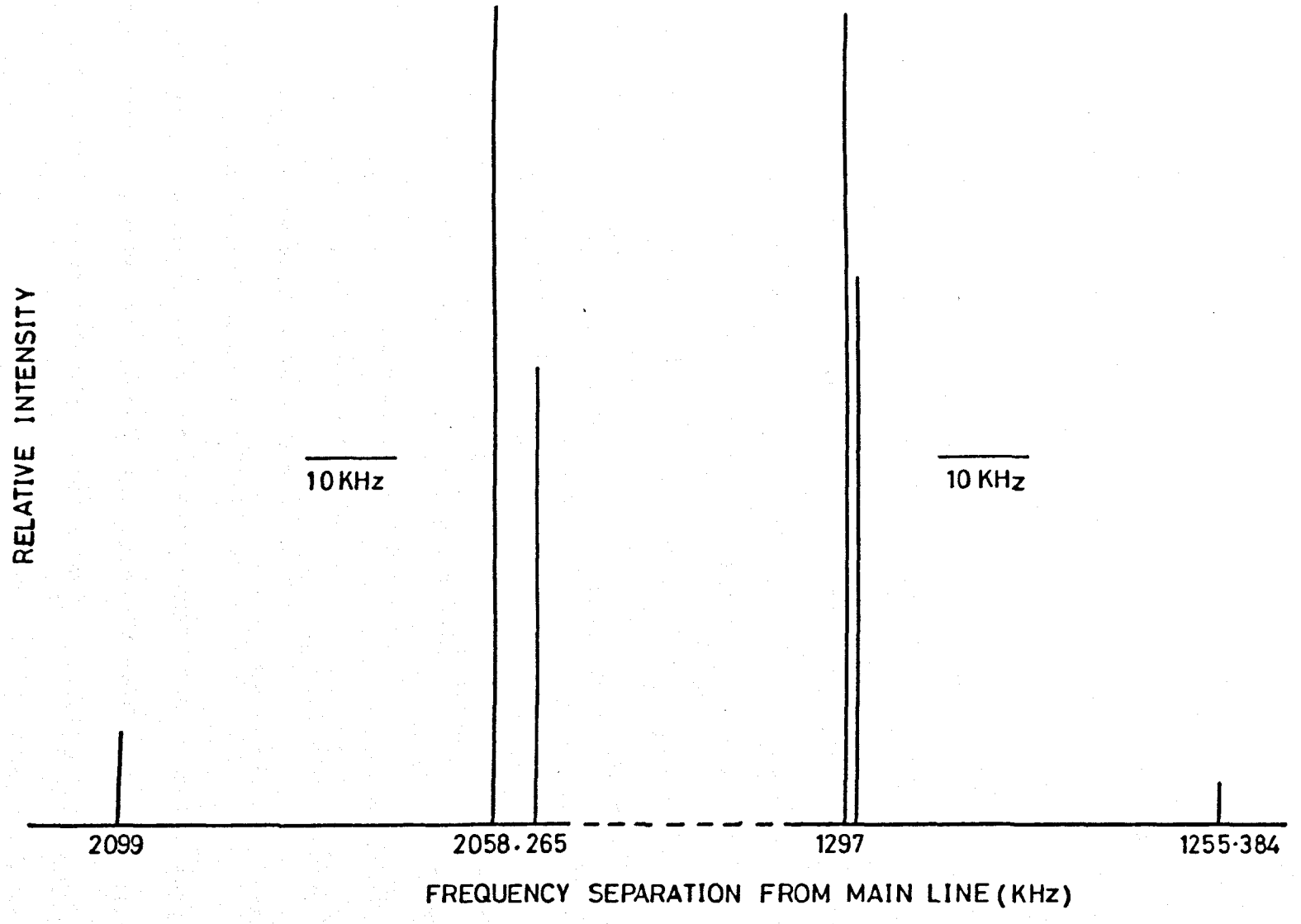

FIG. 18 SPECTRUM OF THE LOW FREQUENCY QUADRUPOLE COMPONENTS OF $J = K = 2$ INVERSION LINE OF AMMONIA.

thus assumed to be approximately equal to those given in Fig. 1.8.

1.4 THE MASER APPLICATIONS

1.4.1 As an Amplifier

The molecular beam maser acts as a sensitive high gain amplifier when it is operated near the threshold of oscillation. Possible noise sources in a maser amplifier are

(a) Shot noise.

(b) Thermal noise and quantum fluctuations.

As for the shot noise, since the maser media particles are uncharged, the only contribution comes from the random fluctuations in the number of particles in the beam. The latter was shown to be negligible in comparison with thermal noise (Shimoda et al., 1956).

Thermal noise is coupled into the maser output through two main sources. First there is the random noise due to cavity losses and second, noise is radiated from waveguides into the cavity through the coupling holes. Together with quantum fluctuations (Shimoda et al., 1957) this results in a noise figure which is comparable to the detection scheme noise. However it should be emphasized that this type of noise decreases very rapidly as the maser approaches its threshold of oscillation (Smith and Lainé, 1967). When the maser is operated much below threshold on the other hand, random fluctuations are quite detectable and in chapter 5 a method for detection of weak spectral lines is introduced in order to minimize such noise.

The internal electric field gain of the maser amplifier can be defined as

$$g = \frac{E_i + E_o}{E_i} \qquad 1.7$$

where E_i and E_o are the strength of the input and the output microwave electric fields respectively. Substituting the appropriate expressions in Eqn. 1.7 yields (Smart, 1973)

$$g = \frac{1}{1 - \eta} \qquad 1.8$$

where

$$\eta = \frac{2\pi L \mu_o}{v} \left(\frac{QN}{Vh} \right)^{\frac{1}{2}}$$

where L is the cavity length, V its volume and Q its quality factor. N is the number of molecules in the upper state, v is the average molecular velocity and μ_o is the permanent dipole moment. The power gain of a maser employing a transmission cavity is given by

$$G = \frac{4 \beta_1 \beta_2 g^2}{(1 + \beta_1 + \beta_2)^2} \qquad 1.9$$

where β_1 and β_2 are the coupling coefficients of the input and the output coupling holes respectively. The maser amplifier characteristics were experimentally investigated by Smart and others. Stable gains in excess of 50db were reported, for an ammonia beam maser (Collier and Wilmshurst, 1966). Measurement obtained by Smart showed a reasonable agreement between theory and experiment. In the exitation range of state selection voltages from 10 to 14.5KV a gain of 10 - 30db was measured.

Although the maser can be employed as a high stability amplifier, its range of usefulness is somewhat limited. First, this is because of the low level of power at which the maser saturates. A

typical saturation output power of an ammonia maser is about 10^{-9}W. Thus it is only for such low input power or less, that linear power amplification can be obtained. Second, the bandwidth of such an amplifier is dictated by the average time of flight of molecules through the maser cavity. For a typical ammonia maser this is about 7KHz. Moreover, high gain (and low noise) is obtained near oscillation. In this case the bandwidth becomes considerably smaller (Gordon, Zeiger and Townes, 1954). For example a bandwidth as narrow as 300Hz was measured with a gain of 20db (Helmer, 1957). In addition to that the maser frequency is restricted by the molecular transition and thus the amplifier is essentially untunable.

One of the earliest applications of the maser amplifier in practical systems was as a high-gain narrow bandwidth amplifier, between a maser whose noise figure was to be measured and a balanced crystal detector (Gordon and White, 1958). A particularly interesting application of the ammonia maser amplifier was its employment as a pre-amplifier to improve the signal-to-noise ratio of an electron spin resonance spectrometer (Gambling and Wilmshurst, 1964; Collier and Wilmshurst, 1966).

1.4.2 As a Spectrometer

The idea of improving a spectrometer's resolution by using a beam of molecules rather than gases in bulk was known to spectroscopists before the discovery of maser. It was already realized that molecules that move perpendicularly to the direction of propagation of an interacting wave reduce their Doppler broadening to a negligible level. The obvious difficulty was that the use of such a beam inevitably reduced the spectrometer sensitivity, because it limited the beam flux entering the region of interaction. The sensitivity of an absorption

spectrometer employing a molecular beam maser was very much reduced in comparison to the conventional bulk gas spectrometer owing to the reduction in the density of molecules in the detection cell, in the process of the beam formation.

The application of maser techniques on the other hand facilitated the enhancement of the molecular beam spectrometer sensitivity by more than two order of magnitude at microwave frequencies. This can be shown with the aid of Eqn. 1.1. Since at the microwave frequency $h\nu/kT \sim 10^{-3}$ it follows that

$$N_b/N_a \approx 1-h\nu/kT$$

and

$$N_a - N_b \approx N_b(h\nu/kT) \equiv N$$

where sensitivity can be assumed to be proportional to the population excess N. If now state selection is employed so that molecules at the lower energy states are removed ($N_a \sim 0$) then the population excess becomes $N' = N_b$. The sensitivity is therefore enhanced by a factor of $N'/N = kT/h\nu$. At $\nu \sim 24$GHz this factor is about 250.

Although sensitivity remained the main obstacle in its application to spectroscopy, the molecular beam maser was used to investigate the spectrum of many molecules on account of its high resolution. A reference should be made to the molecular beam maser system that employs Ramsey's separated two cavity scheme. Kukolich employed the Ramsey-type maser to measure the hyperfine structure of NH_3 with a resolution of about 350Hz. This tremendous resolution is about 200 times better than the Doppler limited absorption cell type of microwave spectrometer. The general advance in instrumental techniques

like digital signal averaging together with the use of tunable open resonators allowed the spectrum of a wide range of molecules to be investigated, using molecular beam maser techniques. A comprehensive list of such molecules is given by Lainé (1975).

Further enhancement of maser spectrometer sensitivity was recently proposed by using the Fabry-Perot type maser (Lainé and Yassin, 1980; see also Ch. 6) and also by detection of weak spectral lines via the low-noise maser oscillation (Yassin and Lainé, 1981; see Ch. 5).

1.4.3 As an Oscillator

If the power emitted from the molecular beam exceeds all losses from the cavity, the maser system becomes self-excited and oscillation builds up from noise within the cavity to a level determined by saturation effects. In such case the maser can be regarded as a source of a highly stable and coherent microwave radiation. The minimum molecular flux required to sustain oscillation is given by (Shimoda et al., 1956)

$$n_{th} = \frac{h\nu^2 A}{4\pi^2 \mu_{12}^2 LQ}$$

where μ_{12} is the matrix element between the two states for the component of the dipole moment along the direction of the microwave electric field and A is the cavity cross section. A list of molecules with which maser oscillation was obtained is given by Lainé (1975) and perhaps the most famous of them is the NH_3 molecule with its strong inversion line at about 23.87GHz.

Much of the intensive work carried with early masers was directed towards its application as a frequency standard. Unfortunately

the high stability of the maser oscillation was degraded by the well known pulling effects caused mainly by cavity detuning and the variation of the amplitude of oscillation during operation. The oscillation frequency as a function of the maser parameters can be written as (Gordon et al., 1955; Shimoda et al., 1956)

$$\nu = \nu_0 + \frac{Q_c}{Q_m} (\nu - \nu_0) f(\theta)$$

where Q_c and Q_m are the quality factors associated with the cavity and molecules respectively (Shimoda, 1960) and $f(\theta)$ is a function of the order of unity, dependent on the amplitude of oscillation. It is shown in chapter 4 of the present work that $f(\theta)$ depends on a variety of parameters including gas pressure, state selection voltage, stray electric and magnetic fields and background pressure. Therefore it may be expected that the most practical method for stabilizing the oscillation frequency is to set the cavity resonance frequency precisely to the molecular transition frequency. Having achieved that, all variations in Q_c, Q_m and $f(\theta)$ become unimportant as $\nu \rightarrow \nu_0$. Methods of cavity accurate tuning included the modulation of Q_m or $f(\theta)$ and a point of cavity tuning was sought where the frequency shift was at a minimum. Q_m modulation could be obtained by the use of Zeeman field applied to the cavity (Hellwig, 1966) although for open resonators the use of a Stark field must also be possible. Modulation of other quantities like gas pressure (Nikitin and Oraevskii, 1962) and background pressure (Strakhovskii and Tatarenkov, 1964) were also employed.

Although frequency stability is influenced by other complicated effects like unresolved hyperfine structure of the transition involved, the molecular beam maser was eventually employed as a frequency standard both in laboratories and in a portable form.

Hellwig (1966) used the inversion line J = 3, K = 2 of ammonia to obtain a stability of 1 part in 10^{11} by the use of sufficiently low beam intensities and a localized magnetic field for cavity tuning. Portable ammonia masers with secondary frequency standard capability and a frequency reproducibility of several parts on 10^{10} were also introduced (Krupnov et al., 1961; Taylor, 1963). All sealed-off masers were based essentially on cryogenic pumping of ammonia to avoid the use of bulky vacuum pumps. A portable maser was also operated in artificial Earth satellite in the vacuum of space and thus without the use of liquid nitrogen for evacuation (Basov et al., 1967). The use of opposed beams and a thermostated Invar cavity produced a relative stability of 1 part in 10^{11} during a single run of measurements. It should be added that such a high stability was obtained under the intense vibrations of launch conditions and that measurements were made via a two-way Earth satellite radio link which itself could introduce phase fluctuations as propagation conditions varied.

CHAPTER 2

SOME ASPECTS OF THE THEORY OF MICROWAVE OPEN RESONATORS

2.1 GENERAL REVIEW

The Fabry-Perot interferometer was first introduced as a resonator at infra-red and optical frequencies by Prokhorov (1958) and by Schawlow and Townes (1958). Subsequently, this type of resonator was employed in a wide variety of areas including wavemeters (Zimmerer, 1962), molecular beam masers (Barchukov et al., 1963; Krupnov and Skvortsov, 1964; Lainē and Smart, 1971; Al-Jumaily, 1979) and in lasers (Javan et al., 1961).

A cavity is regarded to be suitable for molecular beam maser applications if it fulfills the following requirements:

(1) Long time of interaction.

(2) High Q-value.

(3) Wide range of tunability.

In a flat mirror Fabry-Perot type of resonator the stored electromagnetic waves are reflected back and forth in the resonator while both the electric and the magnetic vectors remain essentially parallel to the mirror's surface. The propagation vector is therefore perpendicular to the molecular beam direction. Consequently Doppler broadening is expected to be very small. Moreover, during operation of the maser the pressure in the main chamber is reduced to a level where the mean free path of molecules is of the order of the system dimensions, collision broadening is thus practically negligible. Since the spontaneous decay rate at the microwave frequencies is very low,

the remaining contributions to the line-width of a molecular beam maser signal comes from the finite interaction time of molecules with the stimulating electromagnetic field and saturation effects. By reducing the level of input power, the latter can be made negligible and thus the line-width can be written as

$$\Delta\nu \approx 1.2\ v/L_u \qquad 2.1$$

where L_u is the "useful" extent of the resonator along the beam axis (that is, for $L \leq L_u$ the microwave field inside the cavity is strong enough to induce transitions) and v is the molecule's average velocity. Therefore to obtain narrow spectral lines the useful extent of the resonator along the beam axis must be made as long as possible.

The quality factor of a resonant cavity is defined as

$$Q = 2\pi\nu_0 \frac{\text{Energy stored}}{\text{Energy lost per second}}$$

where ν_0 is the cavity resonance frequency. It follows immediately that

$$W(t) = W_o \exp(-\omega_o t/Q) \qquad 2.2$$

where $\omega_0 = 2\pi\nu_0$, W(t) is the remaining energy after a time t and W_o is the initial energy launched into the resonator at t = 0. It will be shown throughout the present work that for both spectroscopic sensitivity and low oscillation threshold high Q-values are necessary.

A tunable resonator is one whose resonance frequency can be varied, preferably in a simple way. Quite often, spectral lines are not simple singlets but are complicated by the hyperfine structure. To investigate such a spectrum a certain range of tunability is of great practical importance. Furthermore, if the frequency of the spectral line in question is unknown, a wide range of tunability

becomes an ultimate necessity.

Early masers were operated with closed cylindrical cavities. This type was favoured, firstly, because the spectrum of the maser medium employed was known and secondly in order to avoid radiation spill-over due to diffraction from an open ended resonator. Later, as the maser research was intensified it was found that closed cavities suffered several drawbacks.

Apart from having a rather narrow range of tunability they tend to have a low Q-value in the mm-wave spectral region, which gets worse with an increase in frequency. Also, their small diameter increases the difficulty of focusing the molecular beam into the small entrance area. In addition, pressure build-up in the cavity limits their useful length and makes the use of intense beams impractical.

The first Fabry-Perot type masers employed disc mirrors (Barchukov et al.,1963). It had the obvious advantage of wide tunability range and the possibility of the application of a uniform Stark field along the molecule's trajectory. Using fast pumps, much more intense beams could be introduced into it, through the use of nozzles. When used in conjunction with the ladder-type state selector it was found that such a resonator was suitable for both spectroscopic and oscillation application (Lainé and Smart, 1971). However it was also noticed that the Q-value of a typical disc resonator at its lowest order mode is much less than that of the commonly used TM_{010} cylindrical cavity at the same resonance frequency. For example an open resonator which was constructed of copper mirrors with a disc diameter of 15cm gave a quality factor of Q = 2500 (Smart, 1973) while values of about Q = 8000 were measured for a cylindrical cavity 12cm long at about 24GHz (Maroof and Lainé, 1976). While a single beam maser operated

with the above mentioned disc resonator could not oscillate at the main inversion line J = K = 1 of ammonia, a similar maser system oscillated at four hyperfine component frequencies of the same inversion line when operated with the above mentioned cylindrical cavity.

In addition to their low Q values, disc resonators are well known to be very sensitive to the adjustment of mirror parallelism. Bringing the cavity into resonance proves quite often to be very laborious.

To avoid such difficulties, different resonator geometries were suggested. These included the confocal (Boyd and Gordon, 1961), semiconfocal (Marcuse, 1961; Valentin, 1978; De Lucia and Gordy, 1969) and conical resonators (Lainé and Smart, 1971). All of them have in common the property of high Q values due to negligible diffraction losses and the advantage of ease of adjustment. Nevertheless the microwave electric field of such resonators would normally have more than a single maximum along the longitudinal resonator axis. As a result, nodal plane crossings for molecules arise which yields a complicated maser spectral line and thus a loss in resolution.

A type of cavity which has the good feature of tunability in common with the disc type Fabry-Perot and still has very small diffraction losses, is the flat roof-top resonator (di Francia, 1965). One of the resonator mirrors is a flat rectangular plate while the other is composed of two rectangular planes at a quasi-flat dihedral angle, called the roof angle. This type, which will be considered in detail in the following chapter, can be set so that there are no nodal planes along its longitudinal axis. Its insensitivity to misalignment and the fact that its microwave field distribution is extended along its axis of symmetry, (which is also the beam axis) makes it ideal for molecular beam maser spectroscopy. Furthermore ,the strong anisotropy

which results from its geometry may be expected to remove the mode polarization degeneracy known in the disc resonator. Such a property could prove advantageous in some of the maser oscillator applications where frequency stability is needed (see chapter 6).

In order to understand the shape of the spectroscopic signal produced by a maser employing any of the above mentioned resonators and the conditions for oscillation, the spatial distribution and the resonance frequency of the mode should be known. Such modes can be characterized by two mathematical quantities:

(1) The complex electric (or magnetic) field distribution from which the spatial intensity and phase distributions along the mirror's surface can be deduced.

(2) The propagation constant which gives both the quality factor and the resonance frequency.

To calculate these quantities, the Maxwell equations should be solved in the space enclosed by the cavity walls with the appropriate boundary conditions. In the case of a closed cavity this task is relatively simple since for regular symmetries the boundary conditions on the metallic walls are well defined and can easily be substituted into the equations yielding an exact solution. However for open resonators the problem is complicated by diffraction at the open ends and only approximate solutions can be derived.

Approximation methods for tackling diffraction problems at optical frequencies are well known, and all to be done was to formulate them in such a way that they could be applied to open resonators. In a comprehensive publication, Fox and Li (1961) proved the existence of resonant modes for rectangular, circular and confocal Fabry-Perot resonators at optical frequencies. Using the Huygens-Fresnel principle

with some simplifications, they were able to compute numerically the transverse intensity distribution, phase shift, resonance frequency and diffraction losses for a typical laser cavity. Later, the subject was thoroughly investigated and a long list of articles appeared which dealt with the theory of open resonators (Li and Zucher, 1967). An interesting approach was suggested by Vainshtein (1963). It regarded the open resonator modes as identical to those of an open ended waveguide at cut off frequencies. By calculation of the diffraction at the open ends it was possible to find analytical expressions for the field distribution and the propagation constant, although at the expense of losing the Fresnel-zone ripples which appear in Fox and Li curves.

It should be emphasized however, that all these approximations took advantage amongst other factors, of the fact that at optical frequencies the wavelength is much smaller than the cavity dimensions. This approximation which simplifies the calculation a great deal does not hold at the microwave frequencies, especially for maser cavities where the separation of the mirrors is comparable to the wavelength. To overcome that, a further development of the diffraction theory at a microwave frequency was necessary. Noble (1958) used the so called Wiener-Hopf technique (Mittra and Lee, 1971) to find a formula for the diffraction of a scalar field at the end of a semi-infinite parallel-plate waveguide. Using this result the reflection coefficient at the end of a waveguide near cut off was calculated over the complete frequency spectrum (Bates, 1970). It could be interesting to know whether this theory is applicable to a resonator possessing circular symmetry.

Finally it should be made clear that all theories which will be considered in this chapter employ the scalar theory of diffraction. The microwave electric field is thus assumed to be linearly polarized

along a fixed direction. As a result the resonator will be represented by scalar equations. The effect of polarization will be considered in chapter 6.

2.2 THE RESONATOR BASIC PARAMETERS

2.2.1 Mode Designation

The fact that the microwave power is stored in the cavity in the form of standing waves allows some degree of freedom in the mode designation convention. For example, in the Fox and Li iteration procedure the electromagnetic wave which is reflected back and forth by the two identical reflectors is regarded as being equivalent to a wave which is travelling along the resonator axis and diffracted by a series of identical apertures. Since in a flat mirror resonator both the electric and the magnetic field are everywhere tranverse to the resonator axis, the modes obtained in this way are clearly TEM modes. If on the other hand, the resonator is considered as a waveguide section then the direction of propagation is usually taken to be parallel to the resonator's mirrors (Vainshtein, 1963). The mode in this convention is thus a TE or a TM mode.

In the present work the two systems of mode designation will be used. Let m be the number of maxima that the electric field E_x makes with the X-axis and n and q be respectively the number of maxima along the Y and Z axes of a cartesian set of coordinates whose Z-axis is parallel to the resonator axis. If such a mode is associated with a rectangular Fabry-Perot resonator it can be denoted by $TEM_{m-1,n-1,q-1}$; $m,n,q=1,2,3,\ldots$. The lowest order transverse mode is then TEM_{00q-1} and the mode which is usually used for maser work is TEM_{000}. On the other hand if diffraction from a semi-infinite rectangular waveguide is

discussed then transverse modes are denoted by $TE_{m-1,0,q-1}$ where the infinite extent is along the Y-direction.

The TEM modes are also used for the Fabry-Perot disc resonator. Here m and n stand for the number of maxima along the polar coordinates r and θ respectively, in the plane of the disc and the mode is denoted by $TEM_{m-1,n,q-1}$. The lowest order mode is again TEM_{00q-1}.

2.2.2 The Resonator Losses

In addition to diffraction losses, open resonators are known to exhibit considerable conduction losses owning to the finite conductivity of the metals employed. If Q_0 is the quality factor of the unloaded resonator then

$$\frac{1}{Q_o} = \frac{1}{Q_c} + \frac{1}{Q_d} \qquad 2.3$$

where Q_c and Q_d are the quality factors due to conduction and diffraction losses respectively. If α_o is the loss per transit of the unloaded cavity then it can easily be shown that (Zimmerer, 1963)

$$Q_o = \frac{Kd}{\alpha_o} \qquad 2.4$$

where K is the wavenumber and d is the mirror separation. Since at resonance $Kd \approx q\pi$ then Eqn. 2.4 can be written as

$$Q_o = \frac{q\pi}{\alpha_o} \qquad 2.5$$

from Eqns. 2.3, 2.4 it follows that

$$\alpha_o = \alpha_c + \alpha_d$$

where α_c and α_d are the conduction and diffraction losses per transit

respectively.

If a coupling hole is drilled through the wall of one of the mirrors, then the loaded Q-value is given by

$$\frac{1}{Q} = \frac{1}{Q_o} + \frac{1}{Q_i} \qquad 2.6$$

where as in Eqn. 2.5

$$Q_i = \frac{q\pi}{\alpha_i}$$

and α_i is the loss per transit through the coupling hole. The coupling coefficient in this case may be defined as

$$\beta_i = \frac{\alpha_i}{\alpha_o} \qquad 2.7$$

and substituting in Eqn. 2.5 yields

$$\beta_i = \frac{\alpha_i}{\pi} \frac{Q_o}{q} \qquad 2.8$$

Note that β_i depends on both the unloaded Q-value and on the longitudinal mode order. It will be shown in the following chapter that optimum spectroscopic sensitivity is obtained for certain values of β_i. Experimental methods for the measurement of β_i are given in many places (Smart, 1973).

2.3 SOME APPROXIMATION METHODS

2.3.1 The Closed Box Approximation

The idea that the resonant modes of a Fabry-Perot resonator with rectangular mirrors are similar to those of a rectangular box was originally put forward by Schawlow and Townes (1958). Such a geometry is shown in Fig. 2.1. Assuming that the electric field is linearly

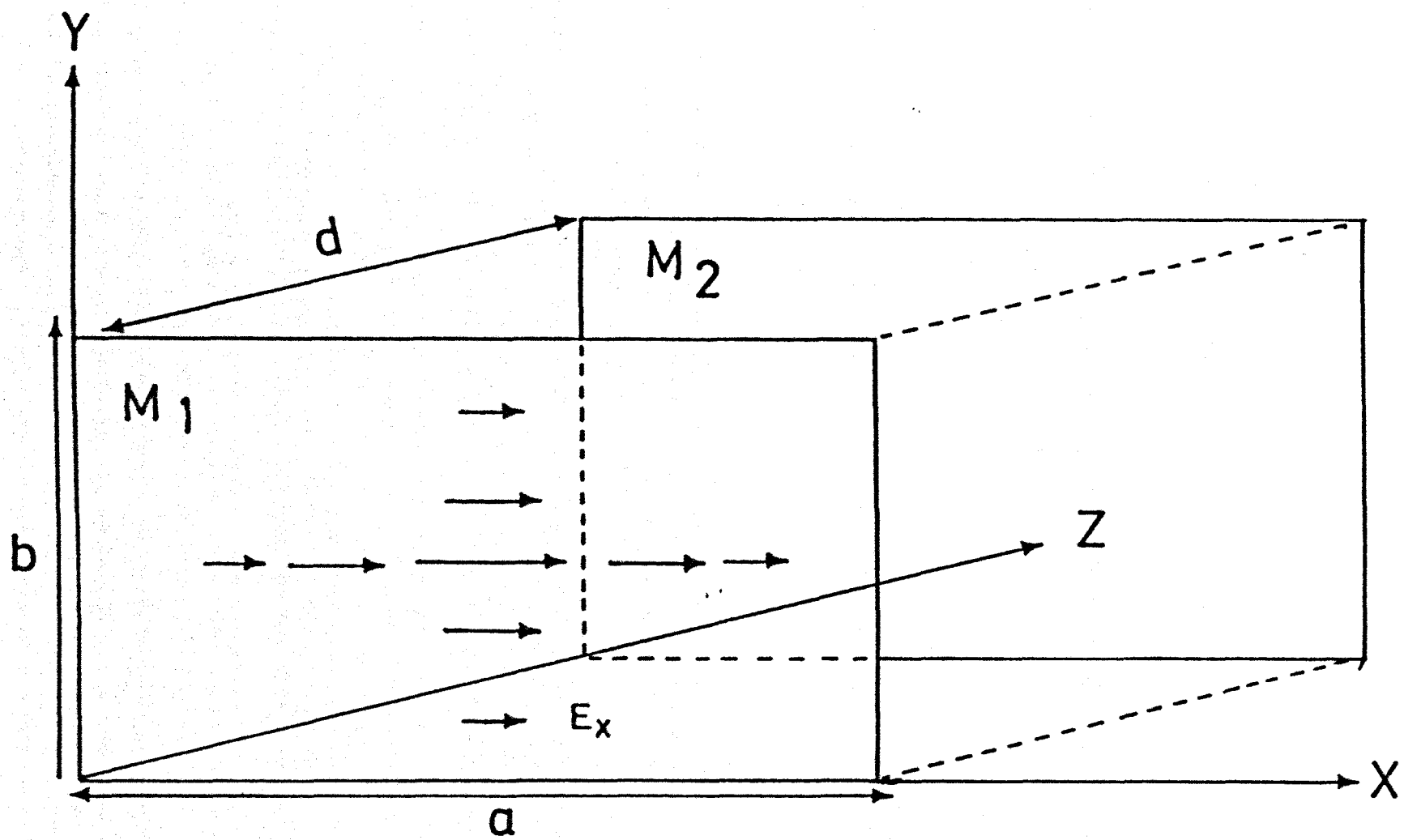

FIG 2·1 THE CLOSED BOX APPROXIMATION

polarized along the X-axis then the nonvanishing TE (or TM) component is given by

$$E_x = A_o \sin(m\pi x/a) \sin(n\pi y/b) \sin(q\pi z/d) \qquad 2.9$$

This solution assumes that E_x vanishes at the boundaries which is equivalent to placing perfect reflectors at the planes y=0, y=b and x=0, x=a. This yields a purely imaginary propagation constant and real resonance frequencies (Montgomery, 1947)

$$\nu^2_{m,n,q} = (c/2)^2\left[(m/a)^2 + (n/b)^2 + (q/d)^2\right] \qquad 2.10$$

The frequency separation between two successive modes along the X-direction can be found by calculating the quantity

$$\nu^2_{m+1,n,q} - \nu^2_{m,n,q} = (2m+1)(c/2a)^2$$

For maser resonators the condition

$$d \ll a,b \qquad 2.11$$

is always fulfilled. Then for low values of m and n it follows that

$$\nu_{m,n,q} \equiv \nu_q \approx (c/2d)q \qquad 2.12$$

therefore the frequency separation of the two lowest order modes is

$$\Delta\nu = (3/2\nu_o)(c/2a)^2$$

where $\nu_o = \nu_q$

This can be written as

$$\frac{\Delta\nu}{\nu} = \frac{3}{8}\left(\frac{\lambda}{a}\right)^2 \qquad 2.13$$

where λ is the resonance wavelength.

For $\lambda \approx 1.25$cm, a = 22cm; $\Delta \upsilon$ = 29MHz which is not far from the experimentally measured values.

The unloaded quality factor of a closed box with lateral dimensions much larger than the width can be shown to be (Yassin and Lainé, 1979)

$$Q_o = \frac{2\pi d}{\lambda \alpha} \qquad 2.14$$

where

$$\alpha = \frac{4\pi \delta_s}{\lambda} \qquad 2.15$$

and δ_s is the skin depth given by

$$\delta_s = \left(\frac{2}{\omega \mu \sigma}\right)^{\frac{1}{2}} \qquad 2.16$$

here μ and σ are respectively the material permeability and conductivity and $\omega = 2\pi c/\lambda$. By comparing Eqn. 2.14 with 2.4 it can easily be argued that α is exactly the loss per transit. Moreover, it can also be shown (Bleaney and Bleaney, 1957), that

$$\alpha = \frac{4}{c}\left(\frac{\pi \nu_o}{\mu \sigma}\right)^{\frac{1}{2}} = 1 - r$$

where r is the reflection coefficient. Substituting in Eqn. 2.14 it follows that

$$Q_o = \frac{kd}{1-r} \qquad 2.17$$

The quality factor given by Eqn. 2.17 is identical to that of a parallel flat plate Fabry-Perot with negligible diffraction losses, regardless of the mirror geometry (Zimmerer, 1963; Barchukov and

Prokhorov, 1961). It describes a wave which is bouncing back and forth between the large reflectors and with each bounce its amplitude is decreased by a factor equal to $1 - r$.

The Fabry-Perot disc resonator can be treated in a similar way. In this case the resonator is approximated to a cylinder whose diameter is much larger than its height. Calculation of its Q-value will inevitably yield a formula, identical to 2.17.

Verification of the accuracy of the above approximation can be made by comparing the Q-values of some constructed resonators with those given by Eqn. 2.17. For example, the Q-value of a conduction loss-limited copper resonator ($\sigma \approx 5.8 \times 10^7 Sm^{-1}$) at $\nu = 24GHz$ as given by Eqn. 2.17 is $Q_o \approx 7300$. The measured Q-value of a lightly coupled copper disc resonator of diameter 15cm on the other hand was 2500 (Smart, 1973). This indicates that diffraction losses of such a resonator are considerable. When the diameter was increased to 22cm the Q-value approached 6000 (Al-Jumaily, 1979) which is not far from the infinite parallel plate value when losses due to coupling are included. The above approximation was also used to calculate the Q-value of the brass roof-top resonator described in the following chapter. In this case the calculated value of about 3800 was in excellent agreement with the measured value for roof angles $\alpha \approx 3^o$. This indicated that diffraction losses of such a resonator were negligible.

2.3.2 Fox and Li Iteration Method

The application of the Huygens-Fresnel principle to open resonators with rectangular mirrors can be explained with the aid of Fig. 2.2.

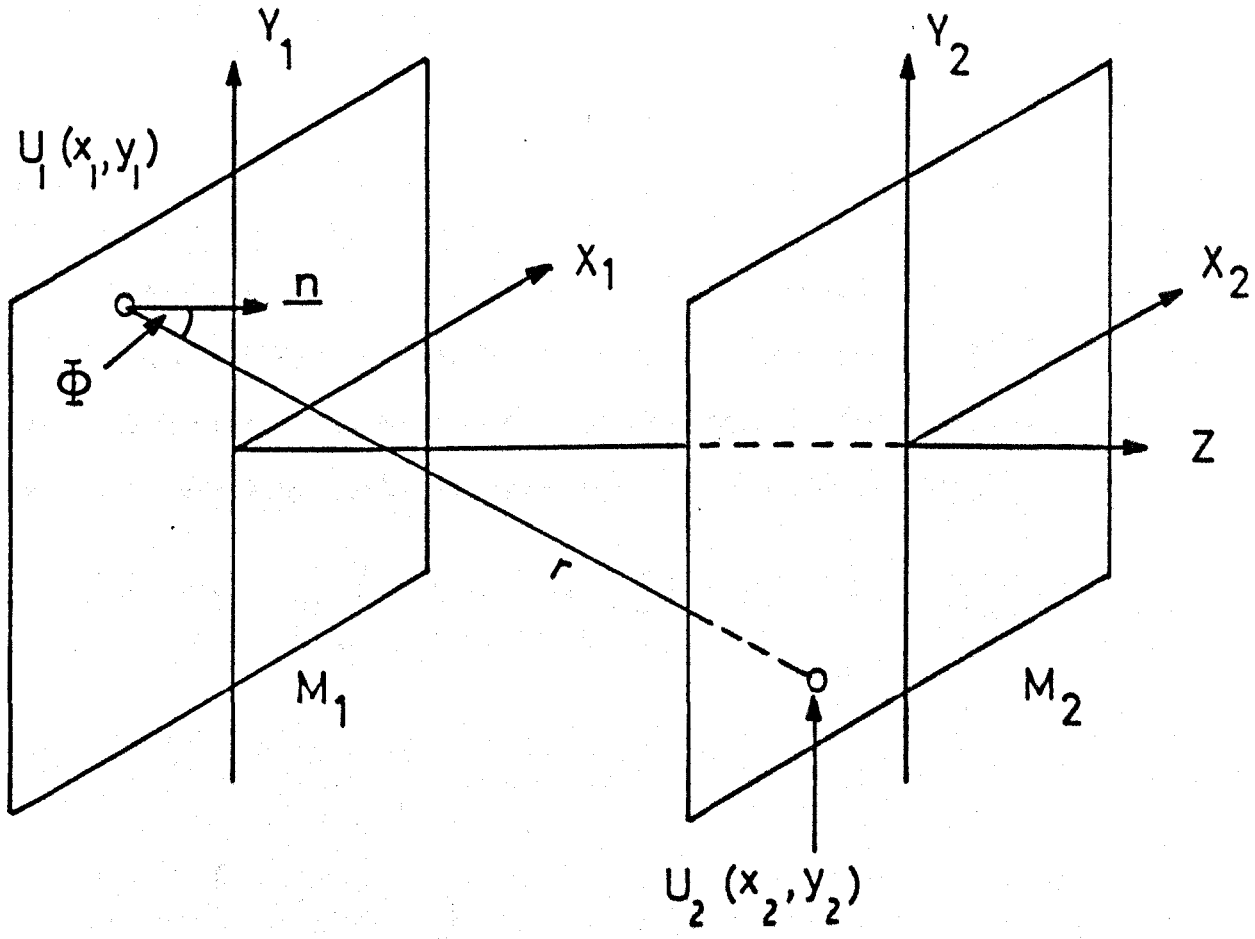

FIG. 2·2 GEOMETRY FOR APPLICATION OF HUYGENS-FRESNEL PRINCIPLE TO RECTANGULAR RESONATORS.

Let the linearly polarized field over the surface of the mirror M_1 be represented by the scalar function $U_1(x_1,y_1)$. According to Huygens' principle this surface acts as a source of electromagnetic radiators. The wave front at a point (x_2,y_2,d) over the surface of the mirror M_2 can be formed by summing over all contributions from the differential Huygens sources at all points $(x_1,y_1,0)$. The analytical expression is given by (Silver, 1949)

$$U_2(x_2,y_2) = \frac{jk}{4\pi}\int_{M1} U_1(x_1,y_1)\left\{\frac{\exp(-jkr)}{r}\left[(1+\cos\Phi) + \frac{\cos\Phi}{jkr}\right]\right\}dx_1dy_1 \qquad 2.18$$

where

$$r = \left[(x_2-x_1)^2 + (y_2-y_1)^2 + d^2\right]^{\frac{1}{2}} \qquad 2.19$$

and Φ is the angle between r and the normal to the surface M_1.

The cavity is said to be at resonance when the functions U_l,(l=1,2,3...) reach a steady state. In other words when the series of functions U_{l+1} calculated after the l_{th} bounce converge to a single function $E(x,y)$, apart from a complex constant η, independent of the coordinates. Therefore at resonance Eqn. 2.18 can be written as

$$E(x_2,y_2) = \eta\int_{M_1} K(r)E(x_1,y_1)dx_1dy_1 \qquad 2.20$$

where

$$K(r) = \frac{jk}{4\pi r}\exp(-jkr)\left[(1+\cos\Phi) + \frac{\cos\Phi}{jkr}\right] \qquad 2.21$$

equation 2.20 is a homogeneous integral equation of the second kind with a complex symmetric kernel $K(r)$. It can be regarded as a special case of the Fredholm integral equation

$$y(x) = F(x) + \int_a^b K(x,\xi)y(\xi)d\xi$$

If now the mirror separation is assumed to be much larger than their dimensions and that $kd \gg 1$, then in the far zone approximation the kernel is given by

$$K(r) \approx \frac{jk}{2\pi r} \exp(-jkr)$$

Furthermore if the kernel is transfered to a new set of coordinates defined by

$$x' = \frac{x_1}{a} \; ; \; x = \frac{x_2}{a}$$

$$y' = \frac{y_1}{b} \; ; \; y = \frac{y_2}{b}$$

then if the conditions

$$\frac{a^2}{\lambda b} \ll \left(\frac{a}{d}\right)^2 \text{ and } \frac{b^2}{\lambda d} \ll \left(\frac{b}{d}\right)^2 \qquad 2.22$$

are fulfilled, it is easy to show that the kernel is separable in rectangular coordinates

$$K(x',x;y',y) = \frac{-jab}{d}\left\{\exp(-jkd)\times\exp\left[\frac{-j\pi a^2}{\lambda d}(x-x')^2\right] \times \exp\left[\frac{-j\pi b^2}{\lambda d}(y-y')^2\right]\right\}$$

by defining

$$N_a = \frac{a^2}{\lambda d} \; , \; N_b = \frac{b^2}{\lambda d} \qquad 2.23$$

$$\gamma = -j\exp(-jkd) \qquad 2.24$$

The resonator becomes represented by two one-dimensional integral equations

$$E_x(x) = \gamma_x \int_{-1}^{+1} K_x(x',x)E_x(x')dx' \qquad 2.25(a)$$

$$E_y(y) = \gamma_y \int_{-1}^{+1} K_y(y',y)E_y(y')dy' \qquad 2.25(b)$$

with the kernels

$$K_x(x',x) = N_a \exp\left[-j\pi N_a(x-x')^2\right] \qquad 2.26(a)$$

$$K_y(y',y) = N_b \exp\left[-j\pi N_b(y-y')^2\right] \qquad 2.26(b)$$

Eqns. 2.25(a) and 2.25(b) can be interpreted as the integral equations of two infinite strips of separation d and widths 2a and 2b respectively. The physical meaning associated with Eqn. 2.25 can then be stated as follows. In order to find the resonant modes of a rectangular resonator, the field distributions E_x and E_y for two independent infinite strip mirrors are first calculated. The characteristics of the actual resonator can then be found according to the relation

$$E(x,y) = E_x(x)E_y(y)$$

and

$$\gamma = \gamma_x \gamma_y$$

and the exact propagation constant can be calculated from Eqn. 2.24.

Another significance of the Fox and Li approximation can be seen from Eqn. 2.26. There, it is shown that in the region where the condition given by the inequality 2.22 is valid, the resonator is

fully characterized by two numbers N_a and N_b known as Fresnel numbers. It therefore follows that resonators with different dimensions and operated at different frequencies must have the same electric field distribution and propagation constants provided that their Fresnel numbers are identical.

From the above discussion it can be concluded that the validity of the Fox and Li integral equation method requires two conditions to be fulfilled. Firstly, the wavelength is much smaller than the resonator dimensions and secondly its Fresnel number is small compared to unity. Consequently the theory outlined in this section cannot be applied to maser resonators at microwave frequencies. Nevertheless the method which is by itself interesting was used by many investigators as a useful check to their theories.

The solution of the integral equations 2.25(a,b) by the method of successive approximations is shown in appendix I. The actual computation showed that convergence becomes difficult for $N > 20$. This result was also quoted by Culshaw (1962). In Fig. 2.3 the computed intensity distribution for a rectangular infinite strip mirror for two different values of Fresnel number is compared with that of a rectangular closed box of dimensions 2a x 2b x 2c. The similarity of the curves is attributed to the small diffraction losses of the Fabry-Perot resonators at optical frequencies.

2.3.3 Vainshtein Generalized Theory

Here the rectangular resonator is again decomposed into two semi-infinite parallel plate waveguides and each is treated independently. However, instead of calculating the diffraction from the mirror aperture, the wave is considered to be propagating along a direction parallel to the surface of the mirrors. Since the waveguide

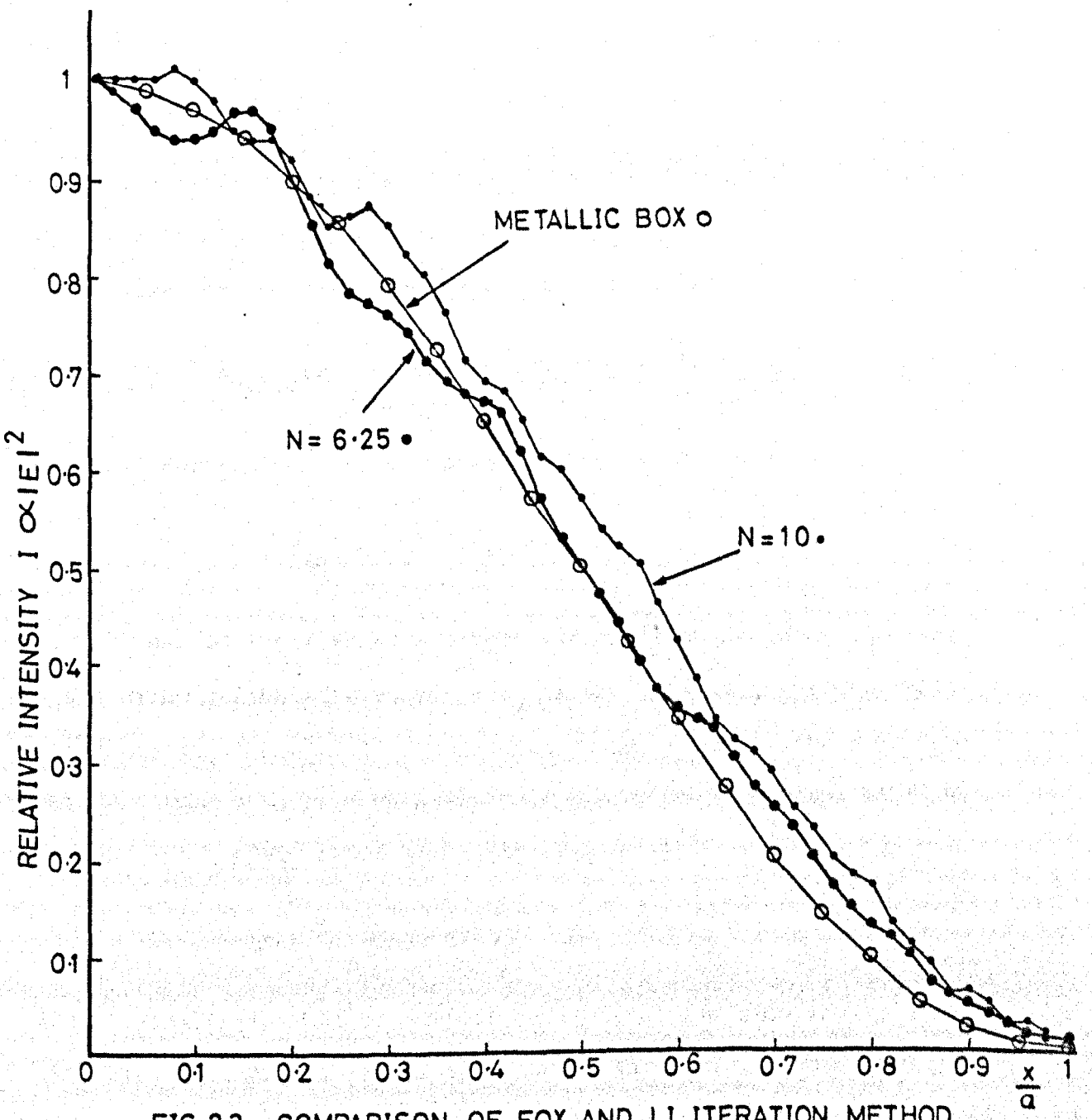

FIG 2·3 COMPARISON OF FOX AND LI ITERATION METHOD WITH THE CLOSED BOX APPROXIMATION.

is near cutoff then when the wave reaches the open end of the waveguide it is reflected back, apart from diffraction losses. Calculating the reflection coefficient at the open end as a function of frequency yields the solution for the resonator parameters.

In Fig. 2.4 a cross section of such a resonator is shown where the microwave electric field is assumed to be polarized along the X-direction. If this is also taken to be the direction of propagation then the resonator modes are designated $TE_{m-1,0,q-1}$. The transverse field inside the resonator can be written formally as:

$$E_{m,o,q}(x) = \exp(i\beta_{mq}x) + R_q \exp(-i\beta_{mq}x) \qquad 2.27$$

where the longitudinal cosine dependence is omitted and where

$$\beta_{mq} = k^2 + (q/d)^2 \qquad 2.28$$

Eqn. 2.27 can be regarded as a superposition of an incident sine-wave and a similar reflected wave where R_q is the reflection coefficient (R_q depends also on m). If the resonator end was closed by a perfect reflector, then $R_q = -1$. Moreover from Eqn. 2.28 it follows that at resonance $\beta_{mq} = m/a$, hence Eqn. 2.27 reduces to

$$E_x \sim \sin(m\,x/a)$$

which is similar to that of a metal box. If diffraction losses are not negligible, Eqn. 2.27 is still valid but with complex values of β and R. The resonance condition can be easily obtained by requiring a standing waves pattern in the resonator. This yields the characteristic equation

$$R_q = (-1)^m \exp(-i\beta_{mq}a) \qquad 2.29$$

Using the usual approximations at optical frequencies, analytical

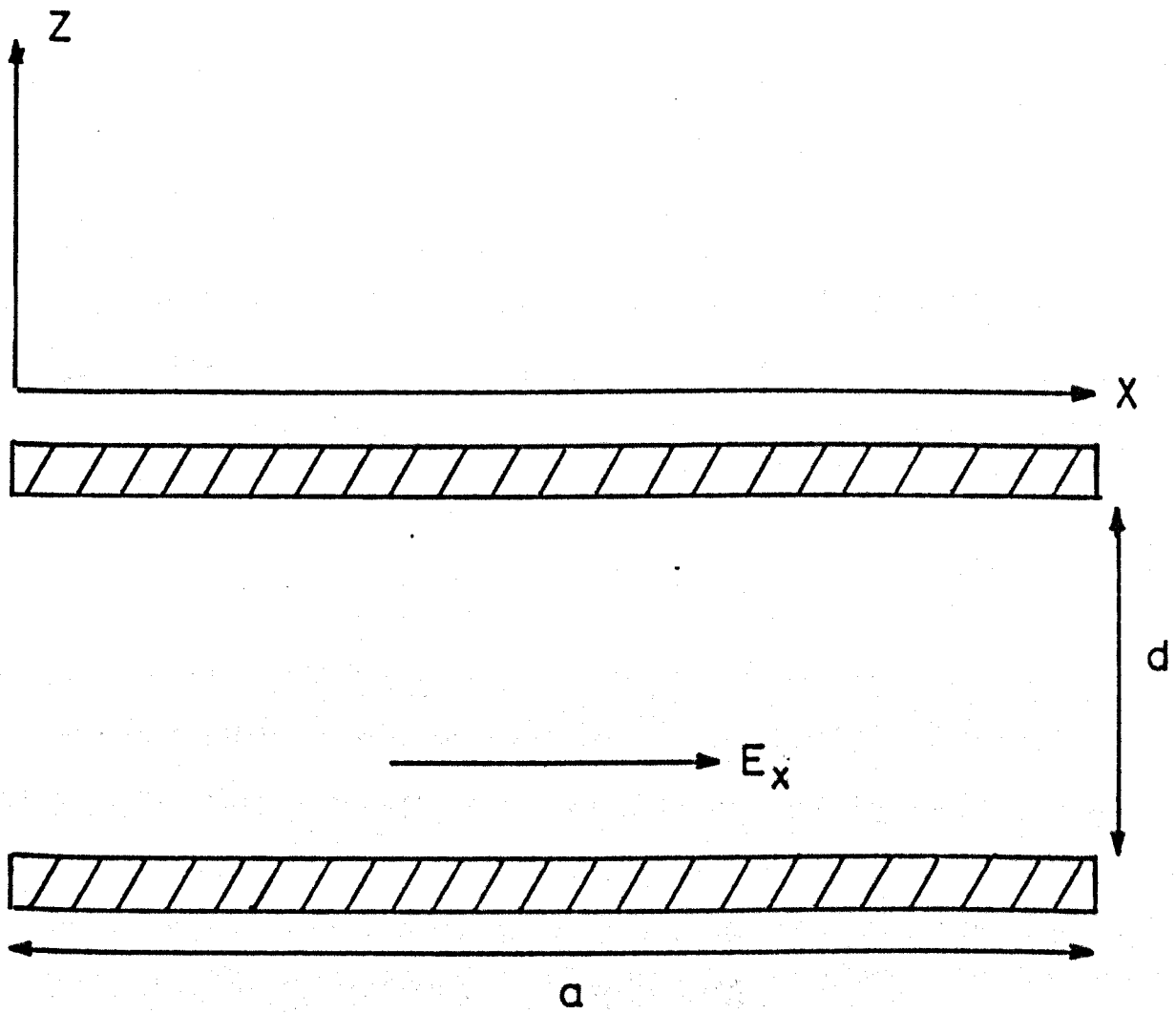

FIG. 2·4 REFLECTION OF MICROWAVES AT THE OPEN END OF A SEMI-INFINITE WAVEGUIDE.

expressions for R_q could be obtained (Vainshtein, 1963). From Eqn. 2.29, β_{mq} and thus the resonance frequency, was calculated. The field distribution could then be found by substituting in Eqn. 2.27.

At microwave frequencies, R_q can only be expressed in terms of β_{mq} according to the relation (Itoh and Mittra, 1974)

$$R_q = \frac{1}{2}\left\{\frac{[\beta_{mq} + k]\ G_+(\beta_{mq})}{\beta_{mq}}\right\}^2 \qquad 2.30$$

where $G_+(\tau)$ is the so called factorized Wiener-Hopf function. Expressions for $G_+(\tau)$ are given in Appendix I. Eqn. 2.29 is then reduced to a simple algebraic equation with one unknown. Although a closed-form solution for it is not possible, β_{mq} and R_q can be found simultaneously using iterative alogarithms. Since all the calculations involved are of a simple arithmetical nature, the computing time here is much less than that required for the convergence of Fox and Li functions.

To apply this theory to disc and roof-top resonators formulae similar to those given by Eqn. 2.30 for these geometries are required. Such derivations are not yet available. However this method promises a comprehensive solution for maser rectangular open cavities at microwave frequencies.

2.3.4 di Francia Approximations for the Roof-top Resonator

A cross section of the flat roof-top geometry is shown in Fig. 2.5. Constructional details are given in chapter 3. Assuming that the cavity is near cutoff, then for small roof angles, both the electric and magnetic fields are parallel to the resonator mirrors. Solutions with the microwave electric field parallel to the X-axis in

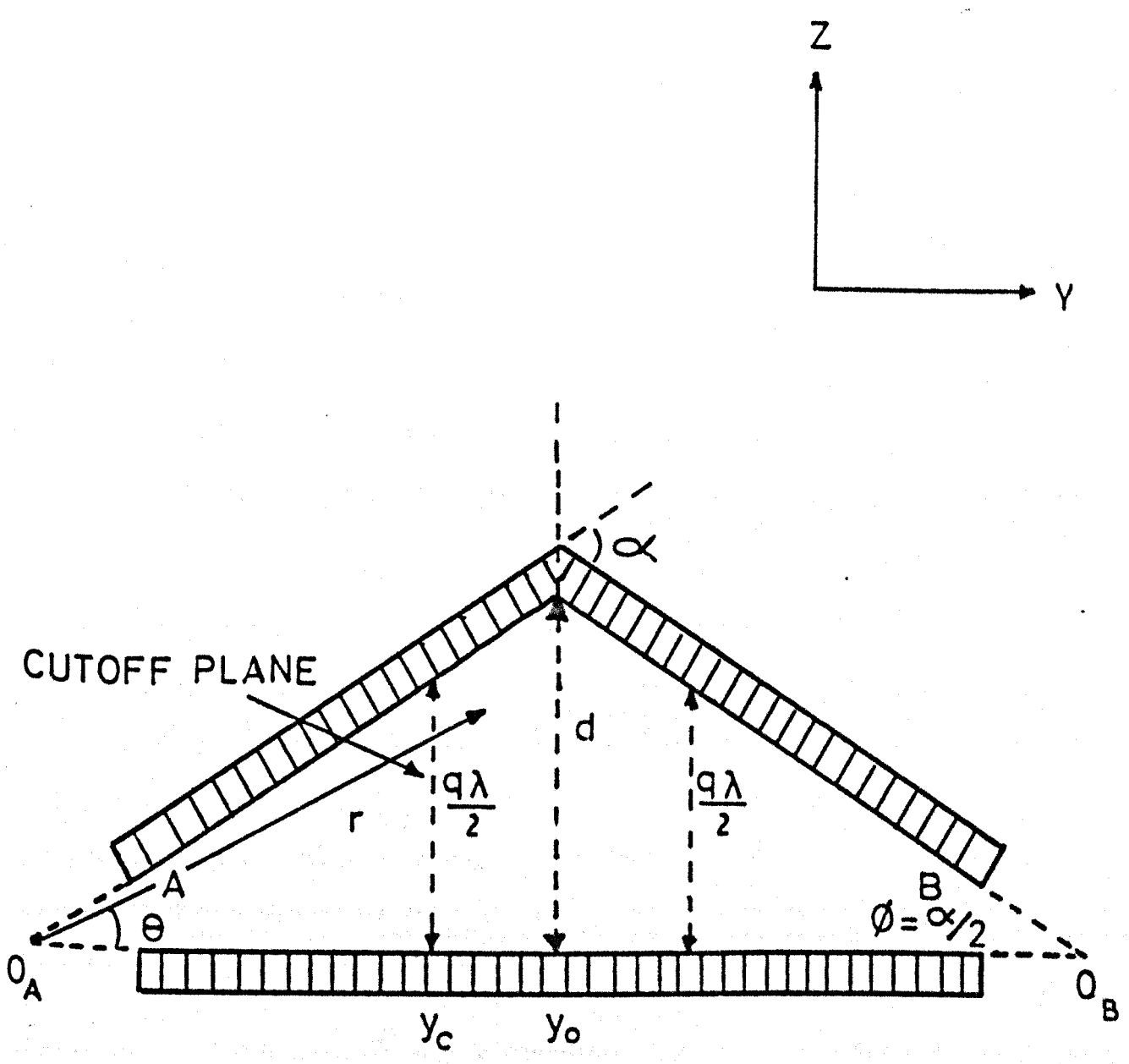

FIG. 2·5 THE FLAT ROOF-TOP RESONATOR

either halves A or B are given by

$$E_x(r,\theta) = J_\mu(kr)\sin(\mu\theta) \qquad 2.31$$

where $J_\mu(kr)$ is a Bessel function of the order μ and the boundary conditions over the metallic walls ($E_x = 0$ for $\theta = 0; \theta = \phi$) requires that

$$\mu = (q\pi/\phi) \qquad 2.32$$

where q is a natural number. For small angles and near the centre of the cavity $kr \approx (kd/\phi)$. Therefore both the order and the argument of the Bessel function are large. Consequently Bessel functions can be replaced by asymptotic expressions (Morse and Feshbach, 1953). The expansion of the Bessel function divides each half of the roof-top laterally (along the y-direction) into two regions with different field distributions according to

$$E_x(y) = \begin{cases} \dfrac{\cos(a\,\dot{y}^{\frac{3}{2}} + b)}{\pi(q\pi\dot{y}/\lambda\phi)^{\frac{1}{4}}} & y > y_c \\ \dfrac{\exp(-a\,|\dot{y}|^{\frac{3}{2}})}{2\pi(q\,|\dot{y}|/\lambda\phi)^{\frac{1}{4}}} & y < y_c \end{cases} \qquad 2.33$$

where

$$\dot{y} = y - y_c$$

$$a = (8\pi/3)\,(\phi/q\lambda^3)^{\frac{1}{2}} \qquad 2.34(a)$$

$$b = 2\pi^2/3 \qquad 2.34(b)$$

Thus, in each half there exists a cutoff plane whose distance from the centre is $W_c = |(y_c - y_o)|$, of height $q\lambda/2$. Inside these planes ($y_c < y < y_o$) the field oscillates as a function of distance, but outside them ($y < y_c$) it decays rapidly. It can be shown that the exponential field equals 1/2 of its maximum value at a distance from

the centre given by (di Francia, 1965)

$$W_{\frac{1}{2}} = (d\phi^{-\frac{1}{3}}/2)\,(3/2\pi)^{\frac{2}{3}} \qquad 2.35$$

for the lowest order mode. For $d \approx 0.65$cm, $\alpha = 3^{o}$; $W_{\frac{1}{2}}$ is of the order of the wavelength. Diffraction losses from the roof strip are thus very small indeed. The field outside the cutoff planes decays so rapidly that it is sufficient to make the strip in the y-dimension only a few wavelength wide and diffraction losses are practically eliminated.

The resonance condition can be obtained by matching the field in the two halves of the cavity at the central plane. The easiest way is to assume that the field exhibits a node or an antinode at the plane $y = y_{o}$. Hence

$$(ay^{\frac{2}{3}} + b) = (m - 1)\,\frac{\pi}{2} \qquad \text{at } y = y_{o}$$

which yields the resonance condition

$$\lambda = (2d/q)\left\{1 - \frac{1}{2}\left[\frac{3\phi(2m - 1)}{4q}\right]^{\frac{2}{3}}\right\} \qquad 2.36$$

for m = 1,2,.... For q = 1, m = 1, $2\phi \approx 3^{o}$ the resonant wavelength is only slightly shorter than that of an infinite parallel plate resonator.

To find the field distribution in the roof-top resonator, the field given in Eqn. 2.33 is multiplied by that of an infinite strip Fabry-Perot. The resonance condition is also found by combining the two resonance conditions.

In the begining of this section it was stated that both the electric and the magnetic fields are practically parallel to the mirror's surface. Also the polarization of the electric field was

assumed to be parallel to the X-axis (Fig. 2.5). In fact, within this approximation (fields parallel to the reflectors) the solution for E along the Y direction should reveal the same results. This is because Eqn. 2.31 will still be valid for the magnetic field which will now be parallel to the X-axis. The derivation can then be carried out in very much the same way yielding an identical resonance condition. In reality, however, there was a frequency difference of about 20MHz between the two directions of polarization. This value depended on the mirror tilt angle and was at a maximum when the roof-top mirror was symmetric with respect to the flat mirror. It could well be that including the other two field components E_r and E_ϑ would create an asymmetry between the electric and the magnetic fields and thus produce the frequency difference between the two polarizations as a function of the roof-angle.

The theory of the roof-top resonator was also treated using the Fox and Li iteration method at microwave frequencies but with small Fresnel numbers (Checcacci, Consortini and Scheggi, 1967; Checcacci et al., 1968). Their numerical computation were in a good agreement with di Francia's theory and with the experimentally measured resonance frequencies. However no mention of the resonance frequency dependence on the mode polarization was made.

CHAPTER 3

A ROOF-TOP RESONATOR FOR MOLECULAR BEAM MASER SPECTROSCOPY

3.1 INTRODUCTION

In this chapter, the operation of a molecular beam maser incorporating a roof-top resonator for the first time is discussed. Although, the ultimate capability of this type of open resonator might not have been fully exploited in this work because of technical difficulties, the following experimental results undoubtedly justify further investigations in the future. Experimental verification that the roof-top spectrometer can have good spectroscopic sensitivity and high resolution has been obtained. To demonstrate the high spectrometer sensitivity, the maser was operated on the ammonia inversion line $J = K = 2$. The resolution was measured employing the known splitting of the quadrupole satellites of the ammonia inversion line $J = K = 1$.

Apart from a few technical modifications, the molecular beam maser system used in the experiments has been discussed previously (Smart, 1973; Lainé and Smart, 1971) and a diagram of its essential components is given in Fig. 3.1.

The main chamber was an aluminium bronze casting in the shape of a rectangular box of dimensions approximately 450 x 200 x 200mm, with rectangular cut-outs of dimensions approximately 400 x 150mm in both of its long sides. It was fitted with a brass lid, which carried two liquid nitrogen traps and closed the top. Two aluminium plates were bolted to the sides of the box. The front plate carried the mechanical and electrical lead-throughs and the back plate carried the

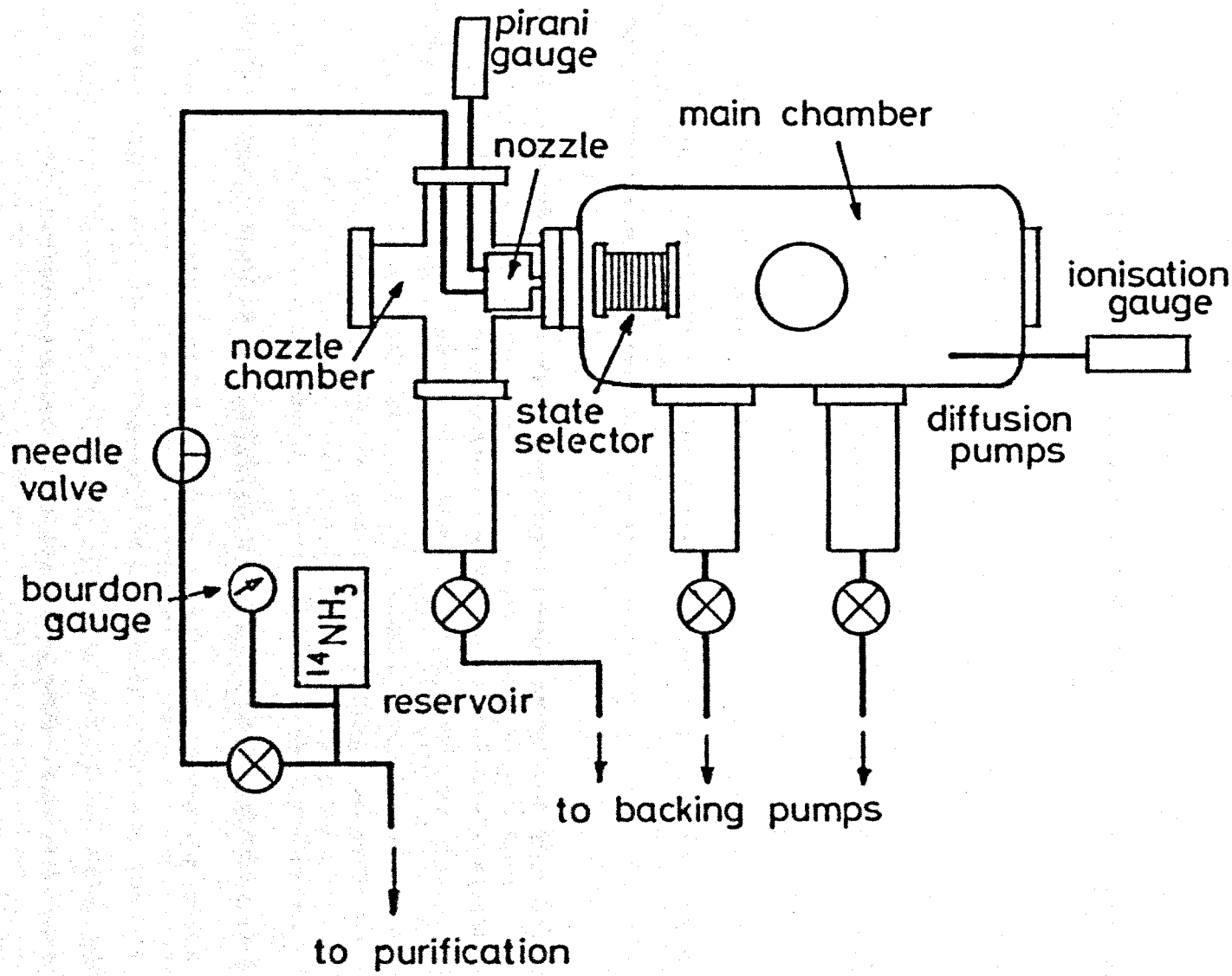

FIG. 3·1 DIAGRAM SHOWING THE MAIN COMPONENTS OF THE SINGLE BEAM AMMONIA MASER.

two coupling waveguides. This provided extra flexibility in using the same chamber with different waveguide and mechanical connections to the outside, simply by replacing the aluminium plates.

The nozzle chamber was a four-port arrangement constructed from brass tubes. One port, carried the skimmer and the state selector which mated with the main chamber. At the opposite end, a smaller port closed by a flange carried both a liquid nitrogen trap and the ammonia supply to the nozzle. The top of the nozzle chamber was closed by a flange which also carried a liquid nitrogen trap.

The pumping arrangement for the two chambers was provided by three Edwards type 203 two inch diameter diffusion pumps. Two were mounted below the main chamber and one below the nozzle chamber. These pumps were charged with silicone oil type 704. Each diffusion pump was backed by its own Metrovac GRD1 rotary pump.

With the aid of the cryogenic pumping by the liquid nitrogen traps, the pressure in the main chamber was 8×10^{-6} torr at best which rose to 1×10^{-5} torr when a molecular beam of ammonia of normal operation intensity (120torr behind the nozzle) was introduced. Such a poor vacuum was just enough for spectrometer operation but made the oscillation threshold very high in terms of the necessary value of EHT which had to be applied to the state selector to reach the oscillation condition.

An improvement on the previous detection scheme (Smart, 1973) was obtained by phase locking the klystron to a high stability quartz crystal by means of a microwave frequency stabilizer. Apart from improving sensitivity this also allowed slow scanning through the spectral lines and thereby permitted the observation of weak quadrupole satellites separated from each other by a frequency of the order of

5KHz. The detection scheme which was employed throughout this study is described in detail in Sec. 3.4. The sensitivity discussion given there will prove to be useful both for resonator design considerations and for the exploration of the new methods of detection presented in later chapters.

3.2 CONSTRUCTION OF THE CAVITY

3.2.1 Design Consideration

The size of a molecular beam maser machine, employing an open resonator in the mm-wave spectral region is mainly determined by the size of the resonator mirrors. Conventionally, a Fabry-Perot interferometer with flat disc mirrors is used. Since diffraction losses continue to be important compared to metal losses in determining the Q value up to a relatively large mirror diameter (25cm for λ = 1.25cm, Al-Jumaily, 1979), masers using such interferometers employ huge vacuum chambers. This implies the use of fast pumps, costly manufacture, and difficulties in handling. In contrast, the use of the roof-top resonator, permits the construction of an efficient, compact machine. The length of the resonator along the beam axis and hence of the main vacuum chamber can be made according to the desired extent of the microwave field which determines the length of interaction, while the height can be made relatively small since diffraction losses through the top and bottom of the resonator are practically negligible. Therefore, the shape and the size of the maser are a faithful expression of the efficiency of its performance. The choice of the mirror dimensions (22cm x 11cm)with a roof angle $\alpha \approx 3^{\circ}$ (Fig. 2.5) in the present work was restricted by the dimensions of a prototype cavity already constructed and an ex isting vacuum system. Because of space restrictions in the main chamber a short state selector was used and

the maser was operated as a spectrometer rather than as an oscillator.

Although the resonator was used in the lowest order longitudinal mode (q = 1) only, it could be easily modified to operate with higher order modes (q = 2,3,...) simply by using longer glass rods as spacers.

In the construction of the roof-top resonator, or indeed any type of open resonator at microwave frequencies two important factors have to be considered. The first is the flatness of the mirrors and the second is the facility of fine tuning from outside the vacuum chamber. Mirrors flatness should be preserved when preparing the surface and also while mounting the mirrors to the cavity frame. Surface imperfections and mirror bending proved to have a strong effect in practice on the Q-value and on the microwave electric field distribution inside the resonator.

Fine tuning is necessary since the cavity resonance frequency is always shifted during evacuation. This is due to the change of the dielectric constant of the medium filling the cavity (air), the pressure applied by the coupling waveguides on the fixed mirror's surface and the cooling of the system by the liquid nitrogen traps. Moreover, temperature variations of the glass rods makes maser operation impossible without fine tuning.

It was also found that final adjustment to mirror parallelizm was best effected by monitoring the maser signal itself. Construction details are given in the following sections.

3.2.2 Cavity Mirrors

As was emphasized, surface imperfections have a considerable effect on Q-values of resonators operating in the microwave region,

especially when low order longitudinal modes are used. Obviously, the amount of tolerable distortion is a function of the resonator Q-value. Let δ be the average surface deviation from a reference flatness. The total distortion of the wavefront after n reflections is $2n\delta$ which can be regarded as negligible if it satisfies the inequality:

$$2n\,\delta \ll \lambda/2 \qquad 3.1$$

The relevant value of n is determined by the number of reflections that a microwave pulse can survive in the resonator which in turn depends on the value of Q. By definition the stored energy drops to 1/e from its maximum value for $n = Q/q_\pi$. The criterion then becomes:

$$\delta \ll \lambda/q_\pi Q$$

If it is assumed that the resonator is conduction loss limited then for q = 1 the following expression is obtained (Yassin and Lainé, 1979)

$$\delta \ll \pi\,\delta_s \qquad 3.2$$

where δ_s is the skin depth. For brass $\delta_s \approx 1.2 \times 10^{-6}$m. If the maximum tolerable distortion is denoted by δ_m, Eqn. 3.2 can be written as:

$$\delta_m \approx \mu\,\pi\,\delta_s \qquad 3.3$$

and for brass

$$\delta_m \approx 3.6 \times 10^{-6}\mu\,(\text{meters}) \qquad 3.4$$

where μ is a constant which can be determined experimentally. If diffraction losses are not large and other surface imperfections are negligible then it follows that

$$0 < \mu \leq 1$$

An investigation of the effect of brass mirror flatness at 1.25cm wavelength was made and a value of $\mu \approx 0.3$ was obtained (Smart, 1973). Substitution in Eqn. 3.4 yields the result that a flatness of $\sim 10^{-3}$mm is satisfactory. The brass mirrors were carefully surface ground. Such a method was found capable of producing a flatness better than 5×10^{-4}mm if care was taken of mechanical distortion of the mirror during grinding. Therefore values of δ_m given by Eqn. 3.3 are not impractical to achieve.

3.2.3 Cavity Frame and Tuning Mechanism

The mirrors were housed in a brass frame with its base bolted firmly and directly onto the bottom of the main vacuum chamber, which was machined flat and made horizontal. The frame consisted of two vertical brass plates(280mm x 150mm) separated by four rods 70mm in length. The flat mirror which carried the coupling holes, was bolted carefully to the front plate of the frame. Since this plate was not made thick enough (6mm), an additional structural support was needed in the form of three brass stands of triangular shape as shown in Fig. 3.2.

The roof mirror (the tuning mirror) was bolted to a rectangular-shaped brass frame. This frame (the mirror frame) carried three 17mm diameter glass rods, two at the upper and the lower corners of one side, (the beam entrance of the cavity) and the third at the middle of the opposite side. They passed forward, through the front plate of the cavity frame, into three micrometer assemblies. Each micrometer assembly consisted of a brass barrel carrying a stainless steel micrometer screw. Coarse adjustment to the desired mirror separation was first obtained by means of the three micrometer screws. Fine tuning and adjustment of the tilt angle was obtained, first by pressing a piece of neoprene rubber against the tuning mirror frame

(Fig. 3.2) and by turning the micrometer screws.

The fine tuning mechanism consisted of a threaded plug which was bolted to a large gear wheel 100mm in diameter and screwed into the rear plate of the cavity frame. By turning the gear wheel the plug could be screwed into or out of the frame and the rubber was compressed or decompressed accordingly. In this way the pressure on the frame of the mirror was varied and a small longitudinal movement of the tuning mirror obtained. Since the cavity frame was thin (5mm thickness), it was bent unequally along its length, but the mirror itself remained absolutely flat. The large gear wheel meshed with a small pinion bolted to the end of a rotary shaft vacuum seal. By turning the shaft outside the vacuum chamber, the gear wheel was rotated to give fine tuning after sealing and evacuation (Fig. 3.3).

An unfortunate disadvantage of the design discussed is that the glass rods were not positioned symmetrically with respect to the rectangular shape. This caused a small deviation from parallelism, effecting fine tuning and applied too much pressure on the single glass rod at the beam exit end of the cavity. To compensate for this effect, a further rotary shaft vacuum seal unit was attached to the single micrometer associated with the relevant glass rod screw, so that a final correction to exact parallelism was possible from outside the vacuum chamber as shown in Fig. 3.2.

3.2.4 Microwave Coupling to the Cavity

Microwaves were coupled to the cavity through two coupling holes positioned symmetrically with respect to the height and length. At first the holes were 2.2mm in diameter and spaced 10cm apart at equal distances from the mirror edges. After testing the cavity on the bench using a crystal vides detection scheme, it was noticed that the

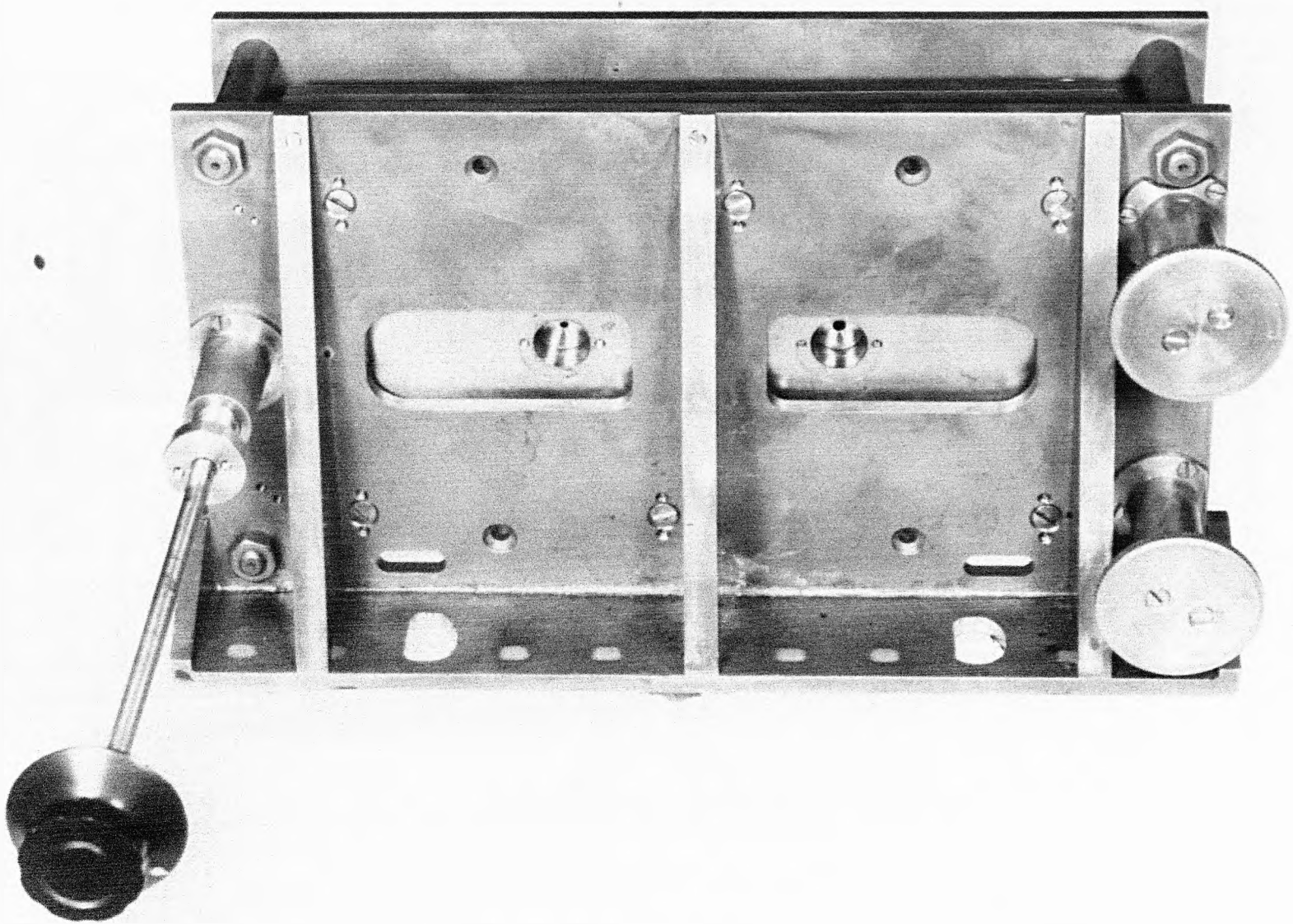

Fig. 3.2 View of the roof-top resonator showing the tuning micrometers and the coupling holes

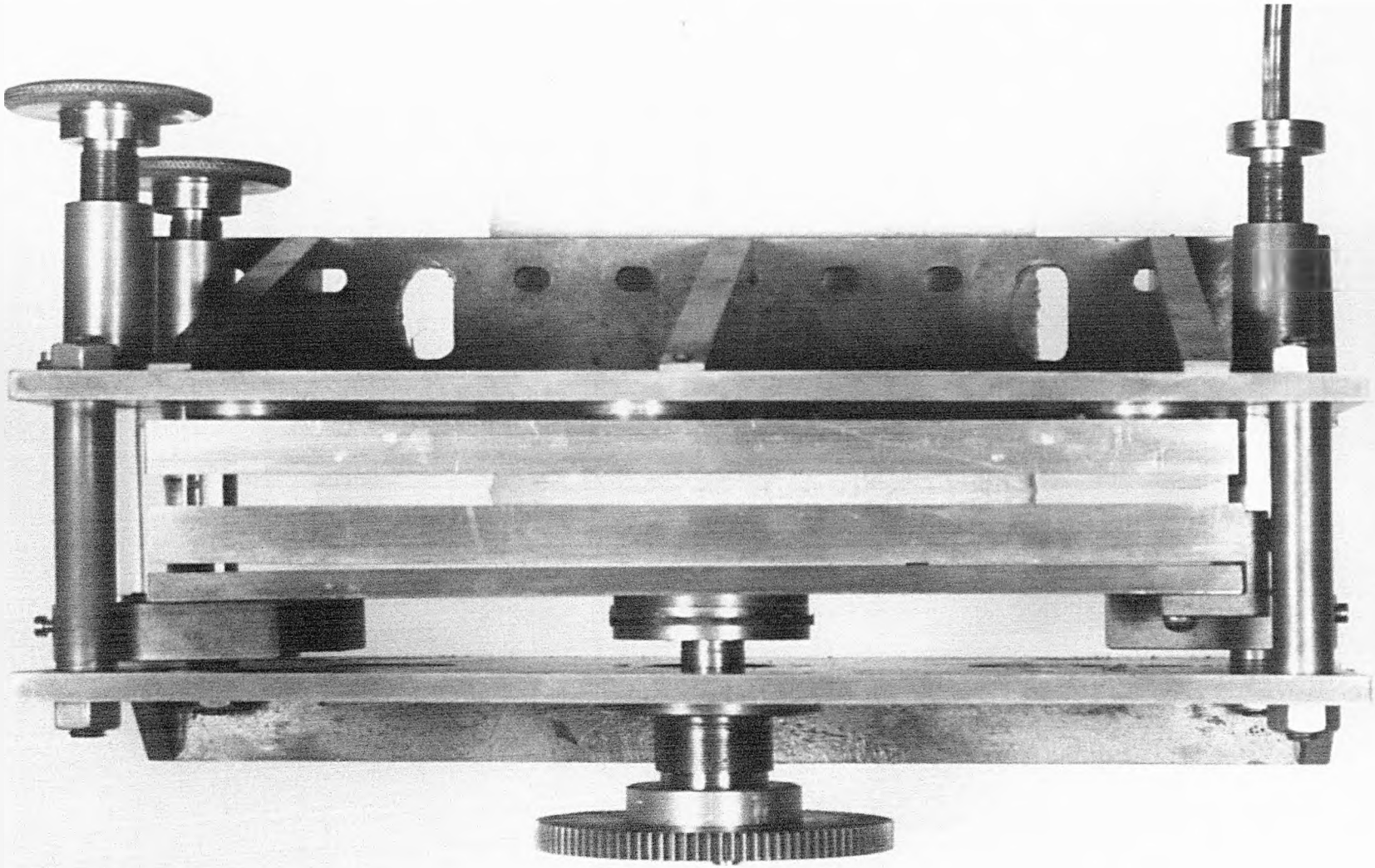

Fig.3.3 View of the roof-top resonator showing the fine tuning mechanism

lowest order mode (TEM_{ooo}) was suppressed in transmission with respect to the higher order modes. This was explained by the fact that low order modes tend to concentrate their energy near the centre whereas the others (being more lossy) propagate more towards the edges. When the fixed (flat) mirror was replaced by another with coupling holes 8cm apart, a satisfactory transmission of the two lowest order modes was obtained. It was noticed at that stage that the effect of the coupling holes on the Q_o-value was not large both because of their relatively small size and also that they were far from the centre (Slater, 1950). When the system was operated as a maser on the inversion line J = K = 3 of ammonia, the ratio of stimulated emission signal-to-noise was poor, although oscillation was set up at a state selection voltage of 15KV. This result was explained by the fact that the signal detected by a superheterodyne receiver depends on the coupling parameters of the cavity, and since the cavity was very lightly coupled, the sensitivity was reduced, whereas the Q-value was high enough for oscillation to be set up. Again, the fixed mirror of the cavity was taken out and the output hole was carefully redrilled, to a diameter of 3.2mm. The coupling coefficient was measured and with external matching of the waveguide to the coupling hole, a maximum value of $\beta \sim 0.3$ could be obtained. A drop in the quality factor was clearly noticed. The new Q-value was only about 80% of the original. As expected, a remarkable improvement in sensitivity was obtained but the oscillation threshold could no longer be reached even when the state selection voltage was raised to 20KV.

The method chosen for making the physical connection between the waveguides and the fixed mirror was a form of choke coupling based on the choke frequently used at waveguide flanges (Harvey, 1963). The method, (including mechanical design details) has been described by

many investigators (Smart, 1973). An important advantage of this method is that the joints are made cylindrical. This enables the waveguide orientations to be varied to any desired angle by rotating a special rotary joint which can couple any two different field polarizations and hence provides the facility of controlling the polarization of both exciting and detected radiation. This facility opened new areas of investigations as will be shown later.

3.3 PROPERTIES OF THE ROOF-TOP RESONATOR

3.3.1 Exploration of the Cavity Modes

In this section the validity of the theoretical discussion developed in Ch. 2 will be examined experimentally. Bench experiments were made to examine the modes of the resonator at a frequency of about 24GHz employing the crystal video detection scheme shown in Fig. 3.5. Exploration of the field and measurements of Q-value were made in transmission via the two coupling holes (Appendix II) while measurements of the coupling coefficients were taken in reflection by measuring the VSWR (Smart, 1973). It should be mentioned that emphasis was put on those properties which were relevant to the resonator application in this study of molecular beam masers.

The electromagnetic field distribution was investigated by the method suggested by Checcacci and Scheggi (1965). A small perturbation object was placed in the field between the mirrors and the power absorbed by it was measured by observing the reduction in power, transmitted by the cavity. This reduction was proportional to the intensity of the field in the vicinity of the perturbation object (Hibben, 1969). Together with rotary joints attached to the input and the output waveguides, both intensity and polarization of the electric field between the mirrors could be explored.

The lowest order mode (TE_{000}) had a single maximum along the resonator axis and was separated from the adjacent mode (TE_{100}) by almost 30MHz. The line-width values of these modes was about 6MHz and two well separated modes were obtained. The frequency separation is in good agreement with the calculation made in Ch. 2. It was also noted that for roof angles from 30' to 3° the field extended along the resonator axis right to the edges. This allowed a long time of interaction of molecules with the cavity radiation field thereby reducing the line-width. On the other hand the field was found to be concentrated near the resonator axis allowing no diffraction losses in the perpendicular direction. This remarkable feature does not only imply an increase in the Q-value but also leads to a practical possibility of enhancing the spectrometer sensitivity (see Sec. 3.5). The width of the field was estimated to be about one wavelength ($\sim$1cm), again with a good agreement with the theory developed in Ch. 2.

3.3.2 Resonator Alignment

Unlike the rectangular Fabry-Perot resonator the flat roof was insensitive to the misalignment of the mirrors. In fact it resonated even when the separation of the mirrors at the top and bottom was considerably different, provided that the apex of the roof-top was kept parallel to the plane of the flat mirror. This result which has a valuable practical application can be interpreted by the fact that the roof-top resonator structure can be considered as a superposition of a roof-top strip and an infinite Fabry-Perot strip. The former resembles the closed cavity structure where alignment has no significant importance since diffraction losses are negligible while in the latter parallelism is rather important since a small deviation from it causes a great deal of diffraction.

3.3.3 Q-Values

Q-values as a function of the roof angle for the lowest order mode were measured by the method described in Appendix II. The results shown in Fig. 3.4 emphasize two important conclusions. Firstly there is a considerable increase in the Q-value when the roof angle exceeds 1° (almost a factor of 2) in comparison with the rectangular Fabry-Perot resonator, and secondly the quality factor approachs a limiting value ($Q \sim 4000$) as the roof angle exceeds 3.5°. The latter was shown to be equal to the quality factor of a Fabry-Perot resonator with infinite plates ie. a conduction loss-limited system (Yassin and Lainé, 1979).

The fact that these results did not show regions of minimum losses as expected by Checcacci et al. (1967) only confirmed the assumption that the cavity studied is not a diffraction loss limited system. Mathematically speaking the calculations made in the latter reference are only valid for a small value of Fresnel number $N = a^2/\lambda d$ (Culshaw, 1962), that is for large values of mirror separation with respect to the mirror dimensions. Physically this means a diffraction limited system.

Finally the theory developed in chapter 2 gives useful design hints. For example at a frequency of ~ 24GHz and for $q = 1$ the following practical values can be chosen for a roof-top resonator:

Length: ~ 25cm determined by diffraction losses of an infinite strip mirror of width 'a'.

Roof angle and roof height: These are determined by the diffraction losses from a roof-top strip of angle α and cutoff planes of length equal to $\lambda/2$. For $\alpha \sim 3^{\circ}$ a roof height of about 5cm would be practical for the lowest order mode.

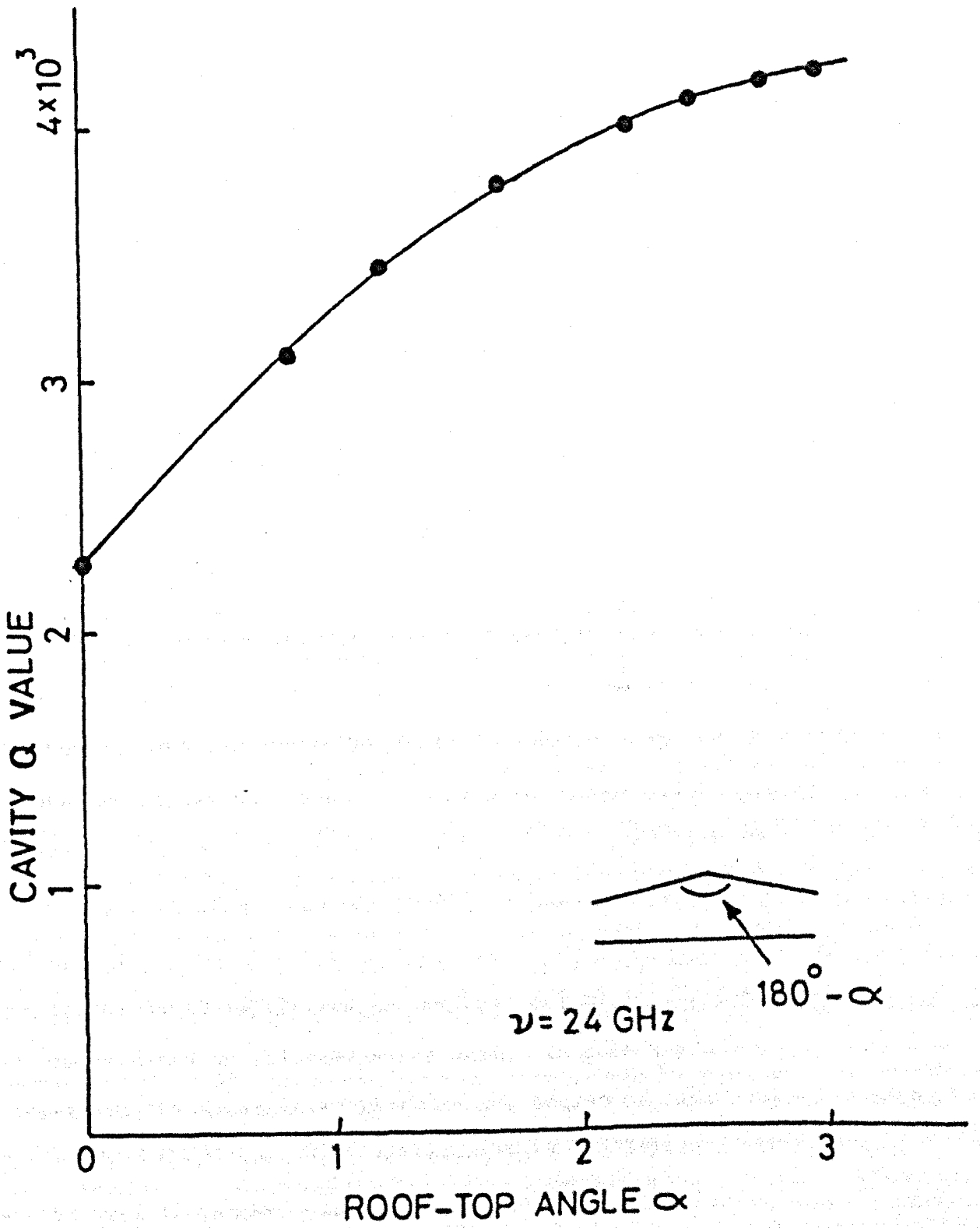

FIG. 3·4 MEASURED Q VALUES OF THE FLAT ROOF-TOP RESONATOR.

3.4 DETECTION OF THE MASER SIGNALS

3.4.1 The Crystal Video Receiver

A quick, simple and a useful method, often employed in microwave measurements is crystal video detection.

Unfortunately, this method, for reasons of sensitivity is not used for stimulated emission detection. Most common applications are cavity mode identification, Q-values measurements and the detection of strong absorption lines. The latter can be easily established by flooding the main chamber with gas while the system is being evacuated. This allows a precise adjustment of the lowest order cavity mode frequency to that of the molecular resonance. A typical experimental assembly is shown in Fig. 3.5.

Power from the klystron is frequency swept by applying a saw-tooth voltage of amplitude 0-50volts and frequency 50Hz to the reflector. The microwave frequency is roughly measured by a calibrated wavemeter. After attenuation the klystron power passes through an isolator which prevents power from being reflected back to the klystron. Power transmitted through the cavity is then rectified by the diode D and appears at the input of the amplifier as a video signal. After amplification it is applied to the vertical plates of the C.R.O which is synchronized by the same sweep unit. In this way a trace which represents the transmitted power as a function of frequency is obtained. Two rotary joints were used to investigate the effect of polarization on the quality factor. As was mentioned in Ch. 2 a frequency difference of about 20MHz was found when the two waveguides were rotated from an orientation where both electric fields were parallel to the beam axis, to an orientation where both waveguides electric fields were perpendicular to the beam axis.

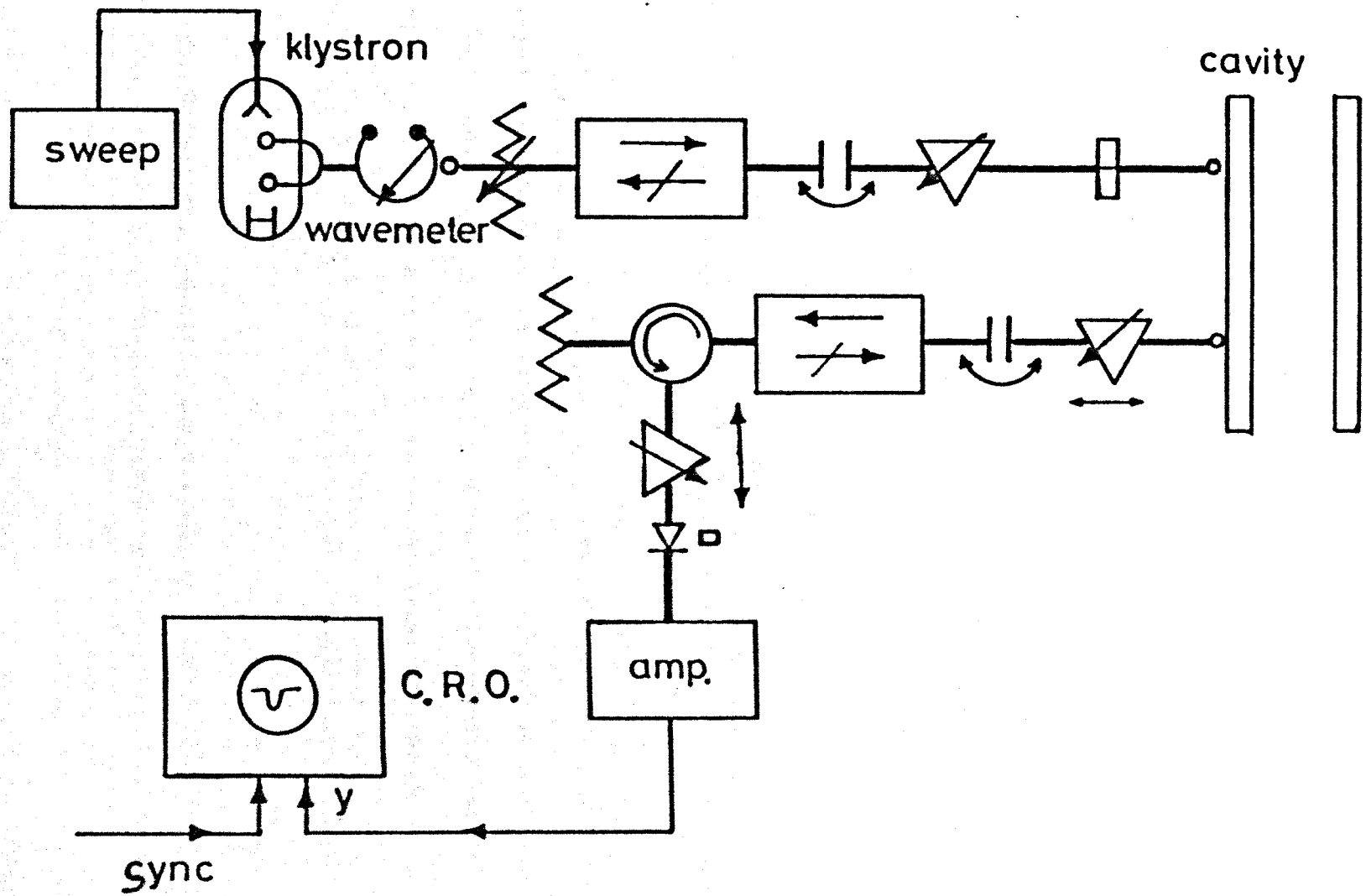

FIG 3.5 CRYSTAL VIDEO DETECTION SCHEME.

3.4.1.1 Signal-to-noise ratio and saturation effects

Two important sources contribute to the noise in a crystal video receiver. The first is "white" noise which is, frequency independent and the other is the "flicker" noise which is inversely proportional to the frequency. The thermal or "Johnson" noise combined with the shot noise can be written as:

$$V_T = \left[4kTB(R_B + R_A)\right]^{\frac{1}{2}} \qquad 3.5$$

where R_B is the video resistance of the crystal (Cordy, 1948), B is the noise band-width and R_A represents the noise generated at the amplifier. Its value is usually taken as 1200Ω. The noise band-width is defined as

$$B = \frac{1}{G_{max}} \int_0^\infty G(f)df$$

where G(f) is the gain response to frequency. First the signal-to-noise ratio due to thermal and shot noise will be determined and then the effect of flicker noise is considered. It should be noted that in both crystal video and superheterodyne detection the stimulated emission signal appears as a change in the power level transmitted through the cavity. In other words the quantity to be compared with the noise is not the emitted power by the beam ΔP_m but another quantity which depends on the particular receiver (Townes and Ceschwind, 1948). In crystal video detection, the rectified voltage as a result of the output power P_o can be written as (Found, 1948)

$$E_d = \Upsilon R_E P_o$$

where Υ is the crystal sensitivity. Therefore the change in E_d as a result of a small change in P_o is

$$\Delta E_d = \Upsilon R_B \Delta P_o \qquad 3.6$$

where ΔP_o is:

$$\Delta P_o = \frac{2Q_L}{Q_2} \Delta P_m \qquad 3.7$$

It can be shown that the power emitted by n molecules in the upper state focused into the cavity at resonance is (Shimoda, Wang and Townes, 1956)

$$\Delta P_m = n\hbar\omega_o \sin^2\theta \qquad 3.8$$

where

$$\theta^2 = W/W_c \qquad 3.9$$

$$W_c = \frac{\pi\hbar^2 A v^2}{16\bar{\mu}^2 L} \qquad 3.10$$

and W is the energy stored in the cavity at resonance due to an input power P_i given by

$$W_i = \frac{4Q_L^2}{Q_1} \frac{P_i}{\omega_o} \qquad 3.11$$

$\bar{\mu}$ is the average of the dipole matrix element ($\bar{\mu} = \mu/\sqrt{3}$). Eqn. 3.10 assumes a uniform field distribution within the cross section of the cavity A but takes into account the field variation along the length L. It also assumes uniform velocity v for all molecules in thermal equilibrium. Substituting in Eqn. 3.6 the following result is obtained

$$\Delta E_d = 2(Q_L/Q_2)\Upsilon R_B n\hbar\omega_o \sin^2\theta \qquad 3.12$$

using Eqn. 3.5 the signal-to-noise due to thermal and shot noise:

$$\frac{\Delta E_d}{V_T} = M(Q_L/Q_2)\frac{n\hbar\omega_o}{\sqrt{kTB}}\sin^2\theta \qquad 3.13$$

where

$$M = \frac{R_B T}{\sqrt{R_B + R_A}}$$

is known as the "Figure of Merit" which contains all the crystal parameters. As a crude estimate of the best signal-to-noise with crystal video detection ($\theta \simeq \pi/2$) take: $Q_2 \approx 10Q_L$; $n \approx 10^{14}$ sec^{-1}; $M = 50$; $\omega_o \simeq 48 \times 10^9$ Hz ; $kT \approx 10^{-21}$ joule; $B \approx 10^3$ Hz; then:

$$\frac{E_d}{V_T} \approx 4$$

It is true that the signal-to-noise given by the last equation can be improved by better coupling, that is increasing the ratio Q_L/Q_2 as much as practical, but even then two main problems remain. The first is related to the poor performance of crystal rectifiers at low frequencies as a result of the "flicker" noise and the other is the molecular saturation at high level of input power.

The spectral distribution of the flicker or the 'excess' noise can be written as (Baker, 1954)

$$G(f)df = \frac{AI^2 df}{f} \qquad 3.14$$

where I is the steady current flowing through the crystal and A is constant. The total noise generated is obtained by integrating

Eqn. 3.14 from f_1 to $f_1 + B$ where f_1 is the lowest frequency accepted by the amplifier and B is the noise band-width. Bosch (1961) showed that the 1/f relation holds accurately from 25Hz to 300KHz for point-contact silicon crystals. Obviously the power of f should become more than unity at high frequencies to allow convergence of the integral but it was shown (Robinson and Bosch, 1957) that this relation is valid up to 45MHz.

In the square low region Eqn. 3.14 can be written as:

$$G(f)df = \frac{\alpha P^2}{f} kTdf \qquad 3.15(a)$$

where

$$\alpha = 5 \times 10^{14} \ W^{-2} \ s^{-1}$$

but it seems more reasonable (Shimoda, 1960) to use the linear relation when the crystal is biased by a small RF signal. Then

$$G(f)df = \frac{\gamma P}{f} kTdf \qquad 3.15(b)$$

and

$$\gamma = 10^{11} \ \text{Watt}^{-1} \ \text{sec}^{-1}$$

the total noise is then:

$$P_N = PkT \ln\left(\frac{f_1 + B}{f_1}\right)$$

So, to compare the flicker noise with the thermal, the noise temperature T_N is defined as

$$T_N = \frac{P_N}{kTB} = \frac{P}{B} \ln(B/f_1)$$

for $P \sim 10^{-8}$Watt $f_1 \sim$ 1Hz; T_N = 7 which corresponds to a noise temperature of about 8dB. Actual measurements show however that the contribution of flicker noise can reach a value of 50dB when the crystal is reverse biased. It should be noticed that at low power both thermal and flicker noise are important. When $P > 10^{-9}$Watt , flicker noise is dominant. To investigate the effect of crystal video detection on resolution it should be recalled that the half linewidth of the emitted radiation is given by:

$$(\Delta\nu) = \sqrt{(\Delta\nu_o)^2 + (\Delta\nu_s)^2}$$

where $\Delta\nu_o$ is the broadening due to finite interaction time. Assuming that the field varies sinusioidally along the cavity axis then (Shimoda, Wang and Townes, 1956)

$$2\Delta\nu_o \approx 1.19v/L$$

$\Delta\nu_s$ is the broadening due to nonzero input power given by (Shimoda, 1960)

$$(\Delta\nu_s)^2 = \frac{E^2\bar{\mu}^2}{h^2}$$

recalling that

$$E^2 = \frac{8\pi W}{AL}$$

and using equations 3.8 - 3.10 the following result is obtained

$$(\Delta\nu_s)^2 = \frac{1}{8}\left(\frac{v}{L}\right)^2 \theta^2 \qquad 3.16$$

and the line width is

$$2\Delta\nu = \sqrt{1.4 + (\theta^2/2)}\ (v/L) \qquad 3.17$$

From equation 3.16 it will be noticed that the line broadening due to input power is proportional to θ, that is to $P_i^{\frac{1}{2}}$. For $\theta > 1$ it is seen that the line broadening due to high input power becomes comparable with that due to finite time of interaction. For good resolution θ must be much less than unity. But from equation 3.13 the sensitivity is proportional to $\sin^2\theta$ and for $\theta \ll 1$ the ratio $E_d/V_T \sim \theta^2$ takes small values.

3.4.2 The Superheterodyne Receiver

In the previous discussion it was shown that the performance of the crystal video receiver for weak maser signal detection is rather poor. Its sensitivity is limited by flicker noise which becomes dominant at low frequencies and saturation effects contribute considerably to the spectral line broadening, at a relatively high input power. It is worth while paying attention to the fact that increasing the modulation frequency does not improve the receiver sensitivity because it requires the use of a wider effective bandwidth (Gordy, 1948). Assuming that the modulation frequency is f_m then the receiver is expected to respond say up to $100f_m$ Fourier components. Increasing the modulation frequency by a factor N will increase the upper limit by the same factor and thereby requires the use of an effective bandwidth N times wider. The result is either that the noise bandwidth is increased or some signal is lost by the same factor. In either case no gain in sensitivity is achieved.

In contrast, the superheterodyne receiver overcomes most difficulties mentioned above. Not only does it practically eliminate the effect of flicker noise by amplifying the signal at 30MHz, but

being a linear receiver makes it more suitable for detection of weak signals on the basis of both sensitivity and resolution. The following argument explains the idea.

Let V_d be the signal detected by a receiver which operates in the square law region and V_s the signal detected by a linear receiver. By definition it follows that:

$$V_d = SV^2$$

$$V_s = GV$$

where S is the sensitivity of the crystal rectifier, G is the conversion gain and V is the signal to be detected which can be written as

$$V^2 = 2ZP$$

where Z is proportional to the waveguide impedance. The ratio of the detected signals is given by

$$\frac{V_s}{V_d} = \frac{G}{S} \frac{1}{2Z\,P^{\frac{1}{2}}}$$

The above equation illustrates that there exists a power level below which the superheterodyne receiver is the more sensitive of the two types of detection.

3.4.2.1 The transmission detection scheme

The particular detection schemes used in the present work differ slightly according to the specific experiment under investigation, but a typical one which includes all the important features of a practical transmission superheterodyne receiver is shown in Fig. 3.6. The klystron (OKI type 24V 10A) is stabilized by a Mos 3600 (Microwave

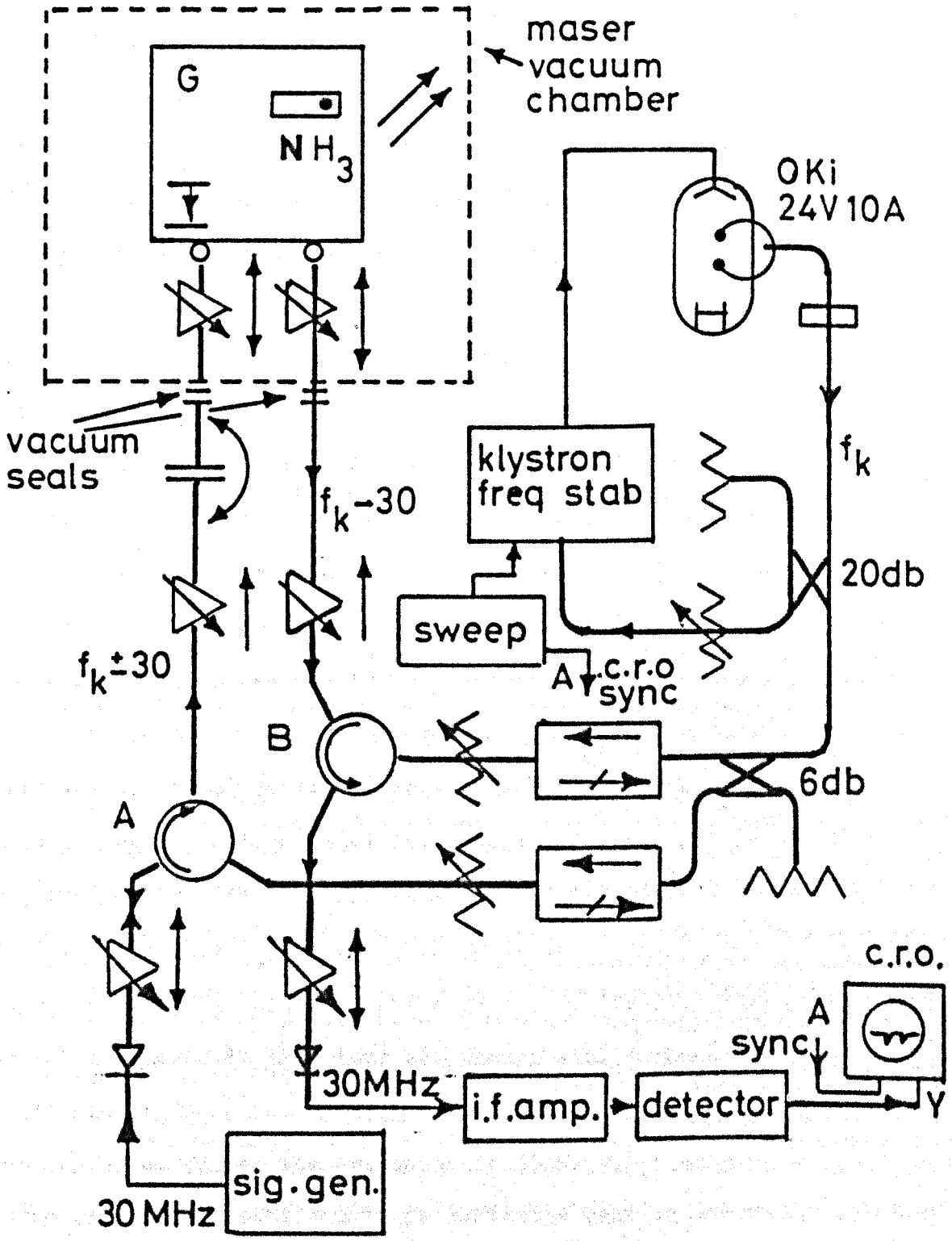

FIG. 3·6 MICROWAVE SYSTEM OF MASER OSCILLATOR-SPECTROMETER.

Systems, INC.) type frequency stabilizer. It provides a frequency stabilization of 1 part in 10^{-8} per hour. The reference voltage from the klystron is supplied by a 20dB directional coupler via an attenuator, which allows a flow of about 1mW power, into the stabilizer input. A sweep facility is also provided by applying a sawtooth voltage of about 1volt amplitude from an external sweep unit via a potentiometer. This allows an easy display of the emission lines and even narrow absorption lines (pressure $\sim 10^{-4}$ torr) can be easily "locked" and displayed. The microwave power is divided into two parts by using a 6dB coupler. One part passes through an attenuator, and an isolator to the circulator A. The impedance of the crystal is modulated at 30MHz by an RF generator so that the power reflected possesses two sideband components of frequencies $f_s = f_k \pm 30\text{MHz}$ where f_k is the klystron frequency. By proper matching the conversion gain of either of the sidebands (say $f_k - 30\text{MHz}$) is maximized and used to stimulate the maser transition at frequency f_o, by altering the frequency of the klystron. This allows the use of a single klystron for both input and local oscillator power without the need of two frequency control systems for separate klystrons. Since the cavity is tuned to frequency f_o and its quality factor $Q_o \gg f_o/30$, all other sidebands are reflected back and absorbed by the isolator. The second part of the power in the other arm passes also through an isolator then an attenuator to the circulator B and arrives at the cavity output coupling hole. Since its frequency is 30MHz off resonance with respect to the cavity frequency f_o, it is reflected back to the mixing crystal through the circulator B. It provides the local oscillator power. The maser signal is coupled to the transmitted sideband and passes through the circulator B to the mixer. If the signal is small compared to the local oscillator power, then the output is a signal at 30MHz whose amplitude is proportional to the amplitude of the maser signal. The

latter is then amplified at 30MHz. After rectification it is applied to the vertical input of the C.R.O., which is synchronized by the same sweep unit. This permits a display to be made of the signal amplitude as a function of frequency.

3.4.2.2 Signal-to-noise in a superheterodyne receiver

It is well known (Gordy, 1948) that superheterodyne detection is linear, and that the output voltage amplitude at the mixer output can be written as:

$$V_o = GV_s \qquad 3.17$$

where G is a constant proportional to the conversion gain and V_s can be written as:

$$V_s^2 = ZP_o \qquad 3.18$$

where P_o is the transmitted power and Z is proportional to the guide impedance. Assuming that the maser signal causes only a small change in P_o then

$$\Delta V_s = \frac{Z^{\frac{1}{2}}}{2} \frac{\Delta P_o}{P_o^{\frac{1}{2}}} \qquad 3.19$$

and the detected signal to be compared with the noise is:

$$\Delta V_o = \frac{GZ^{\frac{1}{2}}}{2} \frac{\Delta P_o}{P_o^{\frac{1}{2}}} \qquad 3.20$$

The noise generated by the receiver is taken as

$$V_N = G\,[4FkTZB]^{\frac{1}{2}} \qquad 3.21$$

therefore the signal-to-noise is:

$$\frac{\Delta V_o}{\Delta V_N} \equiv \quad S/N \;=\; \frac{1}{N_v} \quad \frac{\Delta P_o}{P_o^{\frac{1}{2}}} \qquad 3.22$$

where

$$N_v \;=\; [16FkTB]^{\frac{1}{2}} \qquad 3.23$$

using Eqns 3.7-3.11 the following equation is obtained

$$S/N \;=\; \frac{1}{N_v}\left(\frac{2Q_L}{Q_2^{\frac{1}{2}}}\right)\left(\frac{n\hbar\omega_o}{W_c^{\frac{1}{2}}}\right)\left(\frac{\sin^2\theta}{\theta}\right) \qquad 3.24$$

The expression given in Eqn. 3.24 can be viewed as three multiplying factors. The first depends on the coupling of the cavity to the waveguide, the second is a function of the physical properties of the maser and the third shows the effect of the excitation strength. Each should be maximized for best sensitivity.

In maximizing the quantity $Q_L/Q_2^{\frac{1}{2}}$ (or Q_L^2/Q_2) it is necessary to take into account that the resonator is usually designed to fulfill more than one function. For many practical uses it is desired that the coupling holes are made identical and placed symmetrically with respect to the cavity centre. In other words we demand that $Q_1 = Q_2$. In this case

$$\frac{Q_L^2}{Q_2} \;=\; \frac{Q_o^2\, Q_2}{\left(Q_o + 2Q_2\right)^2}$$

which is a maximum for $Q_1 = Q_2 = 2Q_o$. This gives a maximum value of

$$2\,\frac{Q_L}{Q_2^{\frac{1}{2}}} = \frac{Q_o}{2} \qquad 3.25$$

which indicates that there exists an optimum coupling for best spectroscopic sensitivity. Altering the second factor is not an easy matter because it means changing the parameters of the maser but it may be noticed that the sensitivity is proportional to $n\mu L^{\frac{1}{2}}/Av$. The factor $\sin^2\theta/\theta$ takes its maximum for $\theta \sim 1.16$ and gives a value:

$$\left(\frac{\sin^2\theta}{\theta}\right)_{max} \approx 0.73$$

According to Eqn. 3.16 the sensitivity has to be paid for in terms of line broadening of about 3KHz.

Substituting in Eqn. 3.24 the best signal-to-noise ratio is given by

$$(S/N)_{max} = 0.45 n\hbar \left[\frac{Q_o \nu_o}{W_c F k T B}\right]^{\frac{1}{2}} \qquad 3.26$$

3.4.2.3 Comparison of the two receivers

By Eqns. 3.13 and 3.22 the signal-to-noise ratios in video and superheterodyne detection can be written respectively as:

$$(S/N)_v = \frac{M}{[4kTB]^{\frac{1}{2}}}\,\Delta P_o$$

$$(S/N)_s = \frac{1}{[16FkTB]^{\frac{1}{2}}}\,\frac{\Delta P_o}{P_o^{\frac{1}{2}}}$$

therefore the ratio of the two is given by:

$$R_{v/s} = (2F^{\frac{1}{2}}M)\, P_o^{\frac{1}{2}} \qquad 3.27$$

It is important to notice that the latter result is independent on the radiation process in the maser action. In fact it is valid in any microwave detection process which employs a two port cavity. For $M = 50$; $F = 100$ it follows that

$$R_{v/s} > 1 \quad \text{for} \quad P_o > 10^{-6}\text{Watt} \qquad 3.28$$

which means that the crystal video method is more sensitive only for an output power greater than 1μW. This explains the relatively improved sensitivity of the video receiver in detection of absorption lines, especially when pressure broadening is the dominant factor for determination of the line-width, rather than saturation effects.

Now is it possible to imagine a case where crystal video is favourable for detection of stimulated emission? To answer that it may be recalled that the maximum sensitivity in superheterodyne detection occurs for

$$\theta = (W/W_c)^{\frac{1}{2}} \approx 1.16$$

where

$$W_c = \frac{3\hbar^2 A}{16}\pi\left(\frac{v}{\mu}\right)^2 \frac{1}{L}$$

and

$$P_o = \frac{\omega_b W}{Q_2}$$

For an ammonia spectrometer employing the inversion line $J = K = 3$ ($\mu = 10^{-18}$C.G.S.; $v = 5 \times 10^{-4}$cm/sec) and operated with an open

resonator of length L ≈ 20cm; A ≈ 2cm^2 it follows that

$$W_c \approx 7 \times 10^{-18} \text{Joule or } P_o \approx 10^{-10} \text{Watt}$$

Another fact to be noticed is that the reason why the sensitivities of the two receivers become comparable at high power is not because $(S/N)_v$ increases, but because $(S/N)_s$ decreases. That is, in any case, it is not possible to obtain sensitivities better than those given by Eqn. 3.13 using a crystal rectifier. Therefore the relevant question to be answered is; in what cases must the level of the stimulating power be raised for optimum sensitivity? The answer is for high values of W_c. While the maximum sensitivity in superheterodyne detection is proportional to $(1/W_c)^{\frac{1}{2}}$ as it is seen by Eqn. 3.26, it is independent of W_c in the case of crystal video detection (Eqn. 3.13). If W_c is increased by a factor of 10^4 (say, because μ decreases 100 times) then to sustain the condition of optimum sensitivity W should be increased by the same factor. Since P_o is proportional to W, it reaches the value of 10^{-6}Watt and hence the condition given by Eqn. 3.28 of equal sensitivity is satisfied. Notice that in this case (altering μ) the resolution is not affected by raising the power level, as far as maximum sensitivity is concerned. This result indicates that weak spectral lines saturate at higher levels of exciting power. If loss in resolution is not wanted then μ is the only variable of W_c (Eqn. 3.10) to be considered for a fixed frequency (fixed A). To summarise, it it appears that for most cases, stimulated emission spectra are better detected by a superheterodyne receiver, although there might be special cases where crystal video detection is to be considered. The choice will depend on the level of the output power and the effect of flicker noise.

An experimental varification of the theory developed in the

last sections, has actually been made (Lainé Truman and Hope , 1980). Although a maser which oscillated on several quadrupole satellites of the ammonia inversion line J = K = 1 was used (Maroof and Lainé, 1976) video detection of both oscillation and stimulated emission, although possible, was rather marginal.

3.5 THE ROOF-TOP SPECTROMETER

3.5.1 Sensitivity and Resolution

The roof-top resonator was incorporated in the molecular beam maser described previously and the strong inversion transition J=K=3 of ammonia was chosen for test experiments. A superheterodyne detection scheme was used for detection of either stimulated emission or oscillation, while state selection was provided by a ladder type state selector (Al-Jumaily and Lainé, 1979). With a quality factor of about 4000 (light coupling), stimulated emission was observed on the top of the cavity mode (lowest order), without Doppler splitting, thus confirming that the resonator can be used for molecular beam studies. Although the maser oscillated as the state selection was raised above 15KV, the signal-to-noise was poor due to poor coupling (see Sec. 3.2). After increasing the output coupling coefficient, the cavity was adjusted this time to the inversion line J = K = 1 which is rich in resolved satellite lines. In Fig. 3.7 the main line transition ($\Delta F_1 = 0$; $\Delta F = 0, \pm 1$) obtained by employing three different resonators is compared. The signal in (b) was detected by employing exactly the same maser system but with a circular plate Fabry-Perot resonator, while the signal appearing in (c) was obtained by employing a closed resonator (Krupnov and Shchuko, 1972). The improved resolution of the roof-top in comparison with both is obvious. To measure the actual resolution, the inner quadrupole high frequency side satellite line was

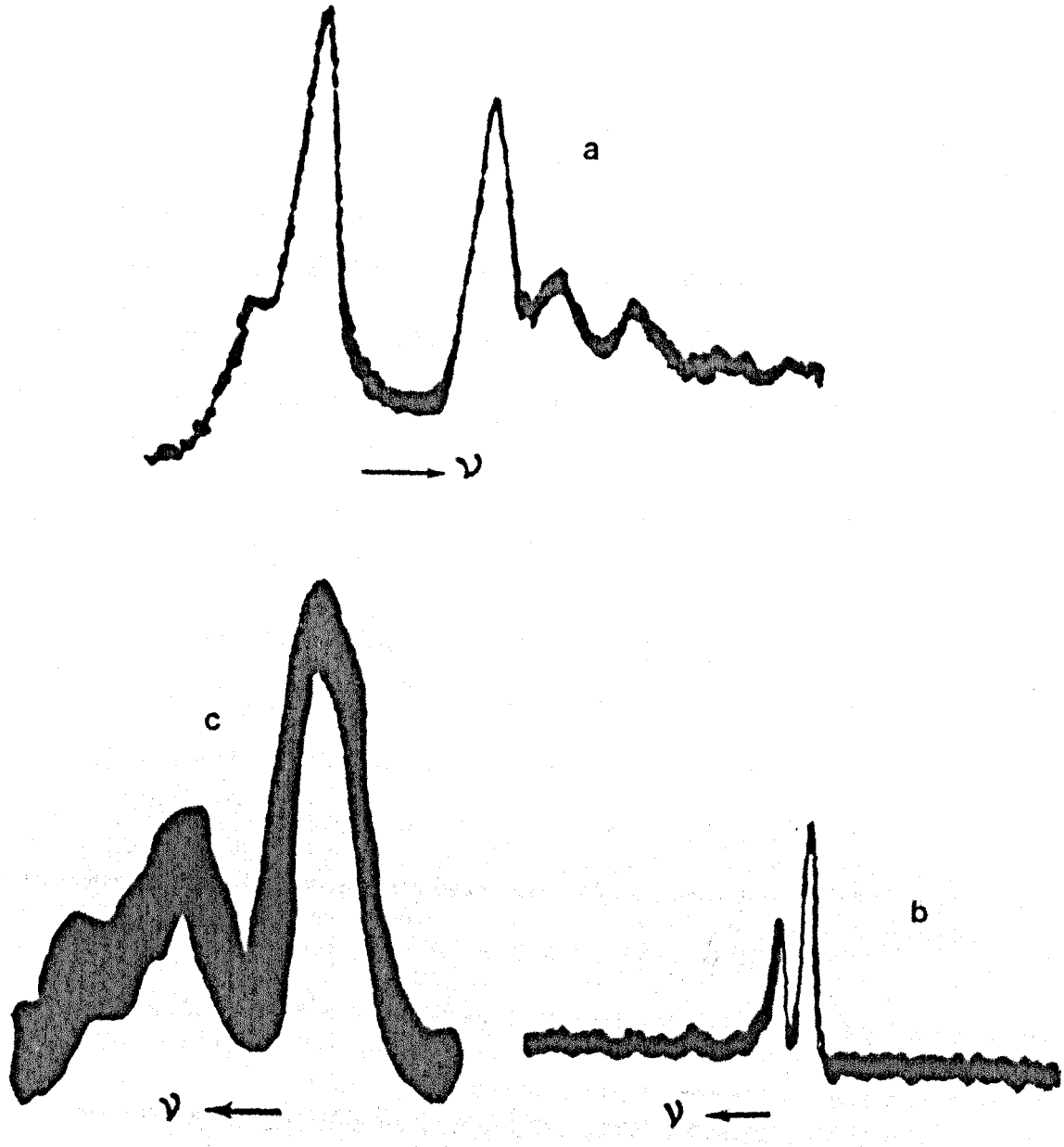

Fig. 3.7 Detection of the main inversion line J=K=1 of NH_3 using different resonators.

(a) The roof_top resonator.

(b) Circular Fabry_ perot (Smart, 1973)

(c) Cylendrical cavity (Krupnov and Shchuko, 1969).

used, where the frequency separation between the spin-spin interaction transitions $(F \longrightarrow F') = (3/2 \longrightarrow 5/2)$ and $(\frac{1}{2} \rightarrow 3/2)$ is about 45.9KHz (Fig. 3.8). Using this calibration the resolution at best signal-to-noise was found to be 6KHz. Following the discussion in Sec. 3.4 it must be seen that the resolution can still be improved if a better sensitivity were available by decreasing the input signal and thereby reducing saturation. It is worthwile emphasising the fact that results obtained in Fig. 3.7, 3.8(a) were taken for a sorting voltage of 8KV only, with a state selector which could operate at voltages as high as 25KV. Knowing that the maser was far from oscillation , it is clear that the sensitivity could be improved a great deal by raising the level of state selection. A good measure of the sensitivity was the observation of the weakest quadrupole satellites of the transition, namely the transitions $(F_1 = 0, F = \frac{1}{2}) \longrightarrow (1,3/2)$ and $(0,1/2) \longrightarrow (1,1/2)$. These transitions have never been reported previously in connection with open resonators and needed a state selection voltage of 20KV to be detectable (Fig. 3.10).

3.5.2 State Selection for the (RT) Resonator

The fact that the electromagnetic field inside the roof-top resonator is concentrated along its axis with a small height requires careful attention. A proper type of state selection improves sensitivity while an inadequate type reduces it. A ladder state selection for instance produces a sheet of molecules with a height which is several times greater than the vertical extent of the field. That means that some of the molecules (which may be most of them) enter the cavity but does not contribute to the signal since the probability of them being de-exited is very small. The result is poor signal-to-noise. This might explain the fact that the signal was optimized for a

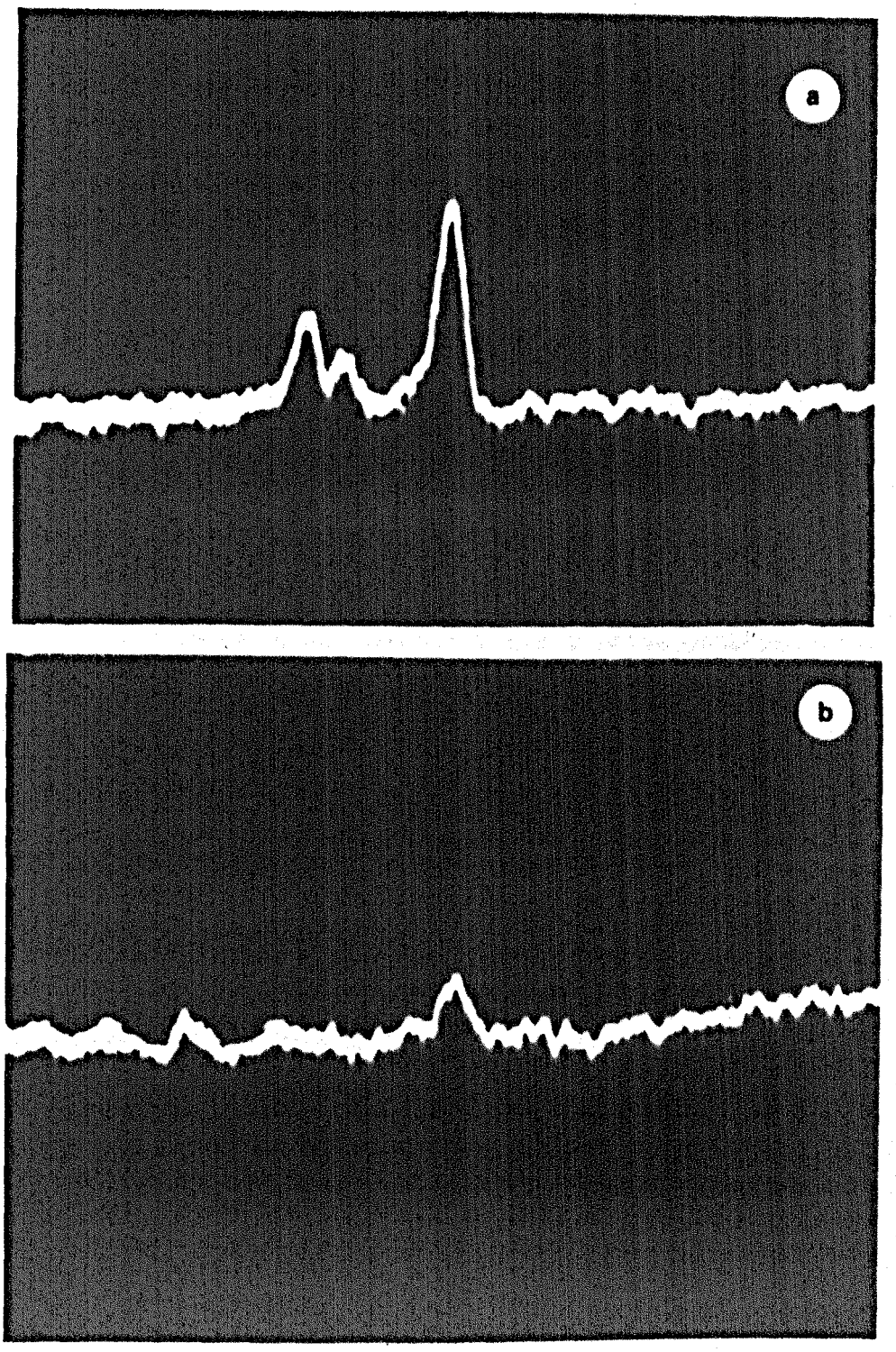

Fig. 3.8 Detection of the quadrupole satellites of the inversion line J = K = 1 of ammonia.

(a) Inner high frequency side.
(b) Outer low frequency side.

relatively low nozzle pressure (about 100torr for nozzle diameter of 0.09mm). Another fact that might be noticed (Eqns. 3.10, 3.26) is that the interaction of a given beam with a particular effective cross section area of the resonator gives rise to an improved sensitivity when this area is made smaller. This area can be reduced considerably in the case of a roof-top resonator and therefore an improved sensitivity is expected, provided an appropriate state selector is used. An attempt was made to verify this by using a ring type focuser (Al-Amiedy, 1979) which seemed to be the most appropriate for this type of resonator. Unfortunately, alignment problems arose in adopting the device for the open resonator system and its full potential was impossible to demonstrate. Nevertheless, when operated on the inversion line $J = K = 2$ a reasonable sensitivity was obtained (Fig. 3.9). The cavity was then tuned to its next higher order mode (two maxima of the electric field along the resonator axis), and a resolved split line resulted as shown in Fig. 3.9(b). Finally the experimental test not only proved the capability of the roof-top resonator of forming a spectrometer of improved parameters for molecular beam studies in the cm-wave region but was very convenient as far as technical difficulties were concerned. Its modification to mm-wavelengths appears to be quite feasible.

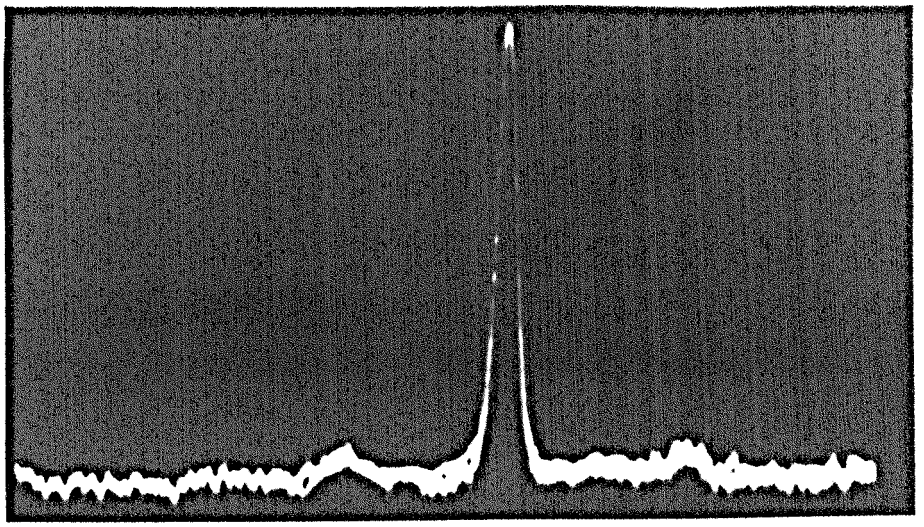

a

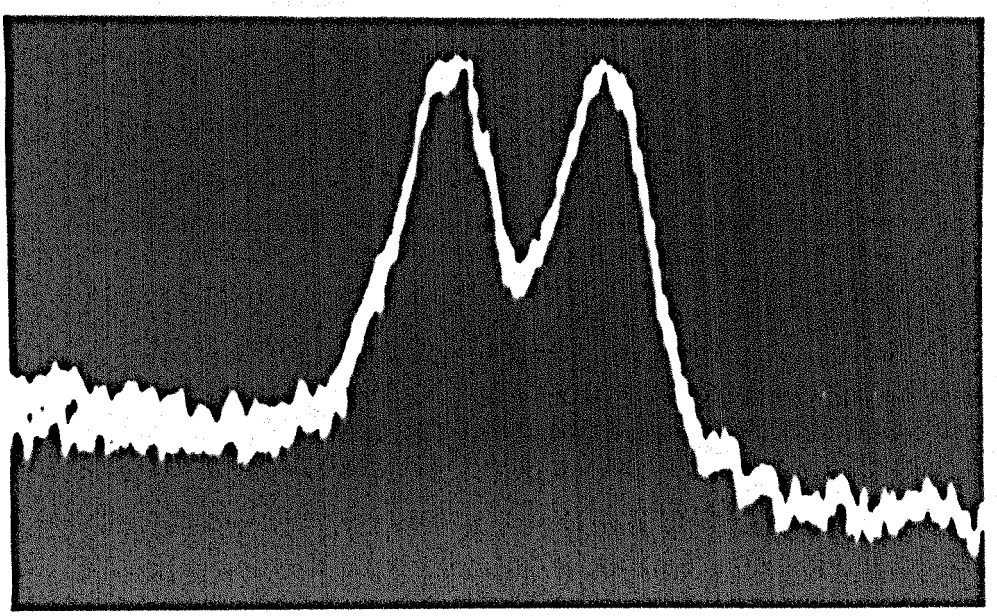

b

Fig. 3.9 Main line of the J = K = 2 inversion transition.

(a) The cavity is tuned to the lowest order mode.

(b) The cavity is tuned to the next higher order mode TEM_{100}.

CHAPTER 4

CHARACTERISTICS OF A MOLECULAR BEAM MASER OPERATED WITH A DISC RESONATOR.

4.1 REPRESENTATION OF ELLIPTICAL OSCILLATION

The amplitude characteristics of the molecular beam maser oscillator employing cylindrical cavities have been investigated both theoretically (Shimoda, Wang and Townes, 1956; Shimoda, 1957; Shimoda, 1960) and experimentally (Barnes, 1959; Bardo, 1969). Conventionally, the way in which the amplitude of oscillation of the maser varied with the two parameters, pressure behind the nozzle and voltage applied to the state selector was observed. The amplitude of oscillation under given conditions could be measured by a method known as "Bandpass display" (Smart, 1973). In this method, the local oscillator is swept through a range of frequencies greater than the amplifier bandpass and mixed with the signal derived from the oscillation itself. The output from the detector is then a display of the frequency response of the I.F. system and the height of the response is proportional to the maser oscillation amplitude.

This method however does not account for the vectorial property of the electric (or magnetic) field associated with the microwave radiation, namely its polarization. In fact it assumes a linearly polarized oscillation with its electric field lying along a fixed axis which is not altered during the course of investigation. In the case of cylindrical cavities, operated at the usually selected TM_{010} mode, this assumption is fully justified since in the cavity, molecules can couple only with microwave field polarized along its

axis of symmetry and thus emit linearly polarized radiation along that axis. In other words the states of polarization of such a cavity (de Lang, 1967) are not an expression of the polarization properties of the molecular transitions and the state selection anisotropy but fully dominated by the anisotropy of the cavity itself. The state of polarization of a TM_{010} cavity can be written as: (R.C. Jones, 1941)

$$\begin{pmatrix} E_x \\ \\ E_y \end{pmatrix} = \begin{pmatrix} E_x \\ \\ 0 \end{pmatrix} \qquad 4.1$$

where E_x is the electric field along the cylinder axis and E_y is orthogonal to it. Equation 4.1 holds irrespective of the properties of the medium and the anisotropy of state selection. Consequently complete information about the latter is not expected to be revealed.

In the case of open resonators however, the situation is completely different. For example the disc resonator which is about to be described or indeed any Fabry-Perot resonator with circular mirrors exhibits no such polarization constraint, but supports any polarization with an electric field parallel to the mirrors surface. It will be shown during the following chapters that transitions of the type $J \rightarrow J$, $J > 1$ drive the mode toward circularity while the anisotropy of the system (state selection included) tends to make it linear. In general, elliptical polarization is therefore expected, with ellipticity and orientation determined by both the molecular transitions and the anisotropy of the system.

Attempts to represent the characteristics of masers employing Fabry-Perot resonators, in the same manner as in the case of cylindrical cavities, yielded a peculiar behaviour of the amplitude of oscillation which could not be fully understood. In these cases what was actually detected is not the amplitude of oscillation but a

projection of the oscillation ellipse along an axis, arbitrarily chosen by the investigator. In fact the concept "amplitude of oscillation" as such was misused since it revealed different behaviours of the oscillation ellipse in accordance with the detected component. For example the oscillation characteristics of the double beam ammonia maser which is going to be described in this chapter were investigated by detecting the projection of the oscillation ellipse along the beam axis (Al-Jumaily, 1979). It was found that under some experimental conditions the "amplitude of oscillation" rose monotonically with increasing the state selection voltage. However, after a certain voltage value it started to drop. This led to the false conclusion that the strength of oscillation in the cavity was reduced because of space reorientation of molecules in the fringe field of the state selector. However this conclusion which might be correct in the case of closed cavities is not accurate for disc resonators since spatial reorientation is only capable of inducing transitions between the closely spaced M levels corresponding to the same upper inversion level (J,K^{+}). The effect will yield a change in the ellipticity of the mode which in turn will be detected and supported by the resonator.

Although the theory of Lamb (1964) predicted the occurence of elliptical oscillation for optical masers, the experimental confirmation for molecular beam masers was first reported by Smart (1973) and subsequently by Lainé et al (1976). Their measurements were facilitated by coupling oscillation power out of the cavity by the use of a rotating waveguide section in conjunction with a coaxial waveguide joint. With such an arrangement, the output waveguide could be rotated so that projections of the oscillation ellipse onto a certain set of co-ordinates were obtained. Assuming that the X-axis was chosen to lie along the molecular beam and the Y-axis orthogonal to it in the

plane of the mirrors surface then the X and the Y components of the oscillation ellipse in complex representation could be written respectively as:

$$E_x = a_x \exp i(\omega t + \psi_x) \qquad 4.2(a)$$

$$E_y = a_y \exp i(\omega t + \psi_y) \qquad 4.2(b)$$

Apart from measuring a_x, a_y as described above it was also necessary to measure the phase difference $\delta = \psi_x - \psi_y$ in order to specify the oscillation ellipse. This was done indirectly by measuring the ellipse major axis a, simply by rotating the output waveguide until maximum oscillation power was detected. Clearly the minor axis b could be measured in the same manner. However for slender ellipses this could not be done with reasonable accuracy and thus it was calculated from the known value of the wave intensity I given by

$$I \propto a_x^2 + a_y^2 = a^2 + b^2 \qquad 4.3$$

Consequently an ellipse that represented the polarization of the maser oscillation under given conditions (for example state selection voltage, molecular beam flux etc.) could be drawn.

However, this method was an awkward one for studies of the detailed behaviour of the oscillation polarization since several measurements were required to generate even a single ellipse, hence rapid changes could not be recorded. For example, the flip phenomenon which will be discussed in detail in the following chapter was not reported by the authors who employed this procedure of measurement. Nevertheless this is hardly surprising because the effect would have been observed if at all as a very small sudden jump in the projection of the oscillation ellipse and even then it could easily have been

attributed to amplitude rather than phase changes. This of course does not prevent a polarization flip occuring and passing unnoticed while rotating the output waveguide or even as a result of cavity frequency drift due to temperature changes. In the following section an alternative method of detection will be described but first new quantities for representation of the maser characteristics should be selected.

From equation 4.3 it can be seen that an adequate choice of parameter to measure the oscillation strength is $a_0 = \sqrt{I}$ rather than a_x or a_y since a_0 is independent of the choice of the axis of co-ordinates as it can be easily proved (Born and Wolf, 1959). Moreover, in order to specify a single state of polarization, measurements of the ellipticity e (the ratio of minor to major axis) and the orientation of the major axis ϑ with respect to the positive X-axis simultaneously with a_0, should be made.

4.2 DETECTION OF ELLIPTICAL OSCILLATION

The experimental set-up which is suitable for investigation of the oscillation behaviour of molecular beam masers employing Fabry-Perot resonators is described in Fig. 4.1.

Oscillation power from the two ports cavity was coupled at each port by means of a rectangular waveguide placed within a brass cylinder that was freely rotatable within a circular hole cut into the non-reflecting side of the mirror, such that its rotation axis was concentric with the coupling hole. This arrangement permitted rotation of the coupling waveguide. One of these waveguide sections served as an analyzer of the maser oscillation ellipse, in a similar way to a polaroid analyzer in optics. This rotatable waveguide was linked into

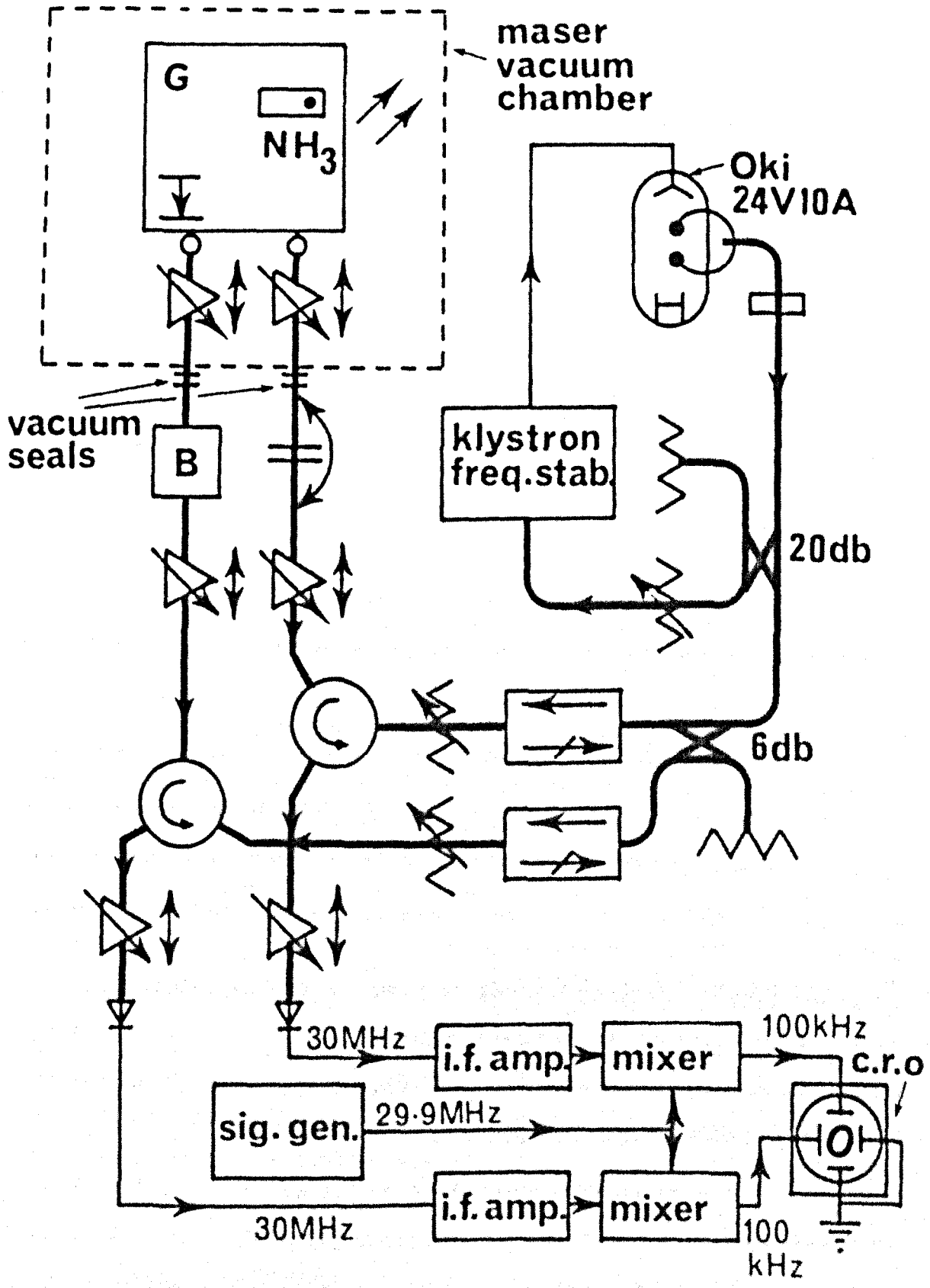

Fig. 4.1 Detection scheme for display of oscillation Polarization

the fixed waveguide system of the microwave detector system via a rotary joint (Kelvin Mfg. Co.,Model No. 111LX). The other waveguide polarization was fixed such that its transmission E vector was parallel to the molecular beam axis (the X-axis). In this way the angle between the E vectors of the microwave field within the two coupling waveguides could be set to any value. The two signals at a frequency $f_o \sim 24$GHz were then sent through the two independent arms of the dual channel double superheterodyne receiver to the 1N26 mixer diodes. The output from the klystron at a frequency $f \approx f_o + 30$MHz was divided by a 6db coupler to supply local-oscillator power to both mixers. Since the L.O. power at both mixers were phase coherent, the two I.F. signals after mixing were also phase coherent. After I.F. amplification at 30MHz (50db voltage gain, 2MHz band width), each output signal was fed into a balanced mixer (Hatfield, type 1754), using a common 29.9MHz frequency-stable signal source at the second L.O. to produce a 100KHz output at a level suitable for d riving the x and y amplifiers of a standard 1MHz bandwidth laboratory oscilloscope. By rotating the rotatable waveguide so that it transmitted microwave power with E vector in the Y-direction, the display of the oscilloscope was a Lissajous figure which represented the polarization ellipse of maser oscillation.

In order to set the zero of phase difference and relate the amplitudes of the components of maser oscillation to the same scale, the oscilloscope display was initially set up with parallel waveguide E vectors and the relative gains and microwave phases adjusted to give a linear oscilloscope trace, set at 45° to the x and y axis. Since the cavity mirrors were circularly symmetric, the spatial distribution of the electromagnetic field inside the passive interferometer was also circularly symmetric. Moreover the two signals were coupled through circular holes with identical diameters and equally spaced from the

mirror's centre. Thus to a good approximation it could be assumed that the two $\underline{E}$ vectors at the coupling points inside the resonator had equal intensity, ellipticity and phase. In principle the approximation could be made as good as desired by more careful measurements of the coupling hole diameters and their spacing. To check the validity of calibration, the level of excitation was varied and also an axial magnetic field perpendicular to the mirror surface was applied while the two coupling waveguides were set with parallel E vectors. No noticable change on the polarization was observed. This also indicated that the zero phase difference and equal amplitudes were preserved by the detection scheme.

The rotatable waveguide was then rotated by 90° in preparation for the Lissajous figure display. A check was made that the relative gains of the two signal paths were not significantly disturbed by the final waveguide rotation by using the fact that circular polarization was obtained under conditions of strong oscillation when a magnetic field $\sim 5 \times 10^{-5}$ T was applied perpendicularly to the plane of the cavity discs (D'Yakonov, M. I., 1966).

The feature of the experimental scheme described above was therefore to allow the behaviour of the oscillation ellipse to be observed visually, without change of loss anisotropy during the measurements. To achieve this it was necessary to phase-lock the klystron to a high stability quartz crystal by means of a microwave frequency stablizer.

Finally it is worthwhile pointing out that the same detection scheme which was used to detect the usual stimulated emission could be exploited to detect the maser oscillation. This was done, simply by inverting the direction of the circulator used in the stimulating signal arm and turning off the sweep.

4.3 THE EXPERIMENTAL SYSTEM

4.3.1 Construction Considerations:

The maser system which is about to be described was originally constructed in order to provide more oscillation power than was available from an already existing single beam ammonia maser. This would facilitate the investigation of several phenomena which could not be explored due to the lack of sensitivity. Another objective achieved was the oscillation on the weak inversion $J = K = 1$ of ammonia (Al-Jumaily, 1979) which has not yet been reported in the open literature.

To obtain more power from the maser, the main identifiable components, namely, gas source, state selector and resonator, had to be constructed according to certain criteria given by the theory of the maser oscillator. According to this theory the oscillation condition is given by

$$\left(\frac{\theta}{\sin\theta}\right)^2 = \frac{n_s}{n_{th}} \qquad 4.4$$

where n_s is the number of state selected molecules per second and the threshold rate of flow n_{th} is

$$n_{th} = \frac{h\nu^2 A}{4\pi^2 \bar{\mu}^2 LQ} \qquad 4.5$$

L is the diameter of the cavity and the other variables have the same meaning as in Ch. 3. For a given coupling coefficient the output oscillation power is proportional to θ. Since θ is a very sharp function of n_s/n_{th} especially for $n_s \approx n_{th}$ a sharp increase in the

oscillation power is expected either by increasing n_s or decreasing n_{th}. If in Eqn. 4.5 we write A = Ld where d is the mirrors separation then as a rough aproximation we obtain

$$n_{th} \propto \frac{1}{Q}$$

which indicated that Q should be increased as much as possible.

Also it can be shown that n_s increases rapidly with increasing the length of the state selector and the input beam flux (Shimoda, 1960). As a crude estimate $n_s \propto l^2$ where l is the length of the state selection (The relation is exact for a 2n-pole focuser). By doubling the length of the state selector and taking into account the fact that the maser system employed two beam sources, n_s is expected to increase 8 fold.

A complete description of the system mechanical design is given by Al-Jumaily (1979). However to understand the way experiments in the present study were conducted a brief description of the essential components of the system is given.

4.3.2 The Vacuum Assembly

A block diagram of the double beam ammonia maser is shown in Fig. 4.2. A three vacuum chamber system was adopted. The two opposite nozzle sources were housed in almost identical side chambers (nozzle chambers) and the disc resonator was fitted to the bottom of the big middle chamber (main chamber). Front and back general views of the apparatus are shown in Fig. 4.3 and Fig. 4.4 respectively (Al-Jumaily, 1979).

The main chamber consisted of a 42cm high, 50cm internal diameter rolled nonmagnetic stainless steel cylinder with 0.4cm wall thickness. An arrangement of six ports fabricated from stainless steel

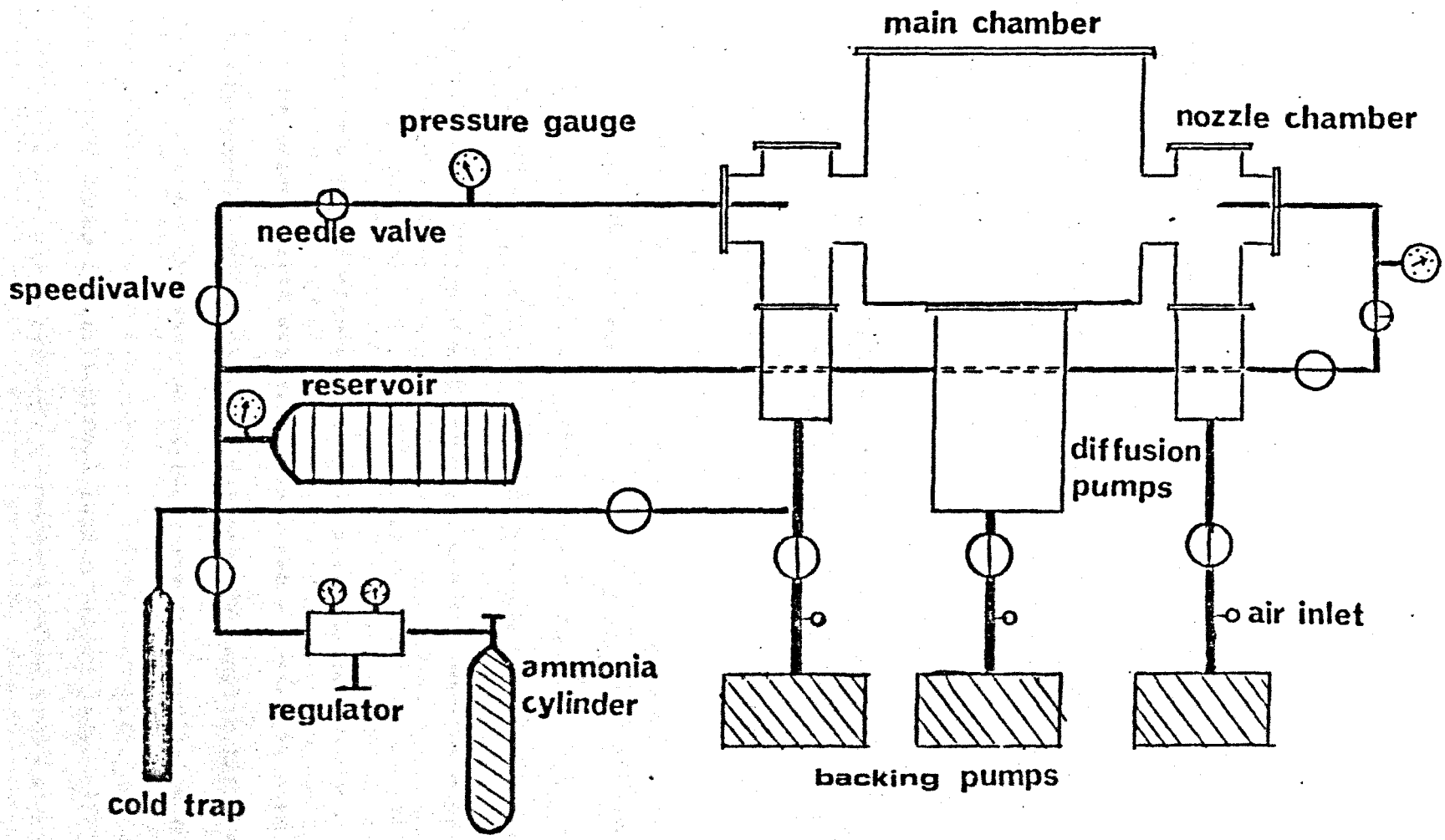

Fig·4.2 Block diagram of maser vacuum assembly and ammonia supply

tube was used. Two cylinders mated with the nozzle chamber and carried the skimmer holder. The front and the back tubes were fitted with identical 2.54cm thick perspex discs. The front disc (Fig. 4.3) carried the two coupling waveguides to the two ports disc resonator and the electrical lead-throughs for thermal tuning, Stark field application and the Helmholtz coils which provide a known value of magnetic field perpendicular to the resonator mirrors. The back perspex window carried the pirani and the ionozation gauges to monitor the pressure in the main chamber and also a rotary shaft vacuum seal to allow fine tuning of the cavity resonance frequency during operation. Two flanges for the tubes of 6.35cm diameter each , carried the electrical lead-through to the state separator from the EHT supply. The top was fitted with a stainless steel lid which carried a liquid nitrogen trap and the base supported a nine inch diffusion pump.

Each nozzle chamber also had a six port arrangement made of stainless steel tubes and joined to a rectangular box. One tube mated with the main chamber and the opposite was closed with a flange and carried both a liquid nitrogen trap and the ammonia supply to the nozzle. The back and front ports were closed by flanges and each carried a liquid nitrogen trap and a rotary vacuum seal for adjustment of the skimmer slit width. The top was fitted with a perspex disc which carried an ionization gauge head to monitor the nozzle chamber pressure and the bottom supported a six inch diffusion pump.

Using 704 siliconeoil (which has 10^{-7}torr limiting pressure) to charge the diffusion pumps, a vacuum of $\sim 3\times10^{-6}$torr in the main chamber could be reached without cryogenic pumping after 2 hours provided the system was not exposed to the atmosphere for long. The pressure in the main chamber dropped to about 8×10^{-7}torr when the liquid nitrogen traps were charged and rose to about 1×10^{-6}torr when

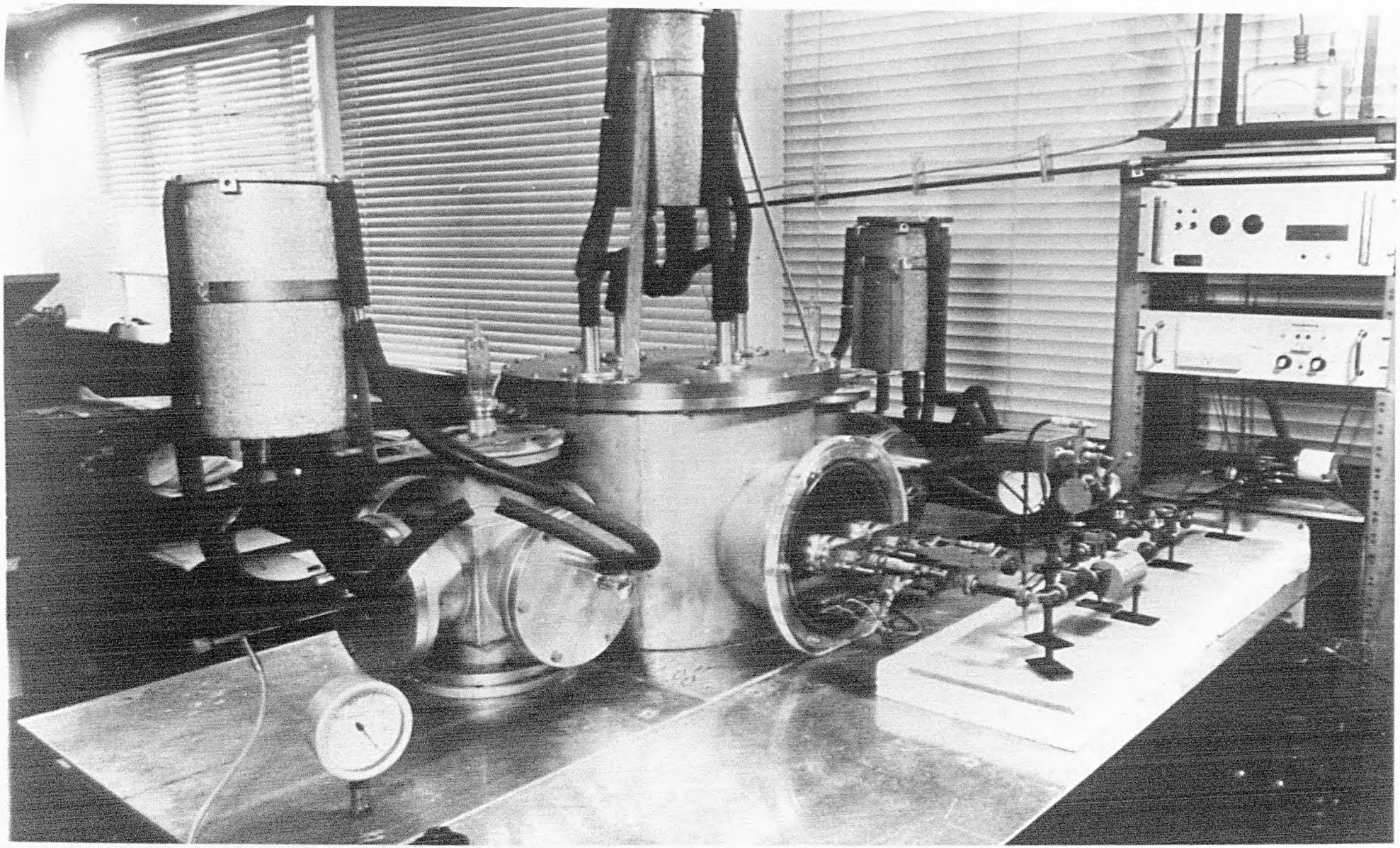

FIG. 4.4 GENERAL VIEW OF THE MASER

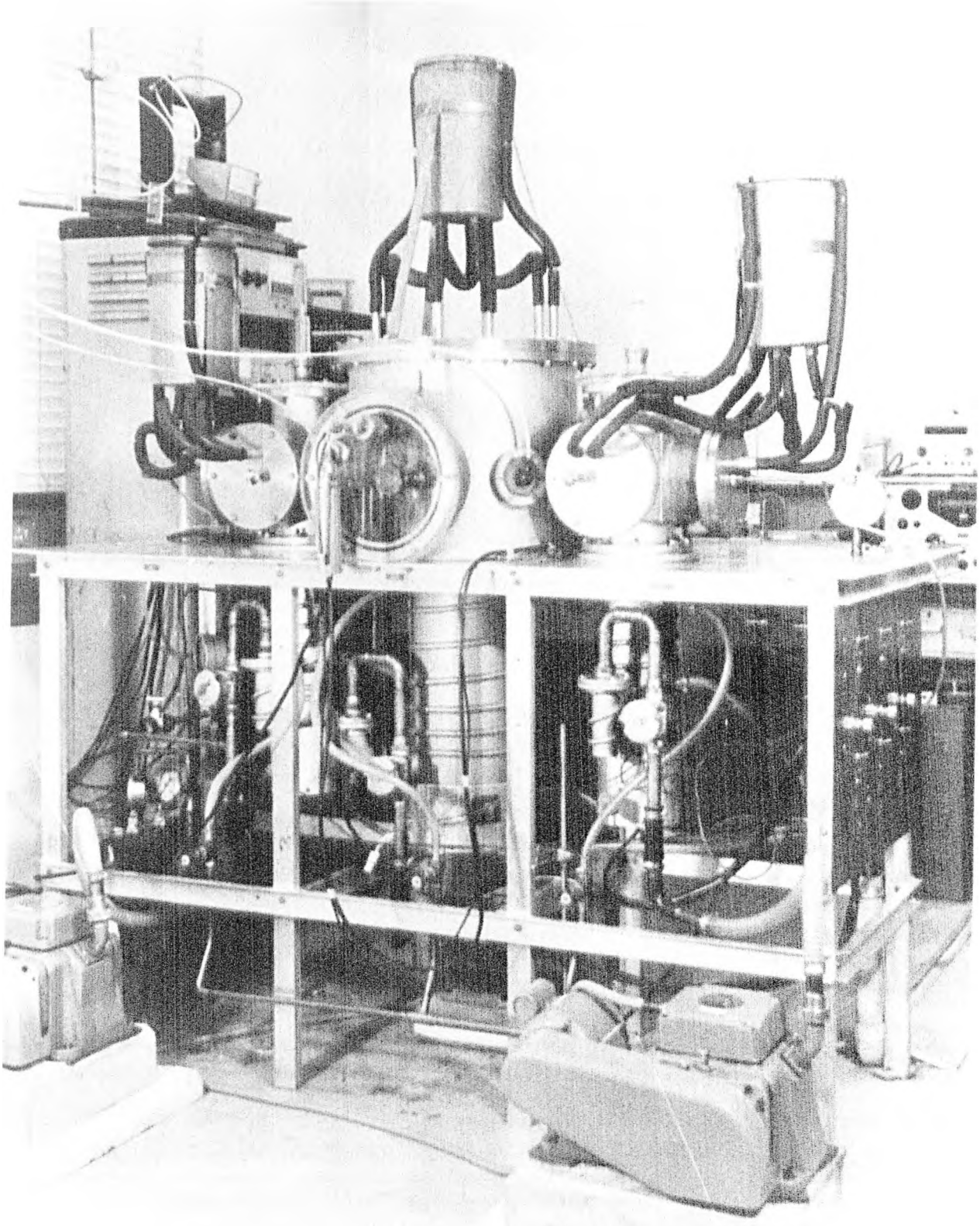

FIG. 4.3 GENERAL VIEW OF THE MASER

the molecular beam was introduced. An important practical feature of the vacuum system was that the oscillation power was found to be very sensitive to the main chamber pressure between 1.5×10^{-6} and 3×10^{-6} torr. In fact for pressures above 4×10^{-6} torr the maser oscillation ceased completely. This unfortunate fact was attributed to the large size of the main chamber and to the rather large distance between the state selectors and the resonator.

4.3.3 The Resonator

The resonator used in the present system was the Fabry-Perot type with plane circular mirrors. The geometry was the most convenient for study of the system anisotropy (for example state selection), the properties of molecular transitions and also Stark and Zeeman spectroscopy. This is due to the fact that all states of polarization corresponding to a given resonant mode were degenerate (see the following chapter).

From previous experiments (Smart, 1973) it was concluded that the quality factor of disc resonators with $\lambda/2$ separation at the microwave frequencies depends on both conduction and diffraction losses. Copper with conductivity $\sigma \sim 5.80 \times 10^{7} sm^{-1}$ was therefore used for the construction of the mirrors while their diameter was increased up to 22.5cm where diffraction losses become negligible. Also it was already known (Barchukov and Prokhorov, 1961) that the Q values of such resonators depend highly on the parallelism and flatness of the mirrors. As a result, an appropriate tuning mechanism was essential to reduce the mirror bending to a minimum level.

As usual, two tuning mechanism were employed. Coarse tuning was used for adjusting the tilt angle and bringing the mirrors'

separation to $\sim\lambda/2$ on the bench and fine tuning allowed the adjustment of the resonance frequency to the molecular transition during operation. Coarse tuning was obtained by adjustments of three micrometer screws, each carried by an aluminum barrel, against three glass rods carried by a three armed frame to which the tuning mirror was bolted. The aluminum barrels were carried by another identical three armed frame to which the fixed mirror was bolted (Fig. 4.5). The frame of the fixed mirror itself was bolted to the front plate of the cavity frame which in turn was bolted firmly into the base of the main chamber. Fine tuning was obtained by turning a shaft from outside the chamber, hence causing a spring attached to the tuning mirror frame to compress or decompress. In this way, the pressure on the three armed frame could be changed causing the tuning mirror to move longitudinally while remaining flat and parallel to the fixed mirror(Fig. 4.6(a)).

Power was coupled into or out of the cavity through two identical circular holes. Their centers lay along a diameter parallel to the molecular beam axis and were symmetric with respect to the mirror center. The coupling coefficient ~ 0.1 for each, compromised the oscillation and the spectroscopic application of the maser.

4.3.4 The Molecular Beams Formation

The ammonia supply system can be seen in Fig 4.2. The source of ammonia was a lecture size cylinder of anhydrous liquid ammonia. Purification was carried out by freezing in a trap cooled with liquid nitrogen and then pumping away the uncondensed impurity gases using the backing rotary pump. The trap was then warmed and the ammonia was allowed to expand into the reservoir. The gas flow from the reservoir to each nozzle was controlled by hand valves and two finely adjustable needle valves. The connection between the needle valves and nozzle

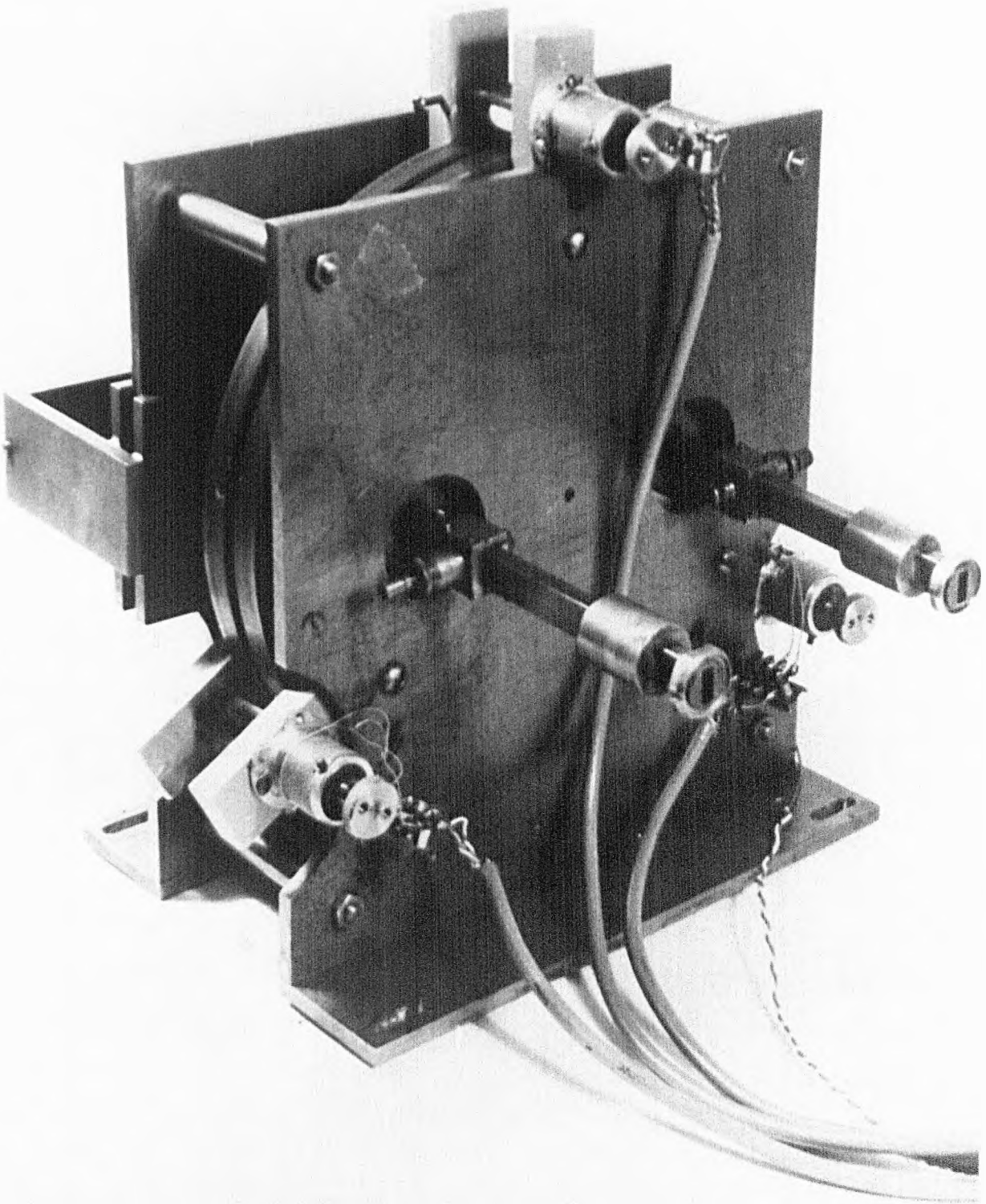

FIG. 4.5 VIEW OF THE OPEN CAVITY SHOWING THE TUNING MICROMETERS, THERMAL TUNING BARRELS AND COUPLING WAVEGUIDES

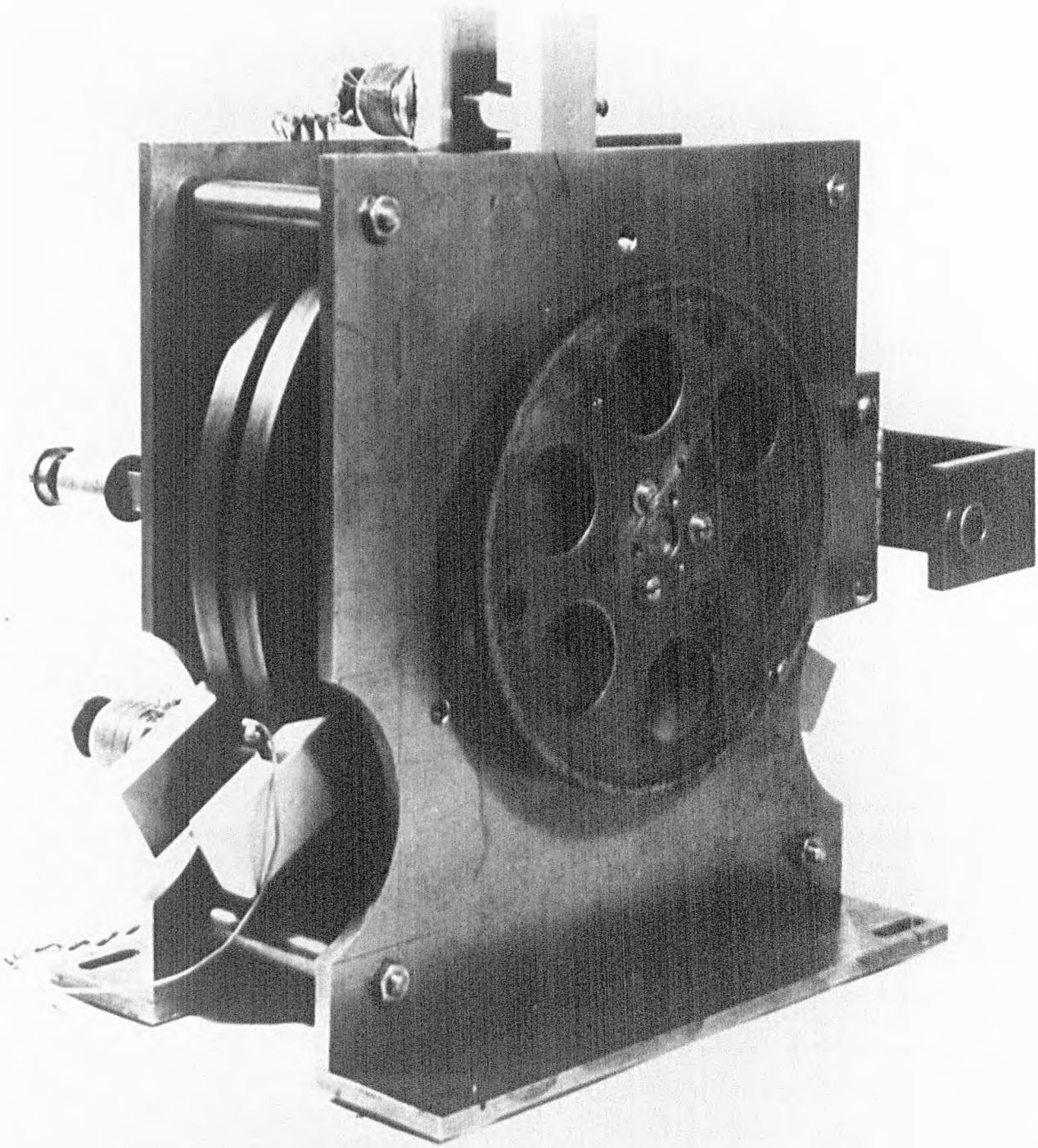

FIG. 4.6(a) VIEW OF THE OPEN CAVITY SHOWING THE GEAR USED FOR FINE MECHANICAL TUNING

holder tubes was by flexible P.V.C. tubes. The pressure behind the nozzle was measured by a gauge with a pressure range 0-760torr.

The beam was formed by allowing the ammonia to expand through the nozzle hole which was drilled into a brass disc 6mm in diameter, soldered to the tube holder. Watch-makers drills were used to make nozzles of about 0.1mm diameter. The gas jet then struck a roof-like skimmer which allowed a collimated molecular beam to advance towards the state separator as a wedge of molecules, while the remaining gas was pumped away.

The nozzle-skimmer combination was found to be advantageous from the viewpoint of high intensity, narrow velocity distribution and rotational cooling of molecules. It provided an intense beam and increased the population of the low lying rotational energy states for state selection and thereby more active molecules for interaction (Kantrowitz and Grey, 1951). From previous experiments (Maaroof and Laine, 1976; Laine and Truman, 1977) it was realized that if the skimmer was shaped to give a flat rather than a pencil-like beam, the advantages of the nozzle-skimmer arrangement could be applied to open resonators. Also, experiments were carried out to compare the nozzle-skimmer with the effuser diaphragm arrangement in conjunction with a disc resonator. It was shown that the former combination revealed much higher spectral line sensitivity and also lower oscillation threshold (Al-Jumaily, 1979). However, for this to be achieved some points in the skimmer design had to be considered.

First, the surfaces of the two pieces of brass which formed the skimmer lips were ground as sharp as possible and highly polished to ensure that the number of molecules which struck the edge and then scattered was minimal. Second, since the skimmer was then to be

immersed in a supersonic stream it was necessary to make the outside angle of the skimmer lips as acute as possible to avoid a detached shock in front of the slit. Moreover, since the beam intensity was highly dependent on the velocity distribution of molecules and on the nozzle pressure (Anderson and Fenn, 1965) then for a given nozzle hole diameter, adjustment of both skimmer-nozzle distance and the width of the slit during operation was essential. This was done by mounting each lip on a brass strip of dovetail cross-section which fitted into slots made in a stainless steel plate thus allowing the jaw to slide to and fro with respect to the other jaw as the mechanical lead-through carried by the nozzle chamber flange was screwed and unscrewed. Also the skimmer plate was fixed on a 10cm long cylinder with a diameter slightly smaller than the nozzle chamber port to give a sufficient large gap for movement in three dimensions. This allowed an easy alignment of the beam to the cavity centre. This together with the longitudinal movement of the holder of the two nozzle tubes enabled the beam flux entering the state selectors to be controlled.

4.3.5 The State Selectors

The transverse ladder type state selector was used in conjuction with a 4mm Fabry-Perot maser (Krupnov and Skvortsov, 1964). In the present system this type was chosen mainly because of two reasons. First it provided a sheet of molecules that suited the spatial distribution of the microwave field inside the cavity and thus allowed as many active molecules as possible to interact with the field and produce stimulated emission. Second, because this geometry was the plane shape analogue of the ring type focuser which showed high efficiency (Becker, 1963). Each state selector comprised a double array part of 22 electrodes and another two parts with 21 electrodes,

each soldered on two pieces of a supporting brass frame as shown in Fig. 4.6. The middle part was tapered so that after the state selector was assembled, the distance between the two planes of electrodes was 0.8mm at the entrance and 4.8mm at the exit. This arrangement was used since it was found that a state selector whose exit area was larger than its entrance area, narrowed the angular spread of the molecular trajectories and thus produced a better focusing effect.

Becker showed that the ratio h/d where 2h is the average separation of the double array and d is the distance between two successive electrodes is the characteristic value of this type of state separator. After some simplifications the focusing force was calculated to be proportional to

$$F(z) \propto \frac{\overline{\partial E^2}}{\partial z} \propto \exp\left(-\frac{2\pi h}{d}\right) \left\{\exp(2\pi z/d) - \exp(-2\pi z/d)\right\}$$

It is easy to show that for $z/d \approx 0$

$$F(z/d) \propto z \approx 0$$

and

$$\frac{\partial F(z/d)}{\partial (z/d)} \propto \exp(-2\pi h/d)$$

Therefore to obtain a reasonable force in the vicinity of the centre h/d must be smaller than a certain value, otherwise molecules travelling near the centre in their lower energy state might be projected into the resonator. An experimental value of $h/d \approx 0.5$ was chosen for the present state separators (Smart, 1973). This was a compromise between obtaining strong focusing action in the centre plane of the separator

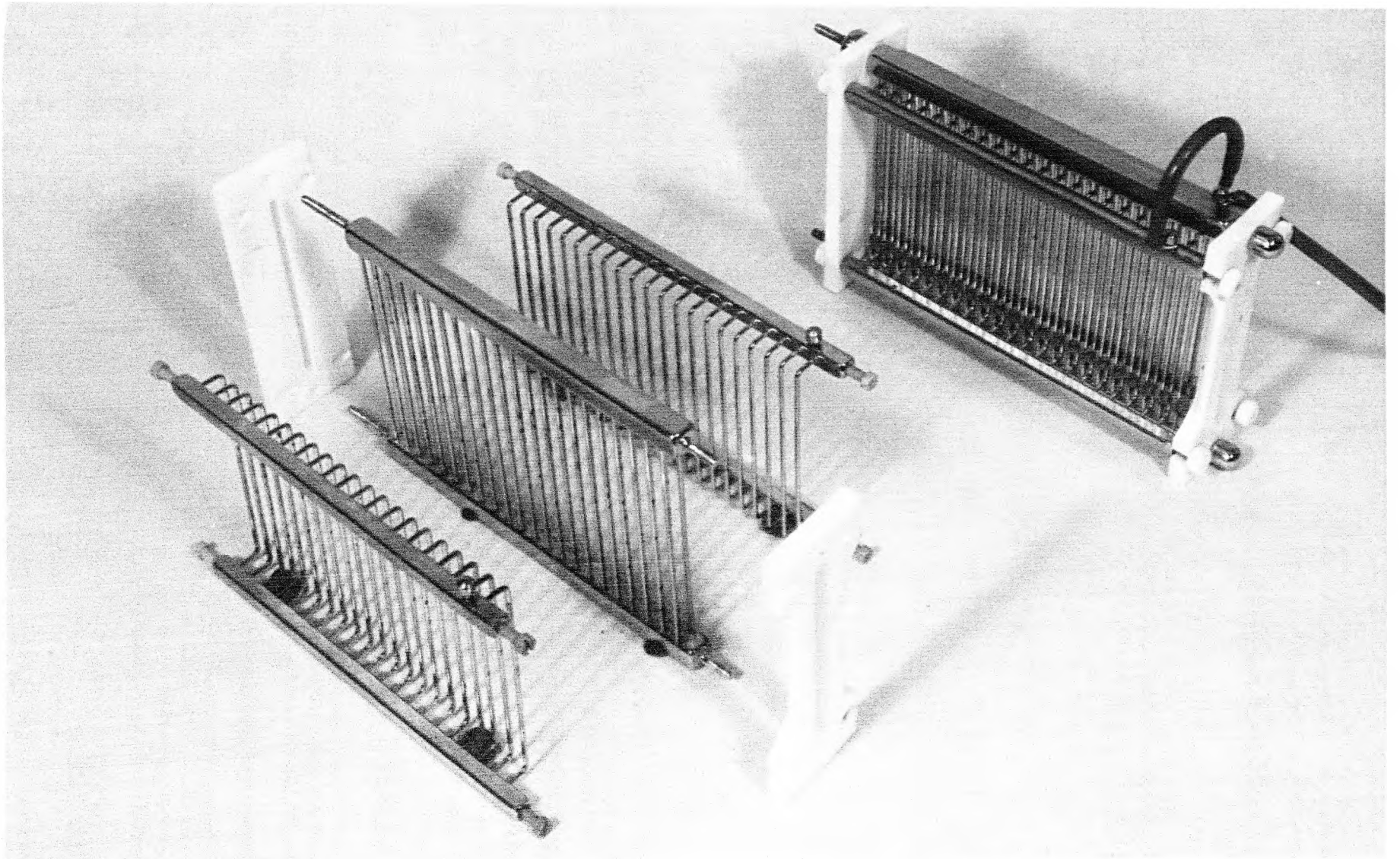

Fig 4.6 The ladder-type State selector.

and maintaining a large cross sectional area with which to capture the molecular beam.

4.4 CHARACTERISTICS OF THE INVERSION LINE J=K=2 OF AMMONIA

The new method of detection was employed to investigate the characteristics of the double beam maser described in previous sections. The strong inversion line J=K=2 of ammonia was chosen for the preliminary experiments. With nozzle diameters of about 0.1mm and pressure of 400torr behind each nozzle, the threshold of oscillation was about 4.8KV. The oscillation power derived from the maser was sufficient to operate the detection scheme and provide a signal-to-noise ratio of 1:15 for the oscillation ellipse display. The main observed features of the oscillation polarization could be summarized as follows:

1) At state selection voltages less than 6.5KV, the oscillation was linearly polarized but inclined at an angle $\vartheta \sim 13^{\circ}$ to the molecular beam axis. It was observed that the ellipticity of oscillation increased monotonically with state selection voltage. Example of this are shown in Fig.4.7. The departure of linear oscillation from the horizontal common axis of the two molecular beams was attributed to deviation in the alignment of the state selectors and to the rotation of the linear oscillation in the cavity in the weak magnetic field of the laboratory (8.8×10^{-6}T). The latter result was first reported by Culshaw and Kannelaud (1964) concerning the polarization of a single mode He-Ne laser operated at the transition J=1 → J=2. The rotation was at first interpre ted on the basis of the molecular transition but later the resonator anisotropy was considered in the theoretical derivation (Kannelaud and Culshaw, 1966). At a state selection voltage $V_s \approx 13$KV the polarization became circular

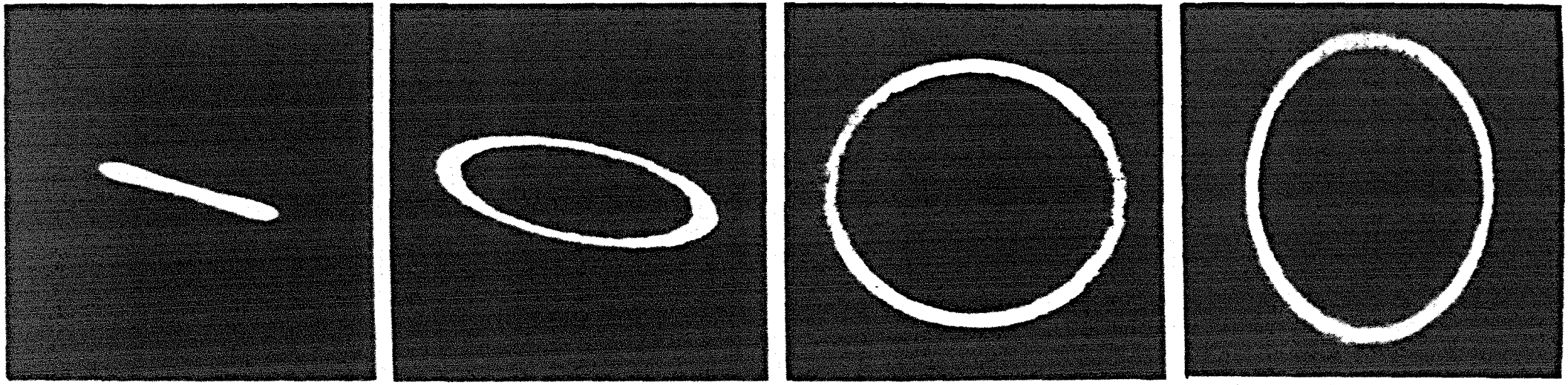

(a) (b) (c)

Fig. 2

while for higher excitation levels the oscillation exceeded circularity, that is it had its major axis pointing in a direction almost vertical to the beam axis, as shown in Fig. 7(d).

2) Tuning the cavity across the molecular transition resulted in reducing the amplitude of oscillation ($a_o = \sqrt{a_x^2 + a_y^2}$). However, no measurable change in the orientation ϑ was observed during the cavity tuning. It was therefore established that the anisotropies of the passive resonator were negligible with respect to the strong anisotropy of the state selector at low voltages.

3) There was slight rotation ($\sim 2^\circ$) of the polarization ellipse as the state selection voltage was raised from 6 to 10KV. This rotation may be attributed to the variation in the angle of rotation as a function of the ellipticity under the earth's magnetic field and to the effect of spatial reorientation of molecules in the fringe field of the state selectors. For larger state selection voltages the ellipticity approached unity and thus the angle ϑ was not well defined. The behaviour of the polarization ellipse azimuth as a function of state selection voltage is shown in Fig. 4.12.

4) For ellipticities $e > 0.2$ there were two stable states of polarization, with different ellipticities and orientations. The polarization ellipse could be flipped from one orientation to the another by slight tuning of the cavity.

5) For state selection voltages less than 9KV which is well below saturation, the variation in the ellipticity was much sharper than the slight rotation of the major axis as shown in Fig. 4.12. Therefore to a good approximation ϑ could be considered constant as a function of state selection. Since the following relations between the ellipse parameters must be fulfilled (Jerrard 1954).

$$\cos(2\epsilon) = \frac{\cos 2\upsilon}{\cos 2\vartheta} \qquad 4.6$$

where $\upsilon = a_y/a_x$

and $\epsilon = \tan^{-1} e = \tan^{-1} b/a$

then for constant ϑ the variation in e is only due to the variation in υ that is in the ratio a_y/a_x. In other words, the state selection induces emissive anisotropy. Moreover, since equation 4.6 must be fulfilled regardless of the phase relation of the two field components it can be argued that emissive anisotropy alone is responsible for the ellipticity variation as a function of the state selection voltage.

A comprehensive explanation of these results including the flip phenomenon which is based on the theory of the maser oscillator at zero and weak magnetic field is given in the following chapters. However, some interesting features of the oscillation characteristics can already be seen by plotting the oscillation ellipse parameters as a function of state selection voltage. In Fig. 8, 9 and 10 the oscillation component parallel to the beam axis a_p, the component vertical to the beam axis a_v and the resultant amplitude of oscillation a_o are plotted for different values of pressure behind the nozzles. These curves were constructed by measuring the ellipse parameters a_x, a_y, a, b, ϑ directly with the aid of a magnifier from the photographic negatives where the Lissajous figures displays were recorded. In the extreme cases $e \sim 0$ and $e \sim 1$ it was more accurate to include only some of the measured parameters in the data while the others were calculated from the well known ellipse relations (Born and Wolf, 1959).

The first thing which draws attention while examining the curves in Fig. 8 is perhaps the somewhat unusual behaviour of the

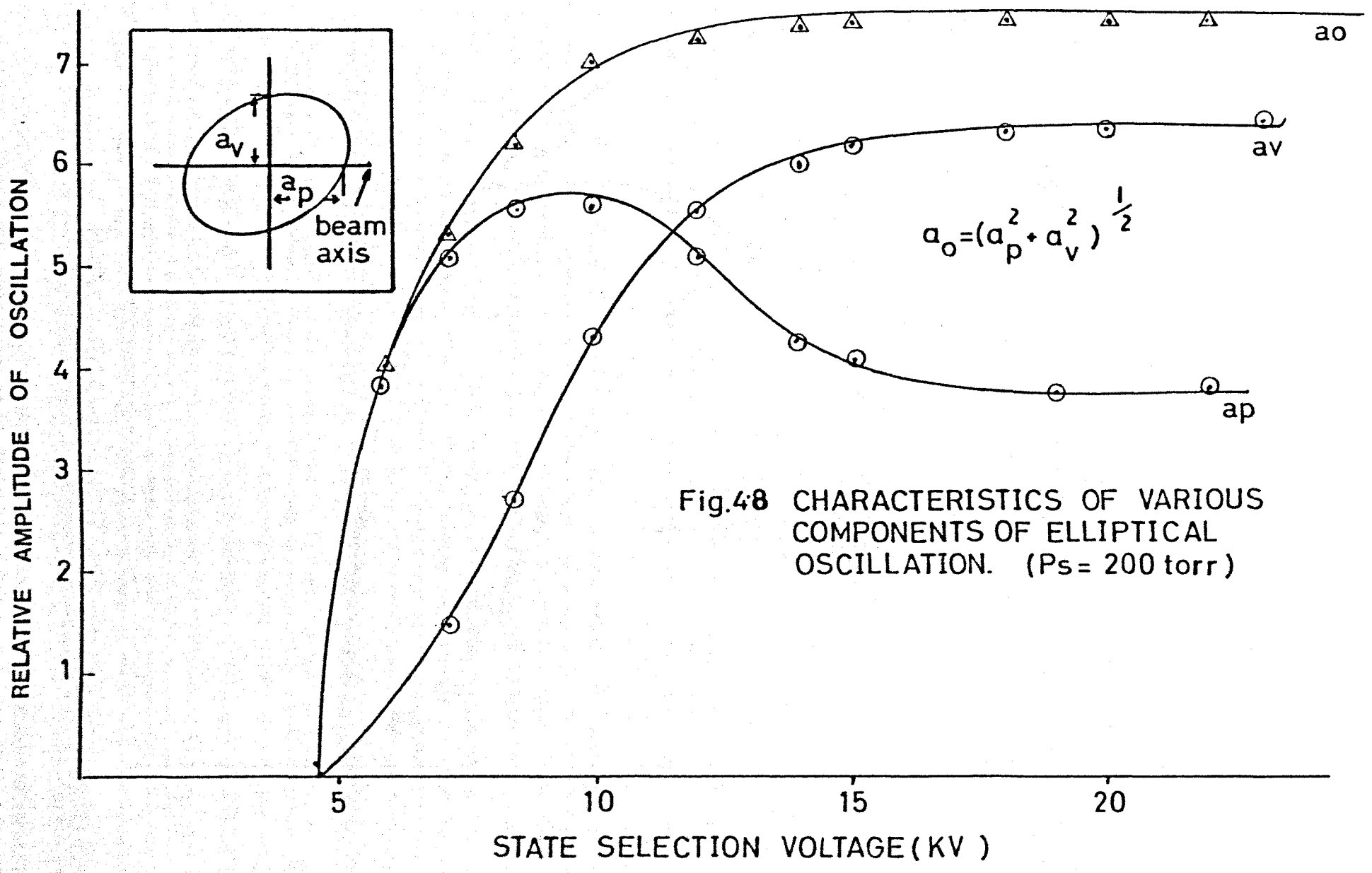

Fig.48 CHARACTERISTICS OF VARIOUS COMPONENTS OF ELLIPTICAL OSCILLATION. (Ps = 200 torr)

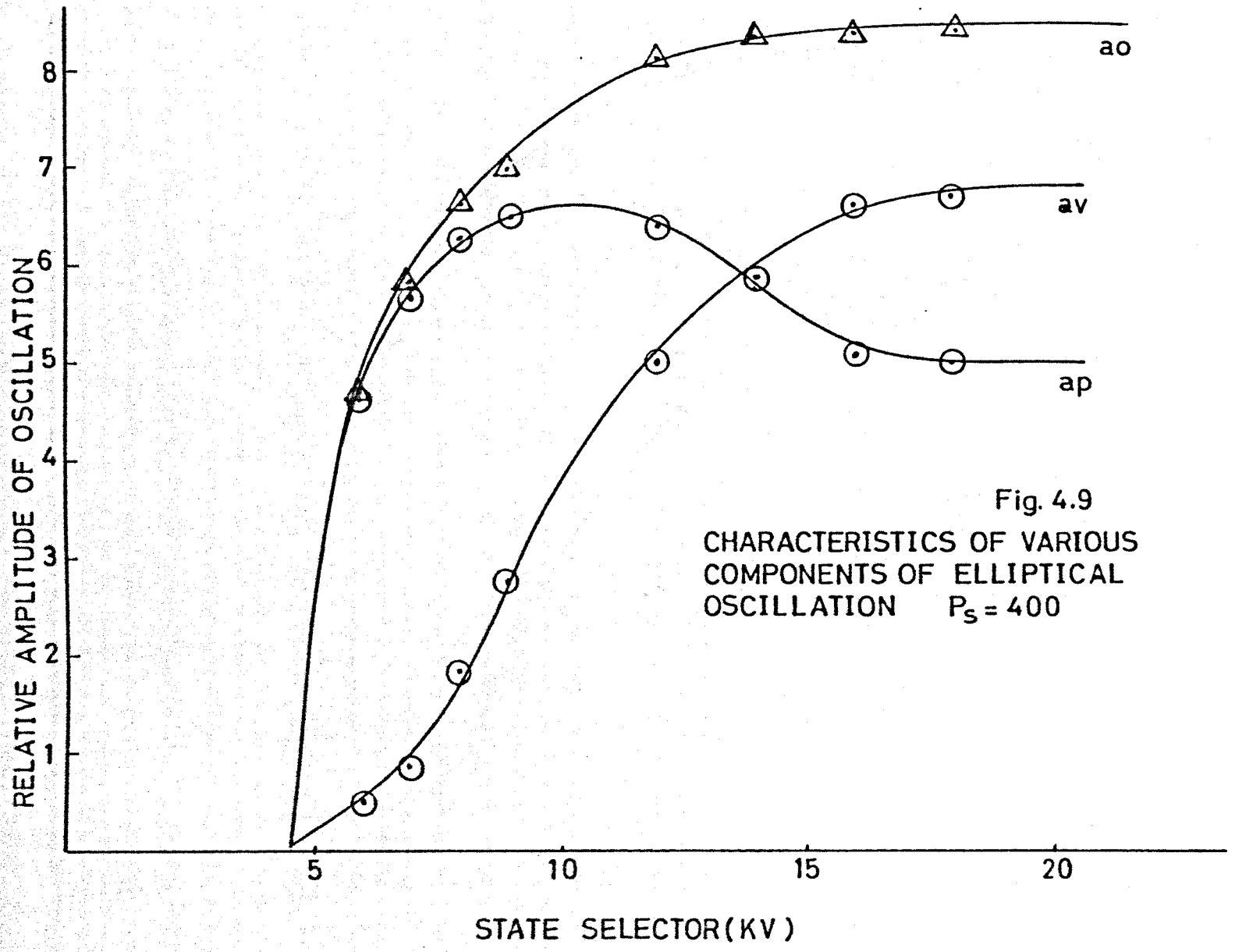

Fig. 4.9
CHARACTERISTICS OF VARIOUS COMPONENTS OF ELLIPTICAL OSCILLATION $P_S = 400$

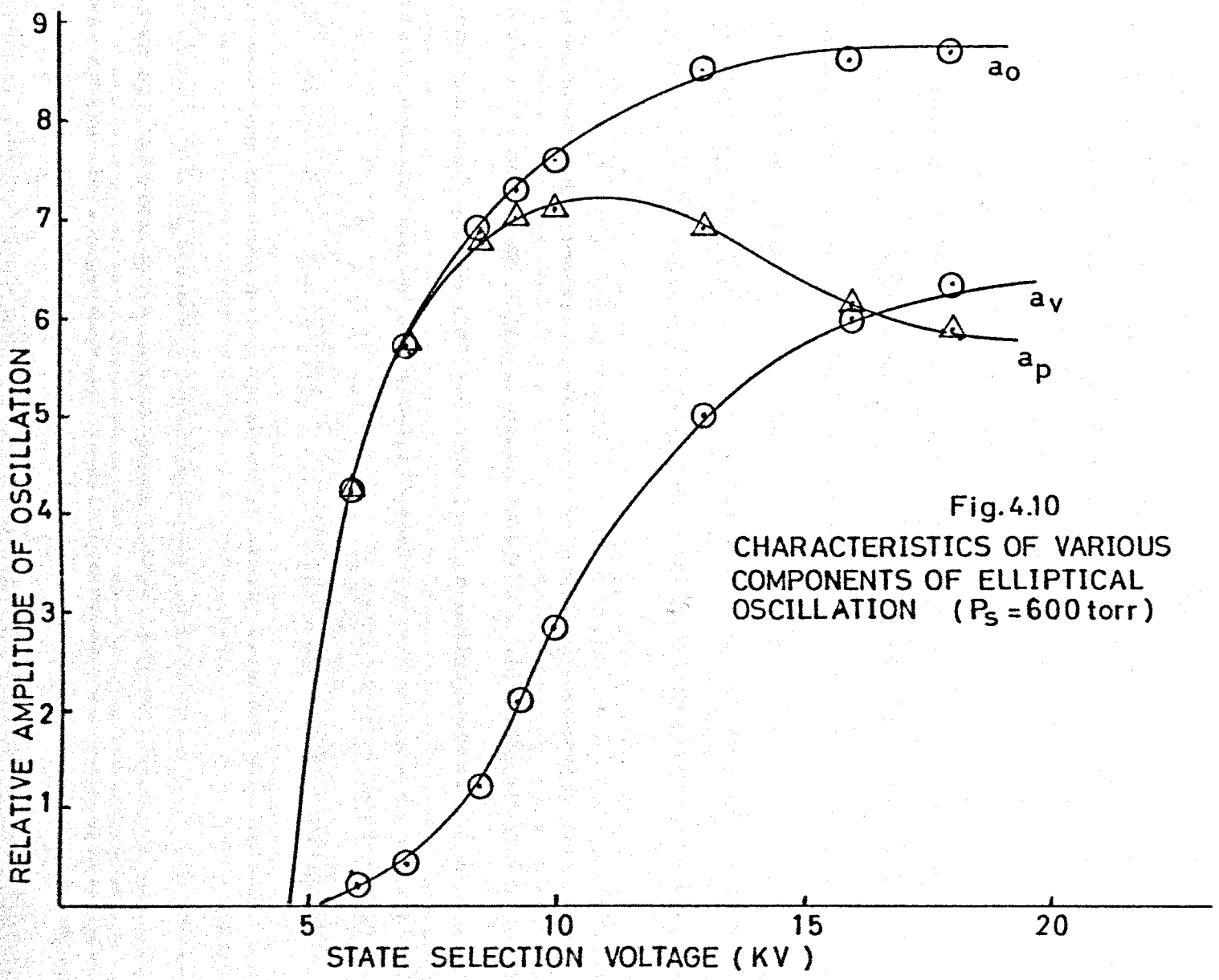

Fig. 4.10
CHARACTERISTICS OF VARIOUS COMPONENTS OF ELLIPTICAL OSCILLATION (P_s = 600 torr)

oscillation component a_p. At state selection voltages smaller than a certain value $V_s = V_d$ it rises monotonically. However at higher voltages, there is a drop in the oscillation component before saturation occurs. The phenomenon repeats itself for different gas pressures but at different values of V_d. The same effect was previously observed by Al-Jumaily (1978) who employed the same maser and the conventional detection scheme (Fig. 3.6) to measure directly the oscillation component parallel to the beam axis without realizing the elliptical properties of the maser oscillations. To help in an explanation of the drop effect the following facts should be considered. First, that its magnitude is well outside the range of error in the measurements. For example, when the pressure behind each nozzle is 200torr the relative drop in the amplitude is more than 20% (Fig.4.8) while the percentage error in taking the measurements is about 7%. Second, although the anisotropy of the resonator and perhaps some imperfections in the state selector design can explain the fact that the oscillation ellipse does not saturate at circularity, they cannot possibly be responsible for a drop in the amplitude of oscillation component. Finally, it is clear from Figs. 8, 9 and 10 that the drop in a_p is not accompanied by a similar decrease in the resultant amplitude of oscillation as the latter continues to increase until saturation. From all that it may therefore be concluded that what actually occurs is not a loss in the energy derived from the beam but a transfer of energy from one polarization direction to another. Such effect can be fully interpreted by the well known spatial reorientation phenomenon (Basov et al., 1964). After leaving the state separator at low voltages molecules no longer have an isotropic orientation in space since molecules which have maximum projection of angular momentum M along the longitudinal field are more efficiently state selected. Those molecules will also interact more strongly with the microwave field polarized along the beam axis and

thus are expected to contribute mainly to the oscillation component parallel to the beam axis. However, above a certain value of E.H.T. the state selection of this type of molecules starts to saturate and thereby a_p becomes more sensitive to the spatial reorientation of those molecules in the region between the state selectors and the resonator. The condition of adiabatic focusing of molecules moving under the effect of an inhomogeneous electric field is given by (Schiff, 1968)

$$\frac{H_{int}}{\tau\hbar\omega_{12}^2} \ll 1 \qquad 4.7$$

where H_{int} is the interaction hamiltonian, τ is the time of flight and ω_{12} is the transition frequency. At $\omega \approx$ 24GHZ the left hand side is about 10^{-6} (Shimizu and Shimoda, 1961) and thus the adiabatic focusing condition is fulfilled. However, at frequencies $\omega_{12} \sim$ 1MHz the above condition is no longer valid and transitions between the closely spaced Stark M levels are bound to occur. The probability for such a transition is given by (Basov et al., 1964)

$$\left|a_{M\pm1}\right|^2 = \frac{1}{\hbar\omega_{int}} \times \frac{(H_{int})_{max}}{\tau} \int_0^{\tau} \exp\left\{ i\left[\int_0 \omega(t)_{MM'}\, dt\right] dt \right\}$$

where ω_{inv} is the inversion frequency. At first $a_{M\pm1}$ increases as a function of state selection. However for voltages greater than a certain value ω_{12} exceeds a certain value so that the condition for adiabacity given by Eq. 4.7 is again satisfied.

It should be emphasized that the oscillation component a_v does not show a drop effect for the simple reason that it saturates at a higher level of state selection. Also since the fringe field of the state selection is longitudinal, molecules which contribute to this component are expected to suffer less from the effect of spatial

reorientation.

The behaviour of the oscillation ellipse as a function of the pressure behind the nozzles at constant state selection voltage is given in Fig. 4.11. The optimum pressure at 9KV is about 350torr while the drop in the amplitude of oscillation at higher pressures is attributed to the collision of molecules in the state selectors and in the resonator.

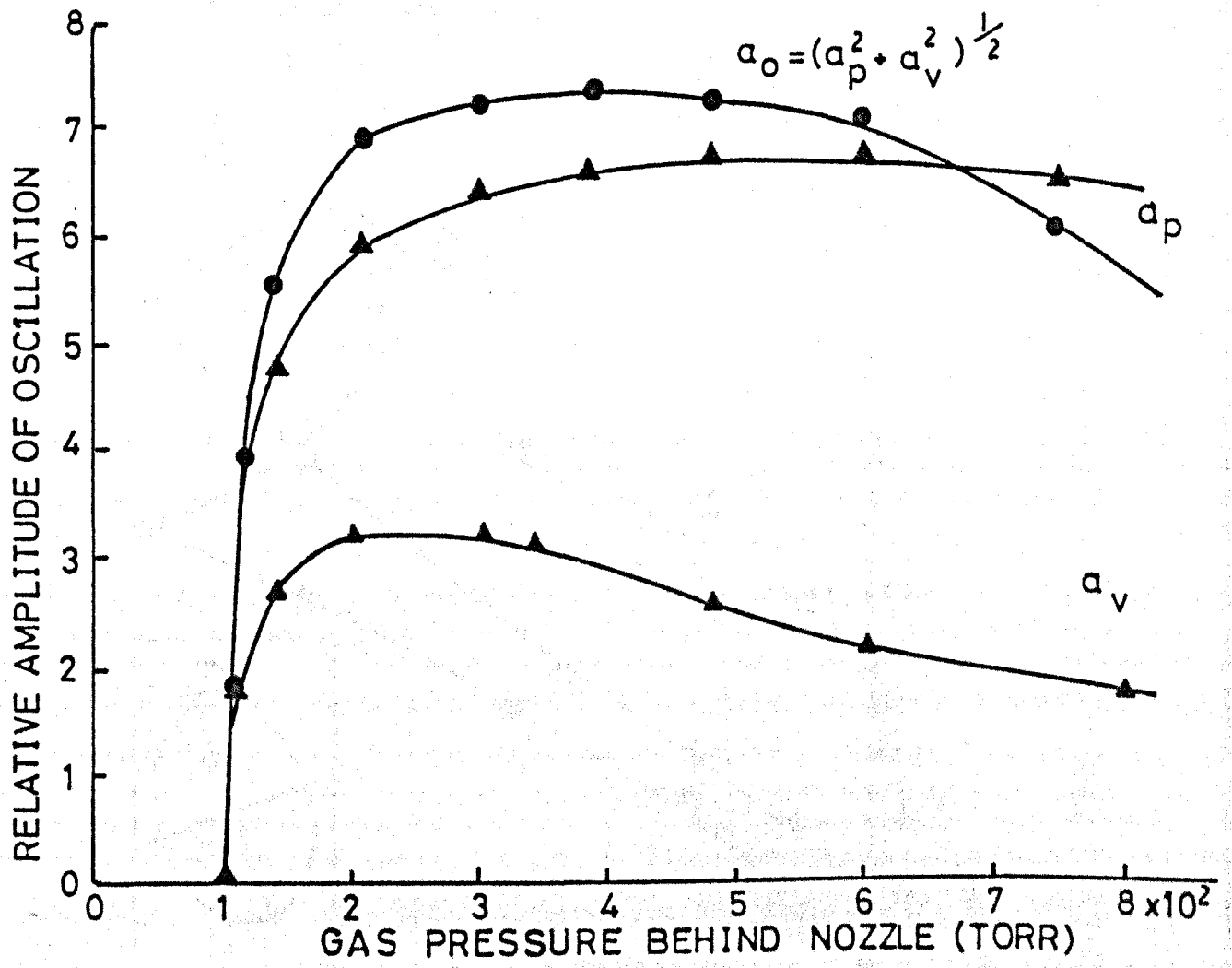

Fig. 4.11 CHARACTERISTICS OF ELLIPTICAL OSCILLATION COMPONENTS ($V_S = 9KV$)

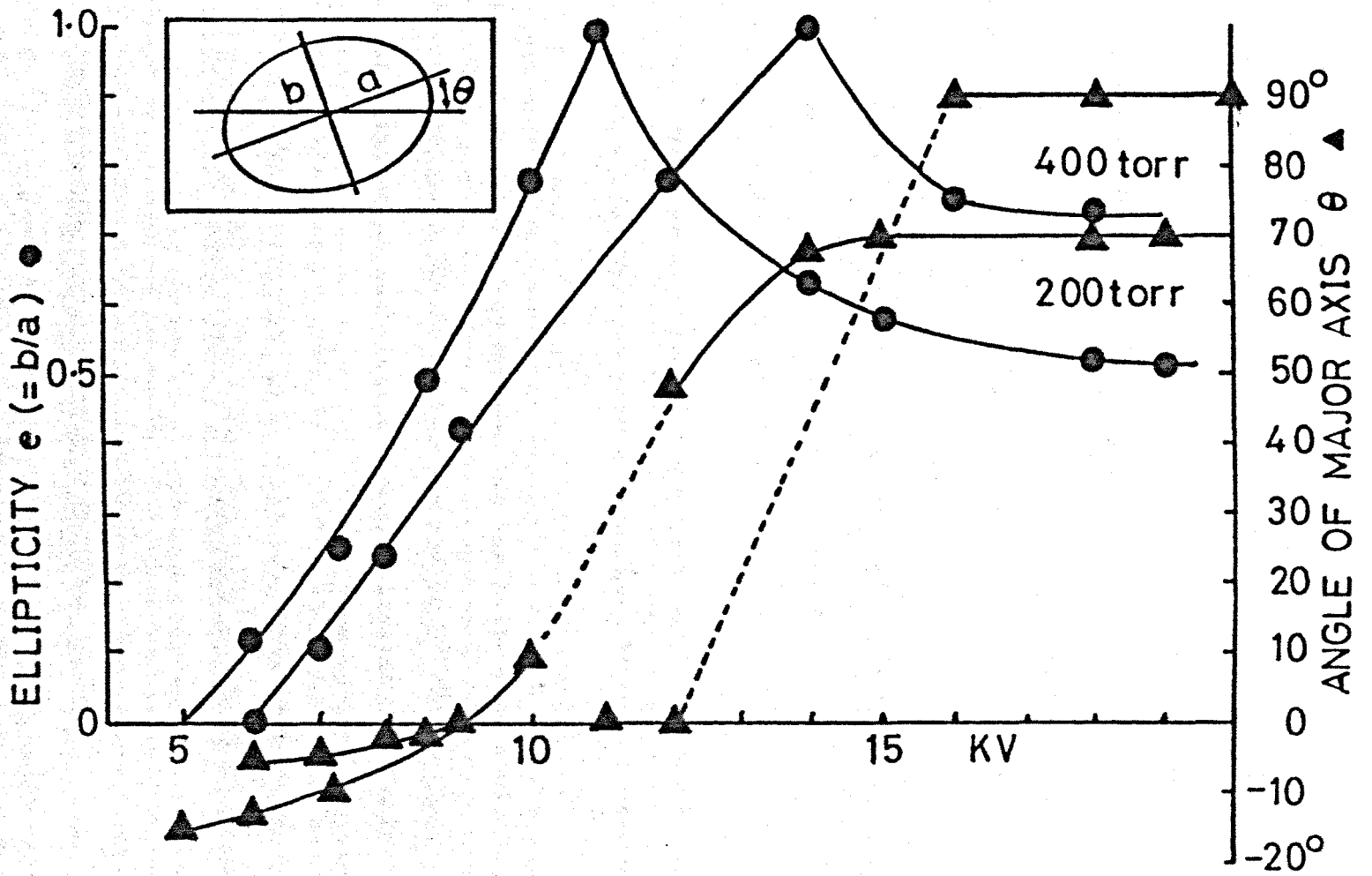

FIG 4-12 PARAMETERS OF ELLIPTICAL MASER OSCILLATION

CHAPTER 5

ENHANCEMENT OF DETECTION SENSITIVITY OF WEAK TRANSITIONS IN A MASER OSCILLATOR

5.1 INTRODUCTION

In chapter 3, the sensitivity problem in the maser amplifier was considered, mainly due to microwave detection noise. The relevant quantity was the noise figure of the receiver. In the present discussion the effect of quantum fluctuations will be taken into account. It will be shown that noise due to fluctuations of quanta is measurable and when it is minimized a significant improvement in sensitivity is obtained.

The effect of such fluctuations will be demonstrated in the detection of the quadrupole satellites of the oscillating inversion lines $J = K = 2$, $J = K = 3$ of ammonia. Moreover an additional enhancement of sensitivity is achieved as the noise figure of the system is reduced by modifying the above method, taking advantage of the fact that the polarization of oscillation becomes circular above a certain level of exitation. Use can also be made of the fact that the azimuth of the polarization ellipse can be rotated under the effect of a weak axial magnetic field before Zeeman splitting occurs.

5.2 RANDOM NOISE IN QUANTUM AMPLIFIERS

It should be emphasized that the type of noise which will be considered throughout the following discussion is not the result of including the effect of spontaneous emission in the calculation. Even if the rate of spontaneous emission is assumed to have zero value, photons will still fluctuate randomly due to the cavity losses. In

amplifier will now be made, but an intuitive insight into the problem can be acquired by the aid of equation 3.26. Since the noise figure F of a receiver is proportional to the noise temperature (Pound, 1948) and since random noise only is considered, then the quantity FkT in Eqn. 3.26 is proportional to kT_c, where T_c is defined by the equation

$$a/b = \exp(-h\nu/kT)$$

For $h\nu \ll kT_c$

$$a/b \approx 1 - h\nu/kT$$

The effective noise temperature of the amplifying system due to random noise is

$$T_c \approx \frac{h\nu}{k} \frac{a}{b - a} \qquad 5.6$$

which of course takes large values for $a \sim b$. On the other hand the effective cavity quality factor (neglecting the coupling for the sake of argument) is $Q_o = (2\pi\nu/b - a)$ and the signal-to-noise ratio is proportional to $Q_o/T_c^{1/2}$. Therefore the signal-to-noise ratio is proportional to $1/(b - a)^{1/2}$ which takes large values for $a \sim b$.

A similar argument can be made using Eqn. 5.3. After reasonable amplification ($t \to \infty$) $G, G^2 \ll 1$ the following aproximations are valid for $a < b$:

$$\langle m \rangle \approx A_o = \frac{c}{b - a} \qquad 5.7$$

$$\langle m^2 \rangle \approx B_o = \frac{c(b + c)}{(a - b)^2}$$

and

$$\sigma^2 = b/c \qquad 5.8$$

classical systems random noise represents the lower limit to the noise of any amplifying process, but for systems employing stimulated emission or absorption of photons, the situation can be completely different as the following example shows. Imagine a waveguide cell filled with active molecules for which the following quantities are defined:

n_o - The number of photons in the cell at t = 0.

a - The probability of stimulated emission per photon per second.

b - The probability of a photon disappearing per second.

c - The rate at which photons are released into the cell by any process other than stimulated emission.

Notice that except for normal absorption by the gas, b includes all losses in the waveguide and that c includes both spontaneous emission and the rate at which photons are released into the cell through coupling holes. The problem is to find the number of photons m in the cell as a function of time as a wave packet is propagated through it.

Although the exact mathematical solution in this case is available, it is sufficient for our purposes to write the dynamic behaviour of the moments of m. It can be shown that (Shimoda, Takahasi and Townes, 1957)

$$\langle m \rangle = A_1 G + A_o \qquad 5.1(a)$$

$$\langle m^2 \rangle = B_1 G^2 + B_2 G + B_o \qquad 5.1(b)$$

where $\langle\ \rangle$ stand for the expectation value of the number of photons m and G is the classical amplification factor

$$G = \exp[(a - b)t] \qquad 5.2$$

and the constants A_i, B_i are given by:

$$A_o = \frac{c}{a - b} \qquad 5.3(a)$$

$$A_1 = n_o + A_o \qquad 5.3(b)$$

$$B_o = \frac{c(b + c)}{(a - b)^2} \qquad 5.3(c)$$

$$B_1 = A_o \left(\frac{a + b + 2c}{a - b} \right) \qquad 5.3(d)$$

$$B_2 = B_1 - B_o \qquad 5.3(e)$$

The quantity which is used to measure fluctuation is

$$\sigma^2 = \frac{\langle m^2 \rangle - \langle m \rangle^2}{\langle m \rangle^2} \qquad 5.4$$

and the resulting random noise is given by

$$N = \sigma \langle m \rangle \qquad 5.5$$

If the system is to amplify the wave-packet it should have $a > b$. Assuming that there is no spontaneous emission and since there is no input signal in this case then $c = 0$. Also since $a > b$ then after large amplification (long interaction time), $G \ll G^2$. Taking all the above factors into account equations 1 - 5 yield

$$\sigma^2 = \frac{a + b}{(a - b)n_o}$$

For $a \gg b$, $\sigma \approx \frac{1}{\sqrt{n_o}}$ which takes small values for $n_o \gg 1$. In this case random fluctuationes represent the lower limit of thermal noise. On the other hand if $a - b$ is small and the frequency is not very low (with respect to $\frac{kT}{h\upsilon}$) then random fluctuations become as important as other sources of noise in the system, say, the detection scheme noise.

Application of the above ideas to the case of a maser

Using Eqn. 5.5, the background signal due to random noise is then

$$N = \frac{c}{a - b} \times \sqrt{b/c} = \frac{(bc)^{\frac{1}{2}}}{b - a} \qquad 5.9$$

The signal emitted by the beam can be calculated as follows. Imagine first that the cavity is empty of active molecules. Hence certain values of a, b and thus of b - a, are established, by the various mechanisms of cavity losses and the input signal. As the molecular beam is introduced, a change ϵ in the quantity a - b occurs resulting in a change S in the average number of photons inside the cavity. S can be regarded as the signal due to stimulated emission (or absorption). By differentiating Eqn. 5.7 we obtain

$$S = \frac{\partial(\langle m \rangle)}{\partial(b-a)} \Delta(b-a) = \frac{c\epsilon}{(a-b)^2}$$

and the signal-to-noise ratio is then given by

$$S/N = \frac{(a/b)^{\frac{1}{2}}}{(a-b)} \epsilon \qquad 5.10$$

where c is replaced by a for optimum sensitivity (Shimoda et al., 1957).

In the case of a maser amplifier this result is not surprising since it simply states that maximum sensitivity is obtained when the system is near oscillation ($a \sim b$). Moreover producing a situation where $a \sim b$ is not an easy task since neither increasing a (more efficient state selection) nor decreasing b (higher Q-value) is trivial. It is not straight forward however to see how the above result applies in the case of an absorption spectrometer. In the latter case $a \sim b$ means that the signal-to-noise ratio due to random noise can be made as large as desired by the addition of excited molecules into the cavity where absorption is to be detected (Townes, 1960).

5.3 APPLICATION TO THE CASE OF THE OSCILLATING MASER

Suppose that a relatively weak hyperfine component of a molecular transition is to be detected. If the usual detection method is used, that is tuning the cavity to the satellite transition frequency, then it may be expected that the oscillation of the main line will be reduced since its frequency will not be set to the top of the cavity mode and therefore it will "see" a lower effective Q value. In this case the random noise of the cavity will be determined by the difference $a_h - b_h$ where a, b corresponds to the hyperfine component in question. since a_h is proportional to the population inversion, and since the line is far from oscillation it is clear that $a_h \ll b_h$ and therefore $a_h - b_h$ is not small. According to equation 5.10 random fluctuations might be significant especially if the noise figure of the receiver is low. If on the other hand detection of the same line is made via the maser oscillation, then a-b is naturally very small and random fluctuations would be considerably reduced. In the following section it will be shown how this can be done experimentally but first an estimate of the expected sensitivity will be given.

It is easy to show that the parameter ϵ which appears in equation 5.10 is related to the gain coefficient γ by

$$\gamma = \frac{\epsilon}{C_o} \qquad 5.11$$

where C_o is the velocity of light, and $\gamma(\nu)$ is defined in the same manner as the absorption coefficient (Yariv, 1971). Using equation 5.7 for $a \approx c$ we obtain

$$S/N = \left[\frac{m_o}{(b-a)b}\right]^{\frac{1}{2}} C_o \gamma \qquad 5.12$$

where m_o stands for $\langle m \rangle$. Knowing that the bandwidth $\Delta\nu$ to which the

cavity system responds is given by (Townes, 1960)

$$\frac{\Delta\nu}{\nu} = (b/a - 1) = \underline{B}$$

Then equation 5.12 yields

$$(S/N) = \frac{C_o}{b}\left(\frac{W}{hB}\right)^{\frac{1}{2}}\gamma \qquad 5.13(a)$$

where $W = m_o h \nu_o$ is the energy stored in the cavity and ν_o, the resonance frequency. Now an expression for b can be found by assuming that the cavity is a short ended waveguide with an attenuation constant $\alpha_o = 4\pi/\lambda Q$ (Townes and Schawlow, 1955). In this case using equation 5.6 for $a \sim b$ it is obtained

$$b = \frac{4\pi}{\lambda Q} C_o \frac{kT_c}{h\nu_o}$$

Therefore

$$(S/N) = \frac{h\nu_o}{kT_c}\frac{\lambda Q}{4\pi}\left(\frac{W}{h\Delta\nu}\right)^{\frac{1}{2}} \qquad 5.13(b)$$

Equations 5.13 are equivalent to formula (15) in Townes' derivation (Townes, 1960) which can be obtained, simply by substituting 1 for S/N. It gives the signal-to-noise ratio for detection via an oscillating system. To compare it with that derived for the usual detection method as given by equation 3.26 it may recalled that the gain coefficient of the maser can be written as (Shimoda, 1960)

$$\gamma(\nu_o) = \frac{nh\nu_o(\Delta\nu_s)^2}{2PL\left[(\Delta\nu_o)^2 + (\Delta\nu_s)^2\right]}$$

where P is the power flow in the cavity and the remaining quantities are defined as in chapter 3, that is

$$(\Delta\upsilon_s)^2 = \frac{8\pi\bar{\mu}^2}{C_o h^2}\left(\frac{P}{A}\right)$$

$$\gamma(\upsilon_o) = \frac{nh\upsilon_o}{4C_o W_c} = \frac{1}{L}\frac{W'}{W_c}$$

where W' is the energy emitted by the beam assuming that each molecule contributes one photon. Substituting in Eqn. 5.13(b) yields

$$S/N = \frac{Q_o}{16\pi}\frac{nh\upsilon_o}{kT_c}\left(\frac{h}{W_c B}\right)^{\frac{1}{2}} \qquad 5.14$$

The above equation gives the estimated signal-to-noise ratio for detection via the oscillating maser. It is worthwhile mentioning that the numerical value that appears in Eqn. 5.14 is not of practical importance since it depends on the level of saturation (the value $W = W_c$ was taken here) and the values of the coupling coefficients. Moreover it should be remembered that the sensitivities indicated by the above equation are achieved only if random fluctuations are the only source of noise and thus the numerical factor which results by substituting typical values does not have much practical significance unless the values of the maser parameters (including efficiency of state selection and the receiver noise figure) are precisely known.

It is interesting to compare the signal-to-noise ratios given by the two different methods assuming random noise is dominant. Dividing Eqn. 5.14 by Eqn. 3.26 it is obtained

$$\frac{(S/N)_{osc.}}{(S/N)_{usu.}} \approx \left[\frac{1}{16} Q_o \frac{h\nu_o}{kT_c}\right]^{\frac{1}{2}} \qquad 5.15$$

The value of T_c will obviously depends on the temperature of the active material and on the value of the coupling coefficients. This is shown

by the relation (Shimoda et al., 1957)

$$T_c = \frac{h\upsilon_o}{k}\left(\frac{a}{a-b_u-b_o}\right)$$

where b_u and b_o are the losses due to the unloaded cavity and the output coupling hole respectively. For an ideal maser $a \gg b$ and $kT_c \approx h\upsilon_o$. Of course it is to be expected that the actual improvement of sensitivity will be less than that given by Eqn. 5.15 since the noise figure of the receiver is not necessarily negligible. Nevertheless it represents a basic improvement on the usual method of detection and its potential will be discussed in the following sections.

5.4 THE EXPERIMENTAL METHOD

Detection of spectral lines via the maser oscillator can be explained by the aid of Fig. 5.1 which shows a schematic diagram of the quadrupole energy levels of the inversion line J = K = 2 of ammonia. Splitting due to spin interaction is omitted for simplicity. By tuning the cavity to the frequency f_o which is equal to the transition frequency ($F_1 \longrightarrow F_1'$, $F_1 = F_1'$) it is possible to make the main line oscillate, provided the state selection voltage is raised above 5KV . If detection of the quadrupole satellite "A" is now desired, then instead of tuning the cavity to the frequency component f_{Q1} and thereby quenching the main line oscillation by increasing cavity losses, the frequency of the stimulating signal is adjusted to equal f_{Q1}. Since the probability of inducing transitions at a given frequency in a cavity is proportional to the number of photons present in the mode at that frequency then by so doing, the transition "A" will be strongly excited relative to the main line transition. Some molecules that would otherwise make transitions at f_o will now be "robbed" from the main line and stimulated to make the transition "A" ($2 \rightarrow 1$) at the

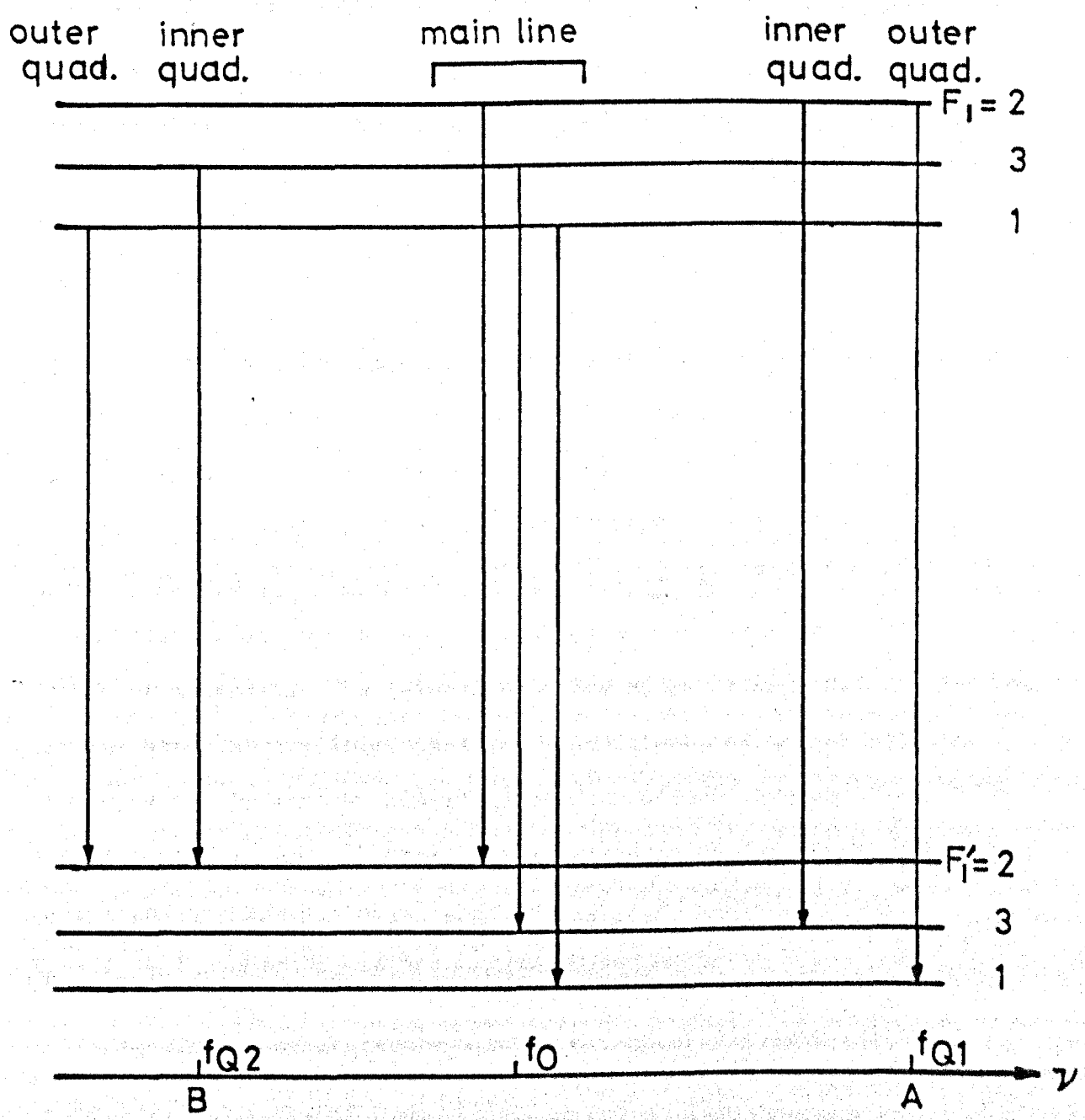

FIG. 5·1 HYPERFINE SUBLEVELS OF THE INVERSION LINE $J=K=2$ OF $^{14}NH_3$ NEGLECTING THE INTERACTION OF THE HYDROGEN SPINS.

frequency f_{Q1}. This accordingly reduces the population of the sublevel $F_1 = 2$ and simultaneously increases the population of the sublevel $F_1' = 1$. Consequently the emission at the main line frequency is decreased and a reduction in the amplitude of oscillation occurs. The spectral shape of the reduction which appears as a dip in the amplitude of oscillation at the appropriate frequency resembles that obtained by the usual detection method except that the latter appears as a positive change ('pip') superimposed on the cavity resonant mode.

In a similar manner, detection of the transition "B" can be made. The transition $(3 \rightarrow 2)$ is strongly excited by adjusting the stimulating signal frequency to f_{Q2}. Therefore the population of the sublevel $F_1 = 3$ will decrease and simultaneously the population of the sublevel $F_1' = 2$ will increase. Again, this will reduce the amplitude of oscillation at the corresponding frequencies allowing the satellite "B" to be detected. The detection scheme shown in Fig. 3.6 can be used for the experimental investigations. Adjustment of the stimulating frequency can be made by altering the modulation frequency f_m. If for example, detection of a satellite with transition frequency f_Q is to be made then the external oscillator frequency is varied so that $f_k + f_m = f_Q$, where f_k is the klystron frequency.

For maser systems employing closed cylindrical cavities operating at the mode TM_{010}, which is the mode with the highest Q value and still has only one maximum of microwave electric field along the axis ($q = 1$), there exists a single state of polarization which is linear, with its electric field along the cavity axis (Singer, 1959). To obtain a maximum oscillation signal it is therefore appropriate to orientate the output wavequide so that it transmits microwave power with its electric field parallel to that axis. For both reflection and transmission closed cavities this also must be the electric field

direction of the stimulating signal, otherwise the input power will be reflected at the input coupling hole. Therefore, at the microwave diode rectifier the transmitted (or reflected) output power is added to that oscillation power emitted by the beam.

Disc resonators however equally support a linearly polarized radiation in any direction parallel to the surface of the mirrors, provided they are completely isotropic. As a result they facilitate the possibility of separating the oscillation from the stimulating power. In general this can be done first by rotating the output waveguide so that it transmits maximum oscillation power, and then the input waveguide is rotated so that its electric field transmission vector is perpendicular to that of the output. As a result no microwave stimulating (side band) power is transmitted and the excitation of the quadrupole components will appear as a pure reduction in the amplitude of oscillation. As it will be shown later, this will provide further improvement in the sensitivity of detection.

Shimoda and Wang (1955) were the first to employ the oscillating maser for observation of the quadrupole components of the inversion line $J = K = 3$ of ammonia in conjunction with a cylindrical cavity. Using the maser oscillations to stablize the klystron they estimated a 50-fold improvement in the signal-to-noise ratio over the usual maser spectrometer. The same method was applied later using a closed cavity operated with the resonant mode TM_{010} (Sircar and Hardin, 1964). In the latter case a klystron which supplied power at $\frac{1}{2}f_k$ was employed. This frequency was then multiplied by taking the second harmonic of a 1N26 diode mixer. Following Shimoda and Wang's method they were able to observe the magnetic satellites of the inversion line $J = K = 3$ of ammonia, using a galvanometer recorder for detection of the changes in the amplitude of oscillation.

5.5 DETECTION VIA THE MASER OSCILLATOR EMPLOYING A DISC RESONATOR

To investigate Shimoda and Wang's method in conjunction with open resonators, the double beam maser system described in the previous chapter with its disc resonator was employed. Both input and output waveguides in Fig. 3.5 were set up so as to transmit microwave power with its electric field parallel to the beam axis (X-axis). The cavity was tuned to 23.72 GHz which is the inversion frequency of the main line J = K = 2 of ammonia. An oscillation threshold of about 5KV was recorded at a nozzle pressure of about 400torr. By appropriate adjustment of the modulation frequency it was possible to sweep the klystron through all four sets of the quadrupole satellites corresponding to different ($F_1 \longrightarrow F_1'$) transitions. All the resolved satellites components corresponding to various ($F \longrightarrow F'$) transitions were detectable. The relative frequency separations were consistent with those quoted by Kukolich(1967).

As an example,detection of the inner quadrupole satellite on the low frequency side of the main line obtained with Shimoda and Wang's method is shown in Fig. 5.2(b). In (a) the same satellite obtained by the usual detection method is shown. Comparing the two signals it is seen that there is an obvious improvement in the signal-to-noise ratio, attributed to the reduction in the random fluctuation noise. However, it may also be noticed that the degree of improvement in sensitivity is greater for the weaker component corresponding to the transition $\Delta F = 0$ (which is not detectable in 'a') than it is for the component corresponding to the transition $\Delta F = +1$. This can be explained as follows: Following the theoretical discussion in Secs. 5.2, 5.3 it was shown that the bigger the value a - b the greater the random fluctuation noise. Therefore, weakly state selected components are expected to suffer more random noise and consequently would benefit most

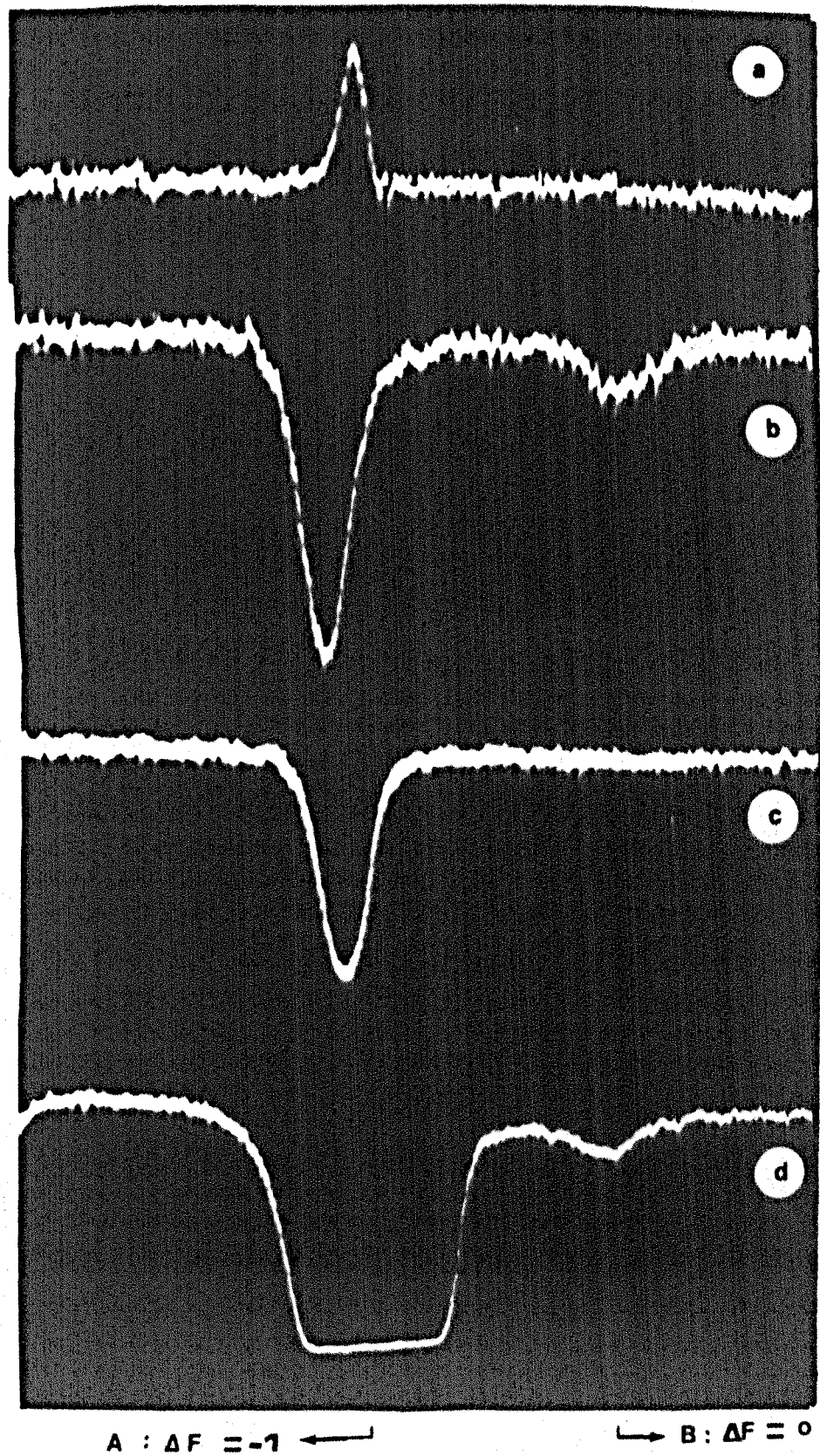

Fig. 5.2 Detection of inner low frequency quadrupole satellite of the J = K = 2 inversion transition of ammonia.

of all from its removal. For example strong components having $a - b \sim 0$, $a \leq b$ are not expected to improve much if detected via the maser oscillation. In addition, it is easily seen that the relative intensity of a spectral component detected via the maser oscillator can be substantially different from the theoretically calculated values for normal spectroscopy (Gunther-Mohr, Townes and Van Vleck, 1954). That is because in the former case the line intensity is not only determined by the effect of state selection on different quantum states but also on the strength of the oscillating main line component to which the line in question is connected. For example the relative intensity of the two mentioned quadrupole components as estimated by Kukolich (1967) is less than 6% while the same ratio as measured from Fig. 5.2(b) is about 10% (see Fig. 1.8).

Another measure of the potentiality of the method is illustrated in Fig. 5.3. There, detection of the outer quadrupole satellite on the high frequency side for both methods is shown. While the component corresponding to the transition $\Delta F = 0$ is just detectable in (a) it showns up clearly in (b). Again the ratio of the two component intensity measured from Fig. 5.3(b) ($\sim$0.5) is substantially different from that deduced from Fig. 1.8 ($\sim$0.1).

The two remaining satellites on either side of the main line showed a similar behaviour. This is to be expected because of the frequency symmetry of the transitions (Fig. 1.7).

Throughout the observations it was noticed that a relatively high input power was needed to excite the quadrupole components in both methods of detection. This is due to the fact that weak components with small dipole matrix elements saturate at a high level of input power (see Sec.3.4.2). As a result of this relatively high power level an

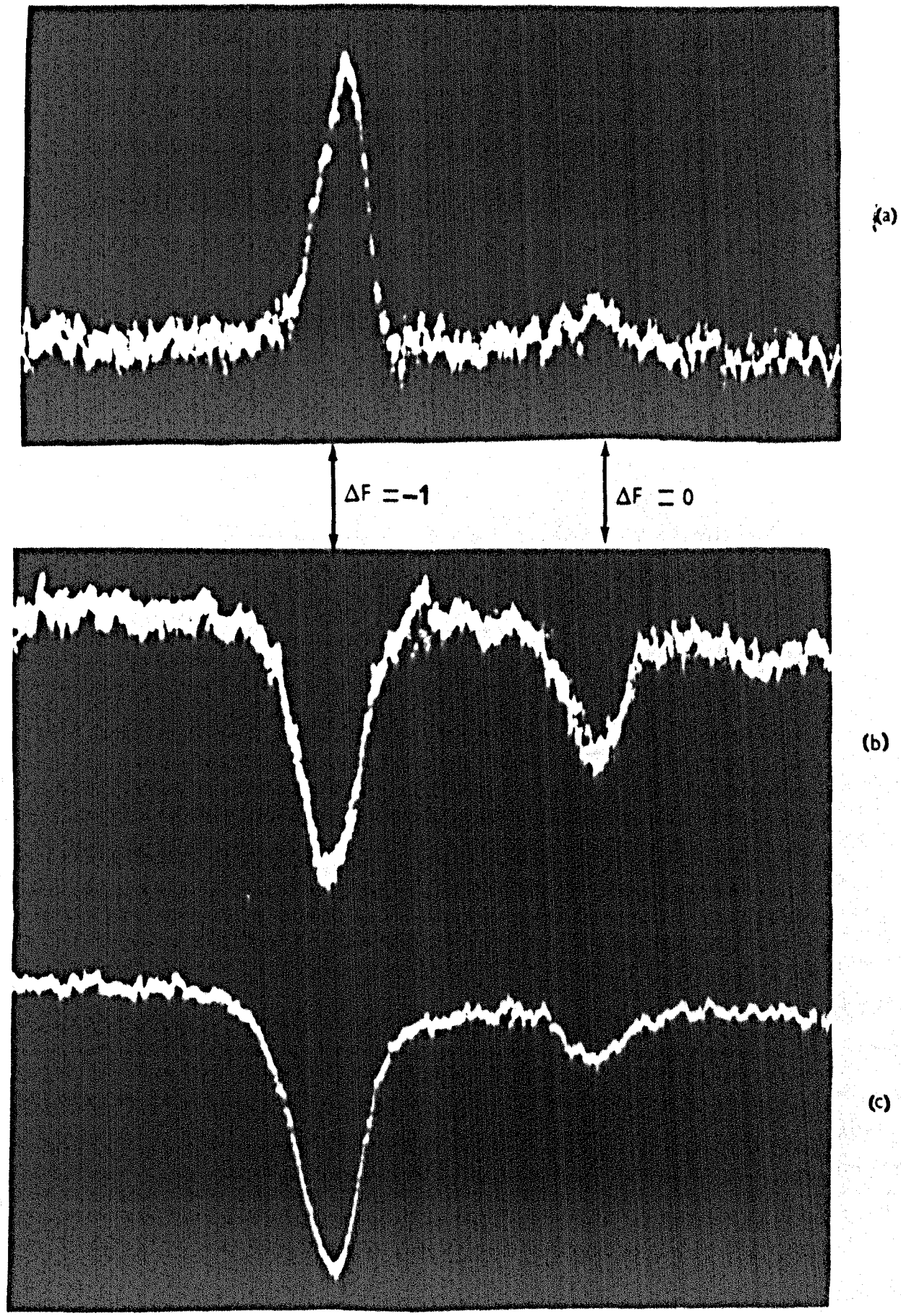

Fig. 5.3 Detection of the outer quadrupole satellite on the high frequency side of the inversion line J = K = 2 of $^{14}NH_3$.

additional noise was introduced to the detection scheme. Firstly, the introduction of high power level with respect to the L.O power at the input of the mixer, makes the latter both more noisy and less linear. Secondly, additional low frequency noise due to the vibrations caused by the rotary vacuum pumps was coupled into the detector through noise modulated power leakage from the microwave joints. These types of noise could be considerably reduced when the above method was modified so that no sideband power could be transmitted, through the resonator, to the detection arm. As was mentioned previously, this could be accomplished by setting the input and the output waveguides do that they transmitted microwave power with their electric fields mutually perpendicular.

An example of detection using the modified method (i.e. detection via the maser oscillator with orthogonal polarizations) is shown in Fig. 5.2(c) and is compared with the same spectral lines detected by both the usual and Shimoda and Wang methods. Since the two signals in (b) and (c) were taken at the same gain of the detection scheme, it can be said that the noise level in (c) was reduced several times with respect to (b). This of course contributed to the further enhancement in the signal-to-noise for the component satellite "A" corresponding to the transition $\Delta F = +1$. However, as it can be clearly seen by comparing the two traces, the ratio of the two satellite components in (c) is different from that in (b). Although the signal-to-noise ratio of the weak component "B" corresponding to the transition $\Delta F = 0$ could be improved by increasing the level of the stimulating input power and thereby saturating the transition "A" (Fig. 5.2(d)), it had to be concluded that the signal which resulted from robbing the oscillating main line by each component was different.

This behaviour is attributed to the fact that the strength of the oscillation robbing by the quadrupole components depends on the

strength of interaction between the state selected molecules and the stimulating microwave field inside the resonator. The latter which is dependent on the distribution of the molecules angular momentum along the input power $\underline{E}$ vector (Basov et al., 1964) is obviously determined by both the spatial orientation of molecules entering the resonator and the polarization of the stimulating input power. Moreover, since the state selection itself is F-dependent it is to be expected that the same F-component will respond differently for different input polarizations and that this response will also vary for different F-components.

As it is shown in Figs. 5.2, 5.3 and indeed as it was found for all the $J = K = 2$ quadrupole satellite, components with $\Delta F = \pm 1$, if detected via the maser oscillation, was favoured when the $\underline{E}$ vectors of the input and output waveguides were orthogonal while components corresponding to the transition $\Delta F = 0$ were better detected with both $\underline{E}$ vectors lying along the beam axis.

5.6 ENHANCEMENT OF THE AMPLITUDE OF OSCILLATION

Throughout the investigation, a phenomenon which had not been reported by previous investigators (Shimoda and Wang, 1955; Sircar and Hardin, 1964) was observed. It was noticed that when the state selection voltage was raised above a certain level, some of the quadrupole satellites components appeared to become dispersive, and at some frequencies, excitation of these quadrupole component caused enhancement rather than reduction in the amplitude of oscillation. This kind of behaviour is shown in Fig. 5.4 where (b) was taken at higher level of EHT than (a) but at the same level of stimulating power.

At first, it was thought that the enhancement was caused by the excitation of a transition which recycled the molecules back to the

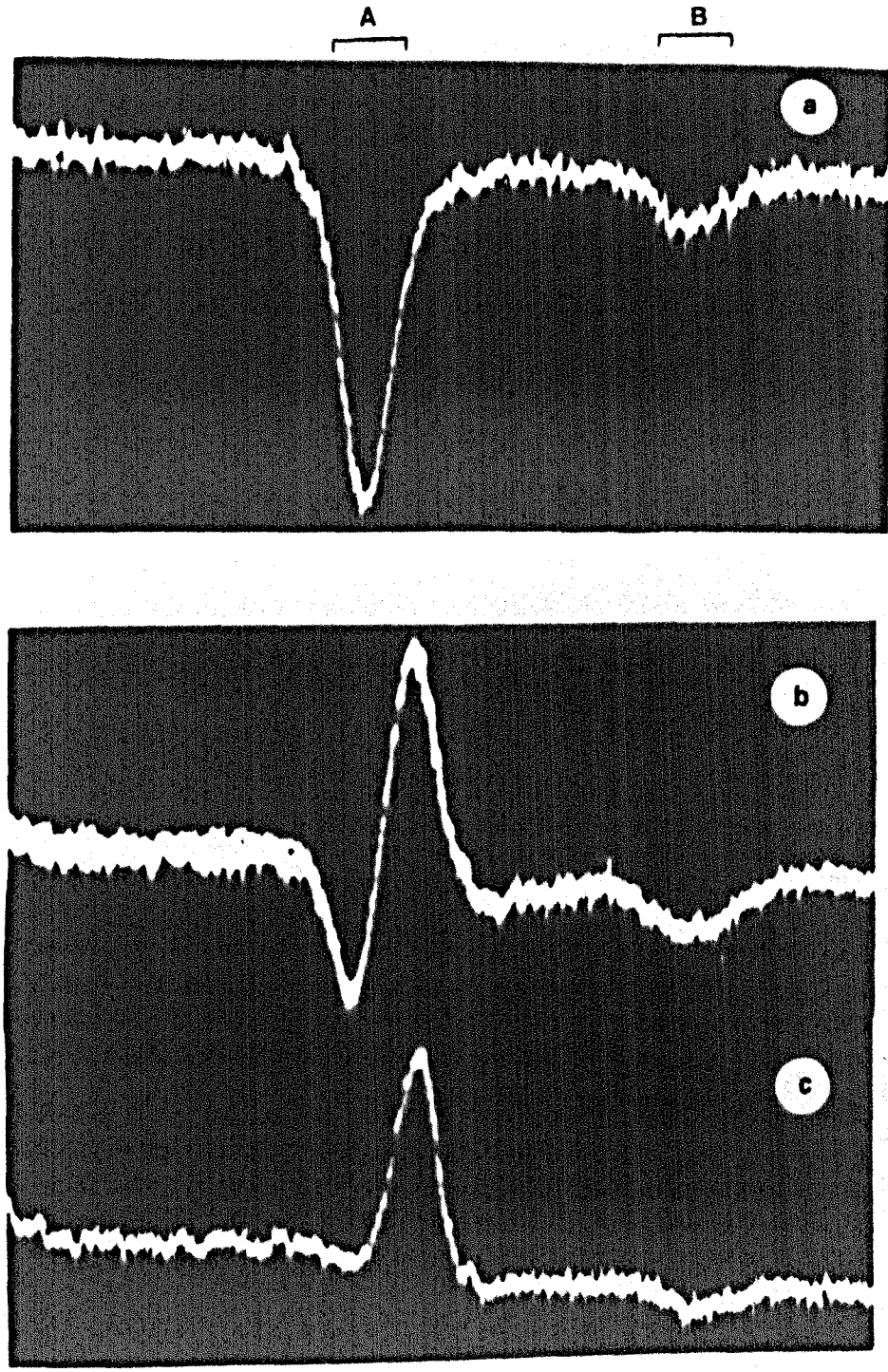

Fig. 5.4 Detection via the maser oscillation of the inner quadrupole satellite on the low frequency side of the main inversion line J = K = ? of ammonia.

(a) V_s = 9KV

(b) V_s = 12KV

(c) as in (b) but lower level of input power.

upper inversion level during their flight in the resonator (Lainé and Bardo, 1971). The idea can be explained with the aid of the schematic diagram in Fig. 5.5 which shows some of the hyperfine transitions involved in forming the quadrupole satellite component "A" shown in Fig. 5.4. As the state selection voltage is raised, the population of the sublevel $(F_1, F) = (2, 3/2)$ increases which cases the transition $(2, 3/2) \longrightarrow (2, 3/2)$ to oscillate strongly. Conditions therefore might be created, under which the population of the sublevel $(F_1', F') = (2, 3/2)$ exceeds that of the sublevel $(F_1, F) = (3, 5/2)$. In this case, excitation of the quadrupole satellite allows the transition $(F_1', F') = (2, 3/2) \longrightarrow (F_1, F) = (3, 5/2)$ which cases the amplitude of oscillation to be enhanced via the transition $(3, 5/2) \longrightarrow (3, 5/2)$.

This assumption was supported by the fact that all satellites components which showed the kind of behaviour described in Fig. 5.4(b) were doublets while the singlets corresponding to the transition $\Delta F = 0$ did not show dispersion. It seemed that one of the doublet members reduced the amplitude of oscillation while the other enhanced it. However, this explanation has one important weakness. The frequency separation of the inner quadrupole doublet components which is about 1KHz (Fig. 1.8) is much less than the frequency resolution of the maser (about 6KHz). Moreover the frequency separation of the two dispersive components was estimated as 5KHz which is nowhere near the theoretical value. Therefore in the absence of a physical process which can explain the frequency pulling of the two doublets numbers, the above explanation of the oscillation enhancement lacks justification.

It should be emphasized however, that this effect was very prominent and easily reproducible. In fact all four doublets corresponding to the quadrupole satellites of the inversion line J=K=2 showed enhancement of the amplitude of oscillation. In Fig. 5.6 another

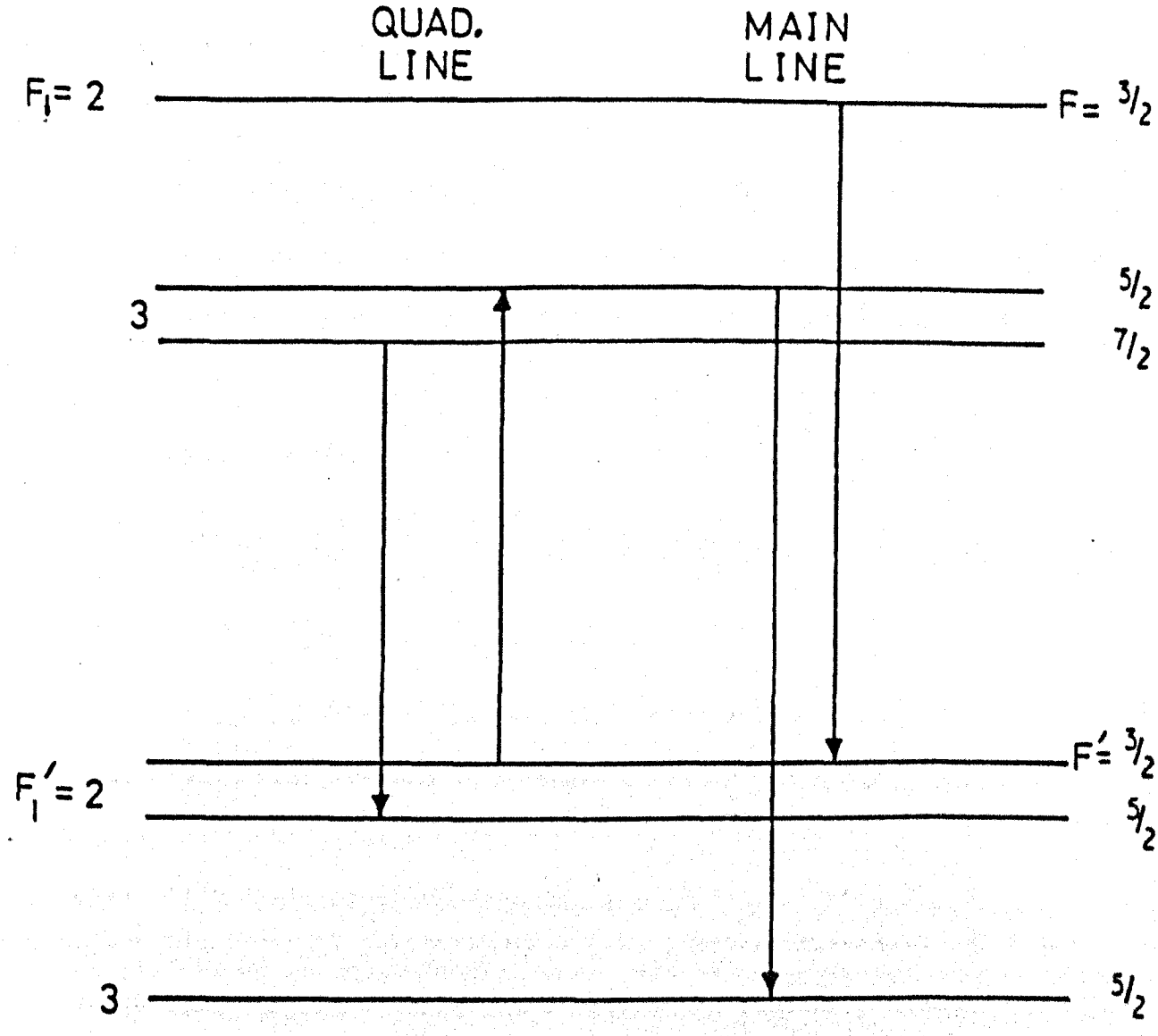

FIG. 5.5 ENHNCEMENT OF THE AMPLITUDE OF OSCILLATION BASED ON PUMPING BY HYPERFINE SPECTRAL COMPONENTS

example is shown were (b) was taken at lower rate of scan to ensure that the effect was not due to rapid passage effects. The frequency separation of this doublet component is about 4.8KHz. It was suggested (Yassin and Lainé, 1981) that some form of Stark splitting via the state selector fringe field penetrating the resonator volume could also have taken place. When the level of the stimulating input power was taken down only enhancement of the amplitude of oscillation occured. No definite conclusion could be drawn as to the precise origin of the oscillation enhancement phenomenon.

5.7 THE EFFECT OF ELLIPTICAL OSCILLATION

In the previous section it was emphasized that throughout the measurements with the modified method, the polarization of the input signal was chosen to lie along a direction vertical to the beam axis, while the output waveguide was set up so that a projection of the oscillation ellipse along the beam axis could be detected. This is simply because this arrangement provided the best sensitivity for state selection voltages below 13KV which reflected the fact that up to this voltage the polarization of oscillation was elliptical,with maximum projection along the beam axis. However, the same sensitivity could be obtained as the input and output polarization signals were interchanged, provided the state selection voltage was raised above 18KV. This observation expressed the fact that the maser amplifier gain profile was found to be less sensitive to state selection voltage than the oscillation polarization. This was verified as follows. The state selection voltage was set to a fixed value. The stimulated emission signal due to a quadrupole component was then examined as a function of the angle θ that the electric field of both waveguides (which were kept mutually parallel) made with the beam axis. For state selection voltages above 9KV no noticeable change in the signal was recorded as θ

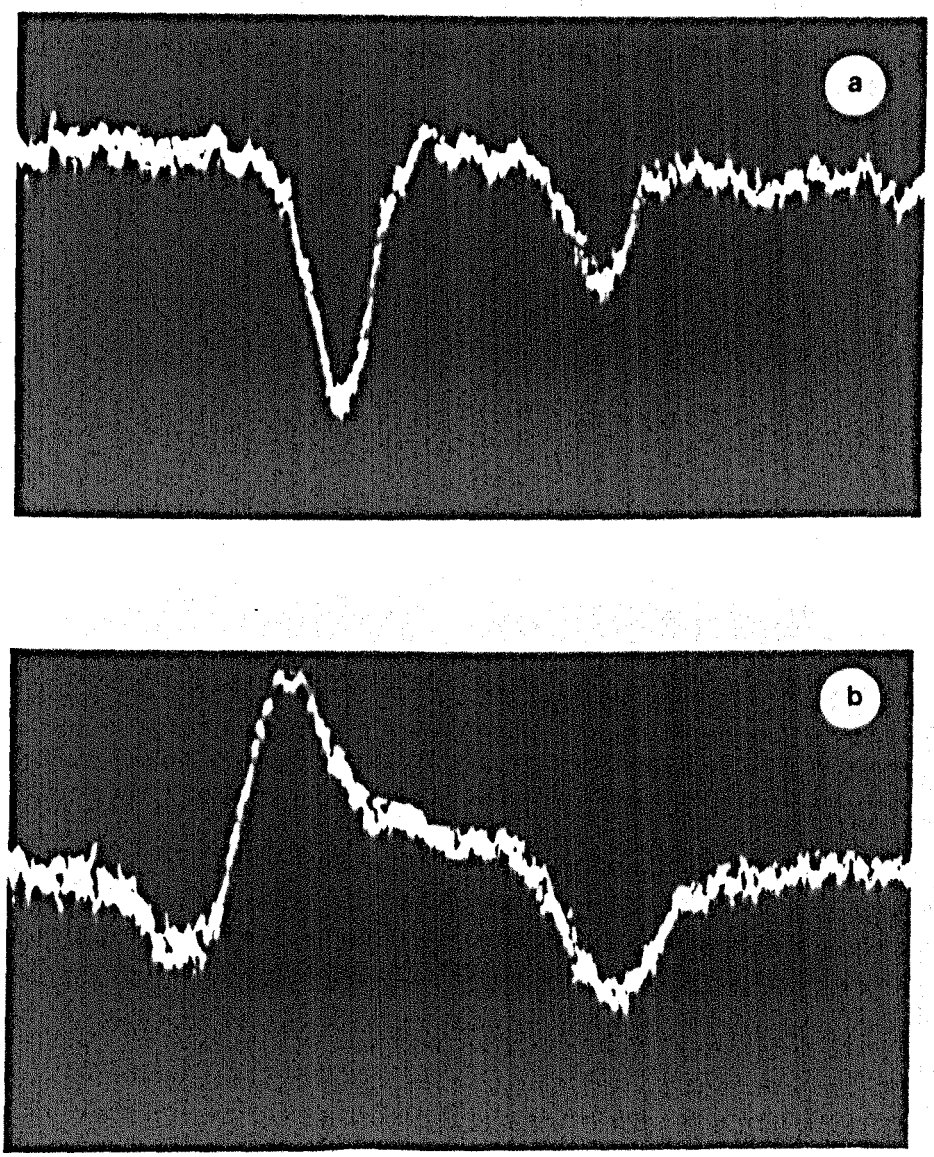

Fig. 5.6 Enhancement of the amplitude of oscillation by the outer high frequency quadrupole satellite of the inversion line J = K = ? of ammonia.

was varied from 0-90°. It appeared to be that this value of state selection corresponded to the value at which the amplitude characteristic curve a_p (see chapter 4) started to saturate. On the other hand it was shown in the previous chapter that changes in the ellipticity of polarization were still measurable up to state selection voltages of 18KV, for nozzle pressures of 400torr. This is because, apart from state selection, the gain anisotropy is dominated by the polarization of the input signal while the oscillation ellipse is affected by other types of anisotropy present in the maser system like mirror coatings, the earth's magnetic field and mechanical alignment.

In other cases however, where the state selection process is more isotropic, the choice of the detected output signal polarization is less critical. An example of that is shown in Fig. 5.8, where, in (a) the method of Shimoda and Wang was employed to detect the outer quadrupole satellites of the inversion line J = K = 3 of ammonia. It was found that if the modified method with crossed polarization was used, then rotating either the input or the output waveguide by 90° with respect to the beam axis, revealed the same sensitivity for the same state selection voltage. Fig. 5.8(b) was taken with output polarization vertical to the beam axis and input parallel to it. Notice that the discussion in the previous section about the effect of polarization coupling on transitions with different F values is still applicable. As is shown, transitions with $\Delta F = \pm 1$ favour orthogonal polarization coupling while $\Delta F = 0$ transitions favour parallel coupling of input - output polarization.

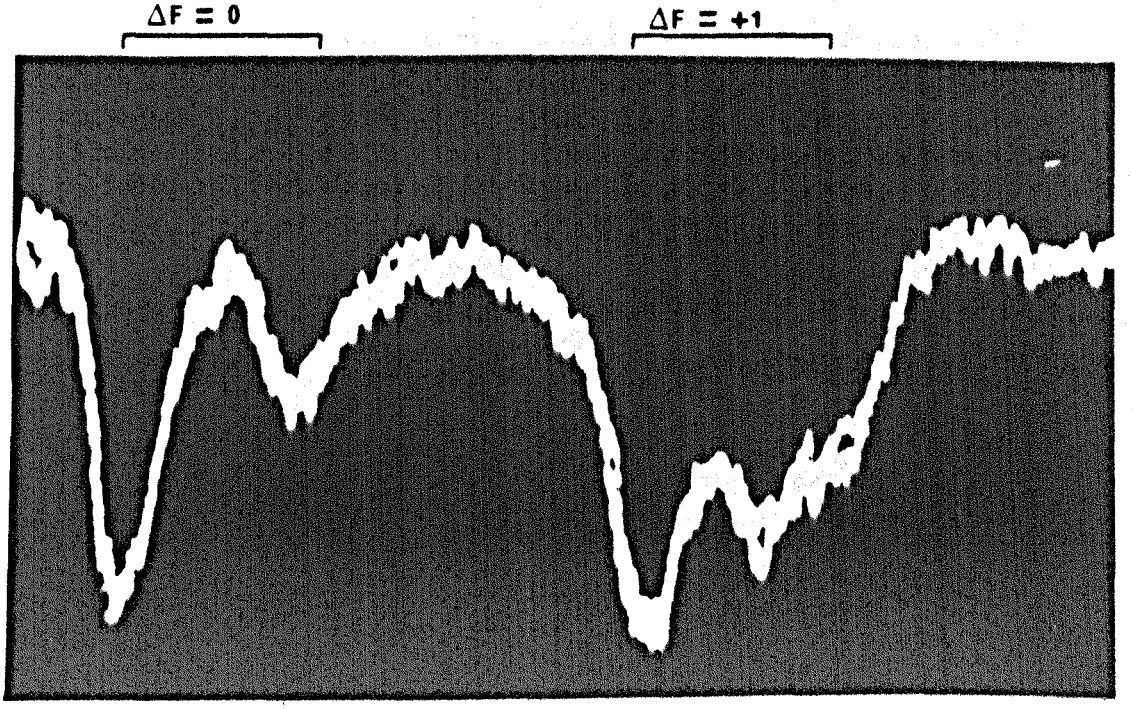

[a]

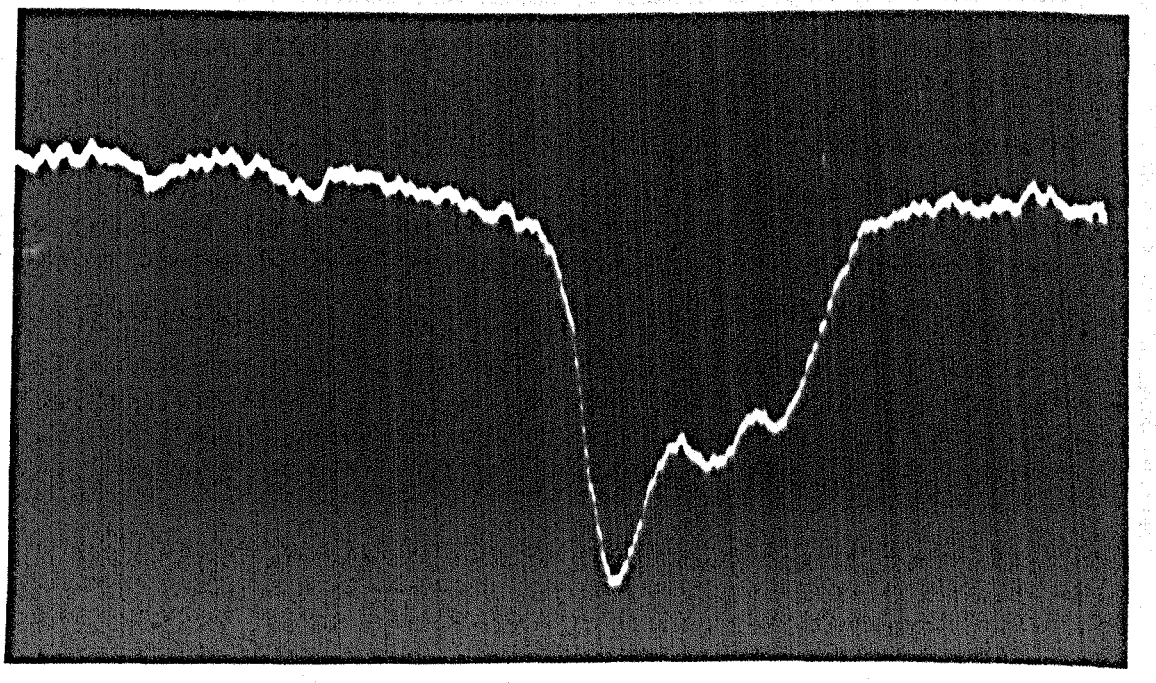

[b]

Fig. 5.8 Detection via the maser oscillation of the outer quadropole satellite on the low frequency side of the inversion line J = K = 3.

(a) Method of Shimoda & Wang.

(b) Modified method with the output waveguide E vector perpendicular to the beam axis.

CHAPTER 6

THE MASER OSCILLATION POLARIZATION AT ZERO AND UNDER A WEAK AXIAL MAGNETIC FIELD

6.1 EIGENSTATES OF POLARIZATION

In chapter 2 the scalar theory of the open resonator was discussed. The electric (or magnetic) field associated with the microwave radiation was assumed to be linearly polarized along a direction which is not altered during the wave propagation (Fox and Li, 1961). Using the scalar theory of diffraction the steady state modes of propagation were calculated yielding the well known TEM resonant modes. Each of these modes is repetitive in two aspects:

(a) It repeats its complex amplitude after a round trip in the resonator apart from a complex constant. Therefore the spatial distribution of intensity is not altered after a round trip apart from a constant reduction.

(b) There exists a single fixed frequency (the resonant frequency) corresponding to this mode.

However, in the presence of anisotropic elements in the resonator, the vectorial aspect of the wave equation must be considered, for these elements influence both the polarization and the resonance frequency of the mode (Dandliker, 1968). Since this will add theoretical difficulties to a problem which is already complicated, it would be more convenient to treat the polarization problem independently (de Lang, 1967). The effect of the various types of anisotropies will be represented by a 2 x 2 matrix which acts on the electric field vector of the resonant mode without affecting its spatial distribution.

In other words, the elements of the anisotropy matrix (Jones, 1941) do not vary as a function of the transverse (x, y) coordinates. As a result each resonant mode (TEM mode) will in general split into two states of polarization with different polarization parameters (ellipticity and orientation) and also different resonant frequencies. Therefore in order that a TEM mode should be a truly resonant mode of the resonator it must repeat its state of polarization after a round trip.

Let the electric field of a given state of polarization be represented by the vector

$$\underline{E} = \begin{pmatrix} E_x \\ E_y \end{pmatrix} \qquad 6.1$$

where as in chapter 4

$$E_x = a_x \exp(i\phi_x) \qquad 6.2(a)$$

$$E_y = a_y \exp(i\phi_y) \qquad 6.2(b)$$

The factor $\exp(i\omega t)$ is omitted and a_x, a_y, ϕ_x, ϕ_y are real. Therefore

$$\frac{E_y}{E_x} = r\cos\delta + ir\sin\delta \qquad 6.3(a)$$

where

$$r = a_y/a_x \qquad 6.3(b)$$

$$\delta = \phi_y - \phi_x \qquad 6.3(c)$$

If ϵ and α are defined as

$$\tan \alpha = r \qquad 6.4(a)$$

$$\tan \epsilon = e = b/a \qquad 6.4(b)$$

then it is easy to show that the polarization ellipticity and azimuth are given respectively by

$$\epsilon = \tfrac{1}{2} \sin^{-1} [\sin 2\alpha \sin\delta] \qquad 6.5(a)$$

$$\vartheta = \tfrac{1}{2} \tan^{-1} [\tan 2\alpha \cos\delta] \qquad 6.5(b)$$

From Eqn. 6.5 it is seen the parameters of the polarization ellipse are determined by the ratio of the cartesian field components and their relative phases. Therefore for calculation of the polarization the absolute value of the mode intensity is not important and thus multiplication of the electric vector by a complex constant does not alter its state of polarization.

6.2 THE ANISOTROPY MATRIX

The anisotropies of the maser system are caused by both the anisotropy of the state selection with respect to the M-values and the initial anisotropies of the resonator. However, in most cases it would be more appropriate to attribute the state selection anisotropy to the passive resonator. Since in a previous chapter the anisotropy of state selection was shown to be emissive, then the effect of the latter is equivalent to a partial polarizer inserted between the resonator discs.

As was mentioned above, the effect of anisotropy can be represented by a matrix of the form (Jones, 1941)

$$M_R = \begin{pmatrix} M'_{11} & M'_{12} \\ M'_{21} & M'_{22} \end{pmatrix}$$

where all the elements M_{ij} are in general complex. This can be written as

$$M_R = F \begin{pmatrix} M_{11} & M_{12} \\ M_{21} & M_{22} \end{pmatrix} \qquad 6.6$$

where

$$F = \sqrt{\det M_R} = f \exp(i\Psi) \qquad 6.7$$

where $f > 0$ and

$$M_{11} M_{22} - M_{12} M_{21} = 1 \qquad 6.8$$

If χ_1 and χ_2 are chosen to denote the eigenvalues of the matrix $(1/F) M_R$ then according to the above normalization it is easy to show that

$$\chi_2 \chi_1 = 1 \qquad 6.9$$

and thus F represents the isotropic reduction per transit in both amplitude and phase (de Lang, 1964). In order that a mode of propagation be an eigenstate of the resonator it must repeat its state of polarization, and thus satisfy the characteristic equation

$$M_R \begin{pmatrix} E_x \\ E_y \end{pmatrix} = \chi \begin{pmatrix} E_x \\ E_y \end{pmatrix} \qquad 6.10$$

The eigenvalues corresponding to such a state are

$$\chi_{1,2} = F \left\{ \frac{M_{11} + M_{22}}{2} \pm \left[\left(\frac{M_{11} + M_{22}}{2} \right)^2 - 1 \right]^{\frac{1}{2}} \right\} \qquad 6.11$$

Notice that in order that M_R will have non-degenerate eigenstates its

eigenvalues must be different. Therefore the condition

$$M_{11} + M_{22} \neq 2$$

must be fulfilled. In this case the two corresponding eigenstates satisfy (Jones, 1942)

$$\left(\frac{E_y}{E_x}\right)_1 = \frac{\chi_1 - M_{11}}{M_{12}} \qquad 6.12(a)$$

$$\left(\frac{E_y}{E_x}\right)_2 = \frac{\chi_2 - M_{11}}{M_{12}} \qquad 6.12(b)$$

From Eqn. 6.5 it is then concluded that there exist two eigenstates of polarization with different values of ellipticity and azimuth, ϵ and ϑ, respectivelly. The various types of anisotropy that might exist in the maser system are:

(a) Isotropic reduction

Here the matrix M_R must only multiply the vector $\underline{E}$ by a complex constant. Therefore it can be written as

$$M_I = F \begin{pmatrix} 1 & 0 \\ 0 & 1 \end{pmatrix} = FI$$

where I is the identity matrix. By direct substitution in Eqn. 6.11 it is easily shown that the eigenvalues of M_I are degenerate ($\chi_1 = \chi_2 = F$), and that the vectors

$$\hat{\underline{x}} = \begin{pmatrix} 1 \\ 0 \end{pmatrix} \quad \text{and} \quad \hat{\underline{y}} = \begin{pmatrix} 0 \\ 1 \end{pmatrix}$$

are eigenvectors. Since any vector $\underline{E}$ in the plane parallel to the mirrors plane can be written as

$$\underline{E} = A_x \hat{\underline{x}} + \underline{A}_y \hat{\underline{y}} \qquad 6.13$$

where A_x and A_y are complex, then any vector of the form

$$\underline{E} = \begin{pmatrix} E_x \\ E_y \end{pmatrix}$$

is an eigenvector of M_I. Therefore a resonator which is dominated by isotropic reduction supports any polarization parallel to its mirrors. Clearly the isotropic resonator is a powerful tool for the study of the anisotropic properties of the maser system (such as state selection) since it preserves the polarization characteristics of the molecular transitions within it.

(b) Pure phase anisotropy

When such an anisotropy acts on a state of polarization it only alters the value of the relative phases (δ) leaving the ratio of the amplitudes (r) unchanged. Let $\underline{E}$ be an eigenstate of such an anisotropy. Therefore

$$M_P \underline{E} = E' = \chi E$$

The components after a round trip then are

$$E_x' = \chi E_x$$

$$E_y' = \chi E_y$$

If the isotropic loss is excluded (det $M_P = 1$) then there must be no energy change in transmission. That is:

$$|E_x'|^2 + |E_y'|^2 = |E_x|^2 + |E_y|^2 = |\chi E_x|^2 + |\chi E_y|^2$$

or

$$|\chi|^2 = 1$$

Therefore the eigenvalues of M_p are

$$\chi_{\pm} = \exp(\pm i\varphi) \qquad 6.14$$

where φ is a real constant. Now if Eqn. 6.11 is rewritten as

$$\chi_{12} = x \pm \left(x^2 - 1\right)^{\frac{1}{2}}$$

where

$$x = \frac{M_{11} + M_{22}}{2}$$

then substitution in Eqn. 6.14 yields

$$M_{11} + M_{22} = \cos\varphi \qquad 6.15$$

A system which exhibits pure phase anisotropy will naturally be composed of retardation plates and rotors only. It is possible to show that the anisotropic properties of such a system can be expressed as a product of a linear birefringence plate and a rotation (Hurwitz and Jones, 1941). The resultant matrix is therefore

$$M_p = \begin{pmatrix} p + iq & z \\ z^* & p - iq \end{pmatrix}$$

where $p = \cos\varphi$ and $p^2 + q^2 + zz^* = 1$. In the absence of rotors and if the oblique axis of the anisotropy coincide with the (x, y) axis then $z = 0$, $q = \sin\varphi$ and

$$M_P = F\begin{pmatrix} \exp(i\varphi) & 0 \\ 0 & \exp(-i\varphi) \end{pmatrix} \qquad 6.15(a)$$

(c) Emissive (gain) anisotropy

The simplest example is the partial polarizer. If the high gain axis makes an angle θ with the x-axis, then the gain anisotropy matrix can be written as

$$M_A = FS^{-1} M_a S(\vartheta)$$

where

$$S(\vartheta) = \begin{pmatrix} \cos\vartheta & \sin\vartheta \\ -\sin\vartheta & \cos\vartheta \end{pmatrix}$$

is the rotation matrix and

$$M_a = \begin{pmatrix} a & 0 \\ 0 & 1/a \end{pmatrix} \qquad a > 0$$

6.3 OSCILLATION POLARIZATION WITH ZERO MAGNETIC FIELD

6.3.1 Theoretical Introduction

To investigate the behaviour of the oscillation ellipse, the equations which govern the dynamic behaviour of the ellipse parameters (ϵ, ϑ) must be derived. In this field, Lamb theory (Lamb, 1964) was a common basis for many authors who attempted the solution of this problem. The main idea of Lamb theory is that the effect of the radiation electric field is to induce a macroscopic polarization P. The vector P must of course obey the Maxwell equations and thus the excited medium must satisfy the equation

$$\nabla \times \nabla \times \underline{E} + \mu_0 M_R \cdot \frac{\partial \underline{E}}{\partial t} + \mu_0 \epsilon_0 \frac{\partial^2 \underline{E}}{\partial t^2} = - \mu_0 \frac{\partial^2 P}{\partial t^2} \qquad 6.16$$

In the above equation the scalar conductivity σ which appears in the original Lamb equation is replaced by the tensor M_R to include the anisotropic loss of the resonator (Sargent, Lamb and Fork, 1967). In general M_R can be written as the sum of the various anisotropy matrices described in the previous sections. Also it will be assumed that the variation of the electric field components in the longitudinal direction (perpendicular to the mirrors) is much sharper than their variation in the transverse directions, i.e. $\underline{E}$ will satisfy the inequalities

$$\frac{\partial E_x}{\partial z}(x,y,z,t) \gg \frac{\partial E_x}{\partial x}, \quad \frac{\partial E_x}{\partial y}$$

$$\frac{\partial E_y}{\partial z}(x,y,z,t) \gg \frac{\partial E_y}{\partial x}, \quad \frac{\partial E_y}{\partial y}$$

This assumption is true at least for the lowest order mode (TEM_{ooq}). According to these approximations the following equations are obtained

$$E_x(x,y,z,t) \simeq E_x(z,t)$$

$$E_y(x,y,z,t) \simeq E_y(z,t)$$

$$P(x,y,z,t) \simeq P(z,t)$$

The second step in Lamb's theory is to derive expressions for $P(z,t)$ in terms of $\underline{E}$ and the applied external magnetic field $\underline{H}$. Such expressions are derived to the third order in $\underline{E}$ and to the first order in $\underline{H}$. This approximation is reasonable for a Zeeman splitting which is small compared to the line-width. Following this approach, several authors (Culshaw and Kannelaud, 1966; Kannelaud and Culshaw, 1966; D'Yakonove and Perel, 1966A; D'Yakonove and Perel, 1966B) were able to extend the theory of polarization in optical masers in order to interpret some of the interesting results that were observed during the investigation of He-Ne transitions. However these theories were

incomplete. For example by setting the value of the axial magnetic field to zero in D'Yakonov equations (D'Yakonov, 1966) there are no such conditions under which circular polarization could possibly occur. Moreover only linear absorption anisotropy is assumed ($Q_x \neq Q_y$). Culshaw and Kannelaud (1964) at first attempted to explain the linearity of the oscillation polarization of some of the He-Ne transitions exclusively in terms of the properties of the molecular transitions, neglecting the anisotropy of the resonator altogether. In a later publication they included the aborptive anisotropy into their calculation as the factor which determined the direction of the linear polarization. Moreover only the transition $J = \frac{1}{2} \longrightarrow J = \frac{1}{2}$ was considered. de Lang (1967) presented an interesting approach to the theory of laser polarization which took account of all the various types of anisotropy. Although his theory was only phenomenological, it seemed to agree quite nicely with experimental investigations.

The first comprehensive quantum mechanical treatement to the polarization problem was first given by Polder and van Haeringen (1965) and subsequently by the extended work of van Haeringen (1967). In this theory, all molecular transitions and the various types of anisotropy were considered. It is along the lines of this theory that the experimental results concerning the polarization of the molecular beam maser oscillation are going to be interpreted. An outstanding feature of this theory is that it shows the behaviour of the polarization variables in terms of phenomenological constants. This results in a fairly transparent set of differential equations for the polarization parameters, thereby allowing a physical insight into the problem even without detailed calculations. If the electromagnetic field inside the cavity is assumed to be monochromatic then it can be written as

$$\underline{E}(z,t) = \varkappa \exp(-i\omega t) + \varkappa^* \exp(i\omega t) \qquad 6.17$$

where $\underline{x}$ is the elliptical basis vector which can be written as the sum of two opposite circularly polarized components

$$\underline{x} = \tfrac{1}{2}\left[A_+ \underline{e}_+ + A_- \underline{e}_-\right]$$

where $A_\pm$ are the elliptical amplitudes:

$$A_\pm(t) = a_\pm(t) \exp(i\psi_\pm)$$

and $\underline{e}_\pm$ are the circular basis vectors

$$\underline{e}_+ = \hat{\underline{x}} - i\hat{\underline{y}} \qquad 6.18(a)$$

$$\underline{e}_- = \hat{\underline{x}} + i\hat{\underline{y}} \qquad 6.18(b)$$

In other words, the elliptical oscillation is written as a superposition of two elliptically polarized ellipses with different amplitudes and phases. By making some approximations (Lamb, 1964), the macroscopic polarization vector can also be written as

$$P = \underline{B} \exp(-i\omega t) + \underline{B} \exp(i\omega t) \qquad 6.19$$

The complex amplitudes B are then expanded formally in terms of x to the third order in x . Substituting in 6.16 and introducing the quantities

$$\epsilon(t) = \arctan \frac{a_- - a_+}{a_- + a_+} \qquad 6.20(a)$$

$$\vartheta(t) = \tfrac{1}{2}(\psi_- - \psi_+) \qquad 6.20(b)$$

$$I(t) = a_-^2 + a_+^2 \qquad 6.20(c)$$

the desired phenomenological differential equations for the ellipticity ϵ and the orientation $\vartheta(t)$ at zero magnetic field are obtained (van Haeringen, 1967)

$$\frac{d\epsilon(t)}{dt} = \frac{1}{8}(\xi_2 - \xi_1) I \sin 4\epsilon + h_1(\epsilon,\vartheta) \qquad 6.21$$

$$\cos 2\epsilon \frac{d\vartheta(t)}{dt} = \frac{1}{8}(\zeta_2 - \zeta_1) I \sin 4\epsilon + h_2(\epsilon,\vartheta) \qquad 6.22$$

where the phenomenological constants ξ_i , ζ_i $(i = 1,2)$ are functions of the molecular transitions and h_1, h_2 are functions of the anisotropy of the system

$$h_1(\epsilon,\vartheta) = \tfrac{1}{2}\left[a \cos 2(\vartheta - \vartheta_a) \sin 2\epsilon + \phi_0 \sin 2(\vartheta - \vartheta_p)\right] \qquad 6.23(a)$$

$$h_2(\epsilon,\vartheta) = \tfrac{1}{2}\left[a \sin 2(\vartheta - \vartheta_a) - \phi_0 \cos 2(\vartheta - \vartheta_p) \sin 2\epsilon\right] \qquad 6.23(b)$$

ϑ_a is the angle that the high gain axis of the emissive anisotropy makes with the x-axis. Similarly ϕ_0 is the magnitude of the linear phase anisotropy whose axes are centred at ϑ_p and $\vartheta_p + \frac{1}{2}\pi$.

6.3.2 Application to the Molecular Beam Maser Oscillation

In the above derivation it was assumed that the process of population inversion of the two energy levels in question is isotropic. This is of course not true at low levels of state selection voltages. However, this difficulty can be overcome by attributing the voltage varying emissive anisotropy to the resonator and assuming the excitation state selection to be isotropic. Therefore a passive isotropic resonator will exhibit an emissive anisotropy whose magnitude depends on the value of the state selection voltage. Before going into experimental details it should be emphasized that the results presented in this section were obtained by employing the same experimental scheme as described in chapter 4. Therefore the behaviour of the oscillation ellipse is studied by displaying it, as a Lissajous figure on an oscilloscope by means of dual channel double frequency conversion from

the maser oscillation frequency (Yassin and Lainé, 1981). Also it seems appropriate to investigate the behaviour of the oscillation polarization at three different levels of state selection voltage, as follows

(1) High level of excitation

After a certain value of state selection (11KV for the inversion line J = K = 3 and 13KV for J = K = 2) the polarization of the maser oscillation changed from elliptical to circular. In interpreting this result it will be assumed that at this level of EHT, the resonator (including the anisotropy of state selection) becomes isotropic. In Eqn. 6.21 this corresponds to the case of $h_1 \approx 0$ and thus

$$\frac{d\epsilon(t)}{dt} = \left[\frac{1}{8}\left(\xi_2 - \xi_1\right) I\right] \sin 4\epsilon \qquad 6.24$$

since the ellipticity must satisfy (Eqn. 6.20):

$$-\tfrac{1}{4}\pi \leq \epsilon \leq \tfrac{1}{4}\pi$$

then Eqn. 6.24 possesses two stationary solutions

$$(a) \quad \epsilon = 0$$

$$(b) \quad \epsilon = \pm \pi/4$$

The first of these, (a), corresponds to linear polarization and, (b), to left or right-handed circular polarization. A quantum mechanical treatment shows that

$$\left(\xi_2 - \xi_1\right) = \frac{2(J^2 + J - 2)}{2J^2 + 2J + 1}\,\xi_1 \qquad \text{for } J \rightarrow J \text{ transitions}$$

where J is the total angular momentum and $\xi_1 > 0$ (in the present

discussion the effect of the hyperfine splitting is neglected since the main line is composed of unresolved hyperfine F-components. Nevertheless the present theory is perfectly valid for an oscillating F-component since the oscillating main line is composed of transitions of the type F⟶F).

For J = 2,3 the value of the term in brakets in Eqn. 6.24 is positive since I > 0. Therefore if ϵ approaches zero along the positive real axis ($\epsilon \longrightarrow 0^+$) then clearly $\Delta\epsilon/\Delta t < 0$. However the left hand side of Eqn. 6.24 in this case is positive. Similarly if ϵ approaches zero along the negative real axis, ($\epsilon \longrightarrow 0^-$) as a function of time then $\Delta\epsilon/\Delta t > 0$ while the calculated value of the left hand side of Eqn. 6.24 in this case is negative. It therefore follows that the solution (a) is not stable for transitions of the type J⟶J, J > 1. On the other hand it is easy to show that either of the solutions $\epsilon = \pm\pi/4$ is stable. It is therefore concluded that the theoretical prediction of circular polarization agrees with the experimental observation.

An immediate result which can be seen from Eqn. 6.24 is the fact that in the presence of the active medium the degeneracy of the eigenstates is lifted ,although the excitation is assumed to be isotropic. It is possible to suppose, therefore that the medium induces an anisotropy of some kind. For transitions of the kind J⟶J, J > 1 preference of circular polarization is shown while for transitions of the type J⟶J + 1 the induced anisotropy favours linear polarization.

(2) Low level of excitation

For state selection voltages less than 6.5KV, the polarization of both inversion lines J = K = 2,3 was linear. In this case the resonator phase anisotropy will be neglected with respect to the strong

emissive anisotropy of state selection. Putting $\phi_0 = 0$ in Eqns. 6.23 and substituting in Eqn. 6.21 and Eqn. 6.22 the following coupled equations are obtained.

$$\frac{d\varepsilon}{dt} = \frac{1}{8}(\xi_2 - \xi_1) I \sin 4\varepsilon + \tfrac{1}{2} a \cos 2(\theta - \theta_a) \sin 2\varepsilon \qquad 6.25(a)$$

$$\cos 2\varepsilon \frac{d\vartheta}{dt} = \frac{1}{8}(\zeta_2 - \zeta_1) I \sin 4\varepsilon + \tfrac{1}{2} a \sin 2(\vartheta - \theta_a) \qquad 6.25(b)$$

with the only stable solution

$$\varepsilon = 0, \qquad \theta = \theta_a$$

Therefore, in the presence of a strong emissive anisotropy the state of polarization is driven towards linearity along a direction which is also dictated by this anisotropy. For the molecular beam maser oscillation at low EHT values, the high gain axis of the emissive anisotropy is clearly the beam axis. Therefore it might be expected that the linearly polarized $\underline{E}$ vector will be orientated along the beam axis. The small angle ($\sim 10^\circ$) that the linearly polarized $\underline{E}$ vector was experimentally found to make with the beam axis is attributed to the magnetic rotation of the plane of polarization under the effect of the magnetic field of the laboratory, and to the possible misalignment of the state selectors to the horizontal. Furthermore, it is seen from the above equations that the azimuth of the linear polarization depends only on the orientation of the emissive anisotropy, regardless of the polarization tendencies of the medium. This explains the fact when the EHT was raised to a level where the polarization ellipse could be flipped to a new orientation of the major axis (say by tuning the cavity), it flipped back by itself to the original orientation when the EHT was taken down to the linear polarization level.

It should be remarked that for EHT voltages up to ~ 7.5KV where e = b/a ~ 10% there was neither a gradual, nor an abrupt flip in the polarization azimuth. To understand this the following quantities are introduced

$$p = n/n_{th}$$

n_{th} is the critical population excess required for oscillation and

$$G(\varepsilon, \theta) = \text{Re } F + a \cos(\theta - \theta_a) \cos 2\varepsilon$$

where F is the isotropic reduction per pass. Then, for small cavity anisotropies (a << F)

$$G(\varepsilon, \theta) \approx \text{Re } F \equiv G$$

Assuming also that the ellipticity is small (which is true at this level of excitation) so that $\sin\varepsilon \sim \varepsilon$, $\cos\varepsilon \sim 1$ it can be shown that (van Haeringen, 1967)

$$\varepsilon = \frac{-\frac{1}{2}\phi_o \sin(\theta - \theta_p)}{2(p-1)GS} \qquad 6.25(c)$$

where

$$S = \frac{(J-1)(J+2)}{5J(J+1)} \quad \text{for } J \longrightarrow J \text{ transitions}$$

Notice that in the above equation ε is small since for these values of EHT $p \sim 1$ and also $\phi_b << 1$ in any case.

Using these approximations it can be easily shown by direct substitution that the azimuth of polarization is given by

$$\frac{d\theta}{dt} = -T\phi_o \sin 2(\theta - \theta_p) - C_2 \phi_o^2 \sin 4(\vartheta - \theta_p) + \tfrac{1}{2}a \sin 2(\theta - \theta_a) \qquad 6.26$$

where

$$T = C_1 \frac{\nu - \nu_0}{\Delta \nu} \qquad 6.27(a)$$

$C_1 > 0$, $\Delta\nu$ is the line width and

$$C_2 = -\frac{S + 1}{8(p - 1)\,GS} \qquad 6.27(b)$$

$C_2 > 0$ for $J \longrightarrow J$ transitions ($J > 1$). Notice that equations 6.26, 6.27 are valid exactly for transitions of the type $J \longrightarrow J + 1$ since with the aid of Eqn. 6.24 it can be easily shown that such a transition favours linear polarization. In our case ($J \longrightarrow J$) the approximation is good for $p \sim 1$. Neglecting the phase anisotropy terms, Eqn. 6.26 can be written as

$$\frac{d\theta}{dt} = \tfrac{1}{2} a \sin 2(\theta - \theta_a) \qquad 6.28$$

For a given sign of "a" there exists a single stable solution. For example for $a > 0$ the solution $\theta = \theta_a + \pi/2$ is stable while for $a < 0$ the stable azimuth is $\theta = \theta_a$. This explains the absence of the polarization flip at low excitation levels as was stated in chapter 4.

(3) Intermediate level of excitation

As the value of EHT was raised above 8KV for the inversion line J = K = 3 and above 9KV for the line J = K = 2 the corresponding ellipticity (b/a) exceeded 1/6. At this stage the oscillation became polarization bistable with the possibility of flipping the polarization ellipse's major axis from one stable orientation to another by tuning the cavity across the resonance line centre.

It would be worthwhile first to consider the case of pure phase anisotropy ($a << \phi_o$). From Eqn. 6.26 it follows inmediately:

$$\frac{d\theta}{dt} = \phi_o \left[T - C_2\phi_o \cos 2(\theta - \theta_p) \right] \sin 2(\theta - \theta_p) \qquad 6.29$$

The stable solutions of Eqn. 6.29 are

$$(a) \quad \theta = \theta_p \qquad \text{with} \qquad T - C_2\phi_o < 0$$

$$(b) \quad \theta = \theta_p + \pi/2 \qquad \text{with} \qquad T + C_2\phi_o > 0$$

and also there exist the unstable solution

$$\cos 2(\theta - \theta_p) = \frac{T}{C_2\phi_o} \qquad \text{for} \qquad |T| < C_2\phi_o$$

This region of instability is equal to $2C_2\phi_o$. In other words, on either side of the oscillation line-centre there exists a stable state of polarization. The azimuth of these states are orientated at $\pi/2$ with respect to each other. Near the line-centre there exists a region of instability as shown in Fig. 6.1. If the cavity is started to be tuned from the left ($\nu < \nu_o$) then far enough from the line-centre the azimuth $\theta = \theta_p$ is stable. As ν approaches ν_o, $T \longrightarrow -C_2\phi_o$ and the region of instability is reached. In this region which extends up to $T = C_2\phi_o$ a flip to the other stable azimuth $\theta = \theta_p + \pi/2$ must occur. It was verified experimentally that the extent of the instability region was highly dependent on the operational conditions (gas pressure, nozzle alignment, etc.,) while the polarization flip itself could occur anywhere in this region, and not necessarily at the line centre.

In the present work the flip angle was much less than the predicted 90°. Nevertheless, the flip phenomenon itself was easily reproducible. The bistability of the maser oscillation is discussed in more detail in the following section. As it might be expected, the behaviour of the ellipticity in this intermediate region of EHT is complicated. As already emphasized, Eqn. 6.25(c) is valid for small

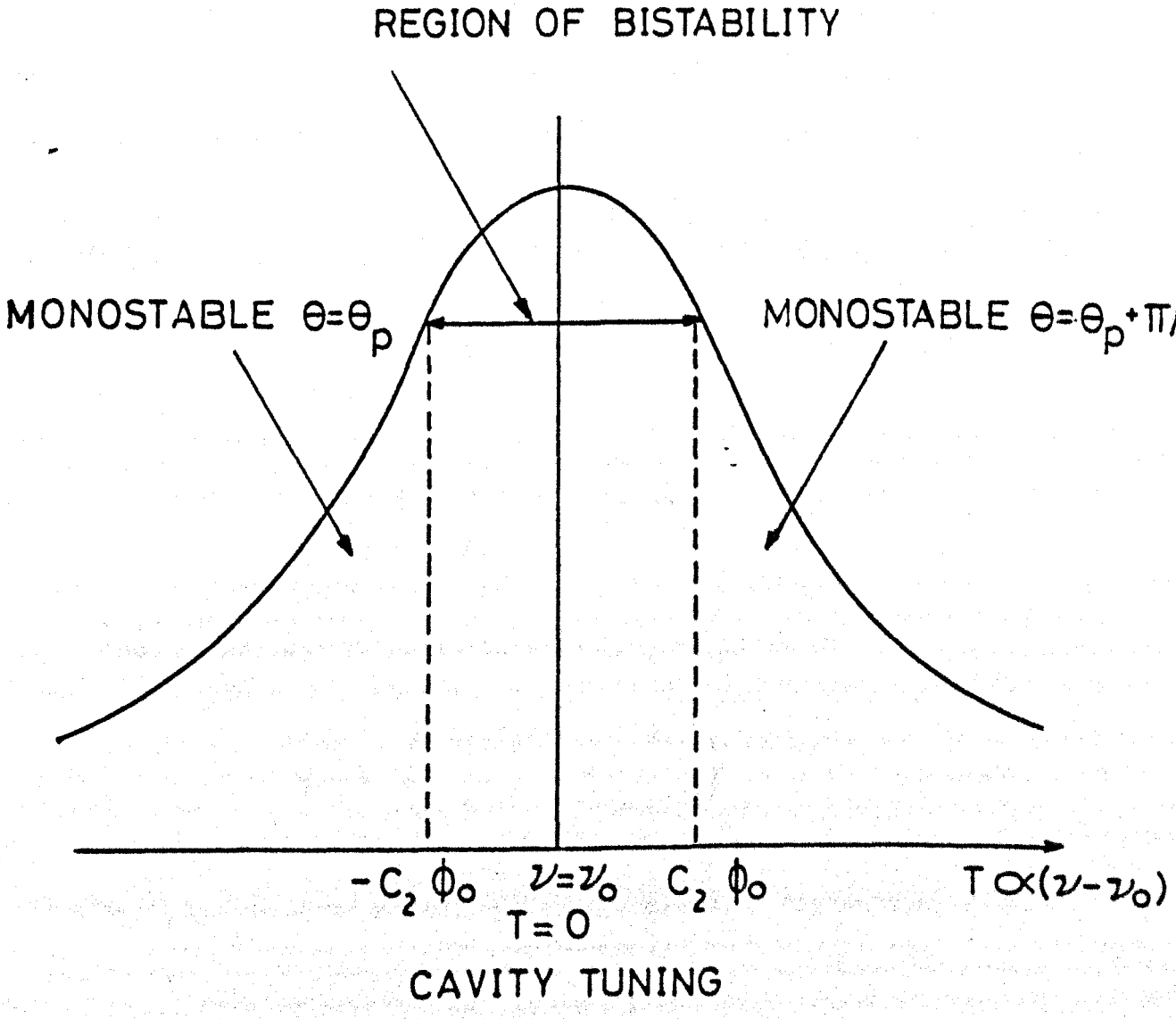

FIG. 6·1 POLARIZATION STABILITY OF THE MASER OSCILLATION IN A CAVITY WITH PURE PHASE ANISOTROPY.

ellipticities only. Although the polarization parameters could be found by numerical computation, nothing would be gained for the understanding of the problem especially because of the great sensitivity of these parameters to the operational conditions and small perturbations in the maser system. Nevertheless an adequate description of the polarization behaviour can be obtained with the aid of the matrix method which was developed in the previous section. From Eqn. 6.24 it was found that the eigenstates of polarization induced by the medium in an isotropic resonator are circular. These states are given by Eqn. 6.18 as

$$\underline{e}_{+} = \begin{pmatrix} 1 \\ -i \end{pmatrix} \qquad 6.30(a)$$

$$\underline{e}_{-} = \begin{pmatrix} 1 \\ i \end{pmatrix} \qquad 6.30(b)$$

The effect of anisotropy of state selection is given by

$$M_a = \begin{pmatrix} a_1(V_s) & 0 \\ 0 & a_2(V_s) \end{pmatrix} \qquad 6.31$$

The effect of emissive anisotropy on the circular eigenstate is then

$$\underline{e}' = M_a S(\theta)\underline{e} = \begin{pmatrix} a_1 \\ -a_2 i \end{pmatrix}$$

Therefore

$$\frac{e'_y}{e'_x} = \frac{e_y}{e_x} \times \frac{a_2(v)}{a_1(v)} = -i\,\frac{a_2(v)}{a_1(v)}$$

Comparing this equation with Eqn. 6.5 it is seen that it represents an

elliptical polarization with an ellipticity proportional to a_2/a_1. At low state selection voltages, $a_2 \approx 0$ and thus the anisotropy drives the mode towards linear polarization along the x-axis. For higher voltages a_1 starts to saturate and a_2/a_1 approaches unity, that is, circular polarization. For even higher voltages a_2/a_1 might exceed unity due to the fringe field, yielding elliptical oscillation again but now with the major axis along the y-axis.

This description of the oscillation polarization, agrees fairly well with the experimental obsevations concerning the polarization of the inversion lines J = K = 2,3. However for the weaker inversion line J = K = 1 no change in the ellipticity was detected as a function of the state selection voltage. For all values of state selection voltage, the oscillation produced a persistent linear polarization along the molecular beam axis. This may be interpreted by assuming that in this case the state selection is completely anisotropic ($a_2 = 0$ in Eqn. 6.31). The phenomenon can be attributed to the fact that the only nonvanishing matrix elements which contribute to the amplitude of oscillation are proportional to

$$\langle J,K,M = 1|H|J,K,M = 1\rangle \quad \text{and} \quad \langle J,K,M = -1|H|J,K,M = -1\rangle$$

Transitions of the type $\Delta M = \pm 1$ yield zero matrix elements (unlike the case of J = 3 where the transitions $M = 3 \rightarrow M = 2$, $M = -3 \rightarrow M = -2$ etc. are allowed). From all this it is concluded that:

(a) In the case of J = K = 1 coupling of state selected molecules and the microwave electric field produces linearly polarized oscillation along the beam axis.

(b) The only transitions caused by the fringe field are $M = 1 \rightarrow M = 0$ and $M = -1 \rightarrow M = 0$. Thus the spatially reoriented

molecules do not possess nonvanishing matrix elements. Unlike the J = 2,3 cases, the spatial reorientation of molecules does not alter the polarization of the oscillation but changes the magnitude of its amplitude.

6.4 BISTABILITY OF THE MASER OSCILLATION

In view of the importance of the maser oscillation stability, the polarization flip phenomenon described above must be studied carefully if the Fabry-Perot maser application as a frequency standard is not to be undermined (Lainé and Yassin, 1981). It was mentioned above, that after a certain value of EET the oscillation of the molecular beam maser became bistable. This value coincided with that at which the amplitude of oscillation component along the beam axis started to saturate. Also it was shown that flips can occur on the account of the linear phase anisotropy alone, and that no flips can occur without it. The theory predicts a flip angle of 90° in the case of pure phase anisotropy and similar flip angles ($\sim 80^{\circ}$) were indeed reported for the single mode He-Ne laser operated at the transition J = 1 ⟶ J = 2 (de Lang, 1967). In the present maser, the flip angle was found to be $\sim 23^{\circ}$ for the inversion line J = K = 3, which confirmed the presence of an emissive anisotropy at these values of EET which was comparable with the linear phase anisotropy of the resonator.

If the term with ϕ_o^2 is neglected for the sake of argument in Eqn. 6.26, then the behaviour of the azimuth of polarization in the presence of both emissive and phase anisotropy is given by

$$\frac{d\theta}{dt} = \frac{1}{2}\left[a\sin 2(\theta - \theta_a) - \phi_o C_1\left(\frac{\nu - \nu_o}{\Delta\nu}\right)\sin 2(\theta - \theta_p)\right] \qquad 6.32$$

For $|a| > |\phi_b|$ flips might not occur since a big value of $(\nu - \nu_o)$ is

required in order that the right hand side could change its sign. Moreover if flips do occur then the flip angle is expected to depend on $(\theta_a - \theta_p)$ and thus its value is not 90° (de Lang, 1967) as in the case of $a \simeq 0$. (Notice that for $a \simeq 0$ the flip occur exactly at the line centre in the above approximation, where $\nu - \nu_0$ changes sign). The assumption that the deviation of the flip angle from 90° is due to the emissive anisotropy is supported by a further experiment with the same equipment and method using the inversion line J = K = ? of ammonia. This line gave a barely measurable flip angle of only a few degrees. For this transition the emissive anisotropy of state selection is stronger than for the J = K = 3 transition. The factors that could have contributed to the phase anisotropy are deviations of the resonator plates from parallelism or flatness, or coupling imperfections and so on.

Switching methods of the polarization azimuth from one stable polarization to another include application of a Stark voltage of 50V between the resonator plates; by transverse deflection of one or other of the nozzle gas sources or by small changes of the local magnetic field by, altering the current of a Helm holtz coil pair which produced a magnetic field perpendicular to the plane of the cavity discs.

The effect of a Stark field is both to broaden the line by an amount greater than the bistability region and to shift the frequency of oscillation. After the field is removed, a new value of $\nu - \nu_0$ is established with the possibility of changing the sign of the term in brakets in Eqn. 6.32, thereby flipping the polarization azimuth. Such a switching method is expected to reveal equal probabilities for both stable orientations. A similar effect can be attributed to the Zeeman pulse apart from the fact that a smaller change in the line width was needed , due to the fact that the application of an axial magnetic

field alters the ratio ϕ_o/a quite strongly. Deflection of the nozzles was equivalent to the introduction of an auxiliary spatial anisotropy. Thus, which particular elliptical oscillation polarization occurs after oscillation quenching is determined by the new net anisotropy ratio ϕ_o/a and the new frequency of oscillation.

In general the two stable states of polarization had different intensities, ellipticities and frequencies as shown in Fig. 6.2. The value of the flip angle was strongly dependent on the oscillation conditions, and oscillation parameter settings could be found though when changes in the azimuth were gradual rather than abrupt when the maser was tuned through the line centre. Bistable operation was also observed using a totally different scheme of detection of the maser oscillation in which the maser output was controlled by a microwave signal introduced at one cavity port and detected from the other. This mode of detection is known as "zero beats" and was used previously to detect the maser oscillation (Smart, 1973). A frequency scan range of ~ 200Hz was obtained by applying a sawtooth voltage to a varactor diode placed across the 5MHz quartz crystal frequency reference of the klystron frequency stablizer. The presence of the maser oscillation was detected on either side of the oscillation quenching region by the obsevation of beats between the sideband signal injected into the cavity and the oscillation itself (Lainé and Al-Jumaily, 1979). It was found that by setting the output waveguide E vector azimuth at about 20° and a high level of sideband power used, oscillation amplitude jumps appeared on the left-hand side of the oscilloscope trace. An example of such an instability is shown in Fig.6.2(b)where two different beat signal levels have been captured on the same photographic trace. The two levels of the beat signal can be understood as the corresponding projections of two polarization

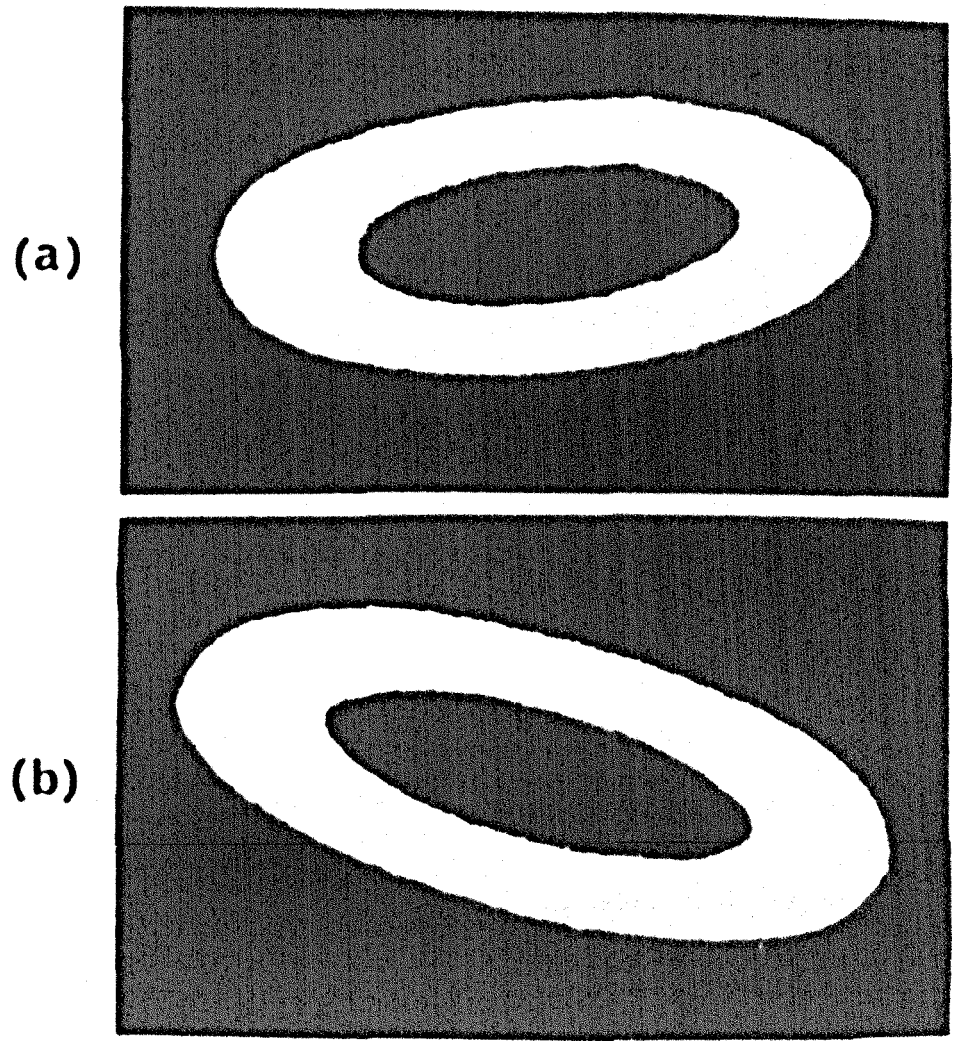

Fig. 6.2 Lissajous figures showing the polarization flip phenomenon using the inversion line J = K = 3 of ammonia.

ellipses with different inclinations with respect to the beam axis. From Fig. 6.3 a frequency difference of about 500Hz between the two signals can be deduced. This frequency difference is directly related to the difference in frequency between the two eigenstates of polarization provided the pulling effects are of negligible magnitude. Flipping of the polarization azimuth in this case is attributed to the flyback of the stimulating power frequency through the maser emission line (Lainé and Yassin, 1981).

When the stimulating input power was increased even further, the oscillation instability ceased and the beats shown in Fig. 6.3(c) appeared. No clear explanation to this phenomenon has yet been found although the beat signal was thought to represent locking of the two stable states of polarization.

6.5 THE MASER OSCILLATION UNDER A WEAK AXIAL MAGNETIC FIELD

6.5.1 Rotation of the Oscillation Plane of Polarization

In the following discussion the applied magnetic field is considered as weak, in the sense that the Zeeman splitting is small compared to the line-width. Also, the discussion is concerned with the behaviour of the maser oscillator near threshold. As was shown in this chapter, the resonator in this case is dominated by the emissive anisotropy of state selection and that the oscillation polarization is linear.

The effect of the axial magnetic field on the maser polarization can also be investigated with aid of the theoretical formulation given in Sec. 6.3. This is done by the addition of a term which is proportional to the field strength in Eqn. 6.25. Since emissive anisotropy alone is assumed, the behaviour of the polarization

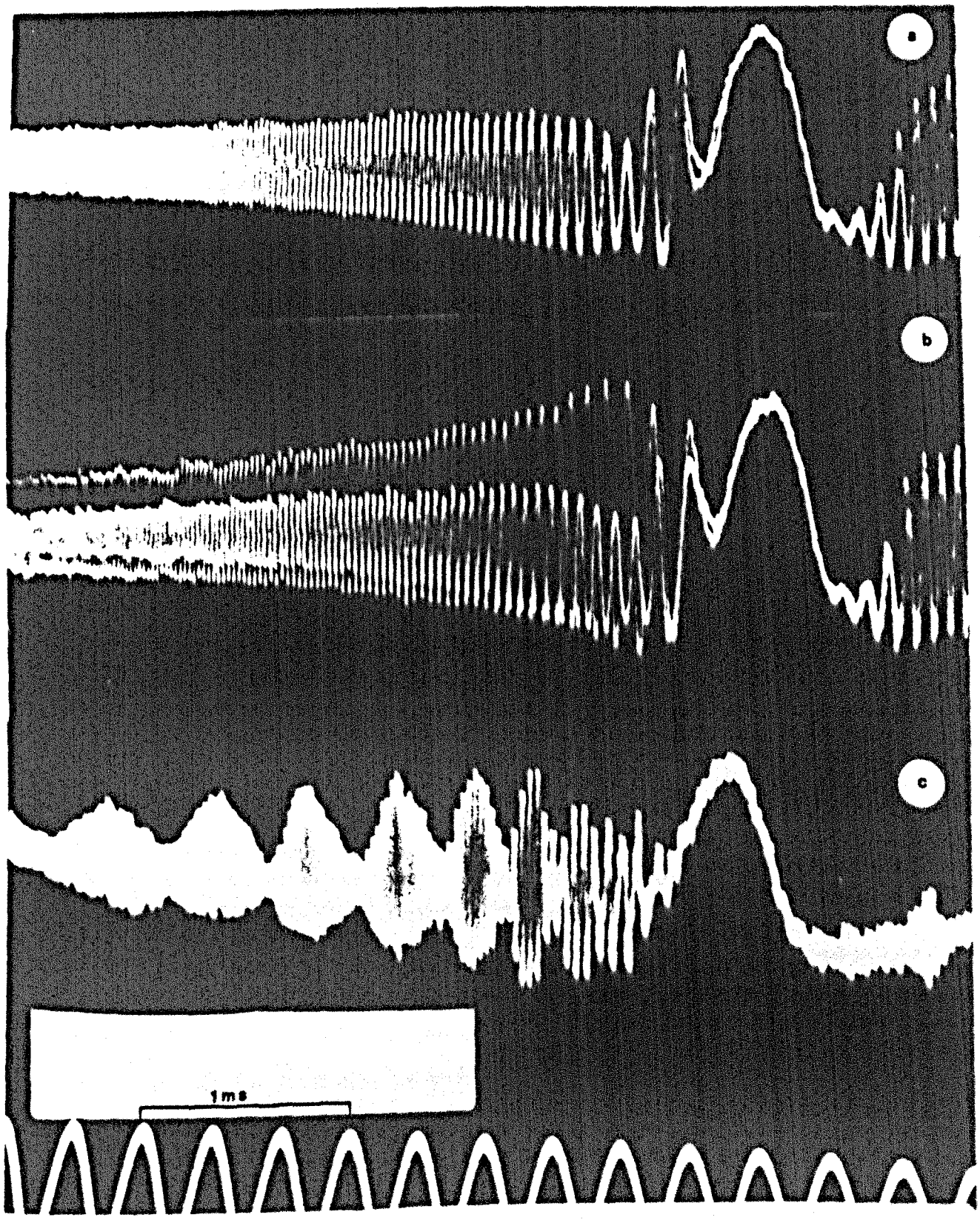

Fig. 6.7 Oscilloscope trace showing beats between the maser oscillation signal on the inversion line J = K = 3 of $^{14}NH_3$ and the stimulating microwave sideband.

(a) Monostable oscillation- low level of input power.
(b) Bistable oscillation- higher level of input power.
(c) Beats obtained by a further increase in the level of input power.

azimuth is given by

$$\frac{d\theta}{dt} = \tfrac{1}{2}a \sin 2(\theta - \theta_a) + bH_z \qquad 6.33$$

where b is a positive constant and H_z is the magnitude of the axial magnetic field. Therefore the stationary azimuth is given by the relation

$$\sin 2(\theta - \theta_a) = -\frac{2bH_z}{a} \qquad 6.34$$

From Eqn. 6.34 it can easily be seen that for $H_z = 0$ the polarization is linear along the direction $\theta = \theta_a$. As H_z increases continuously, so does the stable azimuth until the value $2(\theta - \theta_a) = \pi/2$ is reached. By then, the plane of polarization would have rotated through an angle of $\pi/4$. The corresponding critical value is found from the equation

$$\left|\frac{2bH_c}{a}\right| = 1$$

or

$$H_c = a/2b \qquad 6.35$$

For field strengths greater than those given by Eqn. 6.35 the solution of Eqn. 6.34 is no longer staionary and the plane of polarization rotates at a nonuniform rate. If the magnetic field is further increased so that $bH_z \gg a$, the rotation becomes uniform. Now the rotating ellipse can be considered as a superposition of two counter rotating circular components (Statz, Paananen and Koster, 1962).

From Eqn. 6.33 it can be noticed that the emissive anisotropy is responsible for the rotation of the plane of polarization and indeed for the staionary solutions at nonzero magnetic field. This explains

the absence of beats between Zeeman components at very low magnetic fields and the strong dependence of the field value at which these beats occur, on the cavity tuning and the value of state selection voltage.

de Lang (1967) gave a phenomenological expression for the constant "b" which appears in the above equations. In the theory of van Haeringen the following expression was found

$$b = \mu_B g G \frac{M}{h\Delta\nu}$$

where μ_B is Bohr magneton, g is Lande's factor, G is the isotropic loss, $\Delta\nu$ is the line-width and M is a factor which depends on a variety of parameters, however, its value is of the order of unity. Substitution in Eqn. 6.35 yields

$$H_c = \left(\frac{h\nu}{\mu_B g}\right)\left(\frac{a}{2G}\right)\left(\frac{1}{M}\right) \qquad 6.36$$

As was stated before, 'a' and 'G' represent the anisotropic and the isotropic gains respectively. If the high gain of the anisotropy is taken along the X-axis and the low gain along the Y-axis then

$$a \propto \{Q_x - Q_y\}$$

$$G \propto \left\{\frac{Q_x + Q_y}{2}\right\}$$

where Q_x and Q_y are respectively the effective Q-values of the active resonator near threshold, along and perpendicular to the beam axis. Therefore

$$H_c \approx \frac{h\Delta\nu}{\mu_B g} M \kappa_o \qquad 6.37$$

where

$$\kappa_o = \frac{Q_x - Q_y}{Q_x + Q_y}$$

Eqn. 6.37 is very similar to the equivalent expression obtained by D'Yakonov (1966).

Experimental investigation of the maser oscillation polarization under the influence of a weak axis magnetic field was made and some results are shown in Fig. 6.3. The azimuth of the polarization ellipse with respect to the beam axis is plotted against the Helmholtz coils current which is proportional to the perpendicular magnetic flux. The negative current axis corresponds to the direction of the earth's magnetic field component, parallel to the field generated by the current while the positive axis is antiparallel to the earth's field component. When the current was increased in the positive direction the oscillation ellipse was rotated towards the beam axis. The rotation was accompanied with an increase in the amplitude of oscillation which is a further confirmation to the assumption that the initial rotation at zero current is a result of the earth's field. After rotation through an angle of about -20°, the polarization which was initially made linear by taking down the level of state selection to about 6KV, became elliptical. Further increase of the magnetic field increased the ellipticity and it became circular when the two Zeeman components broke phase lock into biharmonic oscillation at about 5KHz. When the current was reversed, the sense of rotation was reversed but the behaviour was essentially similar.

As was stated at the begining of this section, the present theory is valid only in those cases where the ellipticity remains small. The variation of the ellipticity can then be written as (van Haeringen)

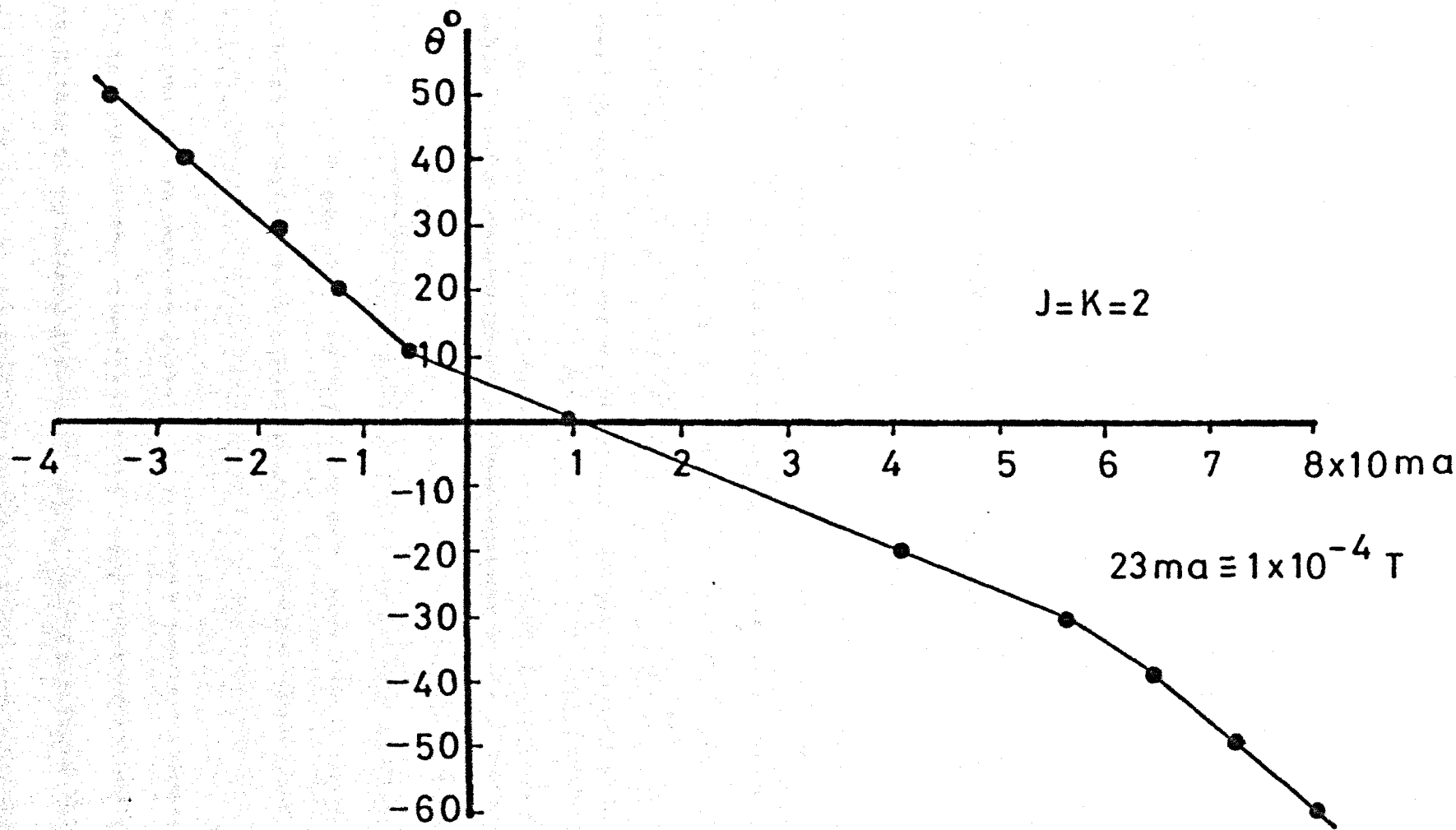

FIG 6.3 ROTATION ANGLE θ OF LINEARLY POLARIZED OSCILLATION IN A DISC RESONATOR AMMONIA BEAM MASER AS A FUNCTION OF MAGNETIC FLUX GENERATING CURRENT.

$$\varepsilon \propto \frac{\tilde{a} H_z}{(\xi_2 - \xi_1) I}$$

where $\tilde{a}$ is a constant which depends on the line-width. The bahaviour of ellipticity as a function of the applied external field depends therefore both on the line-width and the type of transition. For optical resonators, using the He-Ne transition J = 1⟶J = 2 it was reported that the ellipticity increased only slightly as the linear polarization was rotated through 45° (de Lang, 1967). The large variation in ellipticity in the ammonia maser in comparison with the He-Ne laser may therefore be attributed to two reasons:

(1) In the molecular beam maser the line-width is effectively much smaller owing to the elimination of Doppler broadening.

(2) The transition employed in the present work is of the J⟶J; J > 1 type which was shown to have circular tendency. The transition which was used in the laser work however is the J⟶J + 1 type (or the J⟶J; J < 1) which has a linear polarization tendency.

6.5.2 The Faraday Rotation Spectrometer

6.5.2.1 The Faraday effect

It was shown by Faraday (1846) that optical activity can be induced in matter by a constant magnetic field. It was observed that the plane of polarization of a light wave passing through such material, was rotated through an angle φ_m, provided a nonzero magnetic component H_z parallel to the direction of the light propagation was applied. The magnitude of rotation, for small values of H_z was found to be in direct proportion to both the external magnetic field and the length of the light path. This could be expressed by the equation

$$\varphi_m = V_o H_z L \qquad 6.38$$

where V_o is the "normal" Verdet constant.

If the frequency of the incident light is not near any absorption line of the material, then the normal Verdet constan can be written as (Serber, 1932)

$$V_o = (e/2mc^3)\nu \frac{\partial n}{\partial \nu}$$

where n is the refraction coefficient, e and m are respectively the charge and mass of the electron, c is the velocity of light and ν is the frequency of the incident wave.

Values of the normal Verdet constant for gases at microwave frequencies can hardly be found in the literature. This is due to the very small angles of rotation caused by the dipole moment of molecules. For example, the normal Verdet constant of ammonia at optical frequencies is about 19×10^{-6} min./G/cm. To obtain a rotation of 3^o in a gass cell 1m long a magnetic field of $\sim 10^5$G is required. However, when the frequency of the incident ratiation in near a resonant line, the rotation at this frequency is considerably enhanced. The effect in this case is often refered to as circular dichroism (Buckingham and Stephens, 1966; McCaffery, 1971) or as in the present work, "resonant" Faraday rotation, which is directely related to the Zeeman effect. It arises from the fact that the propagation constants of left and right-circularly polarized waves in the presence of an external magnetic field are different. It is therefore expected that rotation of the plane of polarization due to Faraday effect becomes dominant at the same values of magnetic field which causes the spectral line to split into two resolved component. The latter fact was used to distinguish between rotation of the oscillation ellipse due to all

sorts of anisotropies and the Faraday effect. In fact in the method of display which was described in chapter 4, the Faraday effect does not cause the polarization ellipse to rotate in a stationary way as a function of the magnetic field but causes the ellipse to rotate as a function of time when conditions for biharmonic oscillation are fulfilled.

The theory of resonant Faraday rotation in gases was theoretically investigated by Serber (1932). From this theory it could be concluded that the magnitude of rotation was limited by the line-width, although that was not verified quantitively. In reality however, resonator anisotropies at low values of the external magnetic field should be considered. The theoretical treatment is basically similar to the method according to it, Zeeman matrix elements are calculated. The electric dipole matrix elements are essentially of the form $\langle \alpha M | \underline{e}^{\pm} \cdot \underline{\mu} | \alpha' M' \rangle$ which describes the transition between the Zeeman sublevels M and M' of the two energy states α and $\tilde{\alpha}$ respectively for left and right-circularly polarized photons.

The quantum mechanical formula for the rotaion angle can somewhat be deduced from Eqn. 6.38. First Eqn. 6.38 is written in the form

$$\varphi_m \propto \chi_m$$

where χ_m is the magnetic suseptibility. Then the angle of rotation can easily be shown to be given by the relation

$$\varphi_m = \frac{\pi L}{2\lambda} \left[\chi_+ - \chi_- \right]$$

where χ_- and χ_+ are the suseptibilities for left and right-handed circularly polarized photons respectively. $\chi_\pm$ are then calculated

quantum mechanically (Carpentier, 1979) yielding an expression for φ_m .

Since the resonant angle of rotation is inversly proportional to the line-width it is therefore expected that the sensitivity of detection of small Faraday signals in a molecular beam maser would be at least 20 times better than that obtained in an absorption spectrometer. Furthermore, it will be shown that the use of a resonant cavity enhances the rotation angle by more than three orders of magnitude at microwave frequencies. Such properties are of great importance since they permit the avoidance of the complexity of applying a large, homogeneous magnetic field, especially for molecules with small magnetic dipole moment like ammonia.

6.5.2.2 Enhancement of Faraday rotation by the use of a resonant cavity

In the following, the transmission of a polarized wave through a resonator which exhibits a certain anisotropy will be discussed. In the conventional method, the multiple reflection problem was shown to require lengthy calculations even for the isotropic resonator (Rosenberg, Robinstein and Herriot, 1964). Furthermore, in the case of an anisotropic resonator the calculation using this method, although obvious in principle, might prove to be awkward in practice (Carpentier, 1979).

Here, a method which was suggested by de Lang (1967) and uses the matrix method, will be employed. In this method the incident wave (which is assumed to be linearly polarized) is decomposed into two components; each is an eigenstate of the resonator. This is mathematically possible since the two eigenvectors of the resonator can be regarded as the basis for all vectors in the plane of the resonator

discs. Therefore, any vector in this plane can be written as a linear combination of these vectors with complex coefficients. Now since these components are eigenstates of the resonator, the calculation of their transmission through the resonator is straight forward. After each reflection they must repeat their state of polarization and thus they are only multiplied by a complex constant equal to the corresponding eigenvalue.

Let the incident wave be linearly polarized along the X-axis. It is then can be written as:

$$\underline{E}_i = a_+ \underline{E}^+ + a_- \underline{E}^- \qquad 6.39$$

where $E^{\mp}$ are two independent eigenstates of the resonator with eigenvalues $\chi^{\mp}$ respectively. Let the anisotropy matrix of the resonator be given by $\mathbf{M}_a$ and let the transmission of $\underline{E}^+$ be first calculated. From Fig. 6.4 it can be easily argued that the transmitted wave is given by

$$\underline{E}_T^+ = \underline{E}_o^+ + \sum_{n=1}^{\infty} \chi^n t' \underline{E}_B^+ \qquad 6.40$$

where $\underline{E}_B^+$ is the waveform at B

$$\underline{E}_B^+ = \mathbf{M}_a(t\underline{E}^+) = t\mathbf{M}_a(\underline{E}^+) \qquad 6.41$$

and

$$\underline{E}_o = t' \underline{E}_B^+ = \frac{C}{t} \mathbf{M}_a(\underline{E}^+) \qquad 6.42$$

where C = t t' is a constant which depends on the values of the coupling holes and 't' and "t'" are the amplitude transmission coefficients. Eqn. 6.40 can then be written as

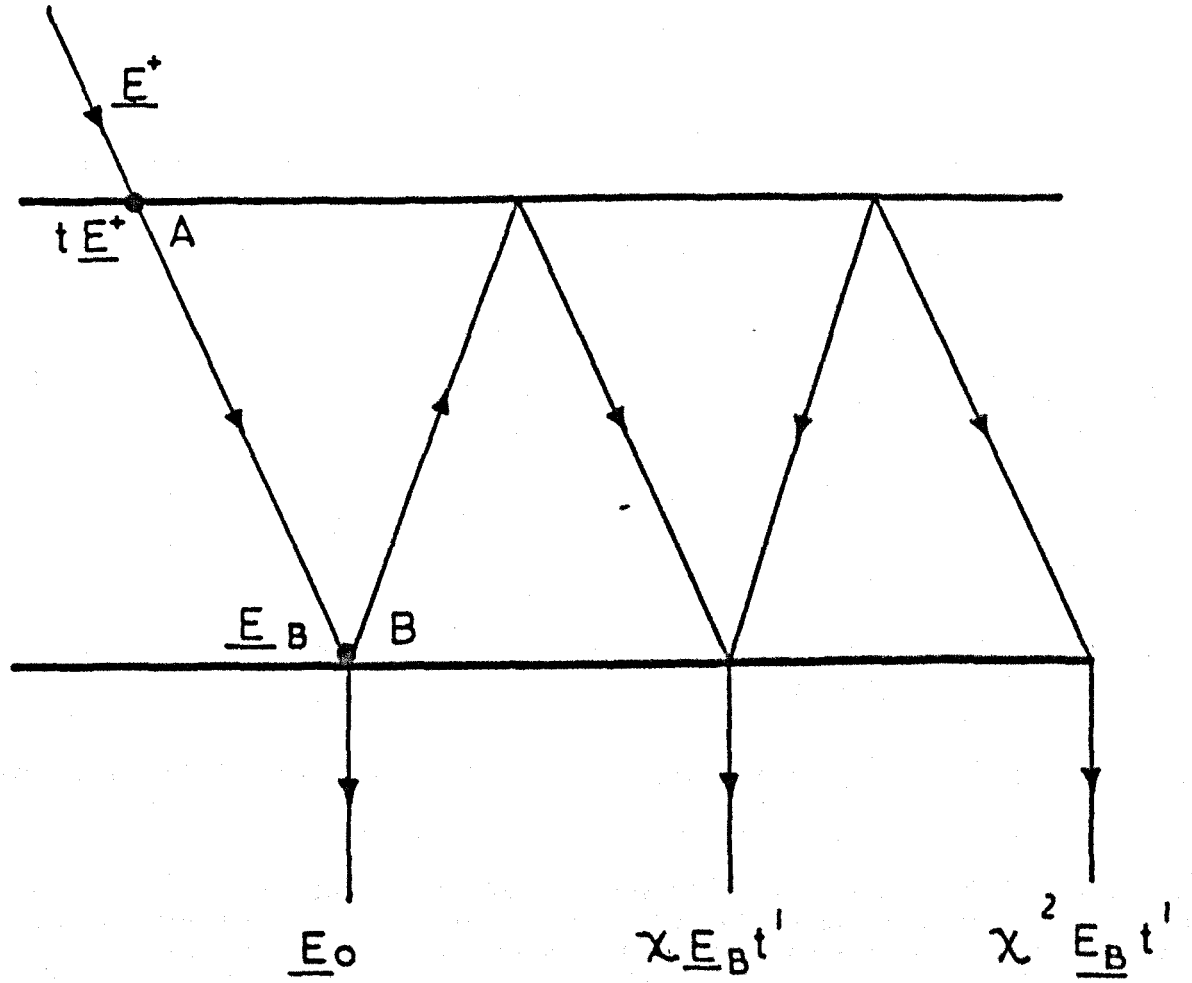

FIG. 6·4 TRANSMISSION OF AN EIGENSTATE OF POLARIZATION BY MULTIPLE REFLECTION IN A DISC RESONATOR.

$$\underline{E}_T^+ = t' \underline{E}_B^+ \sum_{n=0}^{\infty} \chi_+^n = t' T_+ \underline{E}_B^+ \qquad 6.43$$

and similarly

$$\underline{E}_T^- = t' T_- \underline{E}_B^-$$

where

$$T_+ = \sum_0^{\infty} \chi_+^n \qquad 6.44(a)$$

$$T_- = \sum_0^{\infty} \chi_-^n \qquad 6.44(b)$$

The transmitted wave can then be written according to Eqn. 6.39 as

$$\underline{E}_T = a_+ \underline{E}_T^+ + a_- \underline{E}_T^-$$

The polarization parameters can now be calculated from the formula

$$\frac{\underline{E}_{Ty}}{E_{Tx}} = \frac{(a_+ T_+ \underline{E}_B^+ + a_- T_- \underline{E}_B^-)_y}{(a_+ T_+ \underline{E}_B^+ + a_- T_- \underline{E}_B^-)_x} \qquad 6.45$$

So far the above formulas are valid for any type of combined anisotropy in the resonator. The application to some cases of interest will now be discussed.

(a) <u>An isotropic resonator which contains a Faraday rotor</u>

In this case the anisotropy matrix is pure rotation:

$$M_a = \begin{pmatrix} \cos\varphi_m & \sin\varphi_m \\ -\sin\varphi_m & \cos\varphi_m \end{pmatrix} \qquad 6.46$$

where φ_m is the Faraday rotation per pass. The round trip resonator

matrix is simply

$$\mathbf{M}_R = F\, I\, \mathbf{M}_a \mathbf{M}_a$$

or

$$\mathbf{M}_R = F\begin{pmatrix} \cos 2\varphi_m & \sin 2\varphi_m \\ -\sin 2\varphi_m & \cos 2\varphi_m \end{pmatrix} \qquad 6.47$$

The eigenvalues of $\mathbf{M}_R$ can be found from the characteristics equation

$$(\cos 2\varphi_m - \quad)^2 + \sin^2 2\varphi_m = 0$$

yielding

$$\chi_+ = F \exp(2i\varphi_m) \; ; \quad \underline{E}^+ = \begin{pmatrix} 1 \\ i \end{pmatrix} \qquad 6.48(a)$$

$$\chi_- = F \exp(-2i\varphi_m) \; ; \quad \underline{E}^- = \begin{pmatrix} 1 \\ -i \end{pmatrix} \qquad 6.48(b)$$

Thus the eigenstates in this case are circular with opposite senses of rotation. From Eqn. 6.48 it follows that, the coefficients a_+, a_- for a linearly polarized wave along the X-axis are equal. Moreover, from Eqn. 6.41 it is easily shown that

$$\underline{E}_B^+ = t \exp(i\varphi_m)\, \underline{E}^+$$

Substituting the above equation in Eqn. 6.45 and using the fact that $a_+ = a_-$, it follows that

$$\frac{E_{Ty}}{E_{Tx}} = i\, \frac{T_+ \exp(i\varphi_m) - T_- \exp(-i\varphi_m)}{T_+ \exp(i\varphi_m) + T_- \exp(-i\varphi_m)}$$

From Eqn. 6.44 $T_\pm$ are given by

$$T_{\mp} = \frac{1}{1 - \chi^{\mp}}$$

At resonance $F = f \exp(i\Psi) = f$ since $\Psi = 2\pi N$, where N is integer. Therefore $T_+ = T_-^*$ and using Eqn. 6.48 it follows that

$$\frac{E_{Ty}}{E_{Tx}} = \frac{\mathrm{Im}\,(T_+ \exp(i\varphi_m))}{\mathrm{Re}\,(T_+ \exp(i\varphi_m))}$$

Apart from a real factor:

$$T_+ \exp(i\varphi_m) = \cos\varphi_m(1 - f) + i\sin\varphi_m(1 + f)$$

Therefore

$$\frac{E_{Ty}}{E_{Tx}} = \frac{1 + f}{1 - f} \tan\varphi_m$$

and thus the plane of polarization was rotated by an angle

$$\Theta = \tan^{-1} \frac{1 + f}{1 - f} \tan \varphi_m \qquad 6.49$$

and the ellipticity

$$\varepsilon = 0$$

This result indicates that for a perfectly isotropic cavity containing a Faraday rotor the ellipticity of the transmitted wave remains unchanged. For small rotation angles Eqn. 6.49 can be written as

$$\Theta = \frac{1+f}{1-f} \varphi_m$$

Therefore the rotation is enhanced by a factor equal to:

$$M = \frac{1 + f}{1 - f} \simeq \frac{2}{1 - f} = \frac{2}{\alpha}$$

where α is the loss per transit and $f \sim 1$. By definition the above can be written as (Yassin and Lainé, 1979)

$$M = \frac{2}{\pi} \frac{Q}{q} \qquad 6.50$$

where Q is the loaded Q value and q is the longitudinal mode order. At microwave frequencies $Q/q \sim 6000$ and thus $M \sim 5 \times 10^3$. At optical frequencies however, $M \sim 100$. This indicates the importance of using a resonant cavity for enhancing the Faraday rotation angle, especially at microwave frequencies.

(b) Small gain (absorptive)anisotropy with Faraday rotation

From Fig. 6.5 the round trip matrix is given by

$$T_R = \begin{pmatrix} a_+ & 0 \\ 0 & a_- \end{pmatrix} \begin{pmatrix} \cos 2\varphi_m & \sin 2\varphi_m \\ -\sin 2\varphi_m & \cos 2\varphi_m \end{pmatrix} \begin{pmatrix} a_+ & 0 \\ 0 & a_- \end{pmatrix}$$

For small anisotropies, it follows that

$$a_+ \simeq 1 + s$$

$$a_- \simeq 1 - s$$

where $s \ll 1$. Therefore T_R can be written as

$$T_R = \begin{pmatrix} a_+^2 \cos 2\varphi_m & \sin 2\varphi_m \\ -\sin 2\varphi_m & a_-^2 \cos 2\varphi_m \end{pmatrix}$$

If second order terms in s are neglected, then the eigenvalues are

$$\chi_\pm = \exp(\pm 2i\varphi_m)$$

and the corresponding eigenvectors

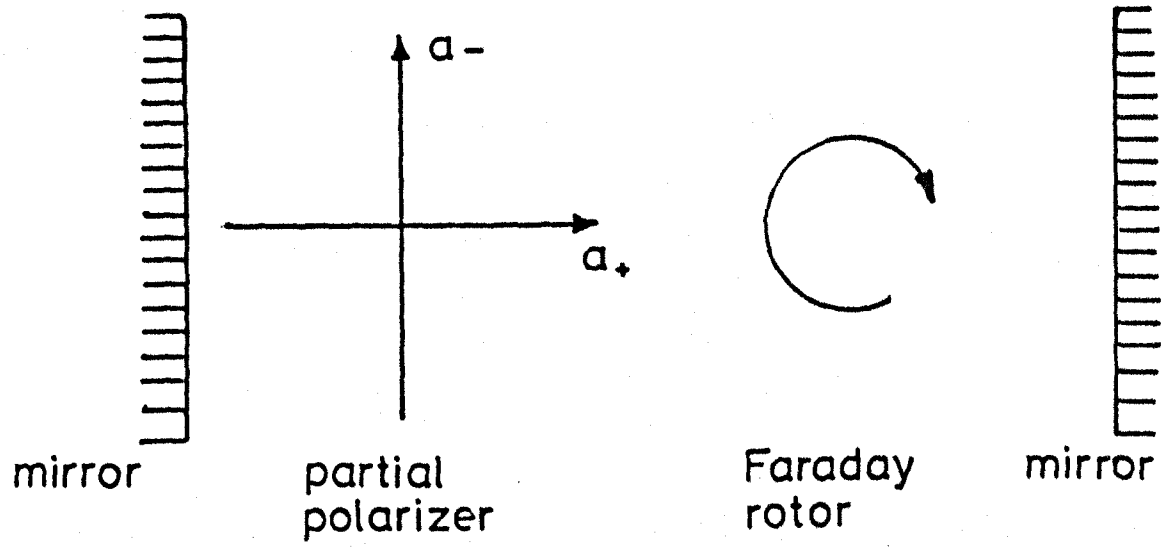

FIG. 6·5 CALCULATION OF THE ANISOTROPY MATRIX IN A RESONATOR CONTAINING A GAIN ANISOTROPY AND A FARADAY ROTOR

$$\underline{E}^{+} = \begin{pmatrix} 1 \\ -r \pm i \end{pmatrix}$$

where $r = 2\cot 2\varphi_m$. Notice that although the two elliptical eigenstates are inclined to the X-axis, they are still orthogonal to each other.

The direct transmittion anisotropy matrix in this case is

$$T_a = \begin{pmatrix} a_+ \cos\varphi_m & a_- \sin\varphi_m \\ -a_+ \sin\varphi_m & a_- \cos\varphi_m \end{pmatrix}$$

and by direct calculation it is easy to show that

$$T_a \underline{E}^{\pm} = \begin{pmatrix} \exp(\pm i\varphi_m) + s\exp(\mp i\varphi_m) \\ \pm i\{\exp(\pm i\varphi_m) - s\exp(\mp i\varphi_m)\} \end{pmatrix}$$

Notice that unlike the isotropic resonator, the eigenstates of T_R, $\underline{E}^{\pm}$ are not eigenstates of T_a and that they become so only if $s = 0$.

Again in this case, the linearly polarized wave can be written as a linear combination of the elliptical eigenstates $\underline{E}^{+}$ with $\alpha_+ = \alpha_-$. Therefore

$$\frac{E_{Ty}}{E_{Tx}} = i \left\{ \frac{\left[T_+\exp(i\varphi_m) - T_-\exp(-i\varphi_m)\right] - s\left[T_+\exp(-i\varphi_m) - T_-\exp(i\varphi_m)\right]}{\left[T_+\exp(i\varphi_m) + T_-\exp(-i\varphi_m)\right] + s\left[T_+\exp(-i\varphi_m) + T_-\exp(i\varphi_m)\right]} \right\}$$

Using the result obtained in (a) it can easily be shown that

$$\frac{E_{Ty}}{E_{Tx}} = \frac{\left[(1+f)/(1-f)\right]\tan\varphi_m + s_1}{1 + s_2}$$

where s_1 and s_2 are small real quantities. It is interesting to notice that although the Faraday rotation angle was altered by emissive

anisotropy, the ellipticity was not.

6.5.3 The Faraday Rotation Spectrometer

Magneto-microwave effects were investigated in esr (Servant, 1975), for paramagnetic gases (Garstens, 1953) and in bulk gas spectroscopy (Carpentier, 1979). It was found that in bulk gas, the rotation angle is very small even for a paramagnetic gas such as O_2 (Carpentier et al., 1979). As a result, detection of Faraday signal required the use of sophisticated electronic techniques such as digital averaging and low noise amplifiers. Even so, large values of external magnetic field (~1KG) were needed in order to obtain a detectable rotation angle.

The great sensitivity and the high resolution of molecular beam masers employing nearly isotropic disc resonators facilitated the study of the resonant Faraday effect in gases and the employment of this effect to produce a new type of spectrometer. In the following some preliminary results for the study of this effect in ammonia are given.

The molecular beam maser described in chapter 4, together with the detection scheme shown in Fig. 3.6 were employed. The incident signal was a linearly polarized wave with its electric field parallel to the beam axis. Its frequency was adjusted to equal the transition frequency of the inversion line $J = K = 2$ of ammonia (23.7GHz). The rotated Faraday signal was detected by rotating the output waveguide so that it transmitted microwave power with its electric field perpendicular to the beam axis. Since the polarization of stimulated emission signal in a maser always follows that of the stimulating input, then at zero magnetic field no signal was transmitted to the output.

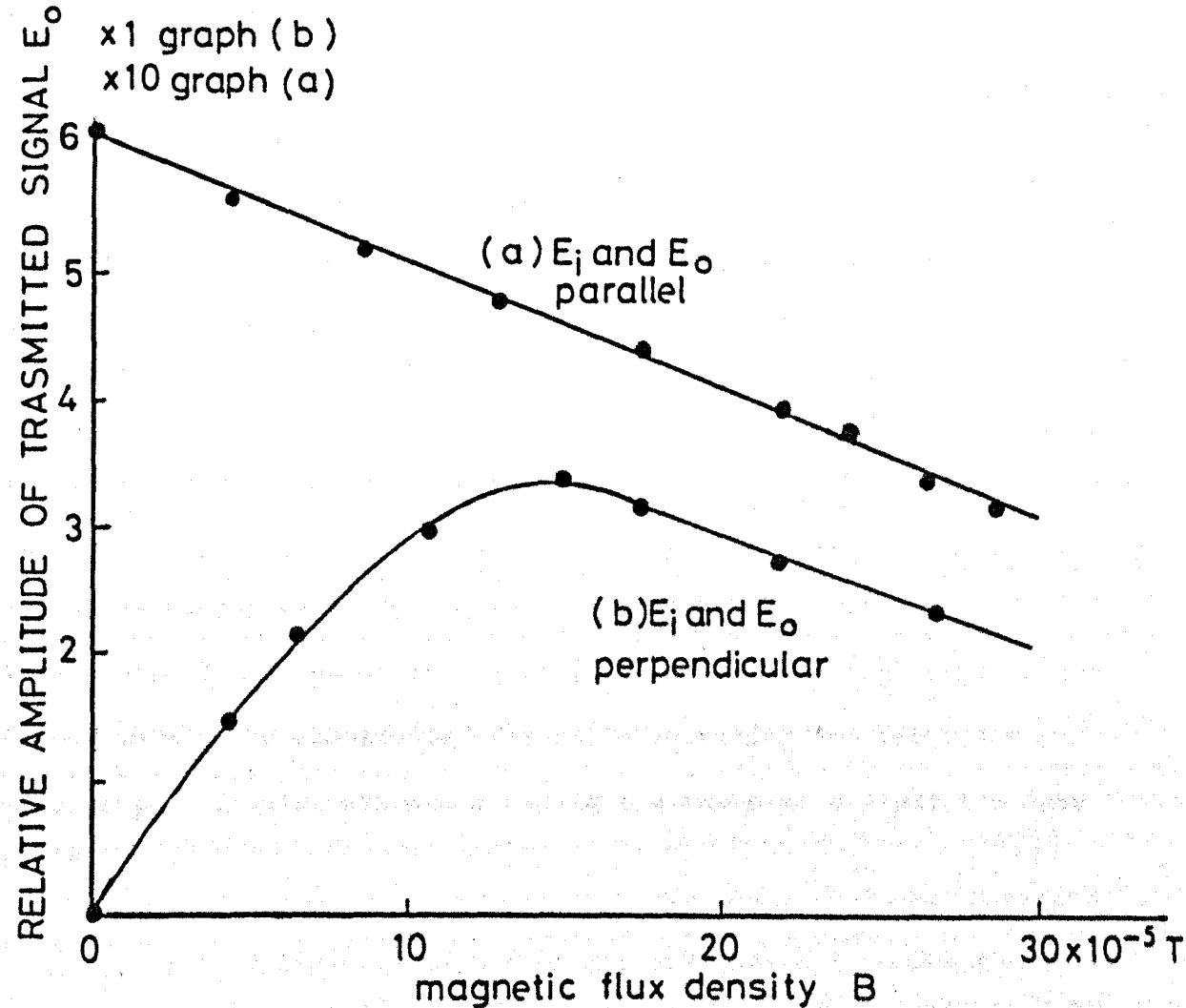

FIG. 6·6 RELATIVE AMPLITUDE OF SIGNAL E_o TRANSMITTED THROUGH MASER DISC RESONATOR WITH MAGNETIC FIELD APPLIED PERPENDICULARLY TO PLANE OF DISCS.

However, when a magnetic field of flux density B adjustable from zero to 3×10^{-4} Tesla was provided by the Helmholtz coils and applied perpendicularly to the plane of the disc, a small Faraday component was detected. It was compared with the component along the beam axis E_o by rotating the output waveguide back to an orientation such that the two waveguide transmission E vector were parallel. From this the rotation angle was calculated and the results are given in Fig. 6.7. The peak of the curve in Fig. 6.6(b) was associated with the onest of a resolved Zeeman doublet splitting and field inhomogeneity broadening as was clearly observed from the displayed signal.

From Fig. 6.7 it can be seen that the linear relation between the angle of rotation and the magnetic field is still preserved in the resonant Faraday effect. By analogy, a resonant Verdet constant V_r can therefore be defined. For ammonia at ~ 23.72GHz a value of $V_r \sim 22$ rad/T/m is obtained. This value which is independent of the cavity Q-value is uncorrected for state selection and resonator anisotropy. It also assumes a negligible value of ellipticity (see Ch. 7).

When electric dipole wiggles, the analogue of nmr wiggles, were produced by rapid passage of the stimulating input signal through the molecular resonance with B = 0, beating of beats was observed when the E-vectors of both waveguides were parallel to the beam axis (Fig. 6.8(a)). When these were made perpendicular by rotating the output waveguide, only the modulation envelope of the wiggle beats remained, since the carrier signal was not transmitted. By comparing the two traces in Fig. 6.8 it can be argued that the signal-to-noise ratio of the signal obtained via the Faraday rotation is a few times better than that obtained in the usual detection method. This is despite the fact that only a small perpendicular component of the stimulated emission

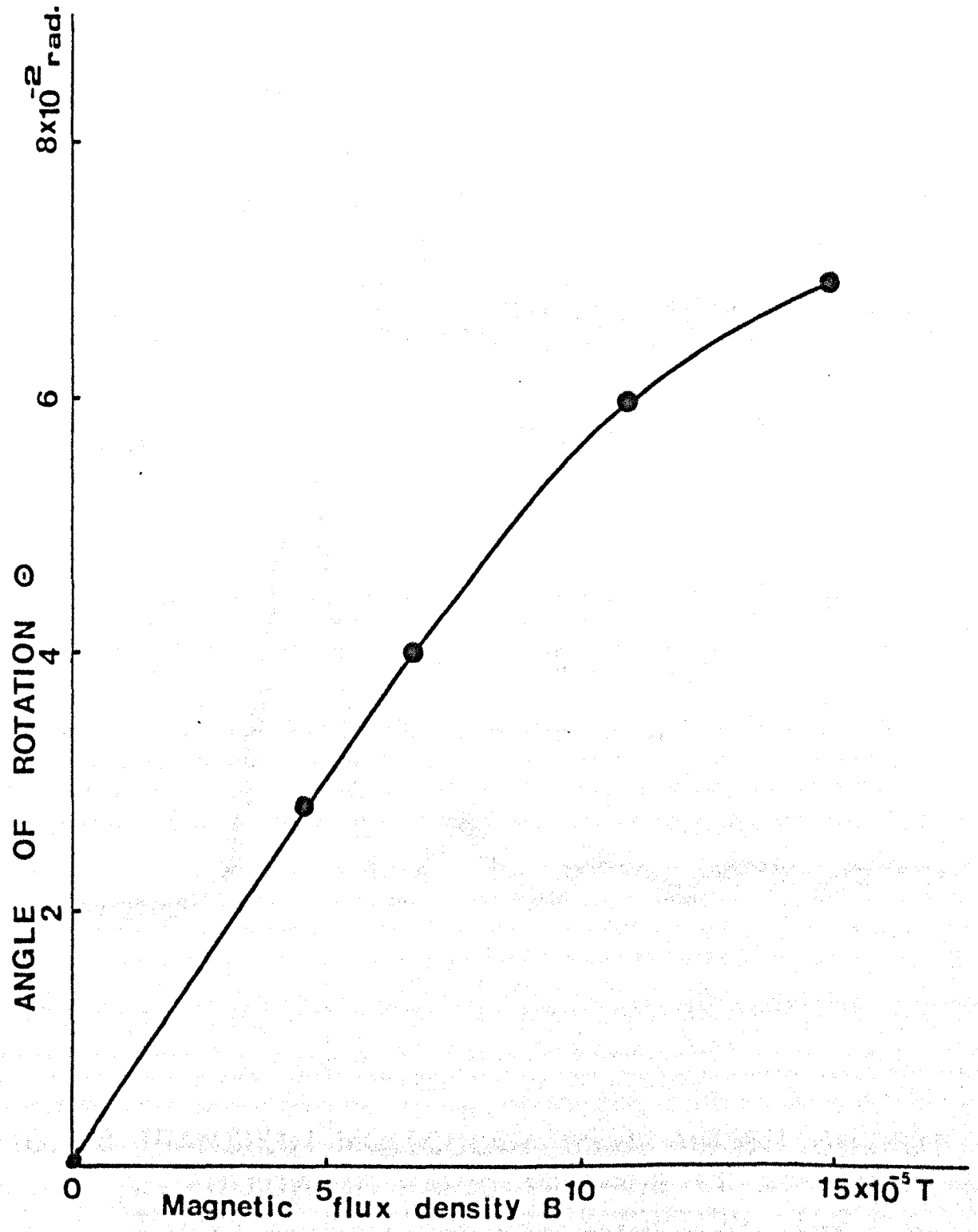

FIG 6.7 ENHANCED FARADAY ROTATION ANGLE AS A FUNCTION OF MAGNETIC FIELD

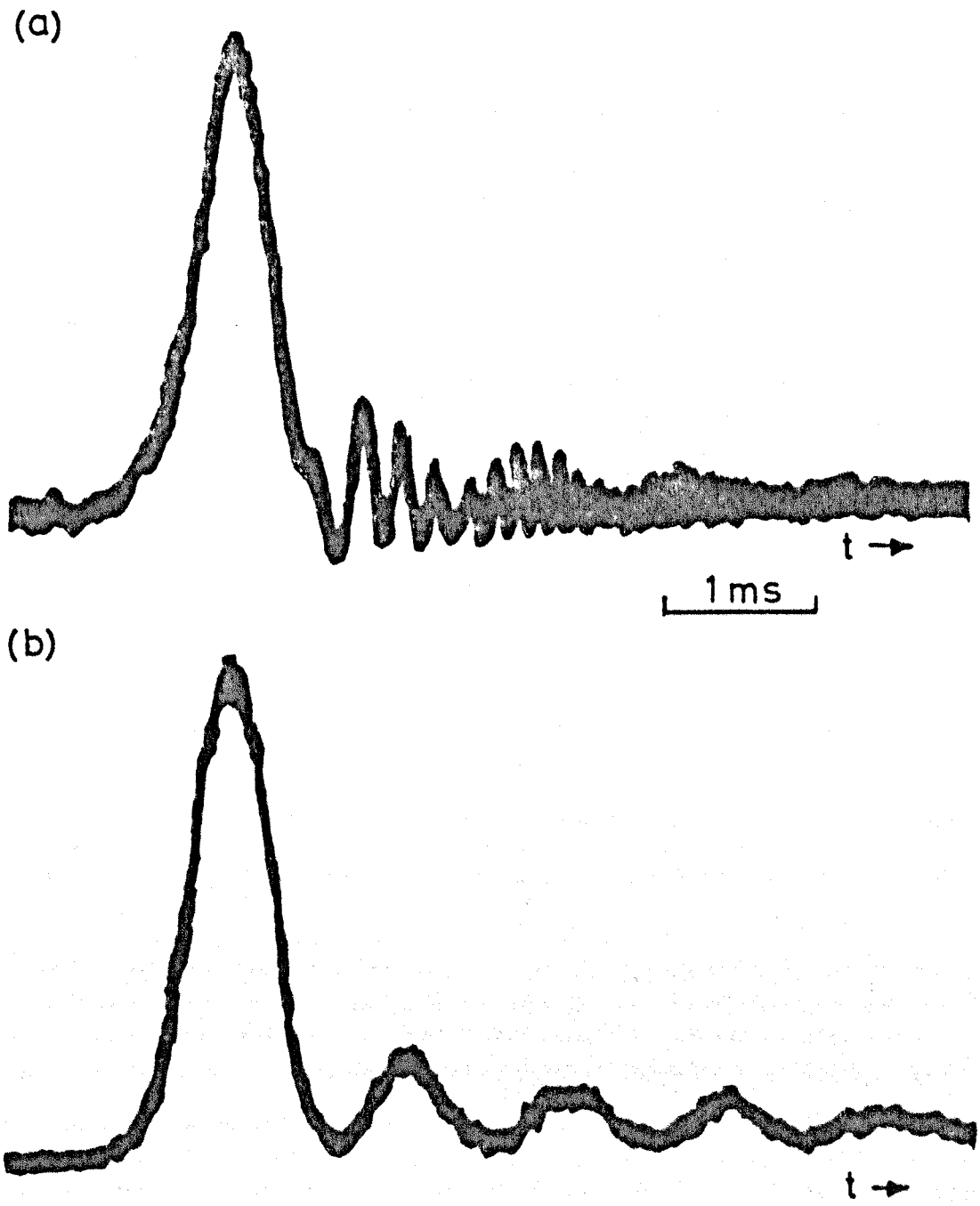

FIG. 6·8 TRANSIENT MOLECULAR BEAM MASER OUTPUT E_o FOLLOWING RAPID PASSAGE OF AN INPUT SIGNAL E_i THROUGH THE INVERSION LINE $J = K = 2$ OF $^{14}NH_3$ WITH WEAK ZEEMAN SPLITTING (a) E_o AND E_i PARALLEL (b) E_o AND E_i PERPENDICULAR.

signal was detected. This inevitably leads to the conclusion that a big reduction in the noise figure of detection had occured. Evaluation of the improvement sensitivity which is attributed to the fact that amplitude modulation noise which is carried by the sideband power is not transmitted to the detector, is estimated in chapter 7.

CHAPTER 7

SUGGESTIONS FOR FURTHER WORK

7.1 ON QUASI-OPTICAL RESONATORS

In chapter 2 some remarks on the theory of open resonators were given. The validity of some of the simple approximation methods given proved to be good in many practical cases. However, it may be concluded that the Wiener-Hopf technique is the most reliable method for calculation of resonator field configurations and resonance frequencies in the microwave spectral range with $\lambda/2$ separation between the mirrors. The application of this method to rectangular parallel plate resonators appears to be straightforward. As for the roof-top resonator it remains to apply this mathematical approach to calculate the reflection coefficient at the open end of an infinite roof-strip, taking advantage of the fact that the roof angle is very small. Moreover the di Francia theory on the roof-top resonator can be generalized in order to calculate the resonance condition when the electric field of the microwave input power is polarized in any direction parallel to the mirrors surface. In this case, further experimental data would be of very great importance. To achieve that, the design of the roof-top resonator described in chapter 3 must be somewhat modified so that it could be operated with higher order longitudinal modes. The quality factor and the electric field distribution can then be measured as a function of the roof angle for the first few values of q (say q = 1,2,3,4,5), and for different polarizations of the input microwave electric field. It is quite possible that for higher q-values, certain values of the roof angle can be found where the resonator losses are at a minimum as was

suggested by Checcacci et al. (1967).

An important advantage of the disc-type Fabry-Perot resonator over the other types of cavities (including the roof-top resonator) is that it allows the application of a uniform Stark field along the molecular beam. The effect of Stark field on the ammonia spectrum was treated both theoretically (Jauch, 1947) and experimentally (Coles and Good, 1951), excluding the effect of the hydrogen spins. To obtain an analytical expression, the problem was divided into two parts. In the first case, the Stark energy was considered weak with respect to the quadrupole splitting. Therefore the perturbed Hamiltonian was diagonalized in the representation $\langle J, I_N, F_1, M_{F_1}|$ where M_{F_1} is the projection of $\underline{F}_1$ along the Stark field. In the second case the Stark splitting was assumed to be much larger than the quadrupole coupling term. Thus the Hamiltonian could be diagonalized in the representation $\langle J, I_N, M_J, M_I|$ where M_J and M_I are the projections of $\underline{J}$ and $\underline{I}_N$ along Stark field respectively. When a tunable disc resonator is used in conjunction with the high resolution molecular beam maser, Stark splitting of the hyperfine components (resulting from the spin-spin interaction) could be observed (Al-Jumaily, 1979). Moreover, both the frequency and the intensity of Stark components were theoretically calculated by diagonalizing the complete Hamiltonian described in chapter 1. Verification of this theory can be obtained by measuring the Stark splitting of the intense quadrupole satellites components of the inversion line J = K = 1 of ammonia. The measurements could in principle be carried out without any particular difficulty using the sensitive double beam molecular beam maser system described in chapter 4 with its klystron stablizer, together with the "pip" frequency marker method described in Appendix II.

7.2 POLARIZATION OF THE MASER OSCILLATION

The elliptical nature of the maser oscillation at low state selection voltages was attributed to the emissive anisotropy of state selection. It was thought that if inversion lines with higher J-values were used, state selection would have become less anisotropic and accordingly transitions of the type J,K ⟶ J,K would approach circularity at lower state selection voltages in comparison to the voltages required for the 2,2 and 3,3 lines. As a result two additional experiments are suggested. In the first, the maser oscillation at the inversion lines J = K = 4 and J = K = 6 at the frequencies 24.139GHz and 25.056 respectively, could be investigated. The OKI klystron in present use is capable of being tuned and of providing enough power at these frequencies while the disc resonator can easily be tuned to these particular transitions without any further modification. The maser system described in chapter 4 together with the double-channel superheterodyne detection scheme can then provide Lissajous figures which represent the oscillation polarization of these transitions. To complete the picture, another experiment of interest could be made. However in this case longer state selectors should be constructed to provide more oscillation power at the inversion line J = K = 1 and perhaps even to oscillate on some of its quadrupole components. This would provide interesting information about the oscillation polarizations of the individual hyperfine components.

From the discussion given in chapters 4 and 6 it can be concluded that frequency stability of the maser oscillator employing disc resonators is degraded due to the polarization flip phenomenon. It was also found that this effect can be eliminated if an external strong emmisive anisotropy is introduced into the resonator. It may be therefore assumed that resonators with strong gain anisotropy would

exhibit polarization constraint which should manifest itself in the absence of the polarization flip phenomenon. To verify this, the roof-top resonator could be incorporated in the double beam ammonia maser and the oscillation polarization investigated in the same way as described in chapter 4. The oscillation polarization vector is then expected to lie along the beam axis (which is also the resonator axis of symmetry) for all values of state selection voltages.

As was always emphasized thoughout the present work the oscillation polarization experiments were carried out with the disc resonator at its lowest transverse mode order TEM_{ooo}. It is well known that if the resonator is tuned to its next higher order mode with two maxima of electric field along the beam axis a Doppler-split spectral line is obtained. It was found that the present maser system could be tuned to oscillate on either of the two components and that when the resonator is tuned to the centre frequency, beats between the two lines of about 7KHz are obtained (Al-Jumaily, 1979). This phenomenon can also be examined using the oscillation polarization method of detection (Yassin and Lainé, 1980). The biharmonic oscillation at the line centre would be observed as a rotation of the polarization ellipse at constant frequency. A polarization flip at each side of the centre may also occur. This may well explain the jumps in the amplitude of oscillation reported by Valentin (1978).

7.3 THE FARADAY ROTATION SPECTROMETER

In chapter 6 it was stated that enhancement of the spectrometer sensitivity could be obtained by detecting the stimulated emission signal via the Faraday effect. Let $(\Delta P)_o$ be the output power emitted by the beam at B = 0 and $(\Delta P)_f$ the perpendicular component of Faraday signal. For small angles of rotation it follows that

$$(\Delta P)_f = (\Delta P)_o \sin\Theta \approx (\Delta P)_o \Theta$$

It was also shown that the signal-to-noise ratio in a superheterodyne receiver can be written as

$$R_o = \frac{(\Delta V)_o}{N_o} = \frac{1}{N_o}\left[(P_o + \Delta P)^{\frac{1}{2}} - P_o^{\frac{1}{2}}\right] \simeq \frac{1}{N_o}\frac{(\Delta P)_o}{2P_o^{\frac{1}{2}}}$$

where P_o is the output sideband power and N_o is the noise voltage. In the detection scheme via the Faraday rotation effect no sideband power is transmitted and the signal-to-noise ratio can be written as

$$R_f = \frac{(\Delta V)_f}{N_f} = \frac{1}{N_f}(\Delta P)_f^{\frac{1}{2}}$$

where

$$N_f = F_f kT$$

$$N_o = F_o kT$$

F_f and F_o are the noise figures for detection in Faraday and the usual spectrometer set-ups respectively. The enhancement in sensitivity in the Faraday spectrometer is then given by

$$\frac{R_f}{R_o} = \frac{1}{2}\left[\frac{P_o}{(\Delta P)_o}\Theta\right]^{\frac{1}{2}}\frac{F_f}{F_o}$$

which shows that the improvement in sensitivity is proportional to $\Theta^{\frac{1}{2}}$. To estimate the reduction in the noise figure let $R_f/R_o \sim 3$ (Fig. 6.8) and $P_o/(\Delta P)_o \sim 9$. Therefore $F_f \sim 0.6\,\Theta^{-\frac{1}{2}} F_o$. For typical rotation angles ($\sim 1^o$) a 7-fold reduction of noise is obtained. This suggests that if lower noise amplifiers than the home-made ones employed in the

present work are used, a more sensitive Faraday spectrometer can be obtained even with such small rotation angles (Lainé and Yassin, 1981).

As was emphasized, the foregoing results were obtained with ammonia which has a magnetic moment of only one nuclear Bohr magneton. Resonant Faraday rotation may also be studied with the present maser system using other state-selectable molecules or radicals. The radical OH (9) would be of particular interest since it has a large magnetic moment. A possible transition is the $^2\Pi_{3/2}$, $J = 9/2$ Λ doublet at 23.82GHz.

So far the ellipticity associated with the Faraday effect has been ignored. It has been assumed that the emerging output wave was also linearly polarized, and that only pure rotation occurred. In fact the linear curve in Fig. 6.7 suggests that at low values of magnetic field the ellipticity is really small, and so can be ignored. However it should be added that measurements of ellipticity are also possible using more or less the same method used for displaying the oscillation ellipse. The detection scheme in Fig. 3.6 can still be used. The Faraday signal is first detected as a 30MHz signal and then it is frequency converted to 100KHz and applied to the vertical input of the oscilloscope. The signal component parallel to the beam axis is now detected in reflection. Using a magic tee, the sideband power can be cancelled by proper matching and the maser signal is also frequency converted down to 100KHz and then applied to the horizontal input of the oscilloscope. In this way the displayed Lissajous ellipse represents both the amplitude and the polarization of the stimulated emission signal. The rotation angle and the ellipticity of the maser signal as a function of magnetic field can then be studied by observing the oscilloscope trace.

APPENDIX I

CALCULATION OF MICROWAVE RESONATOR MODES

I.1 REFLECTION AT THE OPEN END OF A SEMI-INFINITE PARALLEL PLATE SYSTEM

The application of Weiner-Hopf technique to diffraction problems at microwave frequencies contributed a great deal to the theory of open resonators in this region of the spectrum. This is illustrated by the fact that by using this method, the resonator can be represented by an algebraic equation with one unknown. The characteristic equation of an infinite strip mirror of width "a" was shown to be (Eqn. 2.29).

$$R_q = (-1)^m \exp(-i\beta_{mq} a) \qquad \text{I.1}$$

Calculation of the propagation constant β_{mq} requires the knowledge of R_q which is given, in terms of β_{mq}, by Eqn. 2.30. The function $G_+(\rho)$ which appears in Eqn. 2.30 can be written as (Bates, 1970)

$$G_+(\rho) = \left[\sin(kd')/kd'\right]^{\frac{1}{2}} (1 + \rho/k)^{-\frac{1}{2}} \exp(ikd'/2 + I(\rho)) \qquad \text{I.2(a)}$$

where $i = \sqrt{-1}$, $k = 2\pi/\lambda$, $d' = 2d$ is twice the mirror's separation and

$$I(\rho) = \frac{i}{2\pi} \int_A \ln \left[1 + \frac{\rho d'}{(kd' + i\zeta/4)^{\frac{1}{2}}} \right] \left[\frac{\exp(2ikd' - \zeta)}{\exp(2ikd' - \zeta) - 1} \right] d\zeta \qquad \text{I.2(b)}$$

The integration path is along both sides of the branch cut located on the positive real axis in the complex ζ plane. Details of the

integration can be found in Bates. It is also shown there that for $kd \to \infty$ Eqn. I.2 reduces to the expression given by Vainshtein (1963). It was also found that calculations of $G_+(\rho)$ as given by Eqn. I.2 at $kd \sim 1$ is quite laborious and that in this case faster convergence of Eqn. I.1 is obtained by calculating $G_+(\rho)$ from the equation

$$G_+(\rho) = \left[\sin(kd')/kd'\right]^{\frac{1}{2}} \times \exp\left\{\frac{i\rho d'}{\pi}\left[1 - \Gamma + \ln\left(\frac{2\pi}{kd'}\right) + i\pi/2\right]\right\} \times \exp\left[\frac{id'\gamma}{\pi}\ln\left(\frac{(\rho - \gamma)}{k}\right)\right] \times \Pi(\rho) \quad \ldots \quad \text{I.3(a)}$$

where

$$\gamma = (\rho^2 - k^2)^{\frac{1}{2}} \qquad \text{I.3(b)}$$

and

$$\Pi(\rho) = \prod_{l=2,4,\text{even}}^{\infty}\left[\left(1 + \frac{\rho}{\beta_{1m}}\right)\exp\left\{\frac{i2\rho d'}{l\pi}\right\}\right] \qquad \text{I.3(c)}$$

It should be noted that the above derivation is made for an even number of maxima of the electric field along the longitudinal resonator axis. In the case of an odd number of maxima, the treatment is very similar.

I.2 SOLUTION OF THE FOX AND LI INTEGRAL EQUATION

In Ch. 2 it was shown that the integral equation which describes the infinite strip mirror at optical frequencies can be written as

$$E(x) = \gamma \int_{+1}^{-1} \exp\left[-i\sqrt{N}\,(x - x')^2\right] E(x')dx' \qquad \text{I.4}$$

where γ is a complex constant and N is Fresnel number which fully characterizes the resonator at a given frequency. The iterative

procedure for solution of Eqn. I.4 is as follows (Hildebrand, 1952):

(1) Select an initial arbitrary function E_o. For example E_o = constant can be taken.

(2) Calculate a new function $E_1(x)$ from the relation:

$$E_1 = \int_{+1}^{-1} K(x,x')\, E_o(x')dx'$$

and calculate γ_1 by the relation

$$\gamma_1 = \frac{\int E_o(x')E_1(x')dx'}{\int \left\{E_1(x')\right\}^2 dx'}$$

(3) Insert the function $E_1(x)$ and the constant γ_1 in the right hand side of Eqn. I.4 and find a new function $E_2(x)$. A new value γ_2 is then calculated. In general after the n_{th} iteration, the function E_n is computed and a value γ_n is found from the equation

$$\gamma_n = \frac{\int E_{n-1}(x')E_n(x')dx'}{\int \left\{E_n(x')\right\}^2 dx'}$$

The procedure is terminated after the functions E_n and the series γ_n converge to a single function E and a constant γ that give the field distribution and the propagation constant of the resonator respectively.

It is interesting to observe that the iteration process is equivalent to launching a plane wave into the resonator and letting it bounce back and forth between the parallel mirrors. The number of iterations which is required for convergence can thus be associated with the number of bounces which occur until the microwave amplitude

(and phase shift) reaches a steady state. In Fig. I.1 the intensity at the mirrors centre was computed as a function of the number of bounces for a Fresnel number N = 10. It shows that about 300 runs are required before a steady state is obtained. All computed results were programed in FORTRAN using the 7600 C.D.C. Manchester university machine. The programme itself is shown in the following pages.

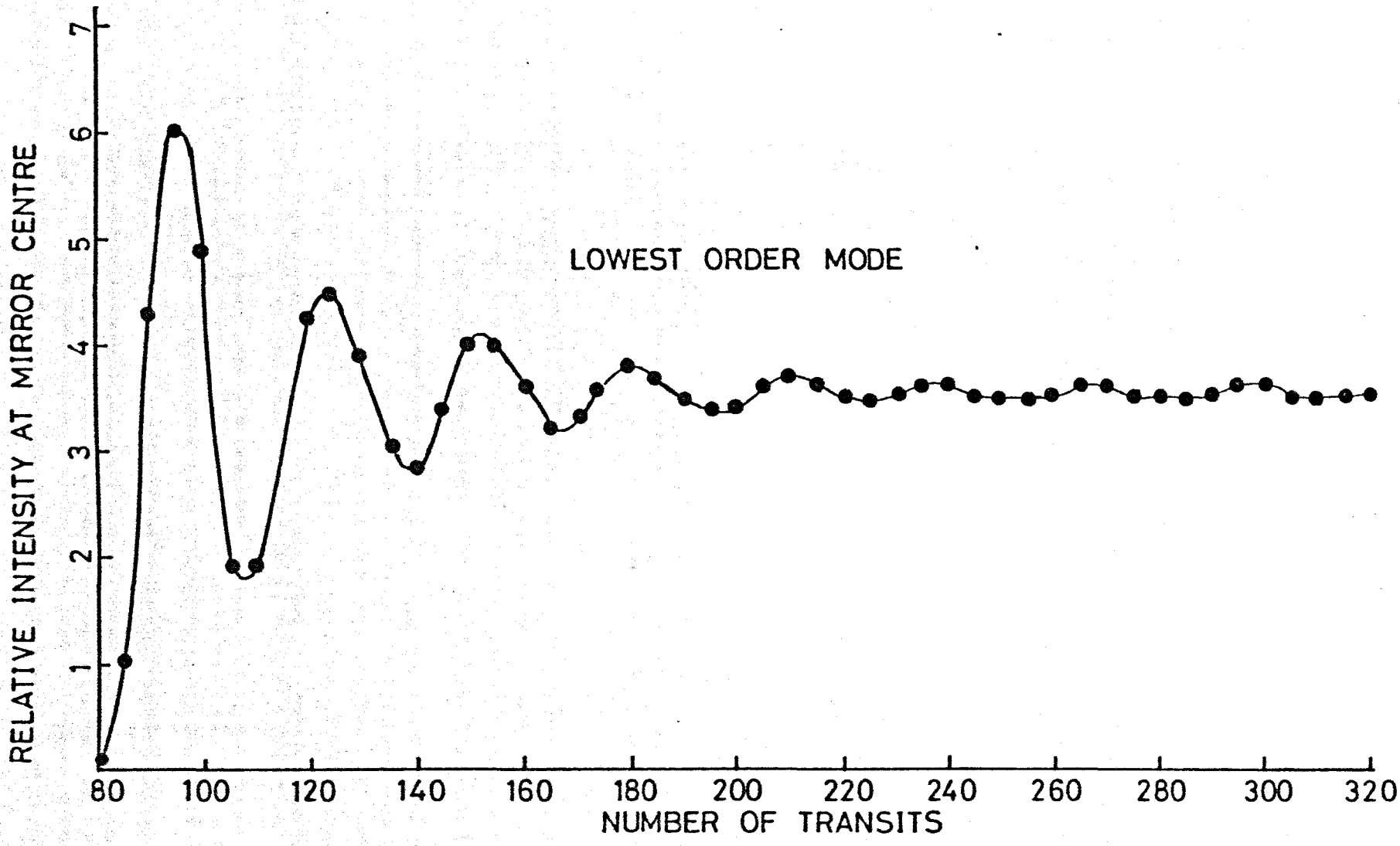

FIG. I·1 CONVERGENCE OF A FABRY PEROT RESONANT MODE.

```
PROGRAM FIRST      76/76   OPT=1 TRACE                    FTN 4.7+470        27/03/79  14.02.39        PAGE    1

      C  GHASSAN YASSIN SOLUSION OF COMPLEX INTEGRAL EQUATION
            PROGRAM    FIRST(OUTPUT,TAPE2=OUTPUT)
            DIMENSION   X(141)   ,Y(141)   ,TEMPRL(141)   ,TREL(141)   ,
           1 TEMPEM(101)   ,TEMG(101)   ,ENGREL(101,101)   ,ENGEMG(101,101)
           1 ,EIGEN(600)   ,CNTR(600)   ,AMPL(141)   ,EGN(600),PHAS(141)  ,
           2 STPREL(141)   ,STPEMG(141)
            COMMON  /LEV2/    ENGREL,ENGEMG
            LEVEL   2   ,ENGREL,ENGEMG
            RELF(A,B)  =  COS(   19.635*(  (A-B)**2  )   )
            EMGF(A,B)  = -SIN(   19.635*(  (A-B)**2  )   )
            X(1)   =   -1
            Y(1)   =   -1
            N  =  101
            L    =    N-1
            M    =     (N-3)/2
            NM   =  (N+1)/2
            KN   =  400
            KP   =  KN-3
            DO  2    K=1,L
            X(K+1)  =  X(K)  +  0.02
            Y(K+1)  =  Y(K)  +  0.02
      2     CONTINUE
            DO 4    I=1,N
            TREL(I)  =  1
            TEMG(I)  =  0
      4     CONTINUE
            K=1
      5     CONTINUE
            DO 7    J=1,N
            TRELT  =  TREL(J)
            TEMGT  =  TEMG(J)
            YT  =  Y(J)
            DO 6       I=1,N
            XT  =  X(I)
            RELFT  =  RELF(XT,YT)
            EMGFT  =  EMGF(XT,YT)
            ENGREL(I,J)  =  RELFT*TRELT  -  EMGFT*TEMGT
            ENGEMG(I,J)  =  RELFT*TEMGT  +  EMGFT*TRELT
      6     CONTINUE
      7     CONTINUE
            CALL    ENGRAL(-1.0,1.0,N,ENGREL,TEMPRL)
            CALL   ENGRAL(-1.0,1.0,N,ENGEMG,TEMPEM)
            CALL    ENTGRL(-1.0,1.0,N,TREL,CIREL)
            CALL    ENTGRL(-1.0,1.0,N,TEMG,CIEMG)
            CALL    ENTGRL(-1.0,1.0,N,TEMPEM,CFEMG)
            CALL    ENTGRL(-1.0,1.0,N,TEMPRL,CFREL)
            DOMEN   =   CFREL * * 2  +  CFEMG * * 2
            EIGNRL  =  (CIRLL * CFREL + CIEMG * CFEMG) / DOMEN
            EIGNEM  =  (CIEMG*CFREL  -CIREL*CFEMG)/DOMEN
            EIGEN(K)  =  EIGNRL
            CNTR(K)  =  TEMPRL(NM)
            ANSLNM  =  TEMPRL(NM)**2  +  TEMPEM(NM)**2
            DO 11        J=1,N
            STPREL(J)  =  (  TEMPRL(J)*TEMPRL(NM)  +
           4 TEMPEM(J)*TEMPEM(NM)  )/ANSLNM
            STPEMG(J)  =  (  TEMPEM(J)*TEMPRL(NM)  -  TEMPRL(J)*TEMPEM(NM)
           5  )/ANSLNM
```

```
SUBROUTINE ENTGRL     76/76   OPT=1 TRACE                    FTN 4.7+470        27/03/79  14.02.39        PAGE    1

            SUBROUTINE    ENTGRL(V,W,N,A,C)
      C   INTEGRAL  OF  A  GIVEN  ARRAY  A  OF  ODD  VALUES   N
      C  V,W, ARE LIMITS  ANSWER  IS  INTERED  IN  C
            DIMENSION   A(N)
            R  =  (N-1)
            H  =  (N-3)/2
            H  =  (W-V)/R
            EVEN  =  0
            ODD  =  0
            DO 20    J=1,M
            EVEN  =  EVEN  +  A(2*J)
      20    ODD  =  ODD  +A(2*J+1)
            C  =  H/3.  *(  A(1) +4*( EVEN+A(N-1) ) +  2*ODD +A(N)  )
            RETURN
            END
```

```
SUBROUTINE ENGRAL    76/76   OPT=1 TRACE                    FTN 4.7+470      27/03/79  14.02.39      PAGE     1

1               SUBROUTINE     ENGRAL(V,W,N,D,B)                                          1
              CINTEGRAL  OF  TWO  DIMENSIONAL  ARRAY  D  OF  ODD VALUES  N                2
              C  V,W,  ARE  LIMITS  ANSHER  IS  INTERED  IN  ARRAY  B                    3
                    DIMENSION     D(N,N)     ,      B(N)                                  4
5                   LEVEL  2,D
                    R  =  (N-1)                                                         5
                    M  =  (N-3)/2                                                       6
                    H  =  (W-V)/R                                                       7
                    DO 50   I  =  1,N                                                   8
10                  EVN  =  0                                                           9
                    OD  =  0                                                           10
                    DO 40    J=1,M                                                     11
                    EVN  =  EVN  +  D(I,2*J)                                           12
                40  OD  =  OD  +D(I,2*J+1)                                             13
15                  B(I)  =  H/3.  *(  D(I,1)  +4*( EVN+D(I,N-1) )  +2*OD  +D(I,N)  )  14.
                50  CONTINUE                                                          15
                    RETURN                                                             16
                    END                                                                17
```

```
CARD NR. SEVERITY  DETAILS    DIAGNOSIS OF PROBLEM

    5   ANSI              THIS STATEMENT TYPE IS NON-ANSI.
   15   ANSI    +         THE TYPE COMBINATION OF THE OPERANDS OF A RELATIONAL OR ARITHMETIC OPERATOR (OTHER THAN **) IS NON-ANSI.
   15   ANSI    +         THE TYPE COMBINATION OF THE OPERANDS OF AN EXPONENT OPERATOR IS NON-ANSI.
```

```
PROGRAM FIRST     76/76   OPT=1 TRACE                    FTN 4.7+470      27/03/79  14.02.39      PAGE     2

                    AMPL(J)  =  STPREL(J)**2  +  STPEMG(J)**2
                    PHAS(J)  =  STPEMG(J)/STPREL(J)
60                  TREL(J)  =  STPREL(J)
                    TEMG(J)  =  STPEMG(J)
                11  CONTINUE
                    IF(K-2)       14,14,17
                17  IF(K-KP)      15,14,14
65              14  CONTINUE
                    DO 8       I=1,MM                                                  43
                 8  WRITE(2,9)   K(I)  ,STPREL(I)  ,STPEMG(I)  ,AMPL(I)  ,PHAS(I)
                 9  FORMAT     (5E23.4)
                    WRITE (2,10)   EIGNRL,  EIGNEM                                     27
70              10  FORMAT     (2F10.5)                                                28
                15  K  =  K+1
                    IF  (K-KN)   12,12,13                                              52
                12  GO  TO  5                                                          48
                13  WRITE(2,19)          (  EIGEN(K)   ,K=1,KN )
75                  WRITE  (2,19)     (CNTR(K) , K=1,KN  )
                19  FORMAT     (  10  (1X,F12.4)  )
                    STOP
                    END                                                                50
```

APPENDIX II

MEASUREMENT OF THE RESONATOR QUALITY FACTOR

A quick method for measuring the loaded Q-value of a cavity can be obtained by using the detection scheme described in Fig. II.1. The klystron reflector voltage is swept with a 50Hz sawtooth waveform so that the cavity response, observed in transmission, can be displayed on the input Y_2 of a dual beam oscilloscope.

By measuring the frequency separation Δf between the half-power points on the cavity response curve, the Q-value can be calculated from the relation

$$Q = \frac{f_o}{\Delta f} \qquad \text{II.1}$$

where f_o is the centre frequency response which can be measured with good precision by calibrating a wavemeter from the known maser transition at ~ 24GHz.

Determination of Δf is made by displaying a marker pip, whose position can be adjusted to coincide with a half power point on the second trace (input Y_1) of the oscilloscope. The marker pip is the beat signal between the swept klystron and a harmonic of a tunable crystal oscillator. The 5MHz oscillator frequency is multiplied 90 times to 450MHz in a frequency multiplier chain (Micro-Now model 101C), and then applied to the diode "A" (1N26A). The 53rd harmonic at about 24GHz is then mixed with the klystron signal at the mixed "B" (1N26A) to produce a zero beat pip on the oscilloscope trace. It is also more convenient to amplify the beat signal by a narrow band radio receiver (Type RA. 117).

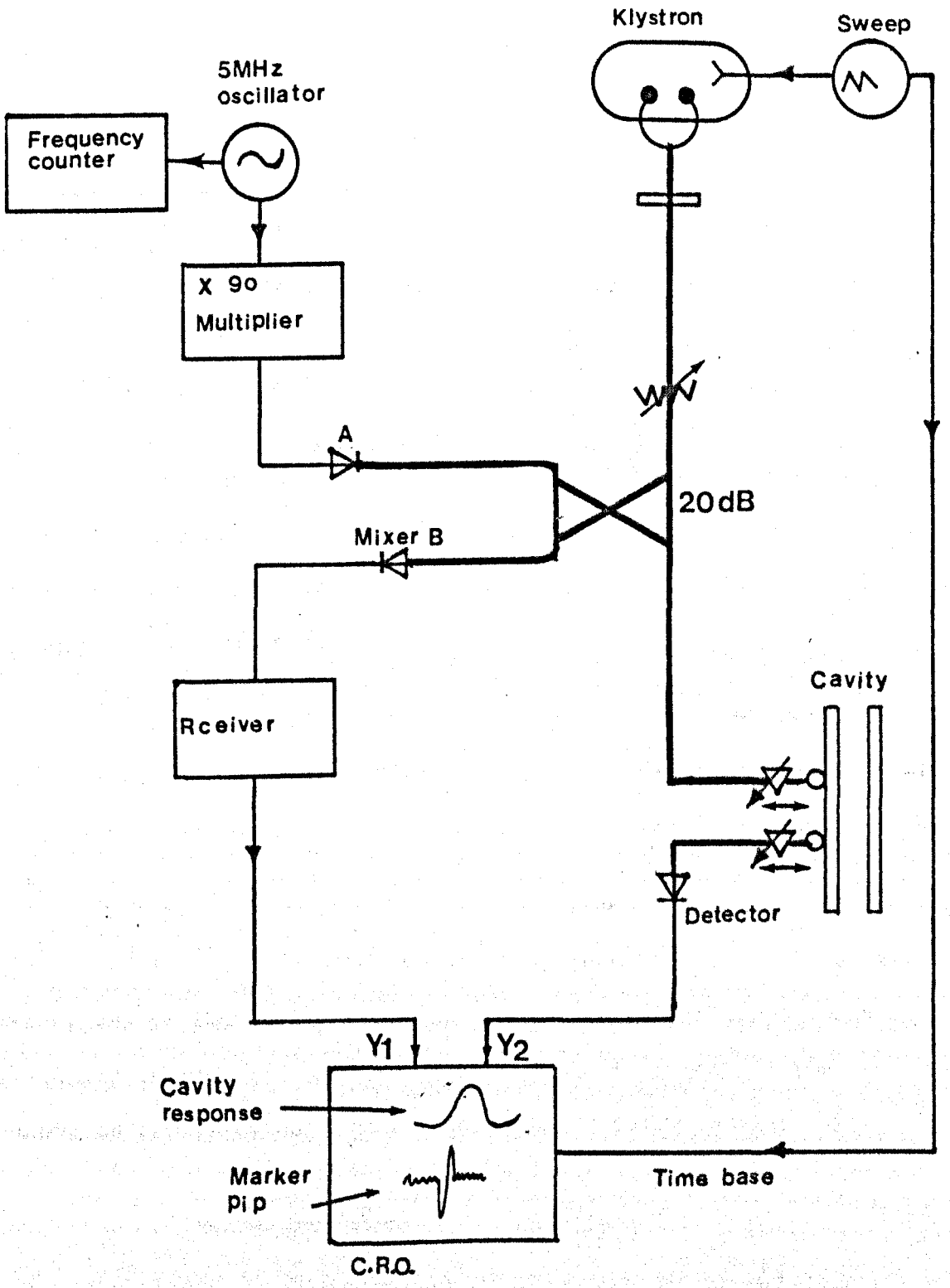

FIG. II.1 MICROWAVE ARRANGEMENT TO MEASURE CAVITY Q-VALUE

The half power point can be founded by either measuring the 5MHz oscillator frequency with a digital counter (at least 6-digits are needed), or by reading the scale of the receiver. To ensure easy operation the following procedure is recommended:

(1) Connect the crystal holder of the diode "A" to the output of the frequency multiplier and switch on XTL. In this position, the 0-1 mA meter reads the crystal current. If 1N26A is used, a current of more than 0.6 mA is needed. The current can be increased by changing the effective capacitance of the cable or by tuning the capacitor labelled C_1 inside the equipment.

(2) The marker pip can be found by tuning both the receiver and the oscillator. The signal-to-noise ratio of the marker can be improved by further attenuation of the klystron power and by decreasing the scan rate.

(3) If Δf is measured with the counter, then the pip is first tuned to the centre of the cavity response and the corresponding oscillator frequency is recorded. In the same way the frequency of the half-power points is recorded, and the loaded quality factor is given by

$$Q = \frac{CF_o}{C F_1 - F_2} = \frac{F_o}{(F_1 - F_2)} \qquad \text{II.2}$$

where C is the multipling factor (90 x 53). If measurements are made with the receiver then first the oscilloscope time base scale is calibrated in frequency units and the line-width is measured directly on the oscilloscope.

The above method was employed to measure the quality factor of the roof-top resonator described in chapter 3 (see Fig. 3.4). For example at a roof angle of $\sim 3^{\circ}$ the frequency counter readings were

F_o = 5.013.1MHz

F_1 = 5.0124 MHz

F_2 = 5.0137 MHz

Substitution in Eqn. II.2 yields $Q \approx 4000$. The estimated error in the measurement is better than 10%.

APPENDIX III

KEY TO SYMBOLS USED IN THE DETECTION SCHEME CIRCUIT DIAGRAMS.

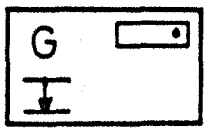

GAS MASER GENERATOR

SEMICONDUCTOR DIODE

RECTANGULAR WAVEGUIDE

ROTATABLE JOINT

MATCHED TERMINATION

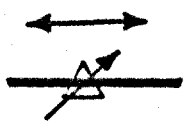

MATCHING UNIT

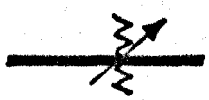

VARIABLE ATTENUATOR

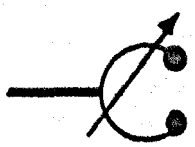

TUNABLE CAVITY RESONATOR

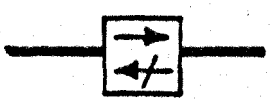

ISOLATOR

CIRCULATOR

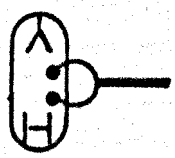

REFLEX KLYSTRON

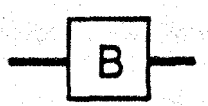

PHASE SHIFTER

DIRECTIONAL COUPLER

REFERENCES

Al-Amiedy, D.H.H. and Lainé, D.C., 1978: Phys. Lett., 66A, 94.

Al-Jumaily, A.M., 1979: Ph.D. Thesis, University of Keele.

Al-Jumaily, A.M. and Lainé, D.C., 1979: Actes du Coll. Opt. Hertz. et Diel., Lille, 27 - 29 June, 161.

Anderson, J.B. and Fenn, J.B., 1965: Phys. Fluids, 8, 780.

Baker, D.K., 1954: J. Appl. Phys., 25, 922.

Barchukov, A.I. and Prokhorov, A.M. and Savaranskii, V.V., 1963: Radio Eng. Electron. Phys. (USSR), 8, 385.

Bardo, W.S., 1969: Ph.D. Thesis, University of Keele.

Barnes, F.S., 1959: Proc. IRE, 47, 2085.

Basov, N.G., Oraevskii, A.N., Strakhovskii, G.M. and Tatarenkov, V.M., 1964: Sov. Phys. JETP, 18, 1211.

Basov, N.G., Borisenko, M.I., Vlasov, V.P., Dubonosov, S.P., Ivanov, N.E., Strakhovskii, G.M., Fedorenko, G.M. and Chikhakhev, B.M., 1967: Cosmic Res., 5, 13.

Bates, C.P., 1970: IEEE Trans., Ap-18, 230.

Becker, G., 1963: Z. Angew. Phys., 15, 13.

Bleaney, B.I. and Bleaney, B., 1957: "Electricity and Magnetism" (Oxford Clarendon Press).

Born, M. and Wolf, E., 1959: "Principles of Optics" (Pergamon Press, Oxford).

Bosch, B.G., Gambling, W.A. and Wilmshurst, T.H., 1961: Proc. IRE, 49, 1226.

Boyd, G.D. and Gordon, J.P., 1961: Bell Syst. Tech. J., 40, 489.

Buckingham, A.D. and Stephens, P.J., 1966: Ann. Rev. Phys. Chem., 17, 399.

Carpentier, J-M., 1979: Docter de Specialite Thesis, University of Lille (France).

Carpentier, J-M., Macke, B. and Segard, B., 1979: Acts du Coll. Opt. Hertz. et Diel., Lille, 27-29 June, 157.

Checcacci, P.F. and Scheggi, A.M., 1965: Appl. Optics, 4, 1529.

Checcacci, P.F., Consortini, A. and Scheggi, A.M., 1967: Appl. Opt. 6, 584.

Checcacci, P.F., Consortini, A. and Scheggi, A.M., 1968: IEEE Trans., MTT - 16, 103.

Coles, D.K. and Good, W.E., 1951: Phys. Rev., 82, 877.

Collier, R.J. and Wilmshurst, T.H., 1966: Phys. Lett., 23, 333.

Condon, E.U. and Shorty, G.H., 1951: "Theory of Atomic Spectra" (Cambridge University Press).

Culshaw, W., 1962: IRE Trans., MTT-10, 331.

Culshaw, W. and Kannelaud, J., 1964: Phys. Rev., 136, A1209.

Culshaw, W. and Kannelaud, J., 1966: Phys. Rev., 141, 228.

Dändliker, R., 1968: J. Opt. Soc. Am., 58, 1062.

de Lang, H., 1964: Philips Res. Repts.,19, 429.

de Lang, H., 1967: Philips Res. Repts., Suppl. No. 8,1.

De Lucia, F.C. and Gordy, W., 1969: Phys. Rev., 187, 58.

di Francia, G.T., 1965: Appl. Opt., 4, 1267.

D'Yakonov, M.I., 1966: Sov. Phys. JETP, 22, 812.

D'Yakonov, M.I. and Perel, V.I., 1966A: Opt. Spectry. (USSR), 20, 257.

D'Yakonov, M.I. and Perel, V.I., 1966B: Sov. Phys. JETP, 23, 298.

Einstein, A., 1917: Phys. Z., 18, 121.

Edmond, A.R., 1960: "Angular Momentum in Quantum Mechanics" (Princeton University Press, New Jersey).

Faraday, M., 1846: Phil. Mag., 28, 294.

Fox, A.G. and Li, T., 1961: Bell Syst. Tech. J., 40, 453.

Gamgling, W.A. and Wilmshurst, T.H., 1964: "Quantum Electronics III" ed. P. Grivet and N. Bloembergen (Columbia University).

Good, W.E., 1946: Phys. Rev., 70, 213.

Good, W.E. and Coles, D.K., 1954: Phys. Rev., 94, 1184.

Gordon, P.J., 1955: Phys. Rev., 99, 1253.

Gordon, P.J., Zeiger, H.J. and Townes, C.H., 1954: Phys. Rev., 95, 282.

Gordon, P.J., Zeiger, H.J. and Townes, C.H., 1955: Phys. Rev., 99, 1264.

Gordon, P.J. and White, L.D., 1958: Proc. IRE, 46, 1588.

Gordy, W., 1948: Rev. Mod. Phys., 20, 668.

Gordy, W. and Cook, R.L., 1970: "Microwave Molecular Spectra" (John Wiley and Sons, New York).

Grastens, M.A., 1953: Phys. Rev., 93, 1228.

Gunther-Mohr, G.R., Townes, G.H. and Van Vlech, J.H., 1954A: Phys. Rev., 94, 1191.

Gunther-Mohr, G.R., White, R.L., Schawlow, A.L., Good, W.E. and Coles, D.K., 1954B: Phys. Rev., 94, 1184.

Harvey, A.F., 1963: "Microwave Engineering" (Academic Press, London).

Hellwig, H., 1966: Z. Angew. Phys., 21, 250.

Helmer, J.C., 1957: Phys. Rev., 107, 902.

Hibben, S.G., 1969: Microwave J. (Nov., 1969), 59.

Hilderbrand, F.B., 1952: "Methods of Applied Mathematics" (Prentic-Hall, Englewood Cliffs, New Jersey).

Hurwitz, H.Jr. and Jones, R.C., 1941: J. Opt. Soc. Am., 31, 493.

Itoh, T. and Mittra, R., 1974: IEEE Trans., MTT-22, 99.

Jauch, J.M., 1947: Phys. Rev., 72, 715.

Javan, A., Bennett, W.R. Jr. and Herroitt, D.R., 1961: Phys. Rev. Lett., 6, 106.

Jerrard, H.G., 1954: J. Opt. Soc. Am., 44, 634.

Jones, R.C., 1941: J. Opt. Soc. Am., 31, 488.

Jones, R.C., 1942: J. Opt. Soc. Am., 32, 486.

Kannelaud, J. and Culshaw, W., 1966: Phys. Rev., 141, 237.

Kantrowitz, A. and Grey, J., 1951: Rev. Sci. Instrum., 22, 328.

Krupnov, A.F. and Shcuko, O.B., 1969: Izv. Vyssh. Ucheb. Zaved. Radiofiz., 5, 1780. English translation: (1972) Radiophys. Quant. Electron., 12, 1385.

Krupnov, A.F. and Skvortsov, V.A., 1964: Sov. Phys. JETP, 18, 1426.

Krupnov, A.F., Naumov, A.I. and Skvortsov, V.A., 1961: Izv. Vyssh. Ucheb. Zaved. Radiofiz., 4, 178.

Kukolich, S.G., 1967: Phys. Rev., 156, 83.

Lainé, D.C., 1975: "Advances in Molecular Beam Masers" in 'Advances in Electronics and Electron Physics' ed Maton, L., 39, 183 (Academic Press, New York).

Lainé, D.C. and Al-Jumaily, A.M., 1978: Electron. Lett., 15, 21.

Lainé, D.C. and Bardo, W.S., 1971: J. Phys. B.: Atom. Molec. Phys., 4, 1738.

Lainé, D.C. and Smart, G.D.S., 1971: J. Phys. D., 4, L23.

Lainé, D.C., Smart, G.D.S. and Corb, A.I., 1976: Annales Scientifiques de l'Universite de Clermont, No. 59, Physique 16e Fasc., 37.

Lainé, D.C. and Truman, M.J., 1977: Phys. Lett., 62A, 322.

Lainé, D.C., Truman, M.J. and Hope, S., 1980: Am. J. Phys., 48, 942.

Lainé, D.C. and Yassin, G., 1981: Proc. VIII Int. Symp. on Molecular Beams, Cannes, 1-5 June, 196.

Lainé, D.C. and Yassin, G., 1981: Bull-Mag. Res. Vol. 2, No. 1-4, 431.

Lainé, D.C. and Yassin, G., 1981: to be published in Phys. Lett.

Lamb, W.E. Jr., 1964: Phys. Rev., 134, A1429.

Li, T. and Zucher, H., 1967: J. Opt. Soc. Am., 57, 984.

Marcuse, D., 1962: IRE Trans. Instrum., I-11, 187.

Maroof, A.K.H. and Lainé, D.C., 1976: J. Phys. D, 9, 175.

McCaffery, A.J., 1971: Nature Physical Science, 232, 137.

Mittra, R. and Lee, S.W., 1971: "Analytical Techniques in the Theory of Guided Waves" (Macmillan, New York).

Montgomery, C.G., 1947: "Techniques of Microwave Measurements" (M.I.T. Radiation Lab. Series Vol. 16, McGraw-Hill, New York).

Morse, P.M. and Feshbach, H., 1953: "Methods of Theoretical Physics" (McGraw-Hill, New York).

Nikitin, V.V. and Oraevskii, A.N., 1962: Radio Eng. Electron. Phys., 7, 814.

Noble, B., 1958: "Methods Based on the Wiener-Hopf Technique" (Macmillan, New York).

Oraevskii, A.N., 1964: "Molecular Generators" (Nauka, Moscow).

Polder, D. and Van Haeringen, W., 1965: Phys. Lett., 19, 380.

Pound, R.V., 1948: "Microwave Mixers" (M.I.T. Radiation Lab. Series, Vol 16, McGraw-Hill, New York).

Prokhorov, A.M., 1958: Sov. Phys. JEPT, 34, 1140.

Robinson, G.T. and Boch, B.G., 1957: Brit. J. Appl. Phys., 8, 275.

Rosenberg, R., Rubinstein, C.B. and Herroitt, D.R., 1964: Appl. Opt., 3, 1079.

Sargent, M. III, Lamb, W.E. Jr. and Fork, R.L., 1967: Phys. Rev., 141, 228.

Schawlow, A.L. and Townes, C.H., 1958: Phys. Rev., 112, 1940.

Schnabel, E., Törring, T. and Wilke, W., 1965: Z. Physik, 188, 167.

Schiff, L.I., 1968: "Quantum Mechanics" (McGraw-Hill, New York).

Serber, R., 1932: Phys. Rev., 41, 489.

Servant, Y., 1975: In "Magnetic Resonance Review" (Gordon and Breach, London) Vol. 4 No. 1, 1.

Shimoda, K., 1957: J. Phys. Soc. Jap., 12, 1006.

Shimoda, K., 1962: In "Topics on Radiofrequency Spectroscopy", A. Gozzini, ed., (Academic Press, New York), 1.

Shimoda, K. and Wang, T.C., 1955: Rev. Sci. Instrum., 26, 1148.

Shimoda, K., Takahasi, H. and Townes, C.H., 1957: J Phys. Soc. Jap., 15, 686.

Shimoda, K., Wang, T.C. and Townes, C.H., 1956: Phys. Rev., 102, 1308.

Shimizu, T. and Shimoda, K., 1961: J. Phys. Soc. Jap., 16, 777.

Silver, S., 1949: "Microwave Antenna Theory and Design" (M.I.T. Lab. Radiation Series, Vol. 12, (McGraw-Hill, New York).

Singer, J.R., 1959: "Masers" (Wiley and Sons, New York).

Sircar, P. and Hardin, J., 1964: C.R. Acad. Sci., 259, 1500.

Slater, J.C., 1950: "Microwave Electronics" (D. Van Nostrand Company, New York).

Smart, G.D.S., 1973: Ph.D. Thesis, University of Keele.

Smith, A.L.S. and Lainé, D.C., 1967: Electron. Lett., 3, 90.

Statz, H., Paananen, R. and Koster, G.F., 1962: J. Appl. Phys., 33, 2319.

Strakhovskii, G.M. and Tatarenkov, V.M., 1964: Izv. Vyssh. Ucheb. Zaved. Radiofiz., 7, 922.

Taylor, E.R.G., 1963: RAE (Franborough) Tech. Note No. WE25.

Thaddeus, P., Krisher, L.C. and Loubser, J.H.N., 1964: J. Chem. Phys., 40, 257.

Townes, C.H., 1960: Phys. Rev. Lett., 5, 428.

Townes, C.H. and Geschwind, S., 1948: Phys. Rev., 19, 795.

Townes, C.H. and Schawlow, A.L., 1955: "Microwave Spectroscopy" (McGraw-Hill, New York).

Vainshtein, L.A., 1963: Sov. Phys. JETP, 17, 709.

Valentin, M., 1978: Il Novo Cimento, 44B, 205.

van Haeringen, W., 1967: Phys. Rev., 158, 256.

Van Vleck, J.H., 1953: Rev. Mod. Phys., 23, 213.

Yariv, A., 1971: "Introduction to Optical Electronics" (Holt, Rinehartan Winston, New York).

Yassin, G. and Lainé, D.C., 1979: Actes du Coll. Opt. Hertz. et Diel., Lille, 27-29 June, 157.

Yassin, G. and Laine, D.C., 1981: Electron. Lett., 17, 156.

Yassin, G. and Laine, D.C., 1981: Proc. Coll Opt. Hertz. et Diel., Toulouse, 14-16 Sept. (in press).

Zimmerer, R.W., 1962: Rev. Sci. Instrum., 33, 858.

Zimmerer, R.W., 1963: IEEE Trans., MTT-11, 371.